Impact of Accelerator Based Technologies on Nuclear Fission Safety: IABAT-project.

Final Report

Co-ordinator: Waclaw Gudowski, KTH

CONTRACT NO**: FI4I-CT96-0012,**
DURATION: **1 MAY, 1996 – 31 OCT. 1999**

Participating institutes:

Commissariat á l' Energie Atomique - CEA
CEA/CE Cadarache
13108 Saint Paul Lez Durance, France

Nuclear Research and consultancy Group - NRG (former ECN)
1755 ZG Petten, The Netherlands

Forschungszentrum Juelich - FZJ
Postfach 1913
52425 Juelich , Germany

Ente per le Nuove tecnologie, l'Energia e l'Ambiente – ENEA- CASACCIA

and **Politecnico di Torino**
via Anguillarese, 301
00060 Santa Maria Di Galeria (ROMA), Italy

Forschungszentrum Karlsruhe - FZK
Postfach 3640
76021 Karlsruhe, Germany

European Institute for Transuranium Elements - ITU
Postbox 2340
D-76125 Karlsruhe, Germany

AEA Technology
329 Harwell
Didcot, Oxon., OX110RA, United Kingdom

University of Uppsala – UU
S-611 82 Nyköping

Chalmers Tekniska Högskolan - CTH
S-412 96 Goteborg , Sweden

Kungliga Tekniska Högskolan - KTH

100 44 Stockholm, Sweden

THE IABAT-PROJECT COLLABORATION

(including contribution to the final report)

G. Ritter, C. Gaudard, S. Soubiale, C. Toccoli, M. Valade, G. Youinou

CEA Cadarache

A. Koning

NRG Petten

P. Phlippen, M.Piontek

FZJ Jülich

P. Ravetto and P. Landeyro

ENEA and Polito

C. Broeders and I. Broeders

FZK Karlsruhe

J. Magill and P. Peerani

ITU, Karlsruhe

R. Cummings

AEA Technolgy Harwell

E. Ramström, B. Fogelberg

Univ. Uppsala

I. Pazsit and V. Arzhanov

CTH

W. Gudowski, J. Cetnar, J. Wallenius, M. Ericsson and Y. Shubin with his group (IPPE)

KTH

Acknowledgements

We would like to thank the DGXII of the European Commission for their support – contract FI4I-CT96-0012 – and particularly M. Hugon for being a competent, effective and stimulating co-ordinator of the Partitioning and Transmutation cluster.

The IABAT project with its many participants and big ambitions would not be able to succeed without a financial support on the national level. We would like especially to acknowledge financial support from the Swedish Nuclear Fuel and Waste Management – SKB. The SKB support helped to co-ordinate efficiently the IABAT project and made possible a smooth merge between the different research tasks.

The IABAT participants would also like to acknowledge the contributions of our collaborators in different tasks, particularly groups from **Paul Scherrer Institut (Villingen)**, **Los Alamos National Laboratory (Los Alamos), Institute of Physics and Power Engineering (Obninsk)**, **University of Mining and Metallurgy (Krakow).**

We would also like to pay tribute to late dr. Pedro Landeyro, ENEA, Casaccia, a member of our team, who unfortunately died before the completion of our project. We keep him warmly in our memories.

CONTENTS

EXECUTIVE SUMMARY

The overall objective of the IABAT project – Impact of Accelerator Based Technologies on Nuclear Fission Safety - has been a preliminary assessment of the potential of Accelerator-Driven Systems (ADS) for transmutation of nuclear waste and, additionally on for nuclear energy production with minimum waste generation. Moreover, more specific topics related to nuclear data and code development for ADS have been studied in more detail.

The IABAT project stimulated very visibly the development of accelerator-driven transmutation research in many institutes in European Union and contributed to the creation of new projects and project proposals for the 5th Framework Programme. Almost every research group participating in the IABAT project has developed further activities in this field.

Three broad tasks have been addressed in the project, covering ADS-System and Fuel Cycle Studies, Nuclear and Material Data Development and Assessment of Accelerator-Technology.

System And Fuel Cycle Studies

Several reactor technologies have been considered for Accelerator Driven Systems. In IABAT we addressed a set of subcritical cores featuring distinctive basic characteristics. These main features are the neutron spectrum, the type of fuel matrix - solid or liquid, and in-core behaviour of uranium and thorium based fuels. The studies focused on neutronics and transmutation potential. They did not try to address important questions concerning fuel and coolant technologies, partitioning and separation chemistry or economics.

Four systems have been studied in detail:

- Liquid Lead and Lead/Bismuth Cooled Fast Systems with Solid Fuel
- Liquid Lead Thermal System with Dispersed Fuel (so called Jülicher Transmuter)
- Fast and Thermal (so called superthermal) Molten Salt Systems

Neutronics studies of the **liquid lead (and Pb/Bi) cooled, solid fuel ADS** show that the extraordinary neutron surplus with ADS would not be a decisive advantage with respect to fast reactor transmutation, if this could not be fully utilized for transmutation purposes in practice. There are several possible options to enhance transmutation potential of ADS, like:

- Transmutation of the long-lived fission products ^{99}Tc, ^{129}I and ^{135}Cs.
- Capture in burnable poisons for flattening of reactivity changes.
- Low-energy capture in absorbers in order to block capture in fuel nuclides and ^{209}Bi (for Pb/Bi cooled systems). Using absorbers to block neutron capture in ^{241}Am and consequently generation of ^{238}Pu.

Studies of the optimized **Jülicher ADS** with a thermal neutron flux and liquid lead as a carrier of low concentration TRU fuel show that it offers a lot of advantages in a continuous operation mode. The TRU inventory in the system is very low, it performs a high TRU consumption rate, the k-value can be kept nearly constant at desired subcriticality and thus the required accelerator power stays constant. In comparison to other options to burn Pu and/or MA it is a very efficient system with a high transmutation rate.

The Jülicher ADS is probably the most unusual ADS proposed until now and there are a lot of difficult technological problems to be solved for this system, like fuel technology, corrosion of liquid lead, high power accelerator, but most of these problems are similar for other ADS-concepts.

Molten salt ADS were assessed in the IABAT project for incineration of transuranium elements and separately, only for minor actinide burning. For molten salt system studies, the following topics were investigated:

- Molten salt composition for a given type of neutron spectrum
- Neutron spectrum of the system
- Fuel feeding strategy to obtain an equilibrium fuel composition
- Accelerator power range matching reactivity swings
- Sensitivity of core parameters to some perturbations

Spallation neutron target studies

The spallation target, being an interface module between accelerator and subcritical reactor, is one of the most important components of ADS and may easily be a technological show-stopper for further development. Consequently, some efforts were put in the IABAT-project to assess the simulation tools for spallation targets and to propose solutions, which may mitigate some of the serious problems arising on merging accelerator and nuclear technologies.

For the liquid **lead cooled, solid fuel ADS** a multiple target system, and with different fuel enrichment levels, have been studied in order to optimize the radial power distribution. The 3-spallation target system shows very good power distribution performance at least at the beginning of life. However, technical difficulties to design a 3-target subcritical core make this option unfeasible for the time being.

To complement target studies **radiation damage to the main ADS components** i.e. core, target container and beam window have been estimated, including contributions from reactor energy range neutrons + high-energy particles. Radiation damage has been quantified in dpa (displacement per atom), specific spallation residuals production and gas releases. Results show that within fairly conservative limits on gas production and dpa, a life time for a target window can be expected to be around 1 year for proton current densities in a range of J_{ave}=25 – 30 μA/cm^2

Development of Simulation Tools and Methodology for ADS Analysis

Development of simulation tools and methodology for analysis of the Accelerator-Driven Systems was focused on following objectives:

- Methodology for monitoring ADS-subcriticality based on the neutron fluctuation analysis
- Assessment of point reactor models for source injected subcritical reactor dynamics
- Solution of space kinetics in one and two space dimensions for fluid-fuel systems and study of the delayed neutron emission worth
- Assessment of three-dimensional time-dependent computational algorithms
- Development of a Monte-Carlo burnup code

Neutron fluctuations can be used to monitor the state of the system in normal conditions, when it is used to determine operational variables such as subcritical reactivity, dynamic response, and to detect the inset anomalies. The theory of neutron fluctuations in ADS was developed in two different contexts. One is the theory of fluctuations in a constant medium with a constant source, in order to use them for monitoring subcritical reactivity. **The theory of the Feynman-alpha and Rossi-alpha methods** was elaborated for subcritical reactors with a spallation source. The second is the development of **the theory of neutron fluctuations, induced by the fluctuations** of the intensity or the position of the source (as a consequence of the fluctuations of the ion beam). The purpose with the latter is to develop diagnostic methods that can be used to detect and identify anomalies in operating ADS.

A **new burnup-code** has been developed in the frame of IABAT-project in collaboration with University of Mining and Metallurgy in Krakow. This code - MCB is a Monte Carlo Continuous Energy Burnup Code, a general-purpose code which can be used for calculation of nuclide densities evolution with burnup or decay, including eigenvalue calculations of critical and subcritical systems and neutron transport calculation together with all necessary reaction rates and energy deposition. The code has emerged from an integration of the well known code MCNP4B, used for neutron transport calculation, and a novel Transmutation Trajectory Analysis code (TTA), which provides density evolution calculation, including formation and analysis of transmutation chains. The codes were integrated on the level of the source code of MCNP. As a result, MCB is compatible with MCNP and complete burnup calculation can be done in one single run. The current version of the code has been distributed among "friendly users" and is under an intensive benchmarking process.

Moreover a number of dedicated code systems for ADS, coupling high-energy transport codes, neutron transport and burnup codes has been set-up and validated giving a confidence in the use applied simulation tools.

Impact on the Risk From High-Level Waste Repositories from Radiotoxicity Reduction Using ADS

A wide-ranging review of repository risk studies has been used to identify which radionuclides would need to be transmuted to reduce risk from a repository. Specific examples have been used to show by how much the inventory of different radionuclides would have to be transmuted to produce reductions in repository risk by factors of 10 and 100.

This study gives **no crystal-clear benefits of ADS for repository radiotoxicity reduction.**

General conclusions are:

- The studies reviewed show the importance of reducing inventories of fission products as well as actinides to reduce repository risk
- In reported repository risk studies there is a wide variation in what are the most significant radionuclides and by how much the inventories of these radionuclides would have to be transmuted to decrease the risk. Variations arise from different assumptions about scenarios, repository design and siting, and other data. ADS should ideally be developed to retain the flexibility to transmute as wide a range as possible of the long-lived fission products and actinides given here.

- It is conceivable that with the use of inappropriate or badly specified materials, in terms of repository risk, the positive benefit of transmuting actinides and fission products could be negated by the creation of activation products.
- The decay daughters of uranium can make a significant contribution to repository risk over long timescales. Significant quantities of uranium could not be transmuted. The waste management of uranium (or thorium) needs to be addressed in a fuel cycle involving ADS.

Proliferation Aspects of ADS

At present, commercially available machines (ADONIS, I.B.A. Belgium) with proton energies around 150 MeV and currents of 1.5 mA (power 225kW), are at the limit of the technology threshold (capacity to produce 100g Pu per year) laid down by the I.A.E.A in their INFCIRC documents. It appears that next generation machines must be specified in the Trigger List and Dual-Use Goods.

In the future, large powerful accelerators may be used for power production and waste transmutation. Because of the size of these machines, they will automatically fall under I.A.E.A. safeguards. It has been shown that during the down time for such systems (e.g. required for fuel reloading), the accelerator beam current can be used for clandestine activities in which significant amounts of weapons grade material can be produced on a timescale of a few days to one month. Steps have to be taken to ensure that this does not occur (for example through the use of power monitors).

Another fundamental difference between a critical reactor and an accelerator driven sub-critical assembly is that the ADS can be used for "isotopic enrichment" and for "fissile material conversion". In the former process, the spallation neutrons can be surrounded by a multiplying medium such as spent reactor fuel ($k_{inf} \approx 0.9$) containing poor grade plutonium to "amplify" the neutron flux. This can then be used to breed pure Pu in the outer blanket. In the latter process, an enriched uranium blanket (containing for example 20% ^{235}U) can be used to amplify the neutron flux. These neutrons are captured by ^{238}U to produce ^{239}Pu. Because the Pu is a different element, it can easily be separated by standard chemical processing.

Assessment of Accelerator Technology

Costing models have been created that allow the circular and linear accelerator options to be compared and the effect of parameter variations examined. Whilst accurate costs can only be obtained from a detailed system design specification, the costing models allow indicative costs to be estimated in a relatively straightforward way. The calculations reported show that cyclotron systems would be more economical, due mainly to the advantage of the cost of RF power supplies. However, it should be noted that many in the accelerator community regard with skepticism the possibility of transporting and extracting more than a 10mA beam current from a 1GeV cyclotron and therefore technical factors may limit the application of cyclotrons.

In collaboration with Los Alamos National Laboratory a reliability study of the LANSCE accelerator has been performed. The reliability and availability of the accelerator in accelerator driven systems is an important issue. Taking into account the fact that proton beams from existing high power proton accelerators trip very frequently, it is indispensable to understand the effect of such beam trips on different subsystems, especially a subcritical reactor. Temperature fluctuation caused by power change in the accelerator beam enforces

thermal transients to reactor structures and beam window, where thermal fatigue or creep-fatigue damage will be accumulated during lifetime. When a large number of severe thermal stress cycles is enforced, there is a possibility of crack initiation and propagation at structural walls.

Some important conclusions of this study are:

- An actual beam trip rate of the LANSCE accelerator is typically 1.6-2.4 trips/hour or 40-60 trips/day. 75% of these trips are shorter than 1 minute. This is almost 4 order of magnitudes more that acceptable for commercial nuclear power installations. It is considered that improvement in the number of trips by a factor of 100 is achievable with today's technology
- The typical downtime of a short trip is 15-20 seconds and the main source of beam trip is sparking in high voltage components, for example the injector column.
- Accelerator trips will be a strongly limiting constraint for a spallation target experiment (e.g. for a liquid Pb/Bi "Obninsk spallation target") due to the load on a target window.
- The temperature swing in the reactor caused by a short beam trip is small due to the thermal inertia of the system; for example, it takes certain amount of time for the coolant to recycle the reactor.

Nuclear and Material Data Development

Several high-energy transport codes exist which contain an intranuclear cascade model that is mainly successful for the primary stages of the reaction, including the production of several types of hadrons. For energies below about 150 MeV, when the predictive power of the high-energy transport codes becomes suspect, nuclear data libraries are required.

In recent years, progress has been made on the following items: (1) a more specific survey of data needs for experimental and evaluated data, (2) consensus on format definition of nuclear data libraries, (3) significant progress on experimental data compilation, (4) the collection of starter files, (5) pilot evaluation projects, (6) recommendation of, and participation in, specialist meetings and benchmark exercises concerning nuclear reaction models.

The fission product yield distributions have been measured for fast neutron fission of ^{232}Th and ^{233}U, which are the main contributors of fission events in systems based on Th fuel. Individual yields of about 180 fission products could be determined. Such data also give a considerably improved basis for predictions of yield distributions using models or systematics.

New phenomenological, spherical, neutron and proton optical model potentials for all isotopes under study here, which are smooth from 0 to 200 MeV, have been created. The potentials are directly applied in multi-step direct calculations to analyze the recent (n,p) measurements.

With a code system centered around ECIS96 and GNASH, 150 MeV neutron and proton transport data files for Fe, Ni and Pb have been created. In collaboration with a Russian group from Institute of Physics and Power Engineering three more data files were created for ^{232}Th,^{238}U and ^{239}Pu. The high-energy part of the data files consists completely of results from model calculations, which are benchmarked against the available experimental data. The

comparison between the data files and experimental data as provided in this report gives an impression of the quality of the evaluations. Although there is obviously future work left regarding fine-tuning of several parts of the data file, we argue that the representation of nuclear reaction information up to 150 MeV is already better than can be attained with intranuclear cascade codes.

I. INTRODUCTION

A self-sustained chain reaction is the very principle of nuclear reactor operation but it also creates non-negligible hazards. One such hazard is the possibility of a criticality excursion, i.e. a potentially possible reactor run-away accident. A reactor run-away (or reactor excursion) accident can lead to an unmanageable power rise and to a disruption of the reactor vessel integrity ending with release of otherwise contained radioactivity. The control of the self-sustained chain reaction, or what we prefer to call - criticality control, relies on the small fraction of delayed neutrons emitted from the fission products a "long time" after the fission event itself. This small fraction of delayed neutrons determines the criticality safety margins, which puts some serious constraints on the fissile fuel composition, e.g. reactors cannot operate on purely minor actinide fuel, because of the very low fraction of delayed neutrons.

What can be done to enhance safety of nuclear fission processes? A lot can be done to improve the design of well-known conventional nuclear reactors; new, better reactors can be designed but it seems today very improbable to expect any radical change in the public perception of conventional nuclear power. In this context, considerable hope and expectation have been expressed for novel systems called Accelerator-Driven Systems (ADS), Accelerator-Driven Transmutation of Waste (ATW) or Accelerator-Driven Hybrid Reactors. All these names are used to describe the same nuclear system, i.e. combining a powerful particle accelerator with a subcritical reactor.

The idea of combining powerful accelerators - with a subcritical reactor for transmutation purposes is not new. Nuclear transmutation itself was demonstrated for the first time by Rutherford in 1919, who transmuted ^{14}N to ^{17}O using energetic α-particles [Ruth20]. I. Curie and F. Joliot produced the first artificial radioactivity in 1933 using α-particles from naturally radioactive isotopes to transmute boron and aluminum into radioactive Nitrogen and Oxygen [Curi34]. It was not possible to extend this type of transmutation to heavier elements as long as the only available charged particles were the α-particles from natural radioactivity, since the Coulomb barriers surrounding heavy nuclei are too great to permit the entry of such particles into atomic nuclei. The invention of the cyclotron by E.O. Lawrence [Lawr39] removed this barrier and opened new frontiers. Now, it is widely known that when coupled with the spallation process, high power accelerators can be used to produce large numbers of neutrons, thus providing an alternative method to the use of nuclear reactors for this purpose. Spallation offers exciting possibilities for generating intense neutron fluxes for a variety of purposes.

Transmutation processes on a larger scale can be realized using different particles, like neutrons, charged particles and even γ-rays. However, neutrons offer the best and most efficient way of transmutation due to lack of a Coulomb barrier and favourable cross-sections. Existing nuclear reactors can be used to perform transmutation, as well as new critical reactors can be designed for transmutation purposes; these options were investigated in some European projects financed by the European Commission during last years.

The first practical attempts to promote accelerators as powerful neutron sources were made in the late 1940's by E.O. Lawrence in the United States, and W.N. Semenov in the USSR. The first such application for the production of fissile material was the MTA project at the Lawrence Livermore Radiation Laboratory. This project was abandoned in 1952 when high-grade Uranium ores were discovered in the United States [AEC53, MTA54].

In the 1960's, Brookhaven National Laboratory presented several proposals for accelerator breeders such as the Na-cooled fast reactor target, the Molten Salt target, the He-gas-cooled target, as well as the LWR fuel regenerator [Stei64]. This concept of the accelerator breeder has also been studied by Russian scientists. Under the guidance of V.I. Goldanski, R.G. Vassylkov [Vass78] made a neutron yield experiment in depleted uranium blocks using the accelerator at Dubna.

The original idea of exploiting the spallation process to transmute actinide and fission products directly was soon abandoned. The proton beam currents required - around 300 mA - were much larger than the most optimistic theoretical designs that an accelerator could achieve. Indeed, it was shown that the yearly transmutation rate of a 300 mA proton accelerator would correspond only to a fraction of the waste generated annually by a LWR of 1 GW_{el}.

To use only the spallation neutrons generated in a spallation target, the fission products would be placed around the target. For the highest efficiency, depending on the material to be transmuted, either the fast neutrons would be used as they are emitted from the target or they would be slowed down by moderators to energies with higher transmutation cross-sections, for example, the resonance or the thermal region. To improve the transmutation efficiency even more it is desirable to surround the spallation target with a subcritical nuclear reactor core (most often called blanket) - an idea, which has been materialized in accelerator-driven systems proposed in last years. ADS using fast neutrons for the incineration of higher actinides was proposed at Brookhaven National Laboratory (PHOENIX-project) and then was carried out for several years in Japan as a part of OMEGA-programme [Gudo97]. Los Alamos National Laboratory has developed several ideas to use ADS using thermal neutrons with a linear accelerator for incineration of plutonium and higher actinides, for transmutation of some fission products in order to effectively reduce long-term radioactivity of nuclear waste as well as for producing energy based on the thorium fuel cycle [Bowm93, Venn93]. In 1993 Carlo Rubbia and his European group at CERN [Carm93, Rubb95] proposed a cyclotron based hybrid system to produce nuclear energy based on the Thorium fuel cycle. It revived significantly a scientific interest for a Thorium fuel cycle in spite of the fact that the main interest in conceptual designs of ADS has focused much more on the transmutation of existing nuclear waste from Light Water Reactors.

Since the end of the 1980´s research in transmutation, particularly Accelerator-Driven Transmutation of long-lived and radiotoxic nuclides has increased all over the world. In particular, interest in ADS for transmutation of nuclear waste (and possibly weapon-grade Pu) and, to a somewhat lesser extent, energy production has increased over the past few years. Different reasons stimulate these research activities in many countries having very different fuel cycle policy: from countries like France, Japan or Russia having "reprocessing" fuel cycle policy for Pu recirculation, through the countries which adopted the once-through fuel cycle (like USA, Spain or Sweden) and ending on the countries without nuclear power at all (Italy, Poland). In France and Japan, where for a decade active research programmes on transmutation have been carried on, new problems concerning the future of fast breeder reactors have stimulated greater interest in Accelerator-Driven Systems. ADS are considered as a viable option for minor actinides transmutation. In USA a road-mapping activity has formulated a DOE programme on Accelerator-Driven Transmutation of Wastes and has tried to define a place for this technology in the US waste management policy [Road99]. In Russia, a few hundred former weapon researchers are currently involved in transmutation related projects, financed mainly by the USA, EU, Japan and Sweden through the International Science and Technology Centre (ISTC). Countries like Italy and Spain have recently started

well-defined research programmes in ADS, while other countries have allocated additional funds to existing programmes (Belgium, Sweden, South Korea, Czech Republic etc.)

The IABAT project - **I**mpact of **A**ccelerator **Ba**sed **T**echnologies on Nuclear Fission Safety - started in 1996 in the frame of 4th Framework Programme of the European Union, R&D specific programme "Nuclear fission safety 1994-1998", area A.2 "Exploring innovative approaches/Fuel cycle concepts", as one of the first common European activities in ADS. The project was completed October 31, 1999.

II. MAIN TOPICS OF THE PROJECT

The overall objective of the IABAT project has been a preliminary assessment of the potential of Accelerator-Driven Systems (ADS) for transmutation of nuclear waste and further on for nuclear energy production with minimum waste generation. Moreover there were few more specific topics related to nuclear data and code development for ADS, which have been studied in more detail.

11 research groups from 6 European countries (France, Germany, Great Britain, Italy, Netherlands and Sweden) participated in this project. Some of the IABAT topics have been completed in collaboration with Paul Scherrer Institut (Villingen), Los Alamos National Laboratory (Los Alamos), Institute of Physics and Power Engineering (Obninsk) and University of Mining and Metallurgy (Krakow).

Three broad tasks have been addressed in the project covering **ADS-System and Fuel Cycle Studies, Assessment of Accelerator Technology** and **Development of Nuclear and Material Data**.

System and Fuel Cycle Studies

System and Fuel Cycle Studies comprised also some theoretical aspects of subcritical systems and spallation neutron target studies.

Several reactor technologies have been considered for Accelerator Driven Systems. In IABAT we addressed a set of subcritical cores featuring distinctive basic characteristics. These main features are the neutron spectrum, the type of fuel matrix -solid or liquid- and in-core behaviour of uranium and thorium based fuels. The studies were focused on neutronics and a transmutation potential, they did not try to address important questions concerning fuel and coolant technologies, partitioning and separation chemistry, neither did address economical assessment.

Four systems have been studied in detail:

- Liquid Lead and Lead/Bismuth Cooled Fast Systems with Solid Fuel
- Liquid Lead Thermal System with Dispersed Fuel (so called Jülicher Transmuter)
- Fast and Thermal (so called superthermal) Molten Salt Systems

For the liquid **lead cooled, solid fuel ADS**, a multiple target system and with different fuel enrichment levels has been studied in order to optimize the radial power distribution. **Jülicher ADS** was developed based on the idea to use liquid lead as a carrier of a low concentrated TRU fuel in a graphite core. Studies were focused on the performance of this type of ADS for different fuel types. In comparison to other options to burn Pu and/or MA it turn out to be a very efficient transmutation system. Some safety aspects have been studied specifically for this ADS.

The **Jülicher ADS** is probably the most unusual ADS proposed until now and there are a lot of difficult technological problems to be solved for this system, like fuel technology, corrosion of liquid lead, high power accelerator, but most of these problems are similar for other ADS-concepts.

Molten salt ADS were assessed in the IABAT project for incineration of transuranium elements and separately, only for minor actinide burning. For molten salt system studies following topics were investigated:

- Molten salt composition for a given type of neutron spectrum
- Neutron spectrum of the system
- Fuel feeding strategy to obtain an equilibrium fuel composition
- Accelerator power range matching the reactivity swing
- Sensitivity of core parameters to some perturbations

Spallation neutron target studies

The spallation target being an interface module between accelerator and subcritical reactor is one of the most important components of ADS and may easily be a technological show-stopper for further development. Consequently, some efforts were put in the IABAT-project to assess the simulation tools for spallation targets and to propose solutions, which may mitigate some of the serious problems arising on merging accelerator and nuclear technologies.

To complement target studies radiation damages to the main ADS components i.e. core, target container and beam window have been estimated, including contributions from reactor energy range neutrons + high-energy particles. Radiation damages have been quantified in dpa, specific spallation residuals production and gas releases.

Development of simulation tools and methodology for ADS analysis

Development of simulation tools and methodology for analysis of the Accelerator-Driven Systems was focused on following objectives:

- Methodology for monitoring ADS-subcriticality based on the neutron fluctuation analysis
- Assessment of point reactor models for source injected subcritical reactor dynamics
- Solution of space kinetics in one and two space dimensions for fluid-fuel systems and study of the delayed neutron emission worth
- Assessment of three-dimensional time-dependent computational algorithms
- Development of a Monte-Carlo burnup code
- Validation of different dedicated code systems for ADS, coupling high-energy transport codes, neutron transport and burnup codes has been set-up and validated giving a confidence in applied simulation tools.

A **new burnup-code** has been developed in the frame of IABAT-project in collaboration with University of Mining and Metallurgy in Krakow. This code, called MCB, is a Monte Carlo Continuous Energy Burnup Code, a general-purpose code which can be used for calculation of nuclide densities evolution with burnup or decay, including eigenvalue calculations of critical and subcritical systems and neutron transport calculation together with all necessary reaction rates and energy deposition. The code has emerged as a integration of well known code MCNP4B, used for neutron transport calculation, and a novel Transmutation Trajectory Analysis code (TTA), which provides density evolution calculation, including formation and analysis of transmutation chains. The codes were integrated on the level of the source code of MCNP.

Moreover a number of dedicated code systems for ADS, coupling high-energy transport codes, neutron transport and burnup codes has been set-up and validated, giving a confidence in applied simulation tools.

Proliferation aspects of ADS

Some efforts have been put to assess proliferation risks related to ADS development and measures have been proposed safeguarding ADS.

Impact on the risk from high-level waste repositories from radiotoxicity reduction using ADS

A wide-ranging review of repository risk studies has been used to identify which radionuclides would need to be transmuted to reduce risk from a repository. Specific examples have been used to show by how much the inventory of different radionuclides would have to be transmuted to produce reductions in repository risk by factors of 10 and 100.

Assessment of Accelerator Technology

Costing models have been created that allow the circular and linear accelerator options to be compared and the effect of parameter variations examined. Whilst accurate costs can only be obtained from a detailed system design specification, the costing models allow indicative costs to be estimated in a relatively straightforward way.

In collaboration with Los Alamos National Laboratory a reliability study of the LANSCE accelerator has been performed in order to assess necessary technological improvements for accelerators to match requirements of the nuclear power systems.

Nuclear and material data development

Evaluated nuclear data files up to 150 MeV for Fe, Ni, Pb, Th ^{238}U and ^{239}Pu

Simulations of ADS physics require nuclear data in much broader energy range than conventional nuclear reactors. Moreover, data for proton interactions may also be important for some material damage problems.

With a code system centered around ECIS96 and GNASH 150 MeV neutron and proton transport data files have been created for Fe, Ni and Pb. In collaboration with a Russian group from Institute of Physics and Power Engineering three more data files were created for ^{232}Th, ^{238}U and ^{239}Pu. The high-energy part of the data files consists completely of results from model calculations, which are benchmarked against the available experimental data. The comparison between the data files and experimental data as given in this report gives an impression of the quality of the evaluations.

The fission product yield distributions have been measured for fast neutron fission of ^{232}Th and ^{233}U, which are the main contributors of fission events in systems based on Th-fuel. Individual yields of about 180 fission products could be determined. Such data also give a considerably improved basis for predictions of yield distributions using models or systematics.

III. DEVELOPMENT OF COMPUTER SIMULATION TOOLS

For the analysis of Accelerator Driven Systems (ADS) the whole energy spectrum of nuclear data from several GeV down to thermal energies has to be covered. The traditional calculation tools for fission reactors use neutron cross-section data in the energy range up to about 10 MeV, like for example WIMS- and ABN-based libraries. Other multigroup neutron data libraries and also special libraries for Monte Carlo calculations (e.g. MCNP) apply energies in the range of the evaluated data libraries like ENDF/B, usually being up to 20 MeV. Modeling of ADS requires not only special routines for simulation of spallation processes but also nuclear data for nucleons (mainly neutrons) interactions at energies higher than 20 MeV. Therefore transport codes and data routinely used for fission reactor calculations have to be combined with high-energy transport codes and data libraries developed for high and medium -energy physics and accelerator technology. Moreover burnup calculations require additional codes simulating time evolution of ADS. Section IX describes in details different approaches to simulations of neutron and proton interactions at energies over 20 MeV. Fig. 1 presents a typical code system for ADS simulation consisting of three main components (this figure exemplifies codes used specifically at FZK):

- Calculation of the neutron source with high energy transport codes like LAHET, different versions of HETC or FLUKA [Nead94]
- Calculation of the steady state reactor with deterministic or Monte Carlo transport codes. In IABAT project different codes were used:
  - Deterministic codes
    - TWODANT [Alco90], D3E [Steh91], ERANOS system [Dori93], MICROX
  - Monte-Carlo codes:
    - MCNP [Brie97], KENO-V
- Burnup/depletion calculations like ORIGEN [Bell73], KORIGEN [Fisc83], KARBUS, ERANOS, SCALE V and CITATION [Fowl70]

Another approach has been adopted by the group from KTH. After preliminary system studies based on the similar code-systems as those developed at FZK, namely coupling of Monte-Carlo calculations with ORIGEN-burnup code (or ORIGEN-like), a new Monte Carlo Burnup code combining steady state and burnup calculations in one single code (see Chapter 2.2). An advantage has been also taken from a development of MCNPX-code at Los Alamos National Laboratory [Hugh97]. MCNPX integrates high-energy particle transport code with a steady state Monte-Carlo transport calculations, i.e. integrates the LAHET code with MCNP [Prae89]. FZK and KTH became "beta-testers" of this code and contributed to its preliminary validation.

This section describes work devoted in the larger extent to code development and gives an idea of how high-energy transport calculations may be merged with standard reactor-like calculations. Minor code adaptations and couplings are briefly described briefly in other chapters, if relevant for understanding of the simulation methodology.

1. Coupling of High-Energy, Steady-State and Burn-up Modules

In connection with the IABAT ADS investigations, a lot of efforts were put into the code development. These tasks were mainly concentrated at FZK, Karlsruhe and KTH, Stockholm.

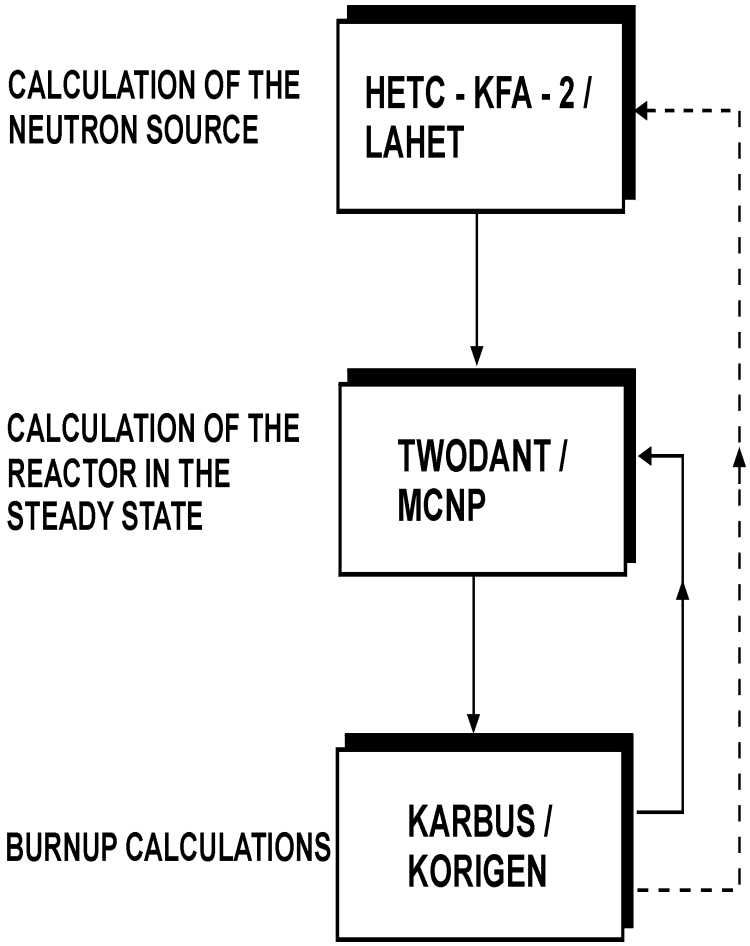

Figure 1. Simplified flowchart for a complete ADS calculation (an example of codes used at FZK).

1.1 High Energy Spallation Calculations

The investigations started with the implementation and qualification of the HETC and MORSE modules from the HERMES [Clot88] code system from the Jülich research center. The MORSE module was soon replaced by the more modern MCNP [Brie97] code. Later on, the LAHET code system LCS from Los Alamos, being an improved coupling of LAHET and MCNP4B was adopted and tested. In Figs 2 and 3 some early results of proton source investigations are given. Fig. 2 shows the distribution of spallation neutrons in an iron cylinder from the irradiation of a pencil beam source of protons with 1000 MeV energy. We may observe that for this beam type a concentrated forward-directed neutron distribution occurs. In Fig 3 the spatial fission rate distributions in a subcritical system with Th/^{233}U fuel is shown for three axial positions of the hitting point of a beam with proton energy 1500 MeV. We may observe that an optimal position between core boundary and mid-plane can be found to obtain symmetric power distributions around the core mid-plane.

All codes mentioned before are based on Monte Carlo simulations, both in the energy region for spallation and in the lower energy region for neutron transport.

1.2 Transport Calculations

In IABAT project, particularly at FZK a strong effort was devoted to the qualification of the discrete ordinate code TWODANT [Alco90] for the transport calculations below a cutoff energy of 10 to 50 MeV, in order to save significant amounts of computing times for simplified geometrical models. In Fig. 4 a comparison of TWODANT and MCNP results is shown for the radial power density distributions in two axial positions of the IAEA ADS benchmark (see also below). The TWODANT results were obtained on an IBM RS6000 workstation in about two hours of computing time, whereas the MCNP code needed several days on the same workstation. Obviously, for simplified geometrical models it is advantageous to apply deterministic codes. A number of design investigations have been carried out with multigroup diffusion calculations (see below).

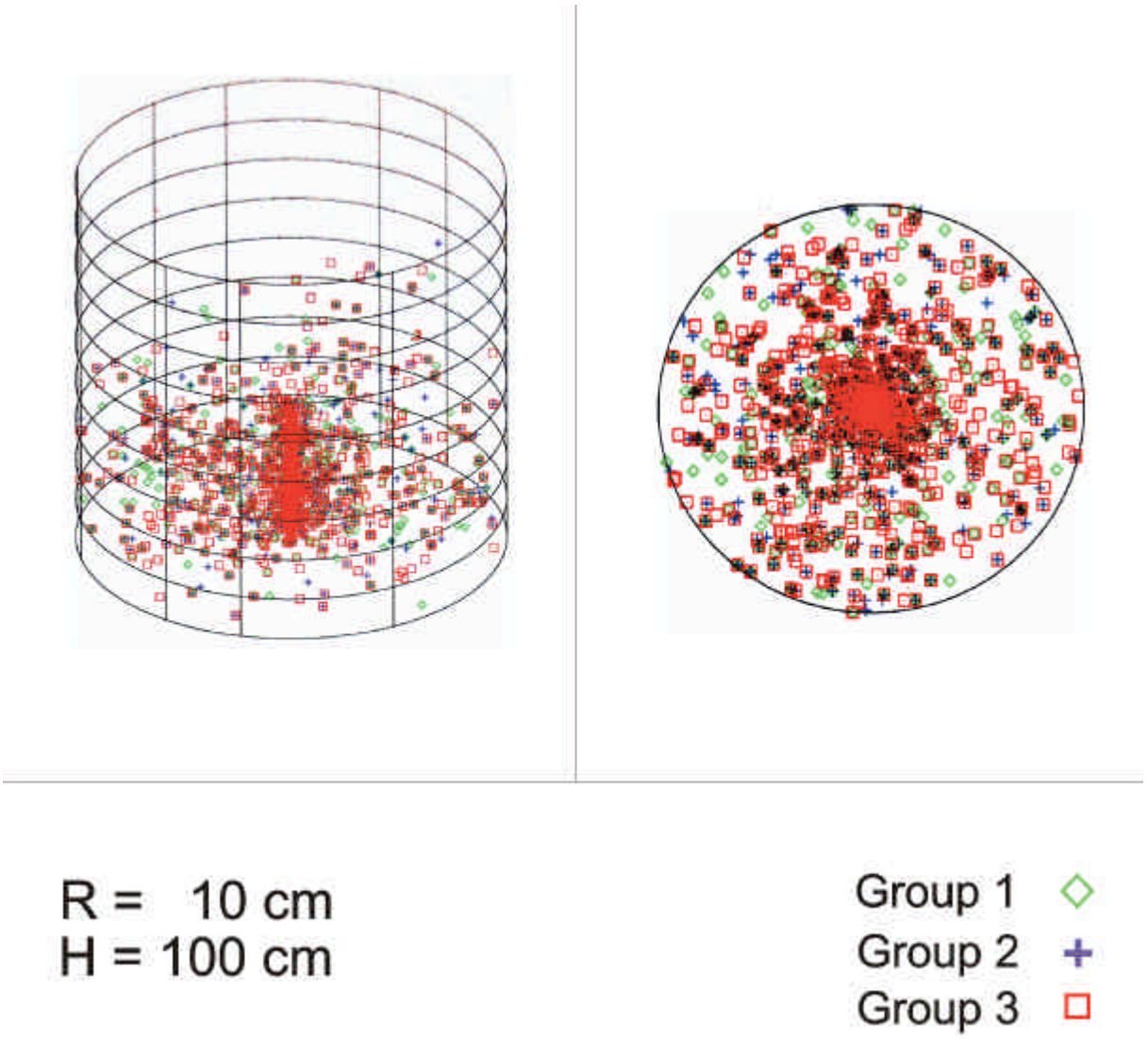

Figure 2. Neutron distribution in an iron cylinder irradiated with 1000 MeV protons.

1.3 Depletion Calculations

A coupling of depletion calculations of the KAPROS/KARBUS [Broe92] code system, developed for critical fast, epithermal and thermal reactors, with the codes HETC/LAHET and MCNP/ TWODANT was implemented and validated.

The KAPROS/KARBUS code system has been developed at FZK since many years. KAPROS [Bach75] is a very flexible fully modular system consisting of a controller program and a large number of independent application modules. The system has been developed on an IBM mainframe computer. The first versions utilized the specific features of the computer environment at FZK with as a consequence that transferring to other computer environments was very problematic. In the past 10 years a portable version for workstations with UNIX operating systems has been redesigned and realized. The first applications were related to fast breeder reactors. In connection with investigations for tight light water reactors the treatment of upscattering in the thermal energy region and of the resonance absorption in the epithermal

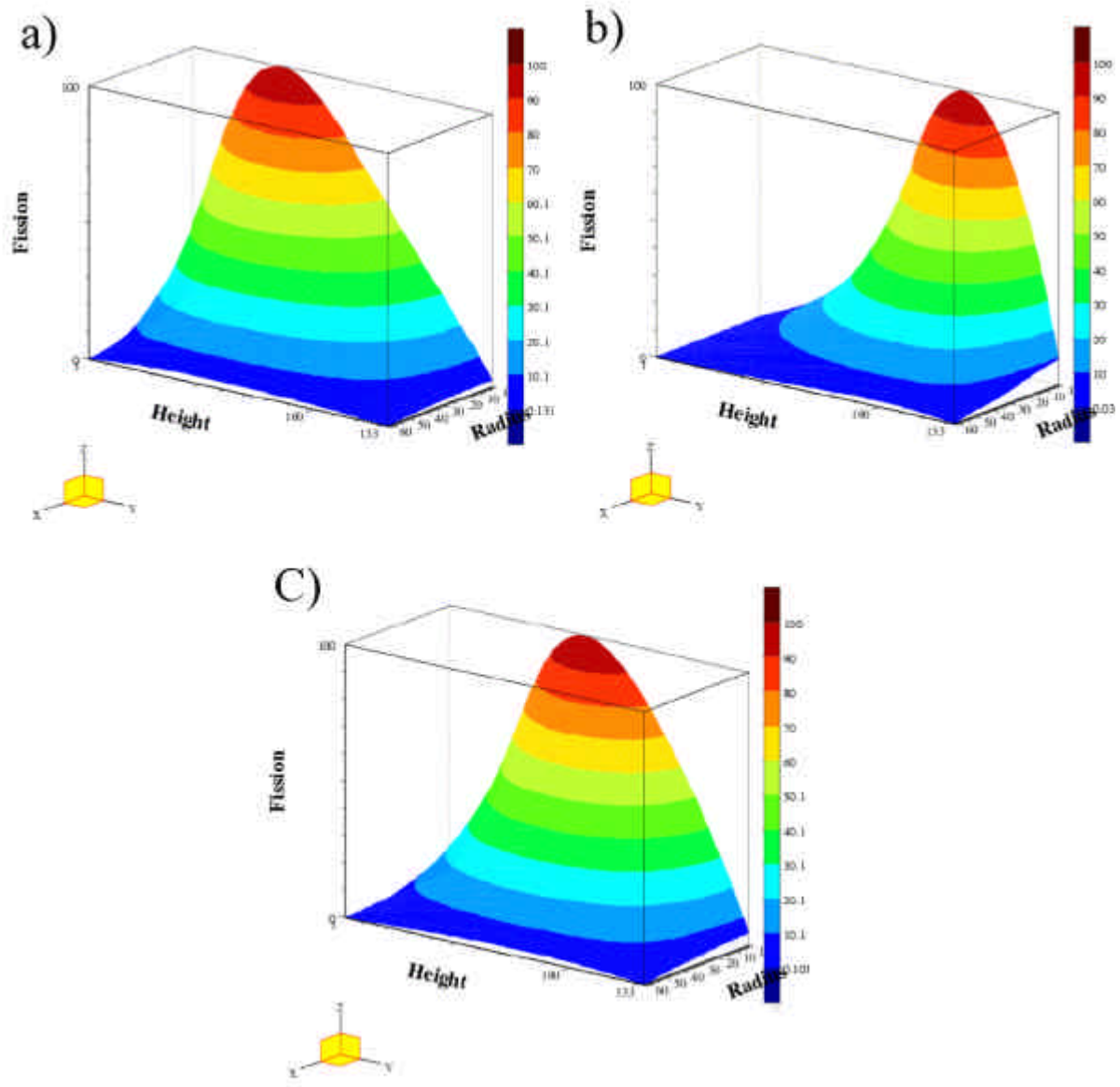

Figure 3. Fission rate distributions for three impact points of a 1500 MeV proton beam. Proton hits the target a) at the bottom of the core; b) at the core midplane; c) 30 cm above the core.

region has been significantly improved [Broe92]. For fuel cycle studies a special module KARBUS was developed. The main tasks of KARBUS are:

- preparation and carrying out of one- to three-dimensional reactor calculations,
- the best estimate preparation of zone-dependent one-group cross sections for use in the depletion module BURNUP.

The module BURNUP is a KAPROS implementation of the program KORIGEN [Fisc83], the well-known FZK depletion code developed from the ORIGEN [Bell73] code.

1.4 Coupling of the Calculation Steps

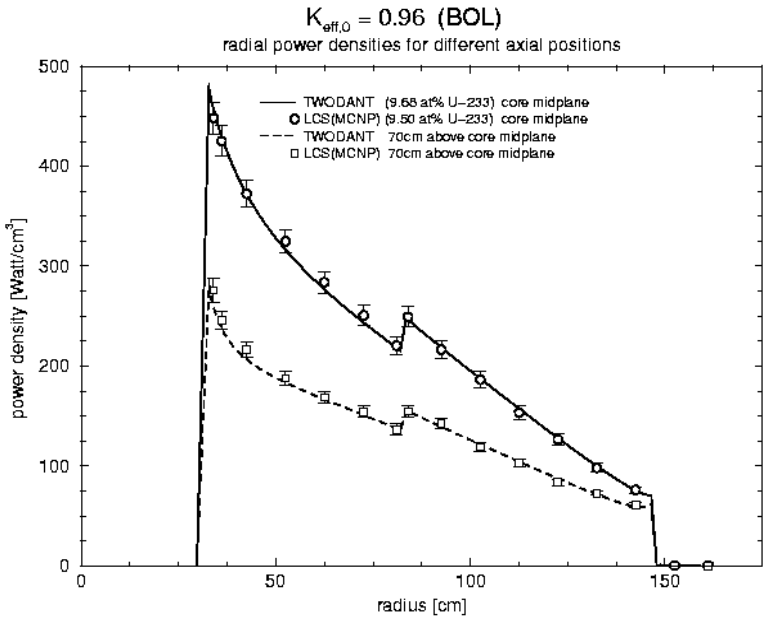

Figure 4. Comparison of radial power density distributions for the IAEA benchmark from TWODANT and MCNP calculations.

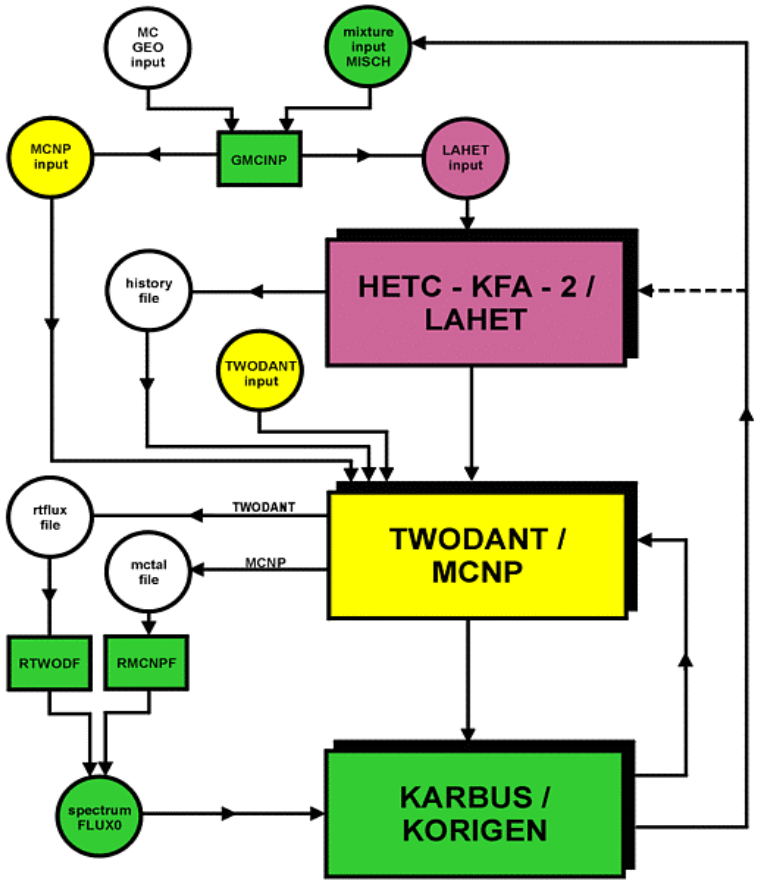

Figure 5. A detailed flowchart for a complete ADS calculation at FZK.

Figure 5 shows a more detailed overview of the calculational scheme used at FZK. This somewhat complicated scheme may be radically simplified using on one side MCNPX, which integrates high energy transport calculation with a steady state Monte Carlo code, or Monte Carlo Burn-up code MCB (described in the next section), integrating steady-state with burn- up calculations. Our ambition is to follow up IABAT tasks and to integrate high-energy – steady state and burnup calculations into one single Monte Carlo code.

However, it should be mentioned that the code system KAPROS presented on Fig. 5 in conjunction with the powerful script languages of the UNIX operating systems is already a very flexible tool for the coupling of advanced computer codes, necessary for ADS simulations.

2. Development of Monte-Carlo Continuous Energy Burnup (MCB) Code

MCB is a general purpose Monte Carlo Continuous Energy

Burnup Code that can be used for calculation of nuclide densities evolution with burnup or decay, including eigenvalue calculations of critical and subcritical systems and neutron transport calculation together with all necessary reaction rates and energy deposition. The code has emerged as a integration of well known code MCNP, version 4B, which is used for neutron transport calculation, and a novel Transmutation Trajectory Analysis code (TTA), which serves for density evolution calculation, including formation and analysis of transmutation chain. The codes were integrated on the level of the source code of MCNP by preparation of so called patch for preprocessor source file of MCNP. As a result, MCB is compatible with MCNP and the whole and complete burnup calculation can be done in a one single run that requires preparation of one input file, which can be slightly enlarged input of MCNP. A flow diagram of the MCB code is presented on Fig. 6.

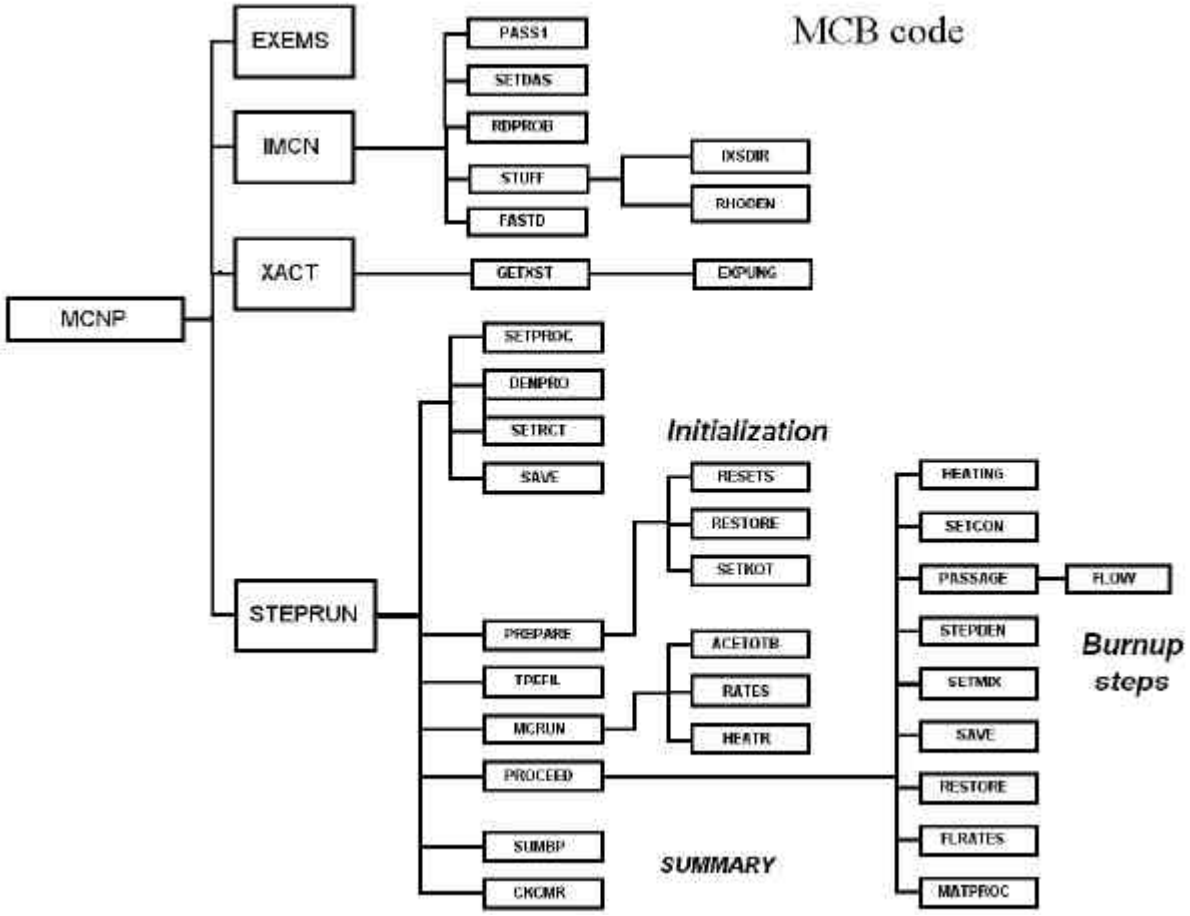

Figure 6. Flow diagram of the MCB code.

2.1 Code Features

System evolution with time of burnup is calculated according to system power or source strength in the user specified periods. The code supports calculations both, in subcritical system with external neutron source, and in critical systems where the neutron flux is adjusted to the required power.

The code is prepared to employ numerous cross-section libraries and data sets to adequately calculate reaction rates and nuclide formation probabilities. It includes the possibility of separate treatment of cross sections for different burnable zones to account for

thermal effects, employment of energy dependent distribution of fission product formation, energy dependent formation of isomer nuclides.

Nuclide decay data is taken from two files. The first one ***TOI.LIB*** is prepared on the basis of Table of Isotopes and describes decay schemes for over 2000 nuclides. The second one ***XS.LIB*** is a decay data file used for ORIGEN code system and it supports energy-integrated ratios of nuclide formation in excited state.

Reaction rates are calculated exclusively by continuous energy method with using transport cross-section libraries or dosimetry cross-section library. The user can specify libraries explicitly or by using default option scheme for library definition that is an extension of the scheme used in MCNP. It allows the user to assign different library to different cells for the same nuclide if needed.

Formation of nuclides in excited states due to neutron capture or (n,2n) reactions is supported by ***XS.LIB*** file while energy dependent isomer formation ratios can be taken from file ***ISB.LIB.***

Energy-dependent fission product yield is calculated automatically according to the specification and the data in the ***FY.LIB*** that contains energy distributions of fission products for every fissionable nuclide.

Heating is calculated automatically during burnup calculations if data with heating cross section are present in the library. In other case, or if required, the user can use an option to calculate heating from fission only. In the current version only heating released in neutron transport are accounted for but extension to photon heating should be expected in the version 1.0.

Time evolution of nuclide densities is calculated with the complete set of linear transmutation chains that is prepared for every zone and time step so it is adjusted to evolving transmutation conditions. The code uses the Bateman method to solve, prepared-on-line and complete, set of linear chains that noticeably contribute to nuclide formation.

Dose of burnable material is calculated on the basis of EURATOM Directive.

The program calculates neutron multiplication of the external source and the fission source as well as neutron multiplication factors. They are used to calculate source importance defined in two ways. The first one is for fission generation and second one is for neutron multiplication. Time evolution of those parameters together with neutron source strength, energy deposition per source neutron and potential dose and activity of material is printed out.

A self-adjusting step routine is available when the user defines allowed variation of k_{eff} or heating. Another control parameter can be used to switch mode of calculation from external source to fission source (k-code) when the current value of k_{eff} reaches specified level.

The program calculates transmutation transitions from nuclide to nuclide and prints them out to one of the output files. Transmutation chains that are formed by the code can also be printed for interesting nuclides.

2.2 Cross-Section Libraries and Data Files

In order to provide accurate transmutation calculations the code must be supported with data files, which allow for complete simulation of neutron transport and nuclide formation. The bulk of data consist of numerous cross-section libraries for calculation of reaction rates

and transport cross-section libraries. The scope of neutron libraries distributed with the MCNP package is limited and lacks libraries for many nuclides, so it is recommended to use an enlarged set of cross sections. Another problem considers the number of available reactions. Since the standard transport library lacks of some reactions, it is recommended to supplement vaster dosimetry libraries to complete the reaction list. In order to satisfy above requirement the code employs simultaneously, transport and dosimetry libraries for one material. The standard XSDIR file is used.

The second part of data files concerns nuclide formation process and radioactive nuclide properties. The decay schemes of over 2400 nuclides, including metastable, were prepared on the basis "The Table of Isotopes 8E" while the dose data of 738 nuclides were prepared on the basis of Euratom Council Directive 96/29/EURATOM. The data file TOI.LIB contains the data describing decay constants with branching ratios, and the values of committed effective dose per unit intake.

Since the formation process of isomer nuclides is not well treated neither in existing MCNP libraries nor in "Table of Isotopes" we need to get necessary data from other sources. The first one is the one-group cross-section library of ORIGEN, which serves for calculation of isomer formation ratio due to decay, reaction (n,2n) or neutron capture. It is attached to the program as XS.LIB file.

Since the ORIGEN file supports only average energy data, for some important cases we have prepared energy-dependent isomer formation ratios making ISB.LIB file. The currently available file contains formation ratios of ^{242m}Am and ^{244m}Am based on Mann & Schenter model [Mann77].

Incident energy and nuclide dependent fission product yields were prepared based on Wahl [Wahl85] model. Produced file FY.LIB contains fission product yields functions for 36 heavy nuclides.

2.3 Input and Output Files

MCB input file can be made from standard MCNP input file by addition of a few cards that will define transmutation system. However in order to describe some complex cases optional material definitions have been introduced.

2.4 Transmutation System Definition

The MCB code can work as the standard MCNP code unless the burnup option is switched on. The card BURN that contains the list of burnable material does the switch. In the burnup mode, the code takes control over user specification of the transmutation condition and gives warning messages in case of user error of specification. Obviously, the program does not perform full checkup of physical consistency of the system definition but checks consistency with program requirements to complete calculations. Without the BURN card the MCNP mode is used and all other burnup control cards are simply ignored but the new option of material definition remains valid. The user can use this feature in case of run trouble to check out if problem lays in system definition for MCNP or for burnup. In order to properly set up the problem the user need to introduce specification of:

- burnable materials,
- libraries required for reaction rates calculations,

- duration of transmutation time periods,
- system normalization with external neutron source strength or thermal power.

2.5 Material and Library Definition

MCB requires an extended number of materials handling which results in the necessity of improving (simplification) material specification from the user point of view as well as material differentiation in order to avoid unnecessary data processing. Since the calculation process is much more complex than in case of pure MCNP the material and libraries should be differentiated. Different treatment is required for abundant materials that influence the neutron transport process and for low abundant material. Moreover, the case is fluent when with transmutation some nuclides disappear while others emerge. Therefore, for the burnup case, libraries for all possibly emerging nuclides must be specified. The material and library definition can be done for such a case using extended material definition option design for MCB, i.e. a combination of M, MB, MR, and MIX cards

Following three categories of material are defined:

i) Transport material - is used in particle transport simulations and also in remaining calculations. It is specified on M card and obviously has its density and assigned library. If isotopes produced in a transmutation chain have no transport cross-sections available, they are treated as burnup materials or a warning is issued that no cross-section data exist.

ii) Burnup material - is not used in transport calculation unless its density accumulate to a certain level, at which its cross section contribution to the total cross section of the cell materials reaches a discrimination level. In such a case the material is ranked-up to the transport material. It is specified on MB card and assigned library is used for calculations of reaction rates.

iii) Residual material - has no defined density and is used only for transmutation transition calculations, so it cannot diminish from the system due to burnup. It does not contribute to the buildup of other nuclides unless it has accumulated as a daughter nuclide due to the burnup. Residual material can be used also for specification of cross-section library for zones when the nuclide is absent at BOL.

The mixing of several materials defined by cards can be done with a MIX option. The mixing option can simplify system definition also for MCNP since a material can be made of its component material, and not only directly of nuclides.

The MIX option can be also used for cross-section library hierarchy definition. This option was prepared for cases where cross-section libraries of nuclides used in the system have different id-numbers and it would be tiresome to specify them all directly. Hierarchy list works in a natural way - the cross section table with highest position in the list will be loaded. Lack of hierarchy list, even for one entry, results in loading only those cross-section libraries that are directly or by default specified for transport. It means that nuclides absent at BOL, but emerging as transmutation products, will have no cross sections loaded. This can produce incorrect results.

An appropriate system definition requires that for every burnable material the library hierarchy list should be formed. There are possible cases when the user does not accept some nuclide cross-section and needs to replace this by other library cross sections. In such case the required nuclide library should be specify directly in one of material cards for burnable material.

The library hierarchy list is also required when the user needs to use both transport library and dosimetry library in order to support full available list of reaction. Since one nuclide cannot appear twice in the material list, it is the only way of using both data libraries.

Other problem appears with metastable nuclides since in case of MCNP libraries there is no distinction between isomers. It is solved by making a new convention of isotope identification, so called ZAID number definition. When a ZAID number represents mass number greater than 300 it is treated as isomer excited state of nuclide. This form of ZAID should be made at the cross section preparation process and XSDIR file should contain it. However since in old libraries ^{242m}Am is represented like a ground state nuclide usage of old libraries would be not proper. For such cases the user can use special option (GTMET) assigning ground state libraries also to the metastable isomer. Additionally, the user can use substitutes of ZAID that is ZA replaced by nuclide or element chemical symbols, in order to simplify material recognition. Currently substitutes of the following form are legitimate:

- Pu239.55c for 94239.55c
- Pb.55c for 82000.55c
- U235 for 92235
- Pb for 82000
- Am242m for 95342 etc.

2.6 Modes of Calculations

Burnup calculations can be done either in a **k-code** mode or a **source mode**. This means that reaction rates are calculated in one of the modes. Also it is possible that the system switches between two modes depending on current value of k_{eff}. In both cases if user wishes to control level of k_{eff} the k-code mode must be used for this purpose. There are few possibilities:

- Lack of the KCODE card will result in omitting k_{eff} evaluation and program will make burnup only in transport mode and can accomplish calculations providing system remains subcritical.
- If the user requires using only k-code then a switch parameter should be put to 0.0. In such a case system will never switch to source mode and will not be able to calculate normalize flux and consequently power of the simulated system must be given explicitly
- Switch parameter controls the choice of calculational mode between **k-code** and **source-mode**
- For time steps with thermal power and source strength set to zero the burnup is calculated as a natural decay and no reaction rates are need to be calculated.

2.7 Benchmarking of the Code

The first extensive tests of MCB code were performed in the frame of NEA/OECD benchmark [Chan99]. Fig. 7 presents a comparison of results obtained with different burnup code systems and different data library sets for a reference ADS system. MCB results are clearly very close to the average. See [Chan99] for more details,

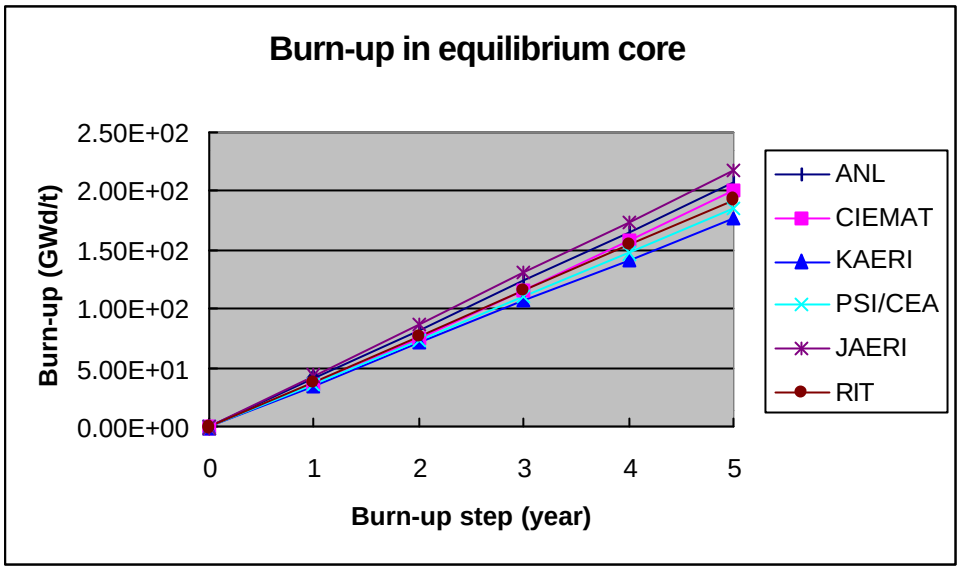

Figure 7. *NEA/OECD benchmarking of the MCB-code against other burn-up code systems. The brown line with a RIT label represents the results of MCB calculations [Chan99].*

IV. SYSTEM AND FUEL CYCLE STUDIES

Several reactor technologies have been considered for Accelerator Driven Systems. In the IABAT project we addressed a set of subcritical cores featuring distinctive basic characteristics. These main features are the neutron spectrum, the type of fuel matrix -solid or liquid- and in-core behaviour of uranium and thorium based fuels. The studies were focused on neutronics and a transmutation potential, they did not try to address important questions concerning fuel and coolant technologies, partitioning and separation chemistry, neither did address economical assessment.

Four systems have been studied in details and are described in details in corresponding sections of this report – see Fig. 1:

- Liquid lead and lead/bismuth Cooled Fast Systems with Solid Fuel – Energy Amplifier (AE) [Rubb95] like systems
- Liquid lead Thermal Neutron System with Dispersed Fuel (so called Jülicher Transmuter)
- Molten Salt Systems: Thermal (so-called superthermal) Molten Salt System (ATW) and Fast Molten Salt System, called JMS –JAERI Molten Salt.

Different objectives were studied for those ADS:

- Plutonium and minor actinide burning (incineration) for uranium-plutonium and thorium-uranium fuel cycles
- Minor actinide incinerations for these fuel cycles
- Energy production based on Th-^{233}U fuel cycle

The first step of the investigations for most of research groups in the IABAT-project was the

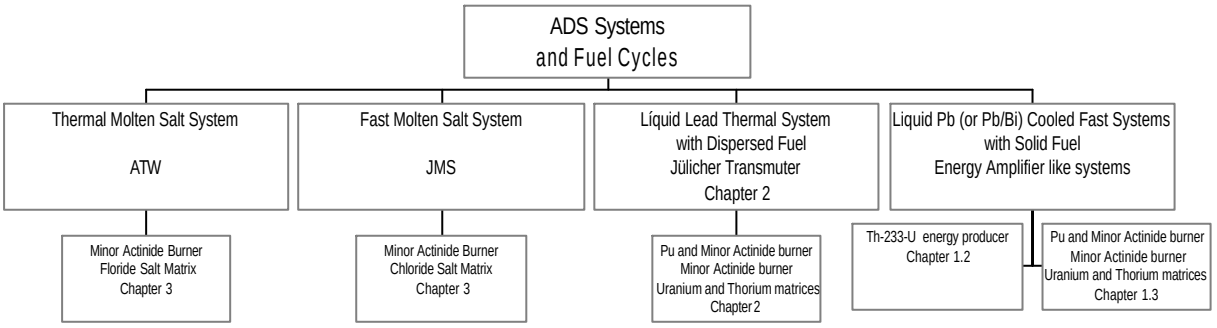

Figure 1. Accelerator-Driven Systems studied in IABAT-project.

implementation and qualification of suitable calculation methods and codes, especially for the description of the spallation processes and for the coupling of the external neutron source with the transport calculations for the subcritical reactor system. For the qualification of the calculation tools participation to several international benchmark investigations was very helpful. The applied high-energy codes could be validated by the participation to the NEA international code comparison of intermediate energy nuclear data [Filg95]. For the validation of the burn-up and of the coupling of the spallation source with the subcritical reactor system, the IAEA ADS neutronic benchmark for lead cooled thorium/^{233}U fuel was a successful undertaking [Sless97] resulting in deeper understanding of subcritical systems and in some novel ideas of mitigating power density problems for ADS.

1. Fast Neutron Liquid Metal Cooled Systems

After some preliminary studies of the capabilities of ADS for the incineration of plutonium, minor actinides and long lived fission products [Broe96], the participation to the IAEA ADS benchmark lead to a number of program developments and resulted in insights of large interest. Especially the power distribution towards the central neutron source proved to be unsatisfactory with radial form factors varying from about 2.5 to nearly 4 (see below). In order to improve these unacceptable characteristics, FZK proposed and investigated an ADS with up to six distributed neutron sources. On the basis of this multi source design a number of more detailed investigations related to the incineration of plutonium and minor actinides have been performed.

1.1 Description of Applied Codes and Models

For the IAEA ADS benchmark investigations a two-dimensional cylindrical model was defined. Comparisons of Monte Carlo calculations with MCNP and deterministic calculations with TWODANT confirmed that for this simplified geometrical model the results of these codes are in satisfactory agreement. For this reason the required depletion calculations were carried out with the much faster deterministic transport code TWODANT. The investigations of the multi-source systems were performed with the diffusion code D3E [Steh91] with triangular geometry, developed at FZK. Some comparison calculations with the widely used CITATION [Fowl70] code showed good agreement. For the depletion calculations two different options of the KARBUS system have been applied:

- Direct depletion calculations with the module BURNUP.
- After each time-step and in each reactor zone mean one-group cross sections are prepared on the basis of mean 69 group fluxes and shielded 69 group cross sections. These one-group cross sections have been applied in the module BURNUP, derived from the (K)ORIGEN code [Fisc83].
- Application of pre-calculated burn-up-dependent macroscopic cross sections with the core simulation program ARCOSI [Broe92].

For each fuel composition a burn-up calculation with sufficiently detailed time-steps and with burn-up up to about 150 MWd/THM is performed on the basis of 69 group cross sections. The 69 group burn-up dependent cross sections are collapsed to 4 group data, using weighting spectra based on fundamental mode calculations. This procedure has been developed and validated for tight light water reactor studies [Broe92] and applies the ^{10}B content of the coolant as an additional parameter. The resulting 4 group macroscopic cross sections are stored on a special library and may be utilized by the core-simulator code ARCOSI. For the fast spectrum ADS applications with thorium and minor actinide fuel the procedure of the 4-group library generation had to be modified. It was found, that for fuels containing isotopes with relatively short decay times like ^{233}Pa (27 days) and ^{242}Cm (162.8 days) the reactivity of the system is sensitive to the flux level in the fuel. Instead of the ^{10}B parameterisation, the power density in the fuel is varied for the generation of the 4 group libraries.

1.2 IAEA ADS Benchmark (Th-^{233}U based Energy Amplifier)

In 1996 the IAEA initiated an international ADS benchmark based on a proposal of Rubbia et al. [Rubb95] for an energy amplifier with a power of 1500 MW_{th} and based on Th-^{233}U fuel in hexagonal fuel assemblies and with lead coolant. Fig. 2 presents a layout of the (R-Z) model for the IAEA ADS benchmark core calculations. Calculations of the neutron-flux density spectra and of reaction rates (total fission reaction rate, fission reaction rates for individual isotopes) have been carried out by IABAT-participants [Broe97, Tuce97] with the transport code TWODANT in S4/P1 approximation. For the calculations multigroup cross sections of a recent 69-energy group constant library have been used (G69P1V03). The nuclear database of most of these group constants is KEDAK-IV [Goel84], some of the group constants have been newly calculated from more recent libraries: e.g. ^{233}U from ENDF/B-6.4 and ^{232}Th from the JEF-2.2 library. In the calculations the temperature of the fuel was 1200K, the temperature of lead and steel was 900K. The neutron source provided with the benchmark data has been transformed to the 69 energy group structure of our group constant set in such a way that for each energy group the number of neutrons per eV was conserved. Table I shows the initial ^{233}U enrichments for the required different k_{eff}-values.

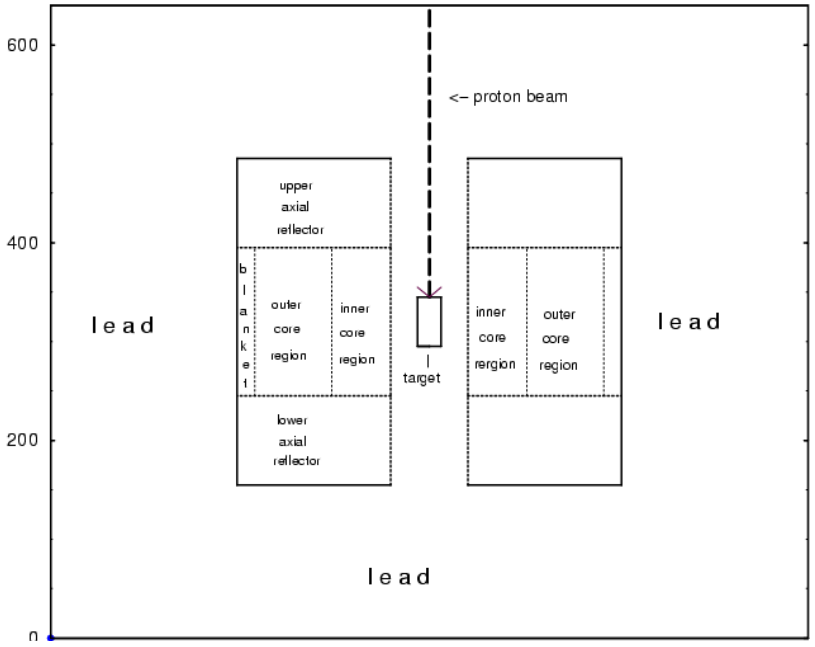

Figure 2. Cylindrical model for the ADS target and spallation product investigations. IAEA-ADS benchmark model [Sles97].

1.2.1 Burnup Behaviour

An important objective of the IAEA ADS benchmark was the determination of the time-dependence of the reactivity of the sub-critical reactor system. In the benchmark specifications the power-level and the time-steps are specified in detail. The cylindrical geometry model-specification contains 5 zones: lead, inner core, outer core, radial reflector and axial reflector. For the burn-up calculations each fuel zone was subdivided into 3 radial and 3 axial sub-zones, leading to a TWODANT (R-Z)-model with 22 zones. During the analysis of the results it pointed out that some other benchmark solutions were based on burn-up

Table I. Initial enrichments of ^{233}U for the different k_{eff} values of the IAEA ADS benchmark.

Enrichment = ratio of atom number densities $^{233}U/(^{233}U + ^{232}Th)$

k_{eff}(BOL)	Enrichment (%)
0.98	10.00
0.96	9.68
0.94	9.36

calculations without sub-division of the fuel zones. For that reason a consistent calculation without sub-division was carried out, leading to a TWODANT (R-Z)-model with 7 zones. In Fig. 3 results for the time-dependence of the reactivity is shown. These results are in good agreement with solutions of other participants. We may observe that for the case k_{eff}=0.96 the influence of the subdivision of the fuel zones is remarkable.

1.2.2 Power Distributions

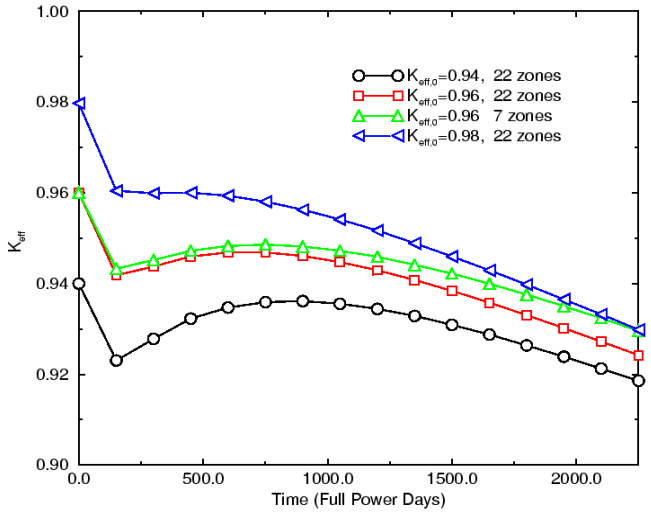

Figure 3. Reactivity of the IAEA ADS benchmark as a function of full power days.

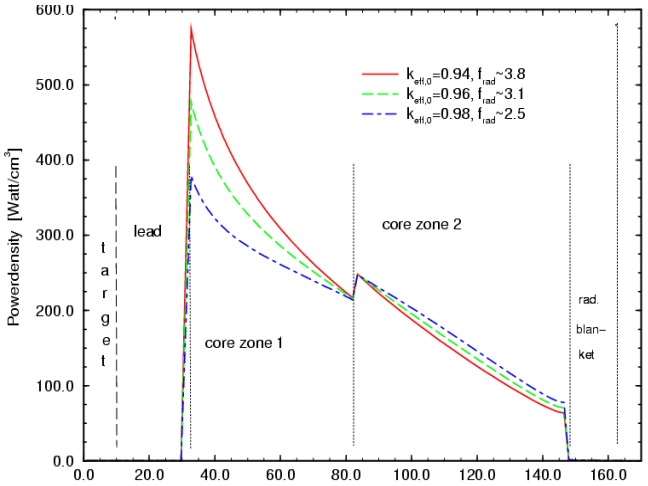

Figure 4. Comparison of radial power density distributions for the IAEA benchmark for three initial values of k_{eff}.

The technical feasibility of an ADS is strongly influenced by the power density distribution in the system. So, another important issue of the IAEA ADS benchmark investigation was the comparison of the radial power distributions for the different sub-criticality levels. In general the agreement between the solutions of the participants was good. In Fig. 4 the radial power density distribution in the mid-plane of the reactor system is shown. Also the radial form-factors, defined as maximum-to-mean power density ratio, are given. We may observe that the form-factor strongly increases with decreasing reactivity of the system. For a sub-critical system the flux–distribution towards the neutron source tends to an exponential shape. For a central neutron source this is in contrast to the smooth shape to the centre of a critical system. The values obtained in the benchmark configuration are not acceptable in large power systems. As a consequence of these observations a considerable effort was devoted to improve the power-density distribution. Although the typical solution for fast critical reactors to increase the fissile enrichment in two to three radial zones also leads to improvements in an ADS,

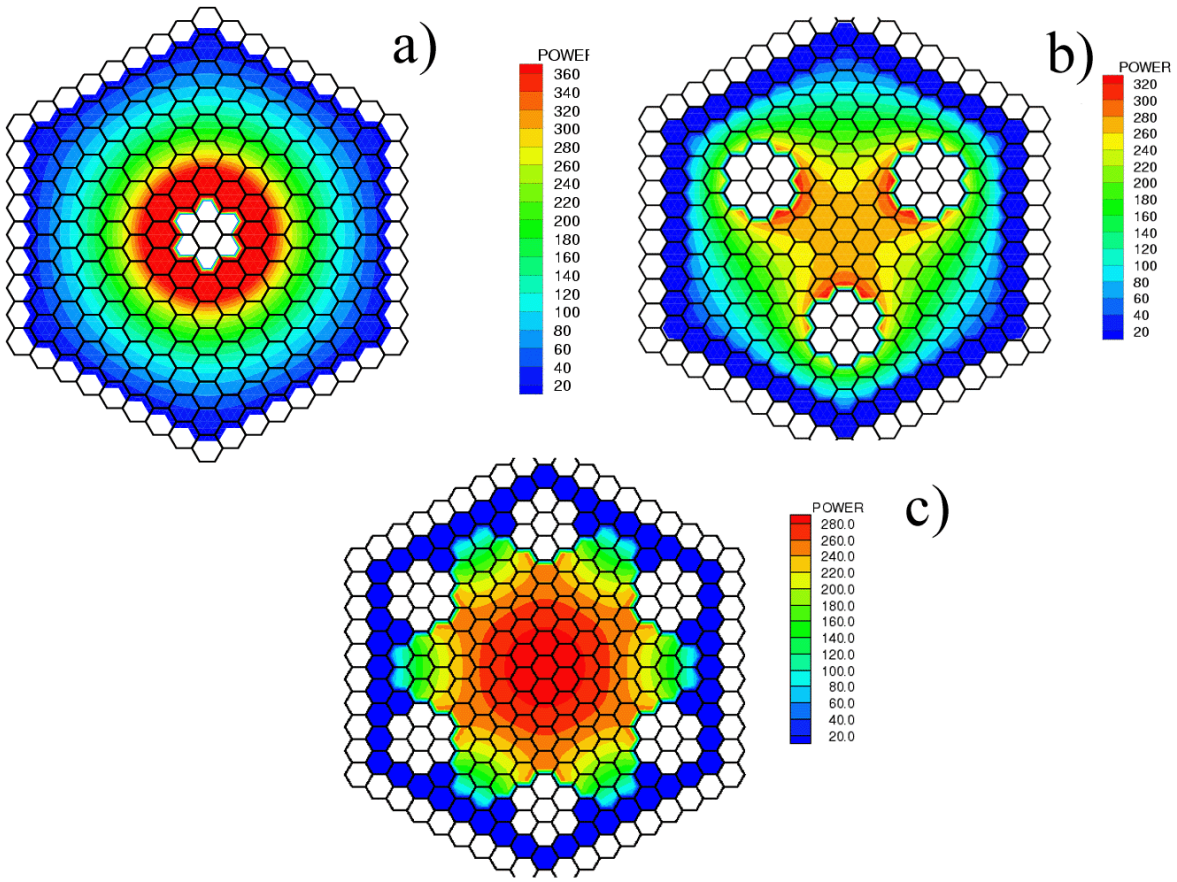

Figure 5. Power density distribution in an ADS with a) one spallation target; b) three spallation targets and c) six spallation targets.

a better solution seems to be to apply more than one spallation source in the system. Exploratory investigations were carried with two to six non-central spallation sources. In the Fig. 5 examples of power density distributions in an ADS with Th/^{233}U fuel with one, three and six neutron sources are shown. In the next section more detailed information is given for multi-source systems for the incineration of plutonium and minor actinides.

1.3 Plutonium and Minor Actinide Burner

One of the main objectives of the ADS investigations was to analyze its characteristics for closing the back-end of the nuclear fuel cycle. An important parameter in these studies is the possible incineration rate of plutonium, minor actinides and long-lived fission products. In the next sections two cases for different fuels are presented. Both cases are based on discharged fuel from pressurized water reactors (PWR) with a mean burn-up of 50.000 MWd/THM. Seven years cooling time and three years fabrication time are assumed for the ex-core times. Other assumptions were:

- All heavy metal fuel isotopes are kept together. The required criticality of about 0.98 has been obtained by mixing with thorium.
- Plutonium and all minor actinides together are kept in two separate stocks. In this case no other fuel is added. The criticality of about 0.98 is obtained by mixing with Zirconium.

1.3.1 Choice of the Number of Spallation Targets

Obviously, power density distributions in accelerator driven sub-critical systems may be improved if instead of one central target several targets are distributed over the core. It is also clear that an increased number of proton sources makes the system technically more compli-cated. In the first investigation a number of six beams quite near to the core boundary was chosen (see Fig. 5 c)). With this arrangement acceptable power factors could be obtained. However, for this system the leakage of spallation neutrons is considerable and the reactivity decreases significantly compared to a system with one central proton source. Therefore the sources were moved to the centre of the core and satisfactory power density distributions could be found with three proton beams (see Fig. 5 b). For this arrangement only a small influence of leakage increase may be observed. The more systematic investigations in reference [Daga99] confirm that the choice of three beams may be a good compromise concerning power density distributions and system complexity. ADS cores with three proton beams and two types of fuel as specified before have been investigated in some more detail.

1.3.2 Incineration in a Thorium Based System

In a first series of investigations the incineration of a mixture of not-separated heavy metals from spent LWR-fuel with 50.000 MWd/THM mean discharge burn-up was considered. The desired sub-criticality was obtained by mixing this fuel with thorium. In Table II the weights and isotopic compositions at begin of life are given.

Table II. Fuel inventory specifications of an ADS core with Th/Pu-MA fuel; (weights in kg)

Material	**Core**	**Reflector**	**Total**
Thorium	12106.0	4735.8	16841.8
Neptunium	140.2	0	140.2
Plutonium	2343.0	0	2343.0
Americium	78.2	0	78.2
Curium	21.8	0	21.8

Plutonium-vector (weight%)				
^{238}**Pu**	^{239}**Pu**	^{240}**Pu**	^{241}**Pu**	^{242}**Pu**
2.7	53.7	23.8	12.3	7.5

Americium-vector (weight%)	
^{241}**Am**	^{243}**Am**
65.3	34.7

Heavy metal from PWR discharged fuel with mean burnup 50.000 MWd/THM
7 yrs cooling, 3 yrs fabrication time

For this fuel burn-up data was prepared up till 140.000 MWd/THM. The reactor core was described by a full 3-D hexagonal geometry with 16 axial layers. Burn-up simulations with 1084 regions with the program ARCOSI were performed until in one region of the model the maximum burn-up of 140.000 MWd/THM is exceeded.

1.3.3 Incineration in Thorium- and Uranium-free Cores

In a further series of investigations the incineration of a mixture of separated stocks of plutonium and minor actinides from spent LWR-fuel with 50.000 MWd/THM mean discharge burn-up was considered. The desired sub-criticality was obtained by mixing these fuel components in a proper way and with about 60% zirconium as matrix

material. In Table III the weights and isotopic compositions of the fuel at begin of life are given. This fuel is very advanced and problems might arise for manufacturing and maintaining. The present results only give information on the characteristics from the neutronic point of view. For this fuel the same burn-up simulations with the program ARCOSI as in the preceding section were performed.

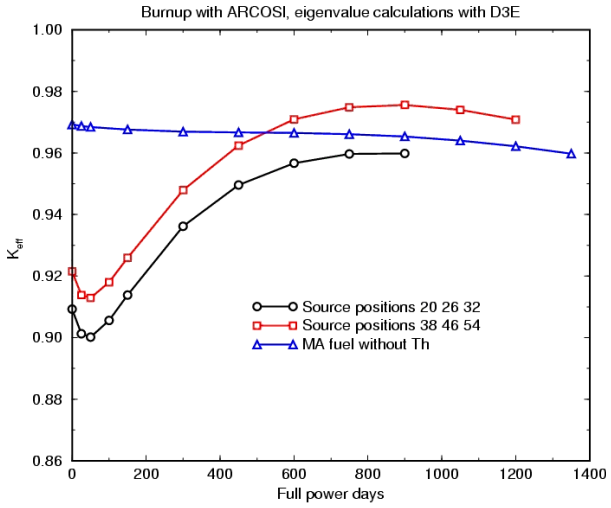

Figure 6. Time dependence of the ADS reactivity with different fuels.

1.4 Results.

In Fig. 6 the burn-up dependence of the reactivity of the systems of sections 1.3.2 and 1.3.3 is shown. For the Th/Pu-MA fuel two different arrangements of the proton sources are investigated, identified by the fuel assembly numbers (20,26,32) and (38,46,54). Obviously, the second case with proton sources somewhat more to the outer boundary of the core is more favourable: the reactivity is slightly higher and the upper limit of the fuel burn-up is reached later, indicating better power density distributions. The Th/Pu-MA results also show the strong influence of the build-up of ^{233}U from ^{232}Th captures with a reactivity increase of about 6% during burn-up. The typical reactivity

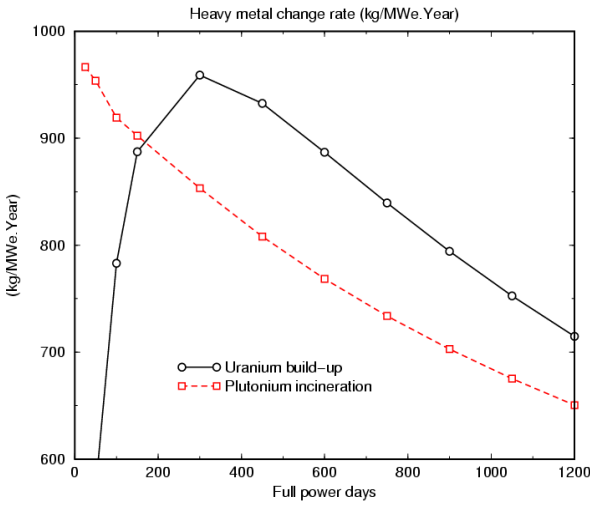

Figure 7. Uranium and plutonium buildup/incineration in a lead-cooled ADS with three proton beams.

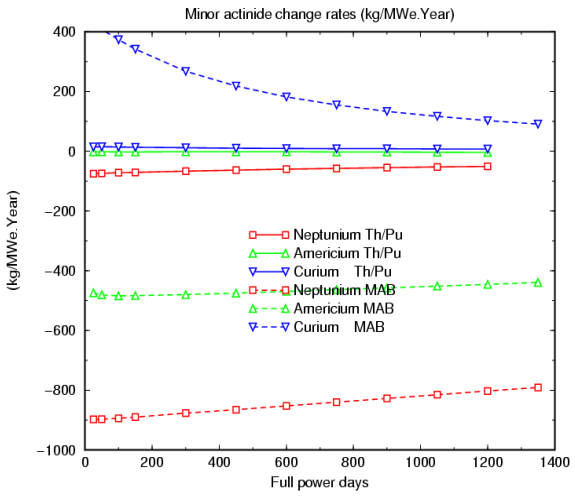

Figure 8. Concentration of minor Actinides in a lead-cooled ADS with 3 proton beams.

decrease due to the ^{233}Pa build-up during the first 50 to 100 days also may be observed. On the other hand, the Th-free fuel leads to a very flat reactivity behaviour. In Fig. 7 the change rates in (kg/MW$_{el}$×Year) of uranium and plutonium in the Th/Pu-MA system are shown. A load-factor 1 and a system-efficiency of 40% are assumed for the normalization to (MW$_{el}$ Year). It may be observed that in this design the uranium production exceeds the plutonium incineration. The change rates for minor actinides are given in Fig. 8 for both cases. The change rates for the minor actinides are small in the Th/Pu-MA system. In the second minor actinide burner system (MAB) the incineration rates of

americium and neptunium are much better. Curium is always produced (changes are always positive). In the MAB system a considerable amount of ^{238}Pu with half-life 87.7 years is produced.

Table III. Fuel Inventory ADS with TRU/Zr fuel

Material	**Core**	**Reflector**	**Total**
Thorium			
Neptunium	3002.4	0	3002.4
Plutonium	2636.4	0	2638.4
Americium	1675.4	0	1675.4
Curium	466.0	0	466.0
Plutonium-vector (weight%)			
^{238}Pu	**^{239}Pu**	**^{240}Pu**	**^{241}Pu**	**^{242}Pu**
2.7	53.7	23.8	12.3	7.5
Americium-vector (weight%)			
^{241}Am	**^{243}Am**		
65.3	34.7		
Heavy metal from PWR discharged fuel with mean burnup 50.000 MWd/THM. 7 yrs cooling, 3 yrs fabrication time			

2. TRU and Thorium Based Fluid Fuel ADS - Liquid Lead Thermal Neutron System with Dispersed Fuel

The section summarizes results of the studies of the „Jülicher“ Accelerator Driven Transmutation System (ADS). Calculations with pure TRU based fuel and with Th-TRU or Th-Pu based fuel have been performed. An unusual fuel option has been chosen - a liquid lead solution of the respective TRU or a dispersion of Pb containing (Pu + MA)O_2.

The calculations were performed in four steps. The first step was basic calculations to find k_{inf} for different fuel compositions and different geometries. In the second part the nuclear safety has been investigated concerning the sedimentation problem for liquid fuels with dispersed oxides. The third the possibility of a batch operation mode of the system has been assessed.

The last part of the neutronic calculations concludes the final fuel composition for a continuous refuelling and reprocessing mode.

2.1 Description of the “Jülicher Transmutation System“

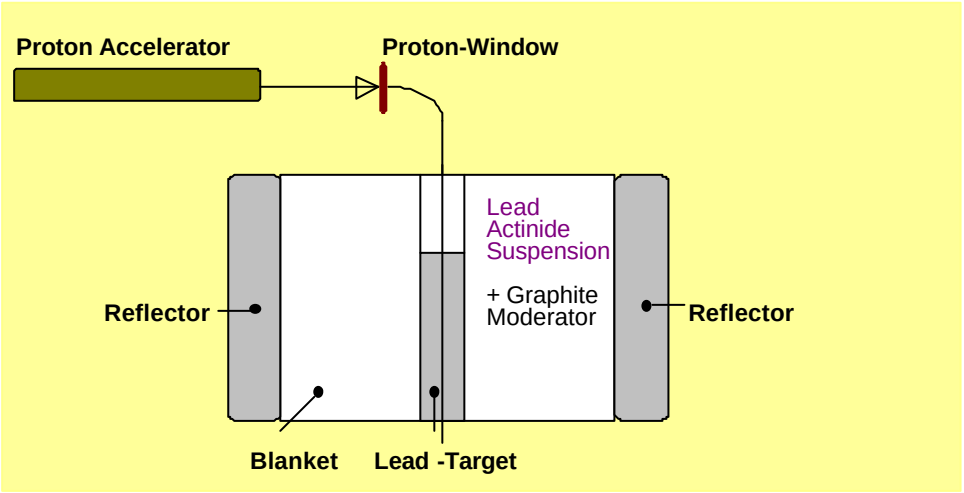

Figure 8. General layout of the Jülicher transmutation system.

The system is composed of three parts. A liquid lead target with a diameter of approx. 1m is placed in the centre. A graphite-moderated blanket with a diameter of approx. 4m, a height of 2.5m and a volume of 29.45 m^3 encloses the target. The graphite reflector with 1m thickness covers the whole blanket. Fig. 8 shows this general layout.

The blanket system consists of a graphite-moderated system, where liquid fuel flows through vertically arranged pipes. The isotopes to be transmuted are mixed in liquid lead, so that lead carries the Actinides and transports the heat from the blanket to the heat exchangers. Fig. 9 shows a sketch of the fuel pin cell used for the calculations. The pipe has a thickness of 3 mm for this study and is assumed as Zr (well knowing that there must be applied an alloy, e. g. with Nb, to get a higher corrosion resistance against liquid lead). This pipe stays in a graphite block for moderation with a gap of 3 mm to the moderator and is arranged in triangular shape.

The system can be designed as a single loop system (with heat exchangers outside the core), which increases the TRU inventory by approx. factor of 4, or as a double loop system (with heat exchangers inside the core), in which the fuel resides the whole time in the core. In this case a second pipe with liquid lead as coolant will enclose the fuel pipe and cool it.

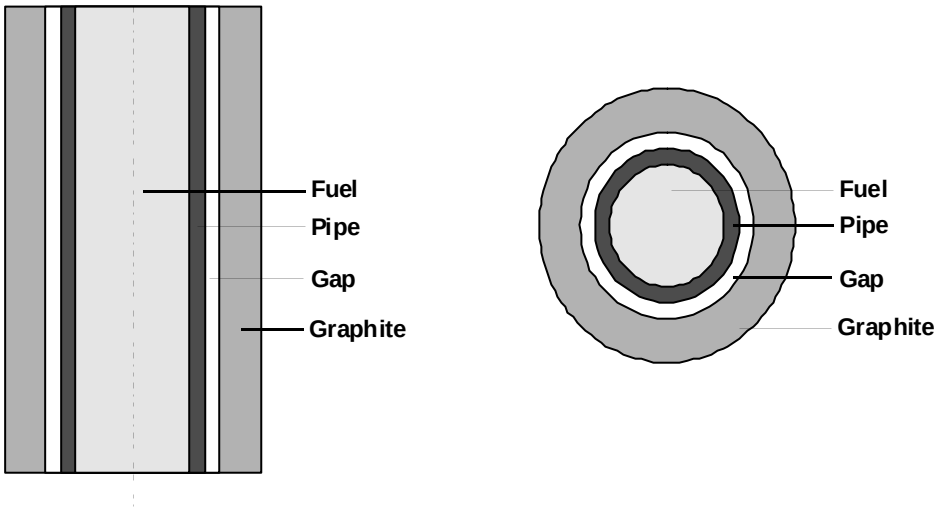

Figure 9. Sketch of the basic fuel cell layout for the liquid lead fuel transmutation system.

All calculations of the 1-dimensional k_{inf} values are done with the code system SCALE 4.2 [Herm89] and the modules CSAS, BONAMI, NITAWL, and XSDRN applying JEF 2.2 based cross-sections, mostly. KENO-V was used to calculate the k_{inf} of a 2-dimensional system, assuming axially varying fuel concentrations in case of sedimentation. They may occur in the case, that a suspension of lead with dispersed actinide oxide particles is applied. MORSE [Naka84] code shows the k_{eff} of the system and the SAS2H module of SCALE allows burn-up calculations for different fuels.

2.2 Basic calculations

The basic calculations show the multiplication ratio of different kinds of fuels in fact of the geometric design of the fuel cell and the Pu- or PuMA-concentration. To find fuel mixtures with a wide range of subcritical behaviour will be the basic for all further steps. The calculations are split in two groups. On the one hand in Pu and PuMA based fuel and on the other hand fuel with a Th ratio.

2.2.1 Pu / PuMA based fuel

The start position for all further calculations are the behaviour of pure Pu of PWR quality in the

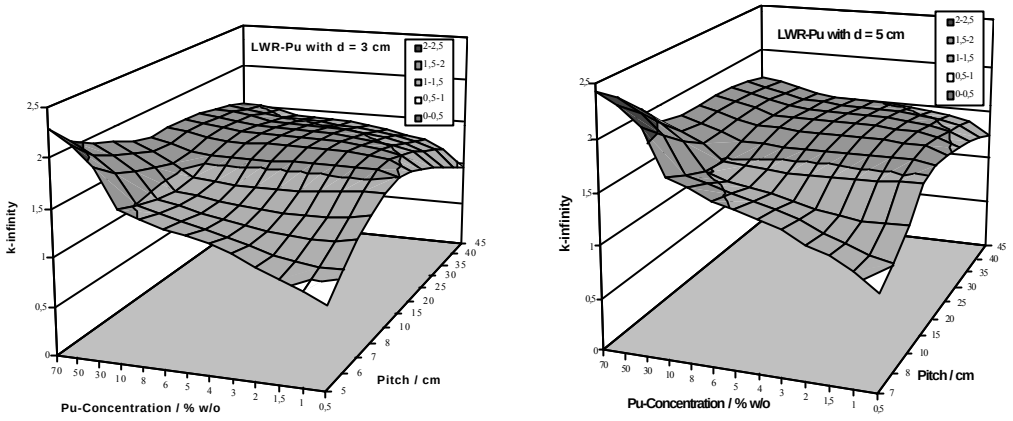

Figure 10. k_{inf} of liquid fuel for different concentrations and pitches at an inner pipe diameter of 3 cm and 5 cm.

liquid lead. As a boundary condition the calculations of k_{inf} depending on the concentration of Pu in liquid lead, the pitch and the inner pipe diameter have been performed. The range of the variations were for the concentration of Pu 0.5 % and the maximum of 70 % in volume assuming the sedimentation of spheres, for the pitch (t) 5 cm to 45 cm and for the inner tube diameter of 3 cm to 12 cm. The conclusion of this first variation is, that a subcritical k_{inf} can be obtained only in a small geometrical and/or loading range. As an example, Fig. 10 shows this fact for a pipe-diameter of 3 cm and 5 cm.

In order to broaden the subcritical range, the fuel composition has been changed in such a way, that the MAs generated in PWR-fuel are also inserted into the liquid lead fuel with varying concentrations. The range of variation for the MA concentration in the TRU-fraction was between 11% (fraction of MA in TRU of PWR spent fuel) and 30%. As a result of the changed TRU composition in the fuel the k_{inf} becomes subcritical in a wide range. Fig. 11 shows this development in ratio to the rising MA concentration applying an inner fuel pipe diameter of 3 cm. In this case the

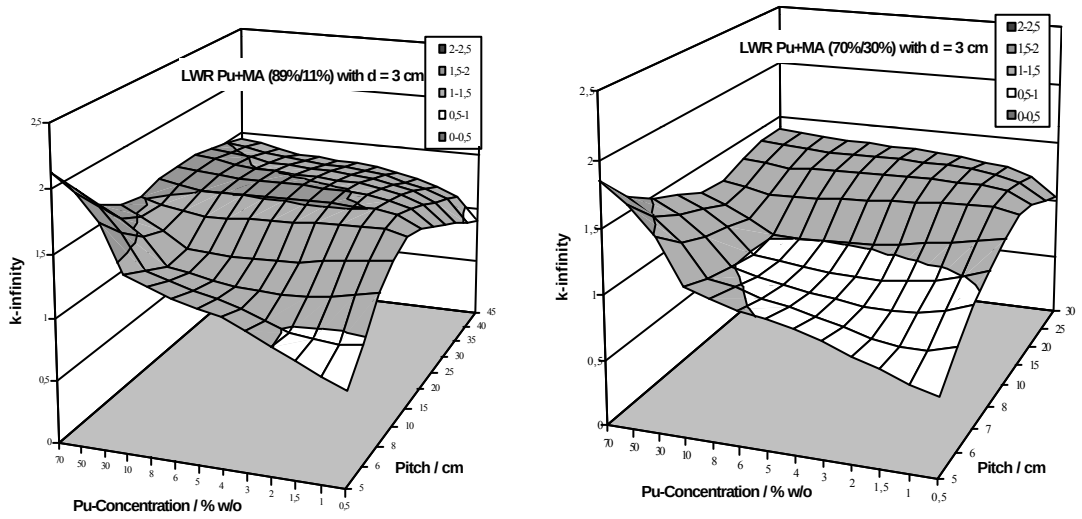

Figure 11. k_{inf} of liquid TRU-Pb fuel with 11% MA and 89% Pu mixed as fuel and TRU-Pb fuel with 30% MA and 70% Pu mixed at an inner pipe diameter of 3 cm.

composition can be used as a base for further 3-dimensional calculations.

2.2.2 Pu-loadings Mixed with Thorium

The general cell layout and calculation procedure are the same like pure Pu / PuMA based fuel. The first investigations start with a mixture of PuO_2 and ThO_2 in lead, both having the same fractions by weight (1:1). The k_{inf} value is calculated in the same way as pure Pu / PuMA fuel while varying the fuel concentration, maintaining the weight ratio between Pu and Th, the pitch and the inner pipe diameter. The ranges of variation were for the Pu concentration from 0.01 % to 35 % by volume, for

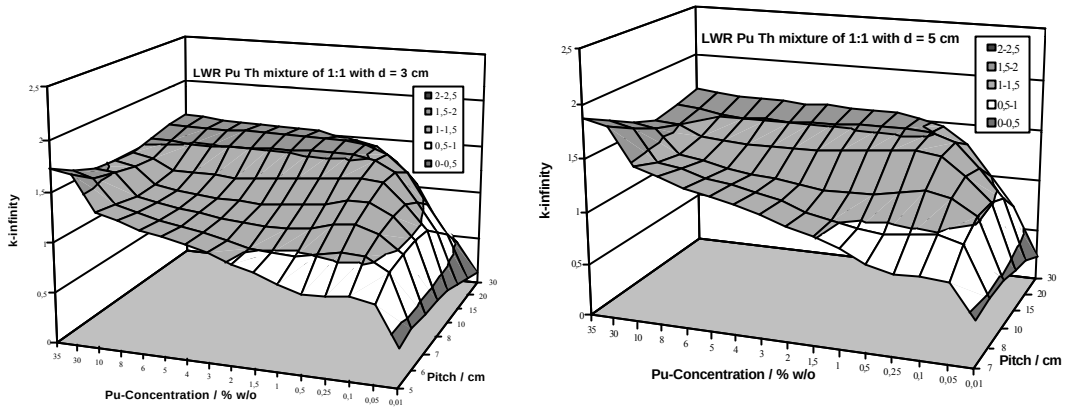

Figure 12. k_{inf}. of liquid lead containing Pu-Th (1:1) fuel mixtures for a pipe of 3 cm and 5 cm inside diameter.

the pitch (t) between 5 cm and 30 cm and for the inner diameter between 3 cm and 12 cm. To obtain the total concentration of actinides in lead, the Pu (TRU) concentration must be multiplied by the sum of Pu- and Th-fractions, i.e. two in this case. The maximum concentration of actinides will be 70 %, the theoretically highest range for dispersion in the fuel.

Fig. 12 shows for the examples of a pipe diameter of 3 cm and 5 cm, that the subcritical range broadens significantly, 2% Pu at a pitch of 5 cm and a pipe diameter of 3 cm or 1.4 % at a pitch of 7 cm and a pipe diameter of 5 cm - compared with pure Pu (see Fig. 10) - but it covers not yet the full concentration, witch is possible in principle. Similar results are obtained with enlarging inner pipe diameters. To open the subcritical range further, the fuel composition has been changed with respect to higher Th contents. The variation for this Pu:Th ratio in the fuel fraction was up to 1:7, i.e. a reduction of the highest Pu concentration in the fuel from 35 % to 8.75 %.

The Fig. 13 shows the development of the subcritical range by changing the Pu:Th ratio from 1:3 (left) up to 1:7 (right) for pipe diameter of 3 cm. For high Pu:Th ratio (i.e. 1:7) and some pitches the subcritical behaviour of the fuel becomes independent from the Pu concentration. This means, that the sedimentation problem gets unimportant for the safety evaluations for this fuel mixtures. With respect to lower Pu:Th concentrations nearly every pipe diameter offers a wide range of geometry and concentration.

2.2.3 Results of the Basic Calculations

In fact of the small subcritical range of pure PWR Pu in the Jülicher ADS, the Pu must be mixed with other compositions. There exist two possibilities. On the one hand a mixture with MAs, which

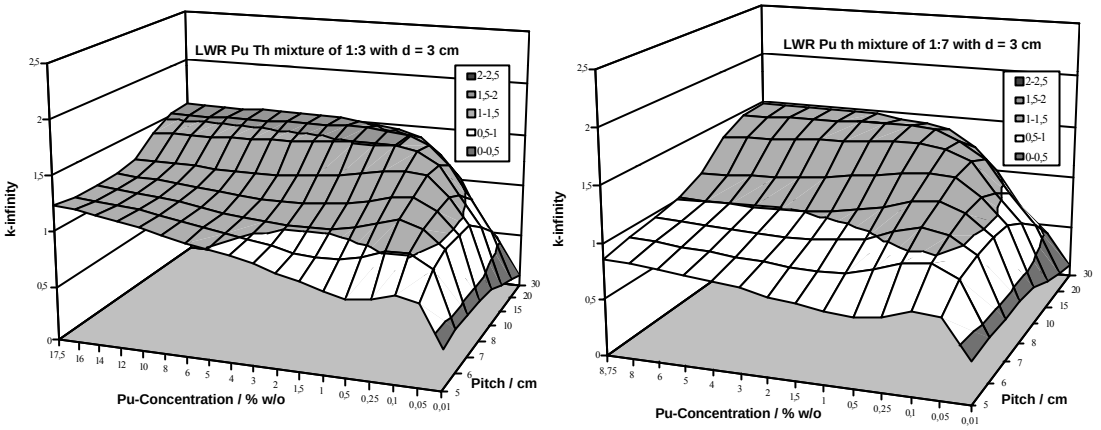

Figure 13. k_{inf}. of liquid lead containing Pu-Th 1:3 (left) and 1:7 (right) fuel mix for a pipe diameter of 3 cm.

will open the subcritical range up to a useful level, but not over the whole concentration scale, or a Pu-Th mixture. The Pu-Th mixture offers the possibility to compose a fuel for ADS will be subcritical independent from the Pu-concentration. But this behaviour occurs only for a high Pu:Th ratio (i.e. 1:7 for a pipe diameter of 3cm). This Pu:Th ratio is disadvantageous for the system (total mass of actinides).

In the same way it is possible to combine both opportunities. This means to build a Pu-MA fuel with Th. Low Th ratio of 1:1 to the PuMA fuel with 70% Pu and 30 % MA for example opens the subcritical range rapidly. Fig. 14 shows this for a PuMA (70%/30%) : Th 1:1 ratio by a pipe of 3 cm. The subcritical ranges grows from 5.5% PuMA-concentration at a pitch of 5 cm without Th up to 10 % PuMA-concentration of the same pitch and a PuMA : Th ratio of 1:1.

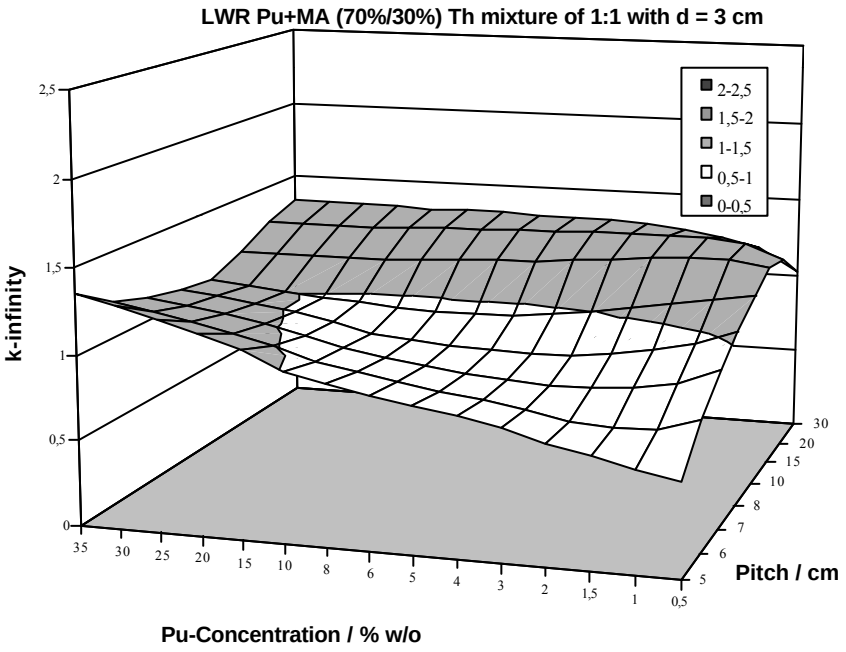

Figure 14. k_{inf} of liquid TRU-Pb fuel with 30% MA mixed and 70% Pu and a PuMA : Th ratio of 1:1 at a pipe diameter of 3 cm.

Consequently three types of fuel, i.e. PuMA-based fuel, Pu-Th-based fuel and PuMA with Th will be investigated in the following steps.

2.3 Nuclear Safety Calculations

In general two kinds of liquid lead based fuels are possible:

– alloy/solution of liquid lead with fuel elements or

– suspension of liquid lead and solid fuel particles, e.g. actinide oxides

Assuming the later fuel type, it is necessary to investigate sedimentation behaviour of the mixture in case of a loss of flow. Especially, for fuels, which cannot guarantee inherent subcriticality over the whole homogeneous concentration range (PuMA-fuel and Pu or PuMA fuel with a low Th concentration), the question of nuclear safety raises.

2.3.1 Sedimentation Behaviour

Sedimentation means an increasing concentration of dispersed actinide oxide particles in some parts of the liquid fuel, while the remainder decreases in concentration. In fact the actinides will concentrate at the bottom, if the circulation stops. The concentration of actinides at the bottom will increase up to the limit of the total mass of actinides in the pipe, to 69% in volume, assuming the theoretically highest concentration of ideal spheres.

To calculate the k_{inf} values of the total fuel pipe, it is necessary to model the axis in 2-dimensional system of pipes and calculate this system e.g. with KENO-V. Fig. 15 shows a sketch of a modified basic cell in X-Y direction and in X-Z direction. The numbers represent the fuel and the

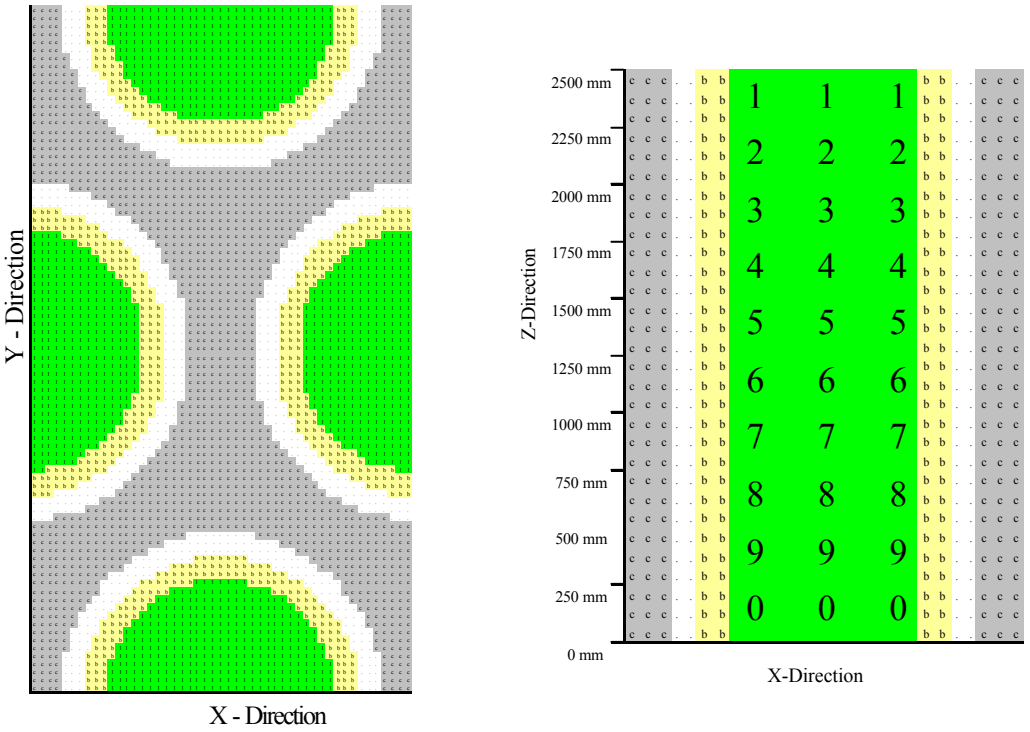

Figure 15. Sketch in X-Y and X-Z direction of modified cell for KENO-V calculation. The numbers represents the fuel zones, the letters the material.

letters symbolise the pipe material (b) or the moderator graphite (c). Every zone includes a homogeneous suspension, thus the whole pipe represents an axially heterogeneous system. . The mainspring of the sedimentation appeals in every zone in the same way, but the effect evince at first in the top area, because in the other zones a balance between drop out into the lower zone and drop in from the upper area exist. In fact of this situation, it is possible and useful to split the effect into different steps. These steps simulate the time progression of the sedimentation in the system; in this case 9 steps are simulated.

The further calculations for an inner pipe diameter of 3 cm and 5 cm comprise three groups of fuel compositions: 1st the PuMA (70%/30%) mixtures in liquid lead, 2nd PuMA (70%/30%) with a dedicated fraction of Th and 3rd pure LWR Pu with a dedicated fraction of Th.

2.3.2 Characteristics of Sedimentation with Initial PuMA - Th Loading

In general the homogeneous PuMA (70%/30%) - Th fuel offers a wide range of subcritical multiplication ratios. Sedimentation can cause that the multiplication ratio for higher concentrations rises rapidly above unity. So all further calculations consider only low initial PuMA or Pu concentrations (< 4%). Fig. 16 shows the behaviour of sedimentation for an PuMA-Th 1:1 fuel with a pipe diameter of 3 cm and a pitch of 8 cm. For the homogeneous mixture, the value of the multiplication ratio rises with the low concentration fuel caused by the better moderation of the Pu. During sedimentation the behaviour of the system changes depending on the initial concentration. The highest concentration (4%) has the highest ultimate k_{inf} value. Another effect of the enhanced moderation is, that the amplitude between the minimum (min) and maximum (max) k_{inf} decreases. For example at 4% initial concentration a change of the amplitude from +0.35 at a pitch of 5cm to +0.16 at a pitch of 8cm results. Finally, the spectrum of k_{inf} values for the different fuels becomes smaller as the moderation increases. This brings up the conclusion, that the multiplication ratio will be dominated for highly moderated systems by the diluted zones with a very low concentration of

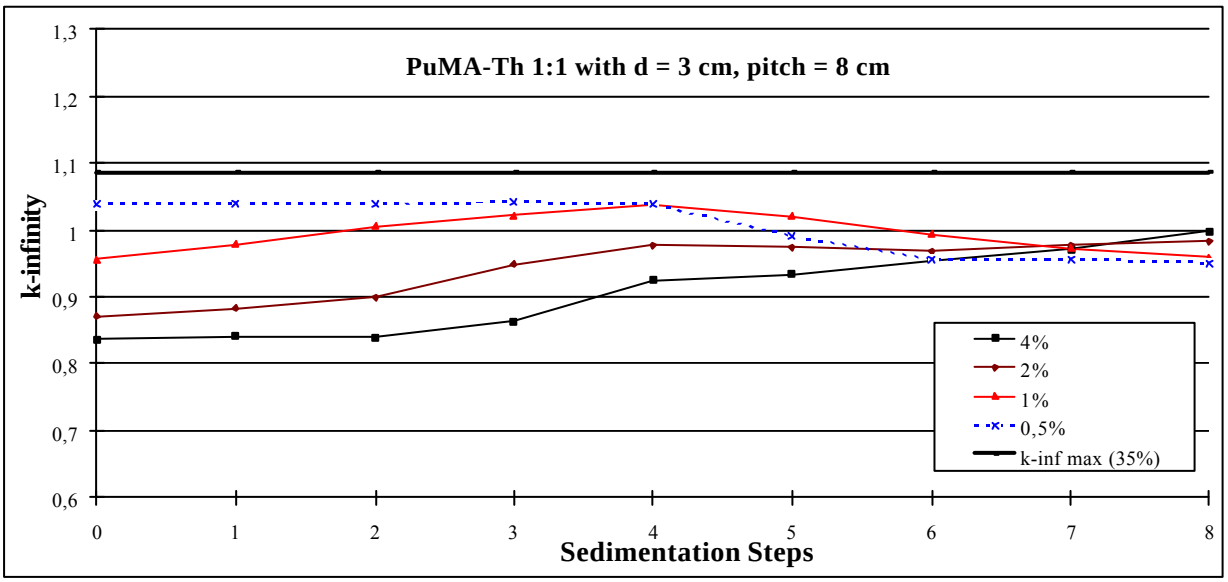

Figure 16. Progress of k_{inf} values for PuMA-Th 1:1 with d = 3cm and a pitch 8cm for mixtures of 4%, 2%, 1% and 0.5% Pu concentration.

PuMA (0.1%). Fig. 17 shows for example four PuMA-Th based fuel mixtures, which have a suitable behaviour for use in ADS. This will be a mixture of 0.5% PuMA-Th 1:1, a 3 cm inner pipe diameter and a pitch of 7 cm, 2% and 4% PuMA-Th with 3cm inner pipe diameter and a pitch of 8 cm and a 2% PuMA-Th 1:1 mixture with a pipe diameter of 5 cm and a pitch of 8 cm will be possible as well. All mixtures show subcriticality while sedimentation progress.

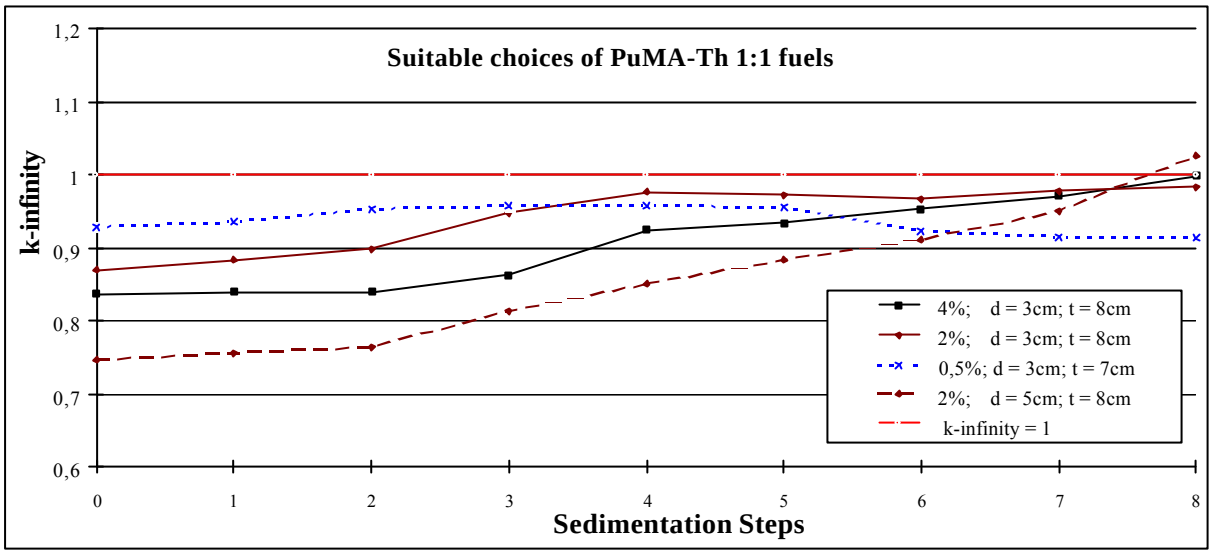

Figure 17. Suitable choices of PuMA-Th 1:1 fuels to be investigated in burn-up calculations.

2.3.3 Characteristics of Sedimentation with Initially Pure PWR Pu - Th Loading

The result of the Pu-Th based fuel show a similar development as the PuMA-Th based fuel, but the min-max behaviour of the k_{inf} ratio changes from a higher start value (step 0) less rapidly. The

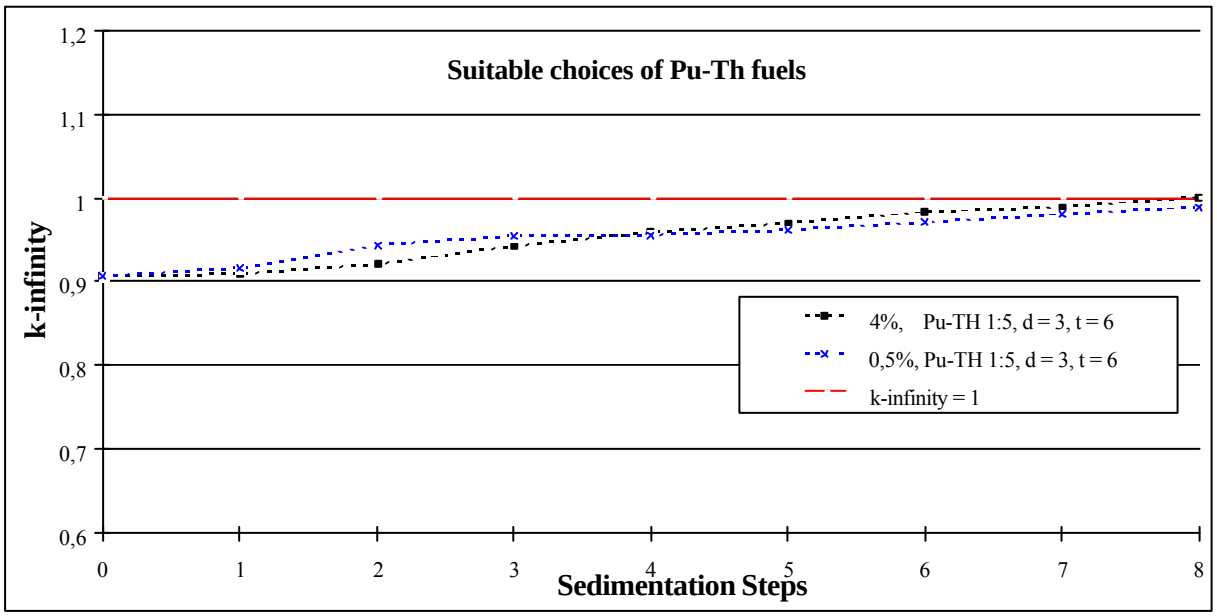

Figure 18. Suitable choices of Pu-Th fuels for further burn-up calculations.

reason for the more smoothly progression is the high Th content. In fact the change of the Pu-Th ratio from 1:5 to 1:3, produces a comparable k_{inf} variation as observed with Pu-Th fuels. The total spectrum for the k_{inf} ratio at the sedimentation end of the different mixtures grows from $\Delta k = 0.17$ (Pu-Th 1:5) to $\Delta k = 0.31$ (Pu-Th 1:3). A larger pitch in this system has the consequence that the multiplication ratio gets more critical during sedimentation. For further calculations the best choices of Pu-Th based fuels with a pipe inner diameter of 3 cm or 5 cm are shown in Fig. 18. There exist several fuels and geometrical compositions where the homogeneous k_{inf} value lays above 0.9 and stays below unity during sedimentation. Especially the Pu-Th 1:5 ratio offers a possibility to work with a higher concentration for a better turnover of Pu.

2.3.4 Characteristics of Sedimentation with Initial PuMA (70/30) Loading

The progress of the multiplication ratio for a PuMA (70/30) fuel, i.e. without Th, during the sedimentation is comparable to the PuMA-Th 1:1 fuel, but with k_{inf} values at higher levels. The higher concentrated fuels (4% and 2%) have nearly the same distinct changing, Δk +0.37 and Δk +0.3, but start on a 0.1 higher k_{inf} level. In fact, there exist among the analysed PuMA for example the 0.5% and 1% PuMA mixtures with a pipe diameter of d = 3cm and a pitch of 7cm, which start at k_{inf} higher than 0.9 and stay subcritical during sedimentation.

2.3.5 Consequences of Sedimentation Behaviour

All three kinds of fuel, PuMA-based fuel, Pu-Th-based fuel and PuMA with Th, offer a wide range of useful fuel compositions and system geometries, which show a subcritical behaviour during sedimentation. The range of possible fuel mixtures starts at very low concentration (<0.5) and rises up to 4% in an approximate pitch and kind of fuel. With the fact that higher concentrations of 4% can be safe in the nuclear point of view, the possibility of a batch mode may be a choice. For lower concentration a continuous refuelling is necessary. This has the consequences, that further burn-up investigations will be split into two groups: one for higher concentrated fuel mixtures in a batch mode system, and the second for low concentrated fuel mixtures in a continuous refuelling mode.

2.4 Burn-up in a Batch Operation Mode

The dedication of higher concentration fuel about 4 % Pu or PuMA, offers the possibility to work with a batch operation mode. This has the advantage, that this system doesn't need any online refuelling or extraction components, which reduce rapidly the engineering expenditure. In front of the burn-up, there must be checked the conditions for the calculation mode. Especially the question of the difference between the 1-D SAS2H code and the 3-D KENO or MORSE code.

2.4.1 Comparison of 2-D and 3-D Calculations

In the fact that the burn-up will be calculated with the 1-dimensional SAS2H code, it is necessary to be able to interpret the results for the 2-dimensional system. A benchmark of the 2-D code SAS2H and the 3-D code KENO and MORSE shows the difference between this modes. If the difference is known, the multiplication ratio of the 2-D burn-up mode can be transform or estimated for the real 3-D system.

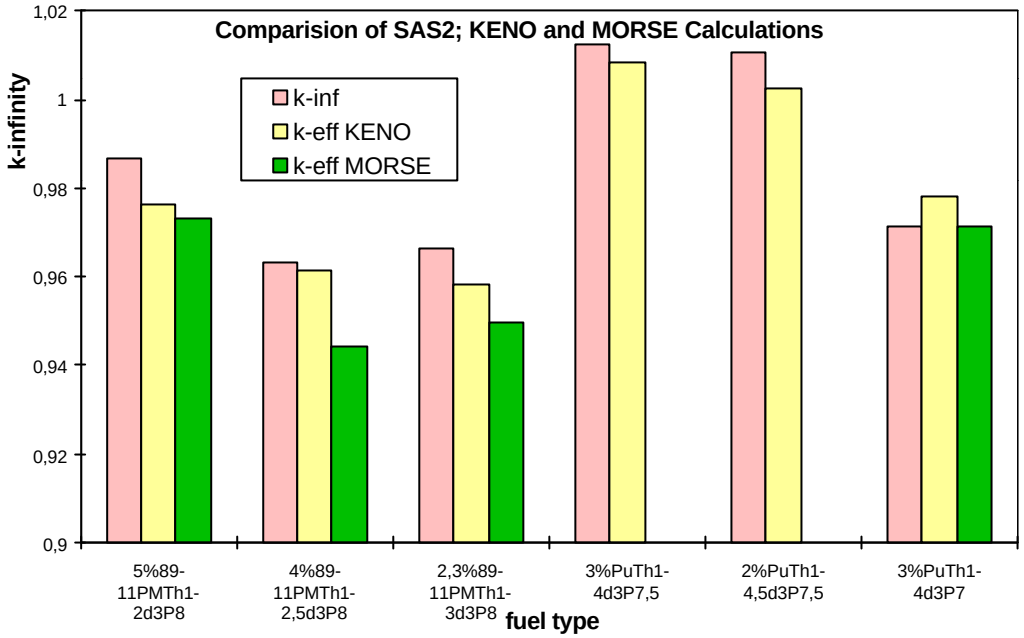

Figure 19. Comparison of SAS2, KENO and MORSE calculations of k_{inf}.

Two different fuel types with an inner pipe diameter of 3 cm have been selected for the benchmark: PuMA-Th fuel and PWR Pu with Th mixtures. For each kind of fuel three cases were investigated. In all cases concentration of Actinides (including thorium) in the fuel has been about 15. The maximum for PuMA or Pu concentration in the mixture was 5% PuMA or 3% pure Pu. thorium fraction varies reaches PuMA:Th $\rightarrow$1:3 or Pu:Th $\rightarrow$1:4.5 for a 2% Pu concentration in the fuel. The results of investigations are shown in Fig. 19. The differences of the calculations are very small and have nearly always the same tendency. The k_{inf} of the 1 dimension SAS2H calculation have the highest value, followed by the KENO 3-D calculation. The MORSE 3-d code conducts to the lowest k value. In general one can approximate the difference between 2-D and 3-D calculation in a first step with –1.7%. This will be the base for further estimations.

2.4.2 k_{inf} Variation with Burn-up

In order to be able to operate ADS in a batch mode it is necessary to find fuel mixtures, which maintain a high k_{inf} value over the burn-up period. The drop of the k-value during ADS operation has to be otherwise compensated by an increased accelerator power.

Two types of fuel have been investigated for batch operation:

- PuMA mixture with Th; and
- PWR Pu mixture with Th.

k_{inf} variation for PuMA-Th fuel

The assessment of the burnup performance of the PuMA-Th based fuel has showed that a wide range of fuel concentrations in different geometrical arrangements can ensure desired evolution of k_{inf} during burn-up. The most preferable compositions are presented in Fig. 20.

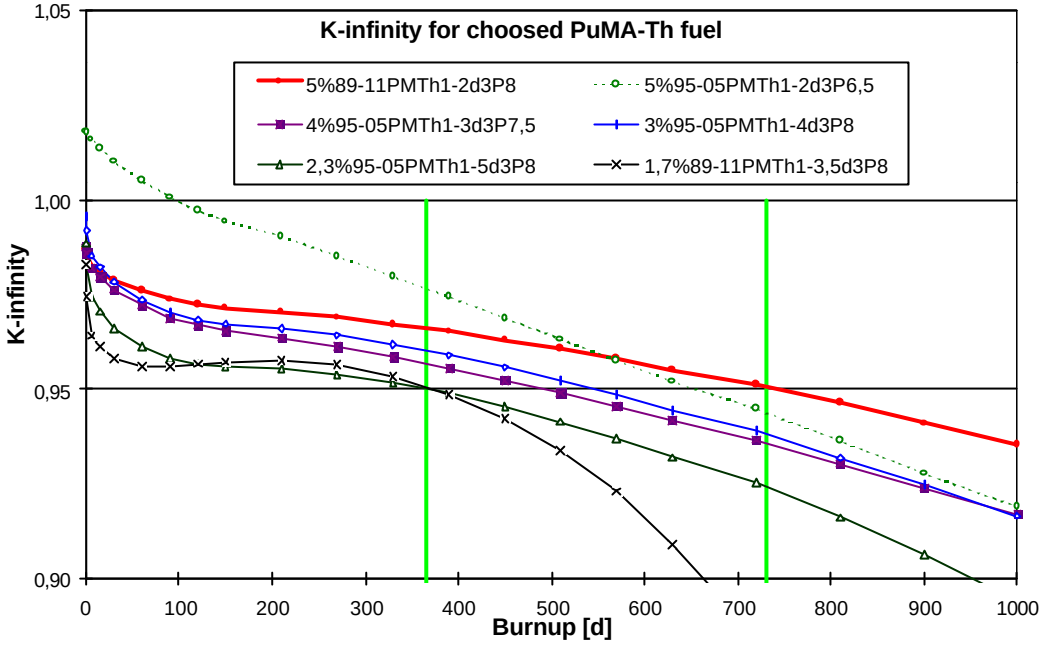

Figure 20. kinf for a group of chosen PuMA-Th fuels during the burn-up

The variation of the k_{inf} during burn-up is rather slow. In fact, the best fuel (5%PuMA(89%/11%) with a PuMA:Th ration of 1:2 at a pipe inner diameter of 3 cm and a pitch of 8 cm) has a k_{inf} drop of 0.8 % after 90 days of burn-up and of about 1.9 % after 330 burn-up days. In general the reactivity of PuMA-Th based fuels decreases by app. -17 pcm/efpd after 90 days and -9 pcm/efpd after 330 days. These results show that the PuMA-Th based fuel with a high enrichment offers good conditions for a batch mode of the ADS. The variation of proton current can be consequently kept in a small range.

k_{inf} variation for Pu-Th fuel

The Pu-Th based fuel does not offer the same flexibility for batch operation as the previous fuel. Fig. 21 presents the best Pu-Th compositions during the burn-up. The reactivity of the mixtures decreases rapidly. So the best Pu-Th fuel (3% pure Pu with a thorium ratio of 1:3 by a pipe inner diameter of 3 cm and a pitch of 7 cm) has a k_{inf} drop of – 2.8 % after 90 days of burn-up and of – 4.4 % after 330 burn-up days. Totally the reactivity of Pu-Th based fuels decreases by app. -37 pcm/efpd after 90 days and -14 pcm/efpd after 330 days of burn-up. Even if Pu-Th fuel shows much worse performance than PuMA-Th based fuel, a batch operation is still possible.

2.4.3 Burn-up Results for a Batch Mode of an ADS

The detailed burn-up results for a batch mode system show the advantages and the disadvantages of this kind of operation. Two cases have been analysed in details.

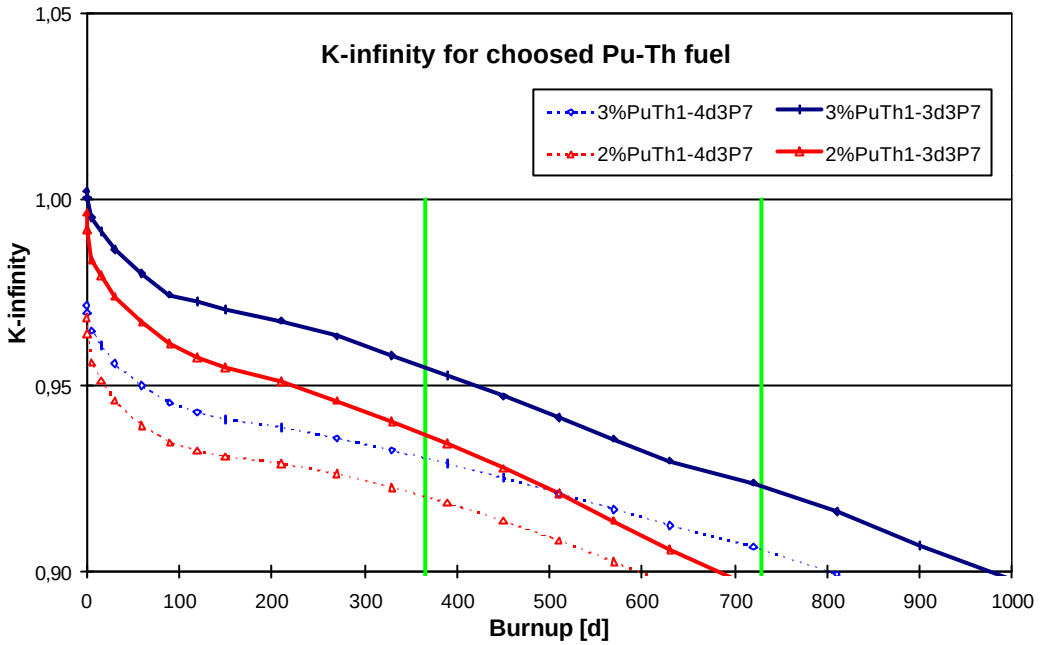

Figure 21. k_{inf} *for some chosen Pu-Th fuel compositions during the burn-up.*

A case of 5%PuMA (89%/11%)-Th 1:2

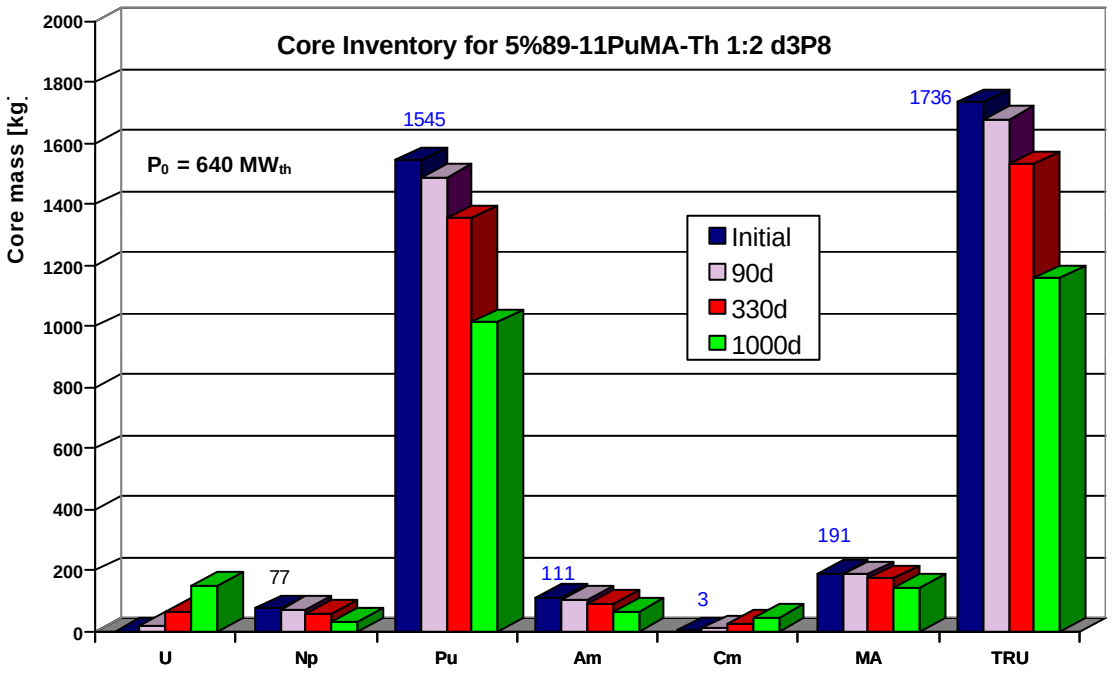

Figure 22. Mass fractions of the core inventory during burnup for the 5%89-11PuMA-Th 1:2 d3P8 case.

The PuMA-Th fuel "5% 89-11 PuMA-Th 1:2" with a pipe diameter of 3 cm and a pitch of 8 cm shows the best behaviour from the point of k_{inf} drop during the burn-up. A cycle length of 330 days has been chosen as an operational mode of the system. The initial k_{eff} was 0.97 and dropped to $k_{eff} = 0.95$ after 330 days of system operation. Consequently, the accelerator current has to rise from 15mA at the beginning to 25mA at the end of the cycle. The mean total flux in the core was 4.6×10^{14} n/cm^2 × s and the mean power density for the system - 21.7 MW/m^3 giving the total power of 640 MW_{th}. The core inventory at the beginning of the comprises of 1545 kg Pu, 1736 kg TRU and 5193 kg heavy metal totally. Fig. 22 shows the inventory in more details. This inventory fractions will be reduce up to the cycle end to 1355 kg Pu, 1594 kg TRU and 4980 kg heavy metal

Fig 23 illustrates the evolution of the element groups during the burn-up. After 330 full power days 19 kg Np, 189 kg Pu, 19 kg Am, and totally 205 kg TRU is consumed. On the other hand, 64 kg U and 22 kg Cm build up. In general 213 kg HM are burnt during 330 full power days.

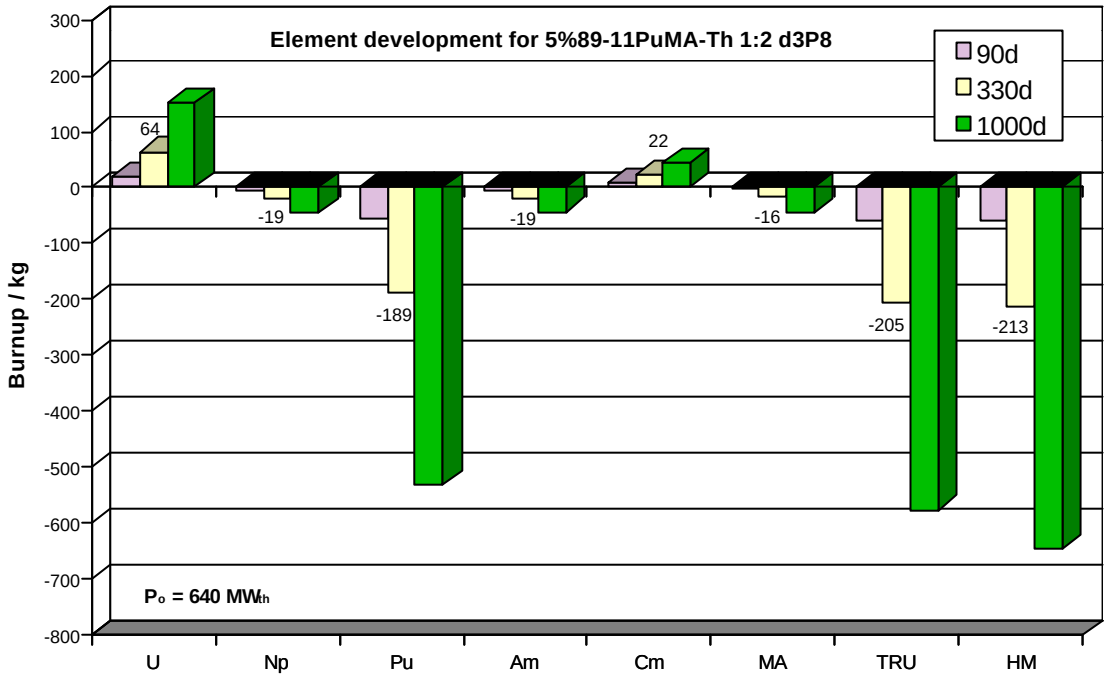

Figure 23. Element evolution with burn-up for the 5%89-11PuMA-Th 1:2 d3P8 case.

A case of 3%Pu-Th 1:3

The 3%Pu-Th 1:3 fuel composition with an inner pipe diameter of 3 cm and a pitch of 7 cm has been chosen as an example for a pure Pu fuel. The cycle length of the system operation has been 330 days. The initial k_{eff} was 0.978 and then dropped $k_{eff} = 0.94$ after 330 days of operation. This k_{eff} drop implies a rise of the accelerator current from 14mA at the beginning of the cycle to 38mA at the end of the cycle. The mean total flux was 6.8×10^{14} n/cm^2×s giving the mean power density for the system of 28.3 MW/m^3. Consequently, the total power was 833 MW_{th}. The core inventory at the beginning of the cycle comprises to 1360 kg Pu and 5425 kg heavy metal in total. Fig. 24 shows the inventory in more details. After 330 days of system operation this inventory has been reduced to 1073 kg Pu, 1100 kg TRU and 5146 kg heavy metal. The nuclide evolution during the burn-up of 330 days is shown on Fig 25. After 330 full power days 287 kg Pu and totally 260 kg TRU will be

consumed. On the other hand, 107 kg U and 19 kg Am, 8 kg Cm will be built up. In general 279 kg HM are burnt during 330 full power days.

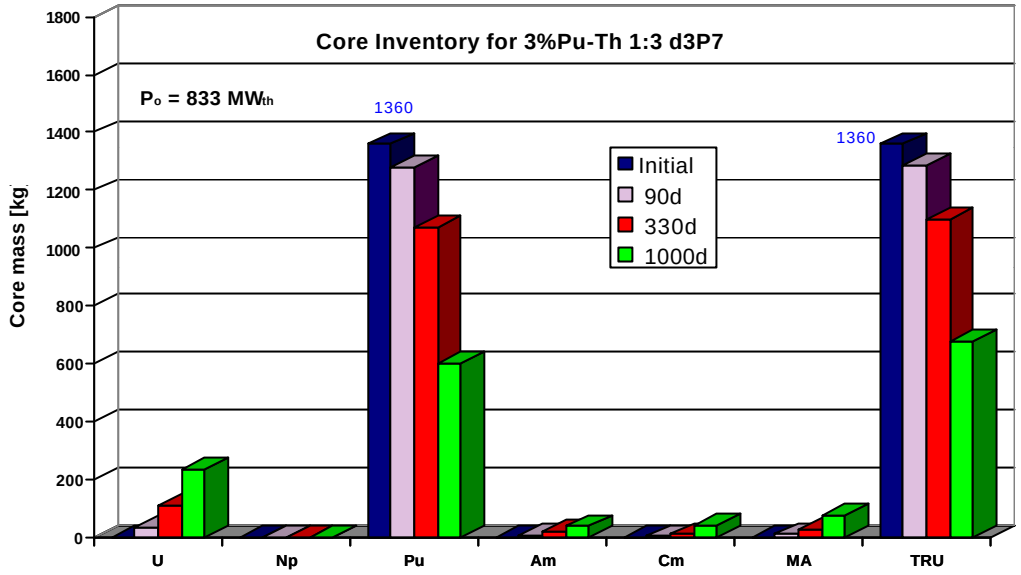

Figure 24. Mass fractions of the core inventory during burn-up for the 3%Pu-Th 1:3 d3P7case.

Both cases indicate a possibility for an ADS batch operation. In fact both fuel compositions have a high transmutation rate of plutonium and the PuMA based fuel for Neptunium and Americium,

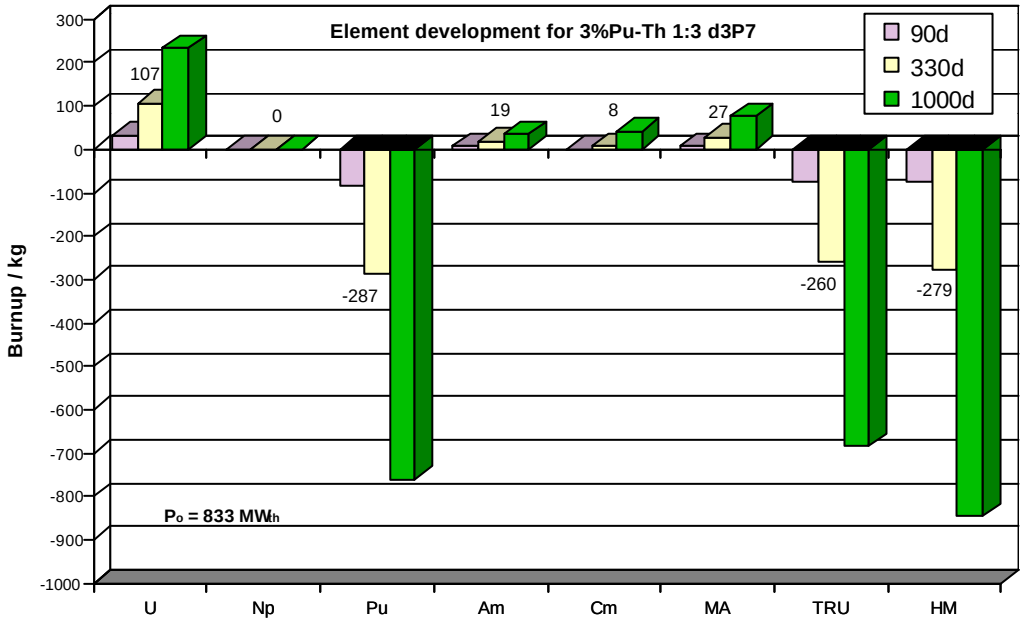

Figure 25. Evolution of elements with burn-up for the 3%Pu-Th 1:3 d3P7 case.

too. The drop of k-value by less than 2 % for the PuMA fuel compositions is very favourable for a batch operation and requires accelerator power changes not more than 70%

2.4.4 Conclusions

In principle a batch operation mode for this ADS type is possible with Pu-Th or PuMA-Th fuels in liquid lead matrix. The batch mode of operation may significantly simplify reprocessing requirements. However the transmutation performance of such system is not very remarkable: the ratio of TRU incineration over discharge is only 0.128 for the 5%89-11PuMA-Th 1:2 fuel and 0.236 for the 3%Pu-Th 1:3 fuel. Moreover the total mass of Pu and PuMA in the system will be relatively large leading to proliferation concerns. From this point of view the batch operation mode may not be preferable.

2.5 Fuel for the Continuous Operation Mode

The liquid fuel offers the possibility to feed continuously fissile and fertile materials and to extract fission products on-line during the system operation. With respect to this fact, a totally different fuel composition than for the batch mode can be used: a low enriched fuel (<0.5% TRU initial). All calculations base on a continuous extraction of a fraction of 50% for the elements Xe, J, Sm, Ce, Nd, Cs, Sr, Y, Mo, Ru, Rh, Pd, Sb, Te, Ba and an extraction fraction of 1.5% to 10% (changing during the burn-up) for Th if present. An extraction fraction of 50% means, that 50% of the available mass from the dedicated element will be extracted/taken out from the liquid lead solution.

In a first step the multiplication ratio is to be checked and in the second step the burn-up behaviour over one year is examined.

2.5.1 Multiplication Ratio of Low Enriched Fuels

The continuous operation mode of the ADS offers the possibility to use liquid lead fuels with a low concentration of TRU. By low TRU concentration fuel it is understood fuel which initially contains more then 99.5% lead as a carrier and less than 0.5% TRU as the fissile/fertile material, respectively. Six types of low enriched fuel compositions were investigated in this study. The type of the fuel have been labelled by a string of number and letters. The first number and element names (e.g.. 0.05%Pu) give the total percentage of fissile (Pu) element in the fuel, the next string shows the ratio in percent of Pu and MA in the fissile material (i.e. 89-11). The thorium based fuel is characterised by numbers describing the ratio of TRU material and thorium (i.e. PuTh1-3), the last term with a letter “P” (e.g. P8) gives the pitch of the system in cm.

Investigated fuel types:

- Pure Pu (PWR spent fuel Pu vector after 10a) with Th based fuel, i.e. 0.1%PuTh1-3P5.95.
- Pu with minor actinides in 89% Pu and 11% MA composition (PWR spent fuel after 10 years of decay) with thorium, i.e. 0.01%89-11PuMATh1-9P6.95.
- Pu with Minor Actinides in a 70% Pu and 30% MA composition with thorium, i.e. 0.15%70-30PuMATh1-3P8.
- Pure Pu (PWR spent Pu vector after 10 years decay) fuel, i.e. 0.05%Pu-P8.

- Pu with minor actinides in 89% Pu and 11% MA composition (PWR spent fuel after 10 years decay), i.e. 0.05%89-11PuMA-P8.
- Pu with Minor Actinides in a 70% Pu and 30% MA composition, i.e. 0.1%70-30PuMA-P8.

All six types of fuel and their system performance are investigated at first with respect to the multiplication factor (k_{inf}) during burn-up, keeping in mind that the accelerator supplies only a limited number of protons. Four different fuels, 0.05%Pu-P8, 0.05%89-11PuMA-P8, 0.1%PuTh1-3P5.95 and 0.1%89-11PuMATh1-9-P6.95 can be stabilised/bring up with a correct refuelling (feeding) mode after a swing nearby the k-value of 1. The 0.1%PuTh1-3-P5.95 fuel needs a longer time to be stabilised nearby the k-value of 1. Especially the lowest concentration fuels with 0.05%Pu or PuMA show a strong influence of the refilling mode. In this case the k-value can be easily adjusted and stabilised/controlled during burn-up by the refilling mode.

2.5.2 Short Time Burn-up Behaviour of Selected Low Enriched Fuels

For the comparison of the different fuels and moderation ratio, it is useful to have a reference with a system power normalised to 1 GW_{th} and a burn-up time of one year (1GW_{th}y). This gives the maximum mass consumption of 375 kg TRU.

Thorium based fuel

Fig.26 shows the result for the 0.1%Pu, 0.3%Th fuel with a pitch of 5.95cm. In one GW_{th}y it is possible to burn 356 kg of TRU while the inventory increases from 54kg/GW_{th}y to 159kg/ GW_{th}y. Just 37kg of MA's are produced. If the PuTh fuel changes to a PuMA fuel, the burnt mass of Pu decreases in the same way like the consumption of MA's (only Np and Am) increases. For the 0.1%89-11PuMATh1-9 fuel with a pitch of 6.95cm the Pu consumption

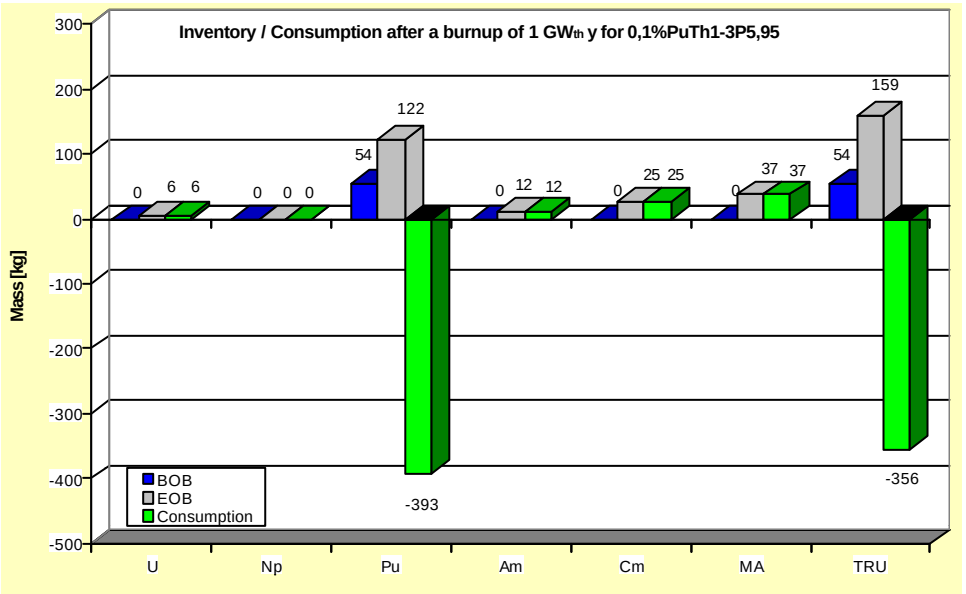

Figure 26. Inventory / consumption after a burn-up of 1 GWth y for 0.1%PuTh1-3P5.95.

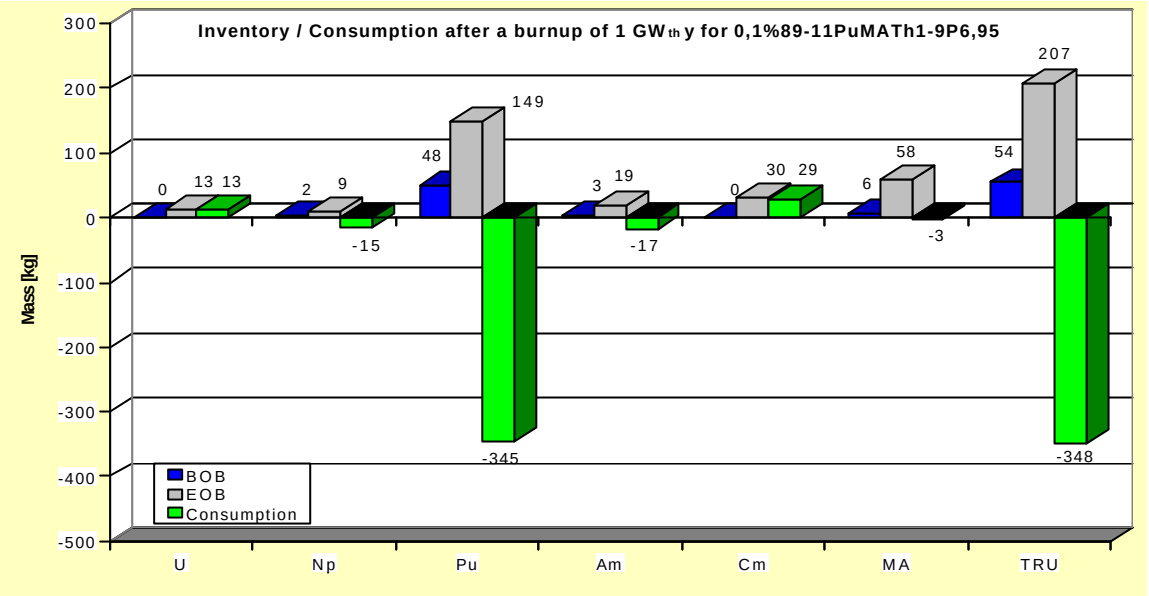

Figure 27. Inventory/consumption after a burn-up of 1 GW_{th} y for 0.1%89-11PuMATh1-9P6.95.

decreases to 345 kg (Fig. 27) and for the 0.15%70-30PuMATh1-3 fuel with a pitch of 8cm Pu consumption decrease to 275 kg (Fig.27). The Np and Am burn-up behaviour changes from a production in a pure PuTh fuel to consumption in a PuMA-Th based fuel. For example in the PuMA-Th fuel with 89%Pu -11%MA 15 kg Np and 17 kg Am will be consumed during one year (Fig.26), and at a higher PuMA ratio (70%Pu-30%MA) 50 kg Np and 96 kg Am (Fig.28) are destroyed. In the case of Cm none of this fuel types is able to burn it down. In total the highest reduction performance of TRU with 363 kg GW_{th}y shows the 0.15%70-30PuMATh1-3 fuel with a

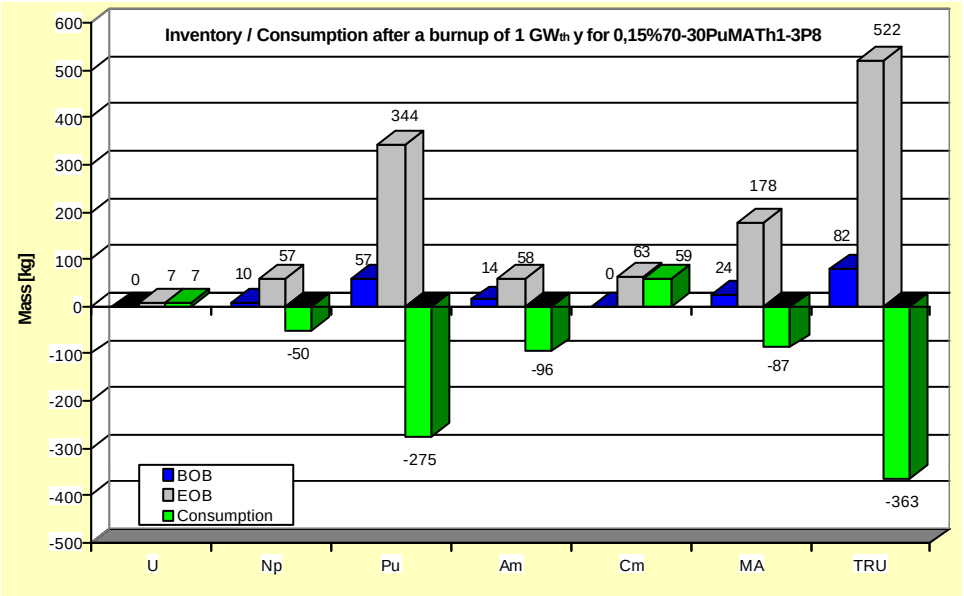

Figure 28. Inventory / consumption after a burn-up of 1 GWthy for 0.15%70-30PuMATh1-3P8.

pitch of 8cm. But this reduction performance must be paid by a high TRU inventory of 522 kg and a decreasing k-value during the burn-up time. The TRU consumption of the thorium based fuel, 0.1%89-11PuMATh1-9 (Fig. 27) destroy only 348 kg TRU in the fact that the system produces and burns a lot of ^{233}Pa/ ^{233}U The burnt mass of uranium can be estimated by 6kg. The consumption of Trans thorium mass will be above 354 kg.

Pure Pu and PuMA fuel

Pure Pu or PuMA based fuels offer the possibility to reduce the initial fissile material fraction down to 0.05% in the liquid lead. With respect to minimize the production of Cm it is necessary to work with well-thermalized neutron spectra. By increasing the pitch to 8cm the production of Cm can be reduced to about 18.3% (from 20.3kg at a 7.1cm pitch down to 16.6kg) with the same fuel and operation mode. Consequently, all further calculations with pure Pu and PuMA fuels apply a pitch of 8cm.

Fig.29 shows the inventory and consumption of a pure 0.05% Pu fuel. The system burns 396kg Pu $GW_{th}y$ and a produces 12kg Am and 17kg Cm/$GW_{th}y$. The total TRU consumption sums up to 367kg. The initial TRU inventory grows only 4.85 times from 27 kg up to 131kg. Using PuMA fuel the ratio of initial TRU and the inventory at EOB increases coincidentally with the fraction of MA's. For the 0.05%89-11PuMA (Fig. 29) fuel the ratio grows by 7.2 times and for the 0.1%70-30PuMA fuel mass at EOB increases by 9.9 times.

Despite of this increasing TRU inventory in the 0.1%70-30PuMA fuel the k-value decreases. With respect to the theoretical consumption of TRU all three kinds of fuel reach approx. 96 %. The difference between the TRU consumption is less then 2kg/ $GW_{th}y$ in total. Nevertheless the Pu burning differences are much higher. As the pure Pu fuel burns 396kg of Pu, the Pu consumption decreases to 363 kg with the 0.05%89-11PuMA based fuel (Fig. 30) and 282 kg respectively for 0.1%70-30PuMA based fuel (Fig.31). The decreasing of Pu burning will be compensated by an increased MA consumption. The 0.1%70-30PuMA based fuel consumes 23.5% Minor Actinides, in fact Neptunium and Americium. In total 6 kg MA are burnt applying the 0.05%89-11PuMA fuel

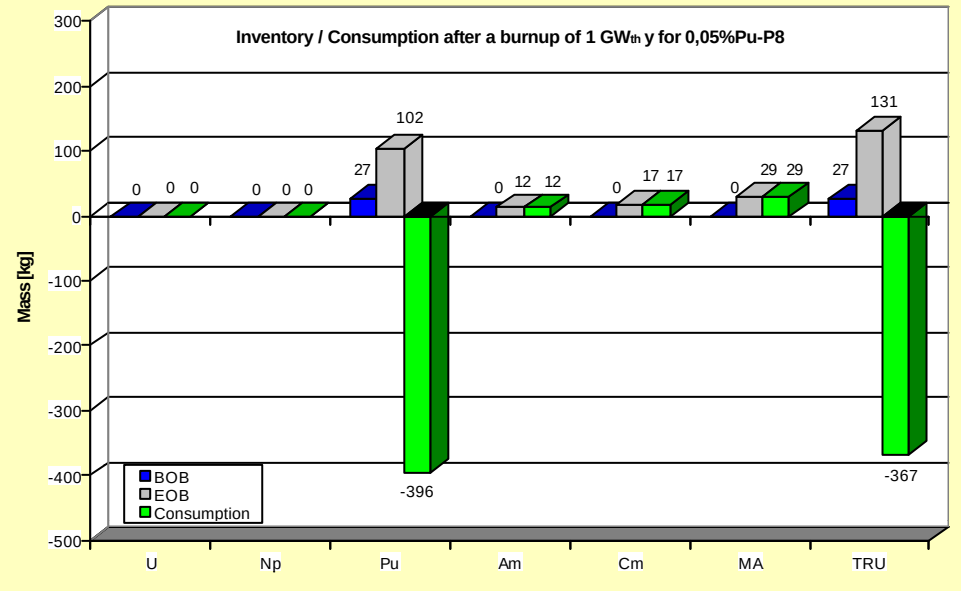

Figure 29. Inventory / consumption after a burn-up of 1 GWth,y for 0.05%LWR-Pu-P8

and 87kg with the 0.1%70-30PuMA fuel, in contrast to the production of 29 kg for the pure Pu fuel. Due to the increase of MA from 11% to 30% in the fuel, the Np consumption increases

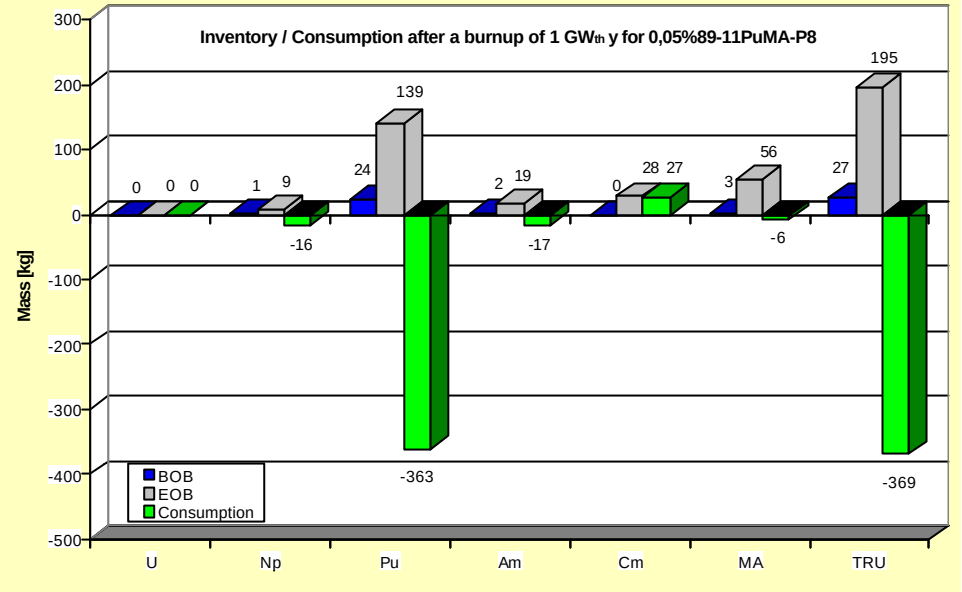

Figure 30. Inventory/consumption after a burn-up of 1 $GW_{th}y$ for 0.05%89-11PuMA-P8.

.

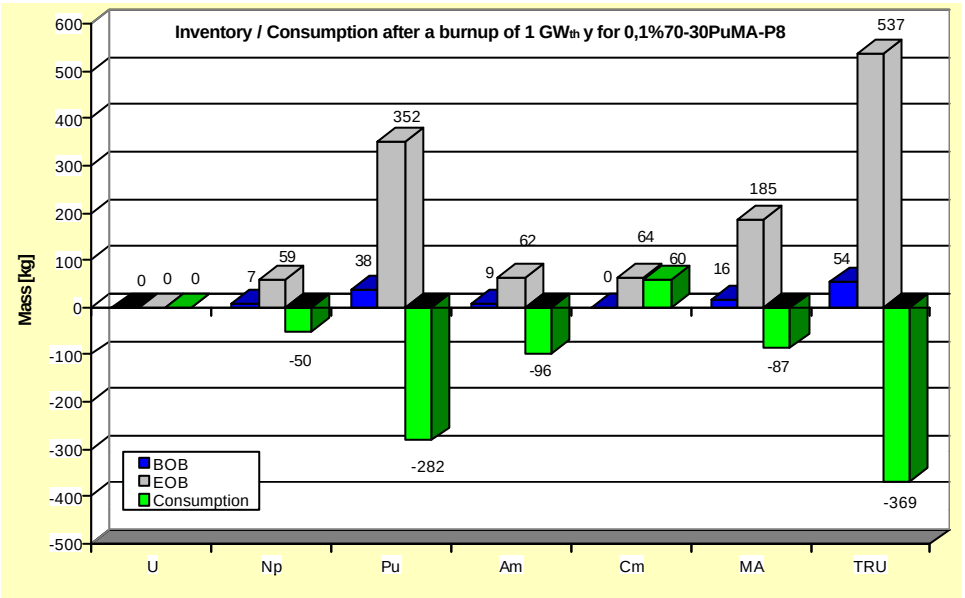

Figure 31. Inventory / consumption after a burn-up of 1 $GW_{th}y$ for 0.1%70-30PuMA-P8.

proportionally (~3.1 times), but the Am consumption increases more than proportional (~5.6 times), while the Cm production shows a less than proportional rise (~2.2 times).

2.5.3 Conclusions for the Liquid Fuel with on-line Reprocessing

In general both fuel types (Th+TRU or only TRU) show a similar burn-up behaviour, but the total TRU consumption will be always a little bit higher for the pure Pu and PuMA fuel group. Th based fuels need, with the exception of the 70-30PuMA fuel, a higher inventory of fissile material to reach the same performance. The Th free fuels show more preferable evolution of the k-value during burn-up. As a consequence, there will be no argument to use Th in the low concentration fuel, especially with the background of the reprocessing problem, the question of thorium solubility in lead and the build up of Pa and U.

With all MA containing fuels, it is possible to burn Np and Am, but Cm will always be produced. To minimize the production of Cm it is useful to work with a well moderated system. A higher consumption of Minor Actinides will be possible, but in this case the inventory increases rapidly and the k-value decreases by time. Looking for a system with minimized fissile material at BOB, the lowest concentration fuel 0.05%Pu and 0.05%PuMA offers the best performance.

2.6 Detailed Analyses of the Burn-up for the Optimised ADS

There are two important questions for the continuous operation mode. First, which elements should be extracted and what will be the extraction rate. Second, which feeding mode is optimal to get high TRU consumption at a low inventory with high and invariant multiplication. In the further analyses a fixed extraction is assumed.

The *extraction ratio* describes the ratio between the extracted mass and the initial mass. An extraction ratio of 0.5 means, that 50% of the existing selected fission products will be extracted, consequently the mass of the selected fission products in the solution is reduced by 50 %. The ratio refers always to the selected elements and up to date mass.

The *refuelling (feed) ratio* describes the proportion of fresh (initial) fuel mixed to the existing fuel. The total mass of resident fuel increases by the amount of refuelled fresh fuel. A refuelling ratio of 0.4 means, that the existing fuel will increase in mass by 0.4 times of the initial mass with the initial (fresh) fuel vector. The reference is the initial fuel mass and isotopic vector.

2.6.1 Optimisation of Fission Product Extraction

The basic burn-up calculations are based on a wide range of fission product extraction. 15 elements (Xe, J, Sm, Ce, Nd, Cs, Sr, Y, Mo, Ru, Rh, Pd, Sb, Te, Ba) should be continuously extracted with a ratio of 50%. As shown above, Th does not offer any advantages for transmutation in this type of ADS, so optimisation investigations have been limited to Pu – MA fuels.

It is assumed that reduction of the number of elements to be extracted reduces costs for reprocessing chemistry. An analysis of the produced fission product quantity during the burn-up combined with a review of their neutron captures cross-sections gave a priority list of the isotopes to be extracted. It was estimated that the extraction of 7 most important fission product elements (Rh, Pd, Xe, Cs, Nd, Pm and Sm) can satisfactorily mitigate the reactivity decrease. Moreover, negative reactivity of the non-extracted fission products can be easily compensated by a slightly higher feeding factor. Fig. 32 shows this comparison for the pure Pu fuel and the PuMA based fuel. The solid lines characterise the burn-up behaviour with respect to the k_{inf} and extraction of 15 elements, the dashed line gives the k-value of the same fuel and extraction of the most important 7 elements. In three years

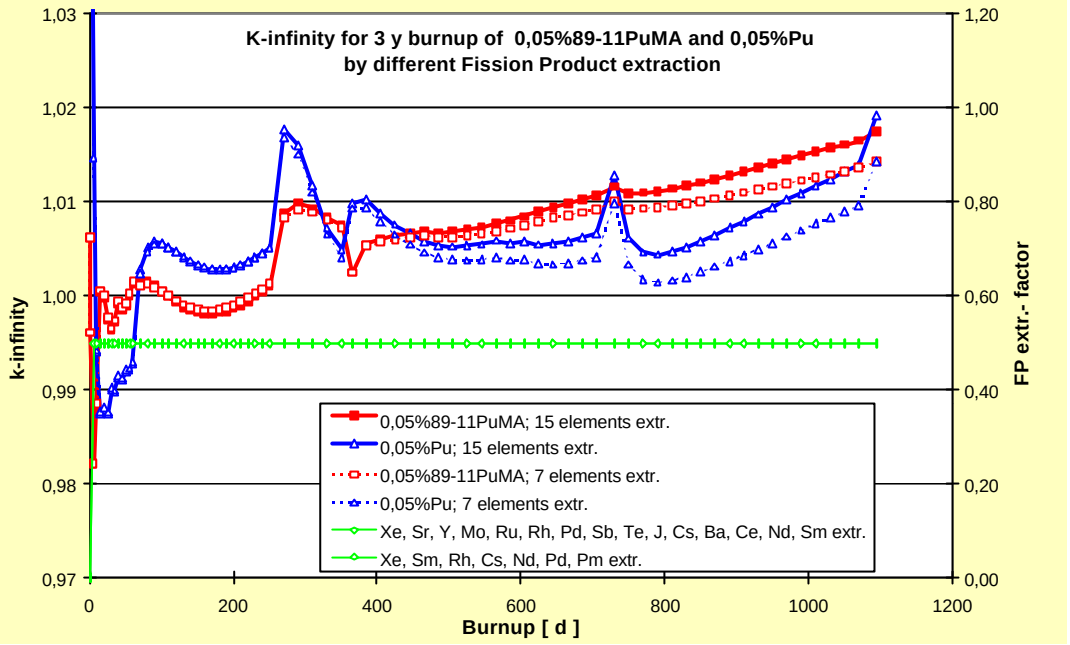

Figure 32. k_{inf} of 0.05%Pu and 0.05%89-11PuMA fuel with different fission product element extraction.

the extracted mass of Rh, Pd, Xe, Cs, Nd, Pm and Sm will be 314 kg (PuMA fuel). The remaining mass of this seven elements stays nearly constant up the second year at 7 kg. In general Rh, Pd, Xe, Cs, Nd, Pm and Sm represent approx. 45% of the total fission products.

In consequence all further calculations have been based on the extraction of only 7 elements (Rh, Pd, Xe, Cs, Nd, Pm and Sm) with an extraction ratio of 0.5. The extraction of Xe is easy due to its gaseous state. For the other elements the reprocessing with organic extraction method and/ or chromatographic splitting could be a possibility. The extraction ratio of 50% is considered to be realistic.

2.6.2 Optimisation of the Feed Mode

The aim of the optimisation of the feeding mode is to get a high TRU consumption with low TRU inventory and a high, stable multiplication without too big reactivity swings.

All optimization calculations were based on the k_{inf} coefficient, knowing, that the k_{eff}, is about 2 % lower then k_{inf}. The difference between k_{inf} and k_{eff} can be easily compensated by an adjustment of feed rate and optimization based on k_{inf} will not be principally different from optimization of k_{eff}. The evolution of k_{inf} for different feed modes is shown in Fig. 33. Starting with the same initial material, different feed modes support optimized value of k_{inf}. The time range is the same. Left y-axes corresponds to the k-values, the right y-axes describes the feed mode. Optimization can give a nearly constant k_{inf} over 3 years, with a value close to 1. An optimal feed strategy gives a very small differences between the max and min values of k_{inf} (~1.4 %). The biggest advantage of the on-line feed mode is, that every required k-value can be obtained and kept stable.

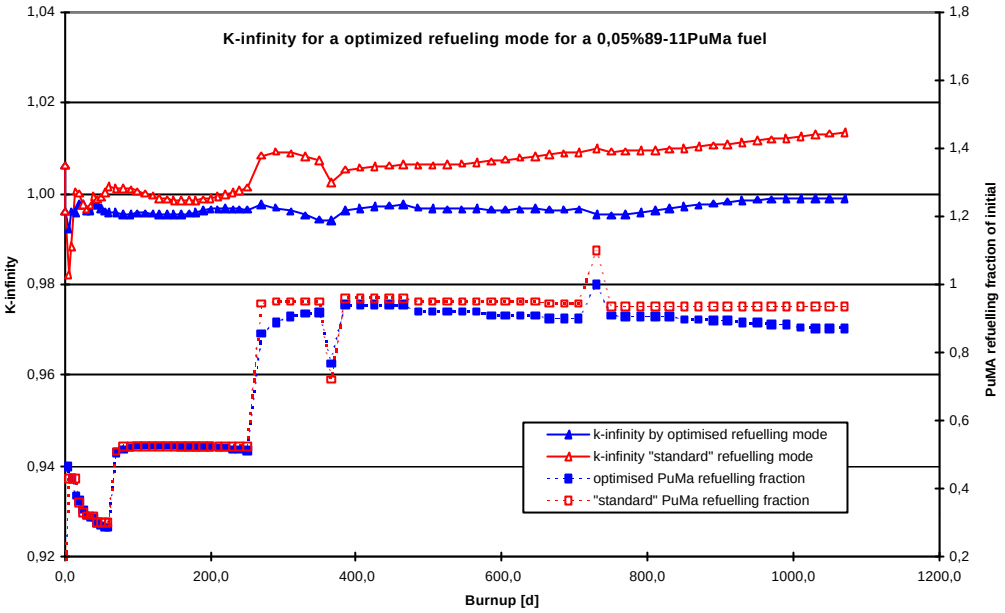

Figure 33. k_{inf}. evolution for an optimal feed of 0.05%89-11PuMA fuel and a normal feed.

2.6.3 Performance of the Jülicher ADS

The ADS was optimized for two different fuels: pure PWR Pu (PWR Pu vector after 10 years decay time) and PuMA (PWR spent fuel after 10 years decay time) fuel. In principle the Pu based fuel offers a higher Pu burn-up in comparison to the PuMA based fuel. The PuMA fuel burns not only Pu, but also Np and Am.

The performance of these fuels is similar. A detailed analysis has been done for the example of the 0.05%89-11PuMA fuel. The burn-up time has been limited to 3 years. Up to this time the MA fraction raises up to 0.25% in the liquid lead, so this period of time is essential from the point of view

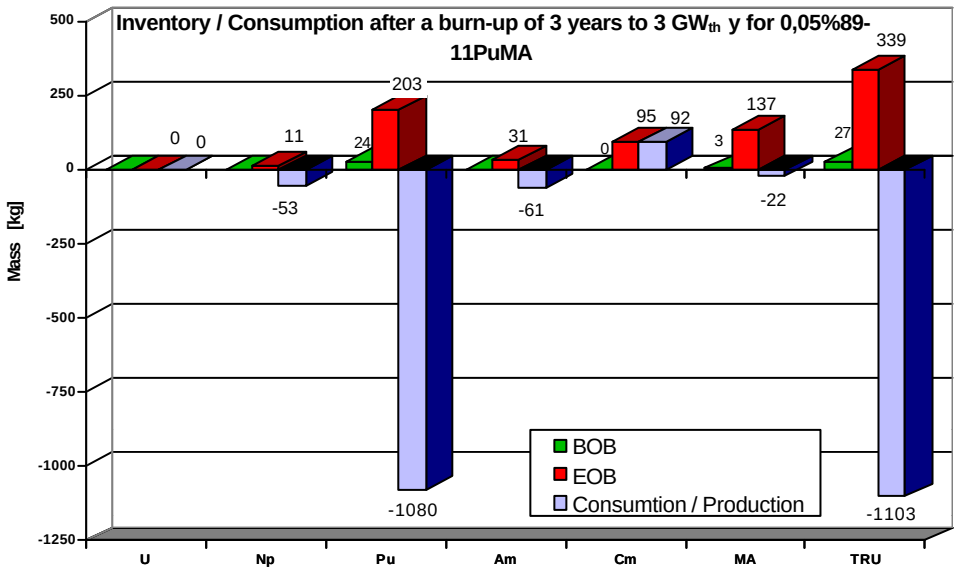

Figure 34. Inventory and consumption after burn-up of 3years at 1 GW_{th} per year.

of the solubility of MA's in liquid lead.

Fig. 34 summarizes the inventory and consumption of TRU for a burn-up of 3 years to 3 $GW_{th}y$. In three years the inventory per $1GW_{th}$ y raises up from 27 kg to 339 kg TRU. This means that the fraction of TRU in the liquid lead carrier grows from 0.05% (BOB) to 0.63% (EOB). In the same time 1103 kg TRU are burned. The biggest part of the consumed mass is Pu (1080 kg), but in the same way Np (53 kg) and Am (61kg) are burnt. The Cm mass grows up to 92 kg. Generally the system reaches a consumption over discharge ratio of 3.25 by 367 kg consumption of TRU per GW_{th} y. Keeping in mind that the thermal power of the plant has been 638 MW, the total TRU inventory in the plant is 217 kg after the burn-up time of three years. This is an important fact with respect to non-proliferation and nuclear safety.

The more detailed overview of the inventory increasing (Fig.35) and consumption behaviour (Fig.36) shows, that in the first year the inventory increases rapidly for Pu and all MA, but later on only Cm increases such rapidly in the 2nd and 3rd year. The other TRU's ascent gets more and more slowly by time. The consumption over the time is nearly constant with respect to the total mass and the kind of elements. In the case of Np and Am an increasing of the consumption during the burn-up time can be detected.

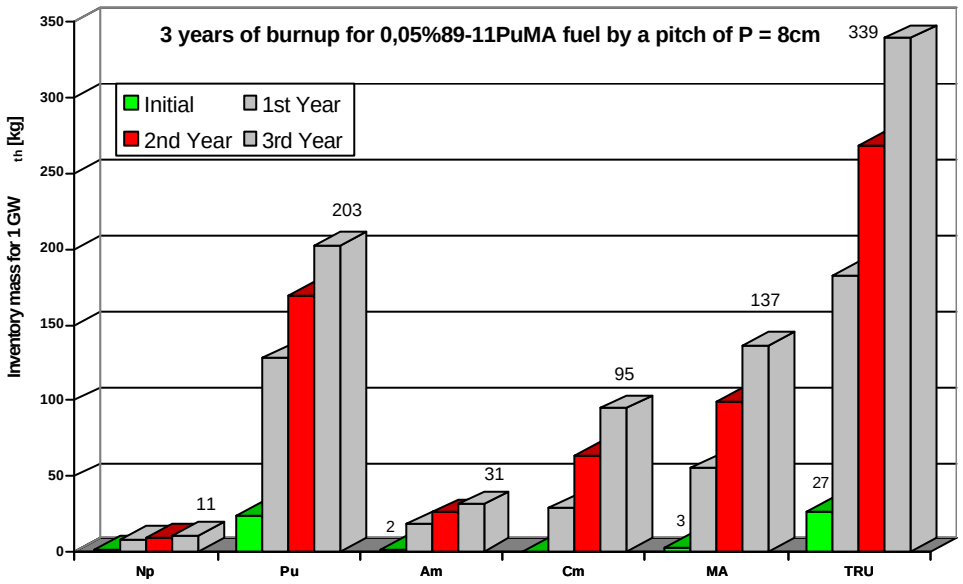

Figure 35. Inventory after a burn-up of 3 years at 1 GW_{th} per year.

During burn-up the ratio of Pu and MA in the fuel changes rapidly. Fig. 37 shows this behaviour. The start position is 89% Pu and 11% MA, with 6.4% Am, 4.4%Np and 0.2% Cm. After one year Am and Np reach a nearly constant fraction of 10% for Am and 3.4% for Np in the TRU. The fraction for Cm increases constantly over burn-up from initially 0.2% up to 28% after three years. The Pu fraction decreases during the same time from 89% down to 60%. Combined with the increasing of the TRU inventory, the fuel will be at the end of the burn-up (EOB) a 0.623%60-40PuMA fuel.

Fig. 38 shows the development of the Pu vector. Starting with the PWR Pu vector after 10 years decay time, the composition changes rapidly during the first 400 days of burn-up. After this time the Pu vector remains nearly constant, with the exception of ^{238}Pu, at 41.7% ^{242}Pu, 20% ^{240}Pu, 16.3% ^{239}Pu, 12.5% ^{241}Pu and 9.5% ^{238}Pu. The ^{238}Pu fraction increases slowly as a result of the

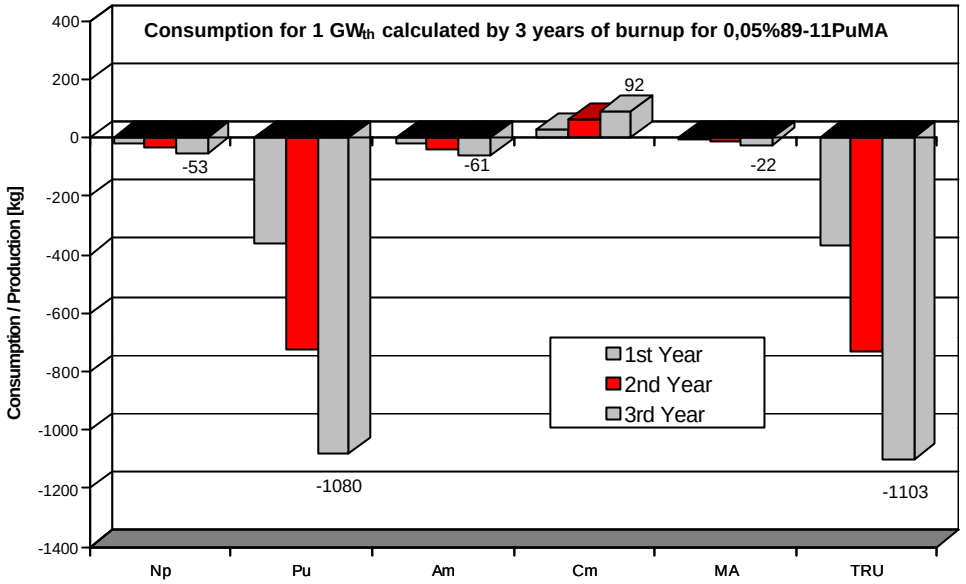

Figure 36. Inventory and consumption after a burn-up of 3years at 1 GW_{th} per year.

decay of ^{242}Cm. Due to this change of Pu vector the number of critical Pu mass (m_c = 10kg/PWR-Pu vector) increases slower, than the increase of the total Pu mass. For example the total Pu mass

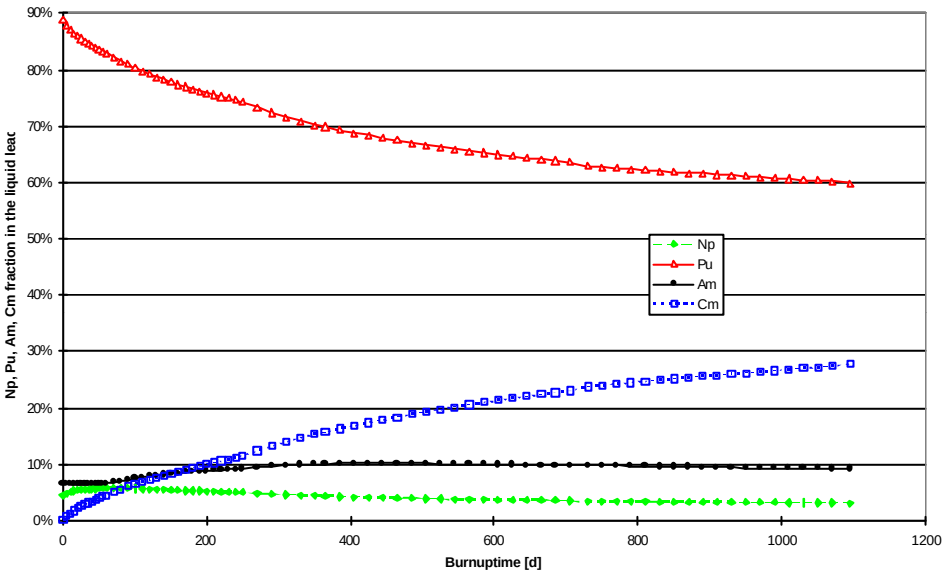

Figure 37. Pu MA composition during a burn time of 3 years for the 0.05%89-11PuMA fuel.

grows from 15.45 kg at BOB to 129.51 kg at EOB by 8.38 times, but the number of critical Pu masses increases only from 1.54 at BOB to 5.37 at EOB. In the case of a single loop cooling system the mass grows by a factor of 4 for BOB and EOB.

After 400 days burn time the Cm vector is dominated by ^{244}Cm (Fig. 38). After 600 days the ^{244}Cm fraction is nearly constant at 77%. The ^{242}Cm decreases to the final level of 9.2%. ^{246}Cm shows an opposite development. The fraction grows constantly to 8% after 3 years. After 600 days

the ^{245}Cm fraction is nearly constant at 4.5%. The total of the remaining Cm isotopes sum up to approximately 1%.

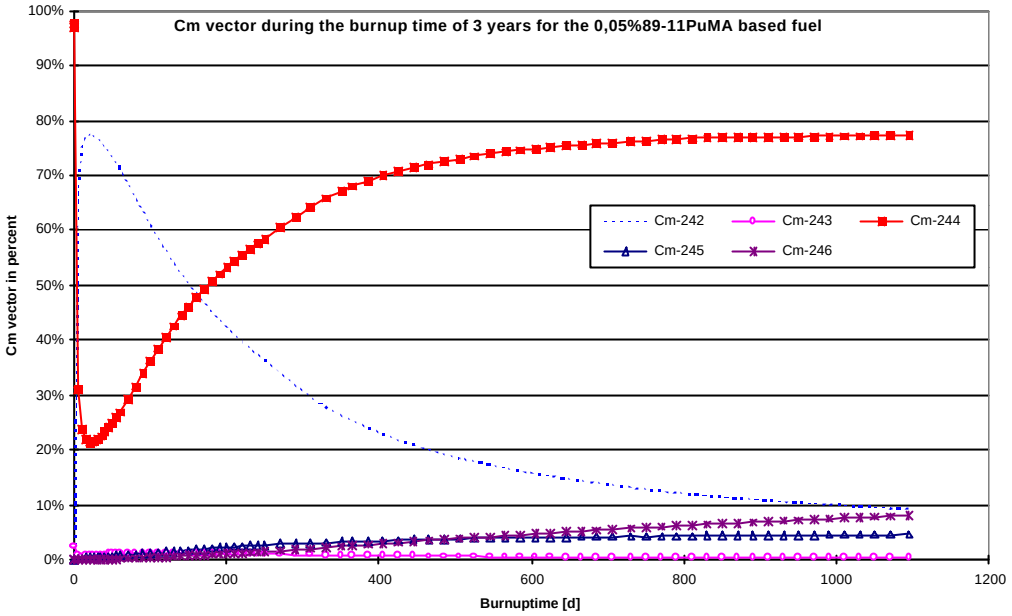

Figure 38. Process of the Cm vector during a burn-up of 3 years for 0.05%89-11PuMA fuel.

Due to the 18.1 year half-life of ^{244}Cm the mass of the most dominant isotope will be reduced after 100 years to less then 2.2%. ^{244}Cm decays to ^{240}Pu. This Pu isotope can be reinserted into the ADS facility.

Fig. 39 shows the mean neutron flux for the system during 3 years. The total flux declines in the first 100 days from 1×10^{15} n/s×cm^2 to 8.3×10^{14} n/s×cm^2. Later on the increasing becomes slightly in 1000 days from 8.3×10^{14} down to 6.8×10^{14}n/s×cm^2. The spectrum is dominated during the whole time by the thermal fraction, however, the fast part increases by time.

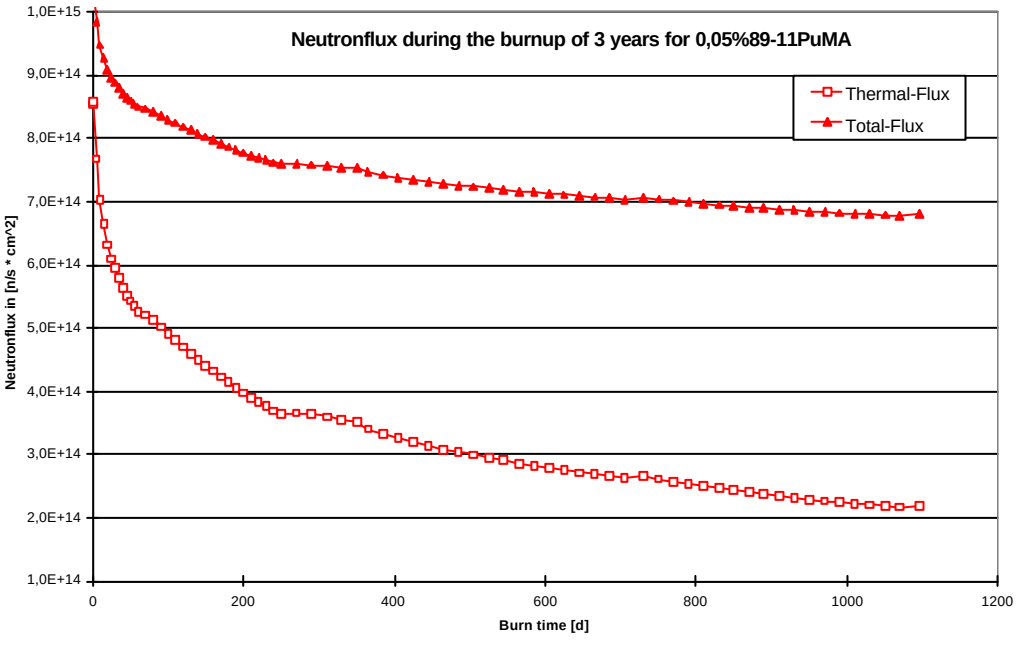

Figure 39. Neutron flux during burn time of 3 years for 0.05%89-11PuMA fuel.

The high and nearly constant k-value results in moderate requirements for accelerator performance. At the lowest k_{inf}-value of 0.992 during the 3 years of burn, which can be extrapolate to a k_{eff}-value of 0.972, a maximum accelerator current of 12.8 mA (k = 0.972) will be needed to produce necessary spallation neutrons (assuming 20 neutrons per proton). For an accelerator of 1.6 GeV the required power would be about 20 MW.

The system behaviour for a pure 0.05%Pu based fuel is similar. The biggest difference is a net-production of Am during the burn-up, in contrast to the consumption of Am and Np by the 89-11PuMA based fuel. On the other hand an increase of inventory is smaller, than for the PuMA fuel. As a result the consumption over discharge ratio is higher (5.42 with a two loop coolant system) with the pure Pu based fuel. At the end of the burn-up the fraction of TRU material in the liquid lead increases from 0.05% (BOB) to 0.36%.

2.7 Transmutation Performance

The optimized Jülicher ADS with a thermal neutron flux and liquid lead as a carrier of a low-concentrated TRU fuel offers a lot of advantages in a continuous operation mode. The TRU inventory in the system is very low, especially applying a double loop cooling system. TRU consumption is high, the k-value can be kept nearly constant at the desired subcriticality level and thus the required accelerator power stays constant. In comparison to other options to burn Pu and/or MA it is a very efficient system with a high transmutation rate.

In order to compare the transmutation performance of different transmutation systems reduction of TRU mass respectively to the radiotoxicity of the waste can be chosen as a criterion. The transmuted mass of TRU should be normalized/calculated for 1 $GW_{th}y$. The reference to the thermal power makes it possible to compare ADS with reactors.

To account for difficulties to work with high masses of Pu and MA (nuclear safety, non-proliferation, etc.), it is useful to establish the ratio of TRU consumption over the TRU discharge as a second coefficient. The higher this value, the better the system performs. For the systems with continuous feed and extraction, an average over the total TRU inventory at EOC over the total TRU consumption should be used.

Table IV summarizes the key results for the Pu and Pu/MA burners.

Table IV. Transmutation performance of different systems.

System	Consumption/$GW_{th}y$ [kg]	Consumption/discharge ratio
„Jülicher“ ADS		
Pu-based fuel	355.5 kg	5.42 double loop / 1.35 single loop
PuMA based fuel	367.4 kg	3.25 double loop/ 0.81 single loop

An additional key variable for ADS will be the requested beam power. Obeying the technical situation and the costs, the beam power should be as low as possible. The maximum needed proton current for the beam is the important data. This value applies to the thermal system power. A conservatively value of 20 neutrons per proton at 1,6 GeV will be helpful to compare the different values.

Table V summarizes the requested proton beam current and the voltage.

Table V. Required proton beam for the ADS.

System	max. proton current [mA]	Power [MW]
„Jülicher“ ADS		
Pu-based fuel	16.8 mA	27 MW
PuMA based fuel	12.8 mA	20.5 MW

3. Molten Salt Subcritical Systems

Molten salt ADS were assessed in the IABAT project for incineration of transuranium elements and separately, only for minor actinide burning. As mentioned before this task was very limited, it **did not address** many important issues like associated partitioning chemistry, corrosion of molten salt and material compatibility, disposal of spent salt, and neither economical assessment. Instead it was focused on some physical characteristics and on assessing neutronics of the system.

The following parameters have been studied:

- Molten salt composition for a given type of neutron spectrum.
- Neutron spectrum of the system.
- Fuel feeding strategy to obtain an equilibrium fuel composition
- Accelerator power range matching the reactivity swing.
- Sensitivity of core parameters to:
  - Feed rate;
  - Accidental configurations;
  - Spectrum shift.

For the molten salt systems a very simple computational model (see Fig.40) has been used and calculations were performed in two separate modules: the high-energy transport (based on HETC code) followed by a low energy range processing that includes transport, depletion and core management.

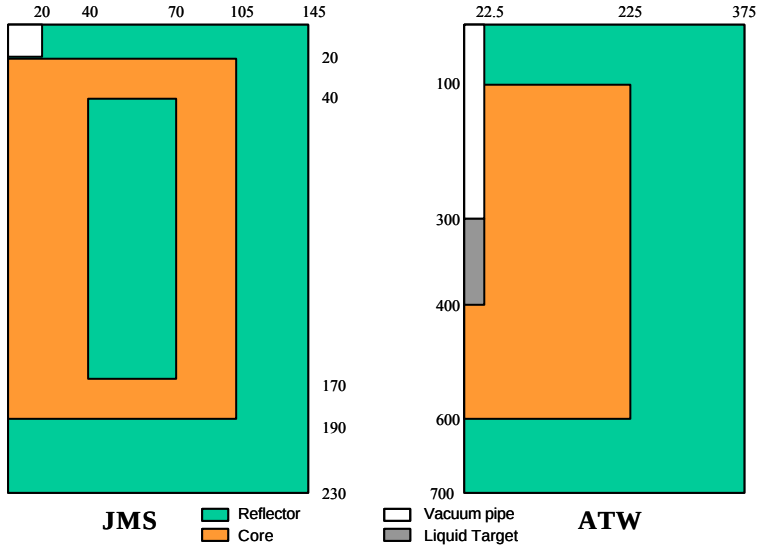

Figure 40. Geometrical model of molten salt systems. JMS –JAERI Molten Salt:a fast neutron molten salt system; ATW – Los Alamos Accelerator-Driven Transmutor of Waste: a thermal neutron molten salt system.

3.1 Description of applied codes and models

High Energy transport calculations have been performed from maximum energy of impinging protons down to a *cut off* level (20 MeV) using a CEA incarnation of HETC code [Bers96] and also a PSI version of HETC.

The Monte Carlo High Energy Transport allows to compute the source of spallation neutrons (see Fig. 41), driving the subcritical core. It also provides distributions of spallation product residuals and enables estimations of irradiation damages to

constructional materials. The spallation neutron source coming from high-energy transport essentially corresponds to isotropic evaporation neutrons with a mean energy ~ 3.5 MeV (for 1 GeV protons on a liquid lead target). These neutrons are registered on a dedicated file and passed to conventional neutron transport module conducting regular "reactor-like" calculations e.g. in a 2-D, deterministic code. Fig. 42 presents R-Z 2-dimensional spallation neutron source passed from HETC-calculation into ERANOS [Dori93] module.

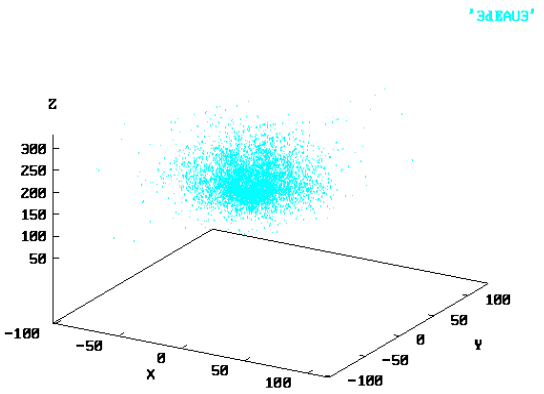

Figure 41. Spallation neutron source in a "Energy Amplifier" like model as a result of the High Energy Monte Carlo Transport in a 3D XYZ view.

Neutron transport calculations for a "reactor neutron energy range" have been performed using the ERANOS code system. Some part of the calculations has been also done with MICROX and TWODANT codes in their PSI versions.

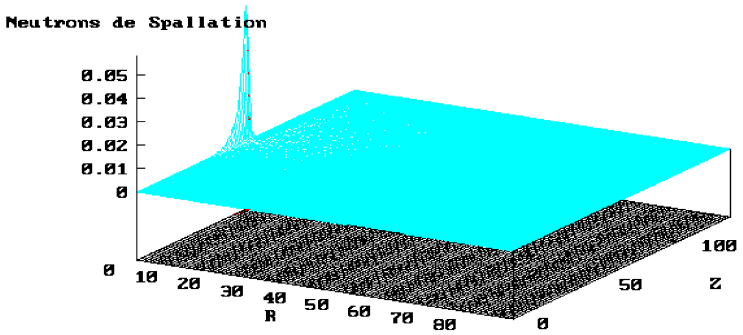

Figure 42. Spallation neutron source (an example of an "Energy Amplifier" like model) prepared for deterministic transport for a 2D RZ geometry in finite diferences S_4 - P_0 computations.

ERANOS is a set of deterministic tools and data for reactor physics developed at CEA. ERANOS consists of the following modules:

- ERALIB adjusted library [Fort96].
- ECCO lattice code [Rimp95].
- Deterministic transport in 2 or 3D (RZ, Cartesian and Hexagonal) by finite elements, finite differences, and nodal methods.
- 3-D Kinetics (nodal).
- Classical & generalised perturbation algorithms.
- Depletion and core management.

ERANOS is currently being validated for ADS calculations using the MUSE experiments [Salv96], [Lebr99].

3.2 Main Features of Molten Salt Systems

Two molten salt ADS have been studied:

- A JAERI Molten Salt - **JMS** - system designed to incinerate minor actinides corresponding to a PWR spent fuel after 3 years of cooling time. Fast neutron spectrum can be obtained due to high concentrations of heavy nuclides in chloride salts. JMS system was proposed by JAERI [Kato92] and its adaptation is described in [Youi98].
- An Accelerator-driven Transmuter of Waste – **ATW** – a thermal neutron system derived from the Los Alamos Accelerator Transmutation of Waste Project [BOWM91] and further developed in [Youi98]. ATW was designed to incinerate the transuranics (TRU's) corresponding to PWR spent fuel after 10 years of cooling time. This objective determines the actinide composition at equilibrium. The specific feature of this system is so called "superthermal" neutron spectrum originating from the fact that a very low concentration of TRU in fluoride salt allows to soften the neutron spectrum.

Table VI characterizes both systems and summarizes some results.

Table VI. Comparison of molten salt systems

	ATW-system	**JMS**
Objective	Incineration of transuranium elements.	Incineration of minor actinides (no Pu).
Fuel carrier	Molten fluoride 79.27 LiF - 20.67 BeF_2 - 0.06(TRU)F_4 99.9925% enrichment of ^{7}Li.	Molten chloride 64 NaCl + 36 (MA)Cl_3:
Volume	80m^3 of graphite, fuel channels ∅ = 1.8 cm.	2.5 m^3
Composition and amount of TRU	100 kg of TRU at BOL ^{238}Pu ^{239}Pu ^{240}Pu ^{241}Pu ^{242}Pu ^{237}Np ^{241}Am ^{243}Am (1.4:51.5:23.8:7.9:4.8:4.6:5.1:0.9)	5 tons of MA' ^{237}Np ^{241}Am ^{243}Am ^{244}Am (56.9:26.3:11.8:5.1)
Neutron spectrum	"Superthermal", due to a large moderation in a high density graphite and low concentration of fissile materials.	Fast.
Target	Molten lead, 22.5 cm in radius and 100 cm in active height.	Molten salt (proton beam impinged directly on fuel carrier).
Power (MW_{th})	**500**	**800**
Transmutation performance	~ 180 kg/year -> 2/3 PWR/year.	290 kg of MA/year, (10 PWRs/year).

Proton beam characteristics	I_p = 11 mA; E_p = 800 MeV.	I = 24 mA; E_p = 1500 MeV.
k_{eff}	0.96 at equilibrium. Large reactivity swing after 1 year.	0.95 (equilibrium) - requires 0.77 at BOL.
Average neutron flux	2.45×10^{14} n/s.cm²	2.06×10^{15} n/cm².s
Power peaking factor : Max/Mean flux	**7**	**15**
Spallation yield	**19.5 n/p**	**25.8 n/p**
Strategy to reach equilibrium:		
Time to reach eq. (years)	~ 20 years for all nuclei except ^{246}Cm	~15
Specific features		Initial high fraction of MA's Pu build-up after 3 years
Strategy to keep k_{eff} constant	After 1 year of operation fissile feed must be higher than fission rate for ~5 years. Otherwise k_{eff} drops after 6 months to 0.65	After four years of operation, an absorber has to be dissolved into the salt in order to anchor k_{eff} at 0.95 *The feed rate remains constant :* An absorber (^{10}B) has to be dissolved into the salt in order to anchor k_{eff} at 0.95 (Equilibrium). *The feed rate is varying :* The feed rate is set to 0 for 6 years so that the inventory decreases to keep k_{eff} = 0.95

Table VII summarizes results on sensitivity studies of molten salt systems.

Table VII. Sensitivity studies

	ATW	**JMS**
Perturbation of the feed rate at equilibrium results		
Feed rate at 50% of default for 24 h	$\Delta k = -32$ pcm	$\Delta k = -1.5$ pcm
Feed rate at 150% of default for 24 h	$\Delta k = +46$ pcm	$\Delta k = +1.6$ pcm
Perturbation of the spallation neutron spectrum	no visible effects.	Softer spectrum changes neutron importance by φ^* - 9 %. Harder spectrum changes neutron importance: φ^* + 8 %.
Accidental situations (with salt volume fraction constant).		
Diameter of the graphite lattice channels increased of 30%	$\Delta k = +1400$ pcm	No data
Diameter of the graphite lattice channels decreased of 30%	$\Delta k = -1700$ pcm	No data
Graphite and salt mixed in a homogeneous dough	$\Delta k = -7500$ pcm	No data
Molten lead of the spallation target voided	$\Delta k = -410$ pcm	No data
A variation of the dimensions in the graphite lattice of ATW	No visible effects on k_{eff}.	No data
A collapse of that lattice, mixed with the fuel, would lead to	a severe *drop* in reactivity.	No data

4. Comparison of Critical and Sub-critical Systems

A first systematic discussion of the different characteristics of possible critical reactor systems (CRS) and accelerator driven systems (ADS) is given in reference [Broe98a]. It is proposed only to compare similar systems, based on the same design principles. Comparisons concerning applied calculation procedures, flux and power distributions, power level control, burn-up behaviour, incineration potential, aspects of dynamics and accident analysis and possible future R&D-work related to fast neutron spectrum designs of CRS and ADS are discussed in this reference. The main arguments for the ADS concepts are usually the improved safety, compared to CRS. Indeed, some ADS objectives hardly may be realized with CRS, e.g. incineration of larger amounts of long-lived fission products or of heavy fuel isotopes with unfavourable properties for the dynamics behaviour (delayed neutron fractions, coolant density and fuel temperature reactivity coefficients, etc.). A comparison of similar fast spectrum CRS and ADS designs shows an improvement of the safety

characteristics of an ADS, caused by the lower required fissile enrichments. However, it is not clear that in fast spectrum ADS recriticality during core damaging accidents can be avoided in all circumstances. In the case core damaging accidents with recriticality cannot be excluded, reconsidering thermal ADS may be a more suitable solution. Finally one has to keep in mind that both **critical and sub-critical burner reactors** only may be run if reprocessing plants with adequate capacity for the fuel cycles of interest are realized.

Fig. 43 shows an attempt to put ADS on "equal footing" with reactors concerning their transmutation potential. The comparison is based on the two key parameters: TRU consumption by 1 GW_{th} year and the fraction of consumption over discharge. (For Jülicher system these values have been calculated for a double loop coolant system which enhances significantly transmutation potential. For a single loop coolant system the fraction of consumption over discharge decreases by approx. 4.).

The serious comparison of ADS and critical reactors is not an easy task and now it is a subject of many studies, including a NEA/OECD study "Comparative Study of ADS and FR in Advanced Nuclear Fuel Cycles" [NEA99]

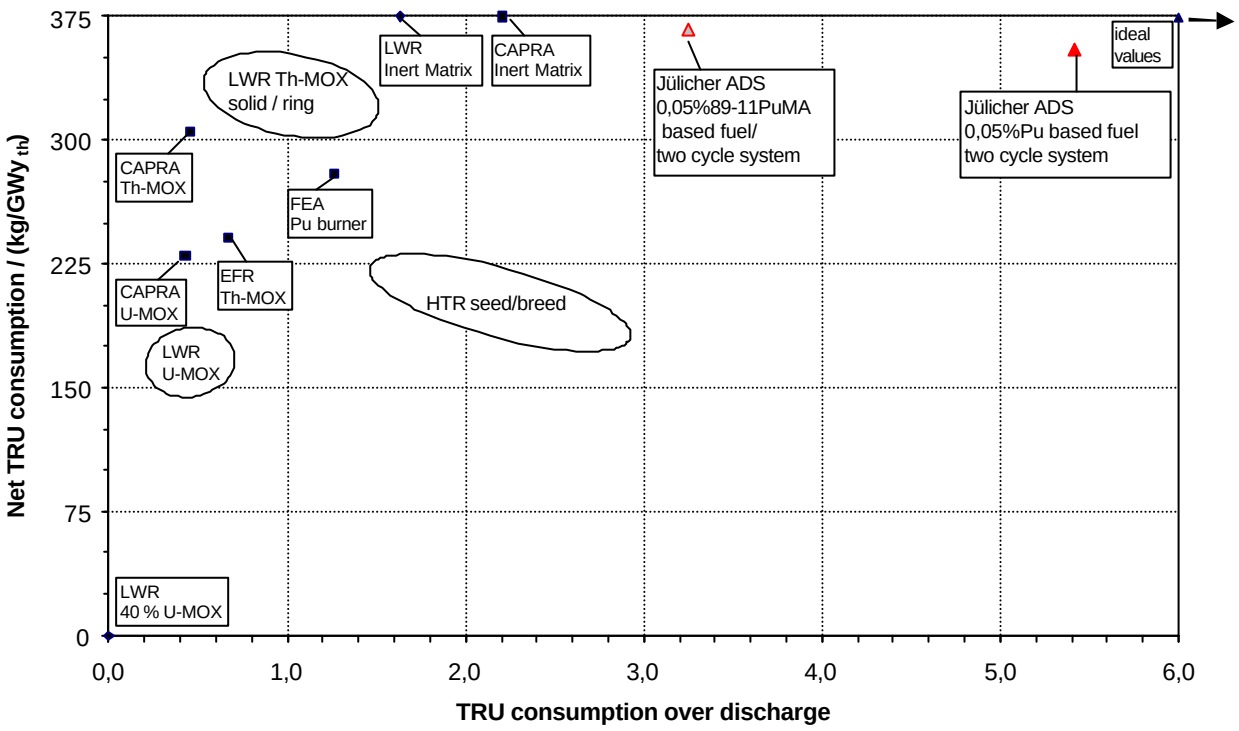

Figure 43. Comparison of Pu / PuMA burner.

5. Proliferation Aspects of ADS

5.1 Introduction

In the 1940s, it was known from work with research accelerators, that bombardment of a uranium target by high-energy protons or deuterons would produce a large yield of neutrons. These neutrons could in turn be used to produce fissionable material through nuclear reactions. In 1941, Glenn Seaborg produced the first man-made plutonium using an accelerator.

During the period 1950-54, the MTA [AEC53, MTA54] (Materials Testing Accelerator) program at Lawrence Livermore (at that time the Livermore Research Laboratory) investigated in detail the use of accelerators to produce fissionable material. Almost concurrently in Canada, Lewis [Lewi52] realised the value of accelerator breeding in the power programme and initiated spallation neutron yield measurements with the McGill cyclotron.

The objective of the MTA program was to show that significant quantities of fissionable materials could be produced reliably and economically compared with the production reactors at Hanford and Savannah River. By the end of 1952, an MTA electronuclear production plant concept known as A-12 had been developed. The accelerator was designed to produce a 500 mA current of deuterons with an energy of 350 MeV. These deuterons would be converted to neutrons, and then to ^{239}Pu through neutron capture reactions with uranium in the target. A production rate of 564 kg plutonium per year at a cost of $230 per gram was estimated for the A-12 concept. In August 1952 the Atomic Energy Commission cancelled the A-12 construction program and limited further work to operation of a less powerful (35 MeV deuteron) test accelerator and other experimental investigations. In the period to 1954 considerable improvements in the accelerator and in particular to the target physics resulted in an improved concept known as C-50. The accelerator was designed to produce a 320 mA current of deuterons with an energy of 500 MeV. Although the annual production rate of plutonium was unchanged, the estimated cost per gram was almost halved to $124.

The project ended in 1954 and the documents were declassified in 1957. Apparently the MTA was considered far from being a practical application!

A materials production accelerator - the "Electronuclear Reactor" - was patented in 1960 by Lawrence et al [Lawr60] for *"commercially adequate quantities of materials which must be produced artificially by nuclear reactions"*. The targets considered were natural uranium and thorium and the artificially produced materials were ^{239}Pu and ^{233}U respectively. At Chalk River in Canada, the Intense Neutron Generator (ING) [Barth66] concept was hailed as "*of potentially great significance in the long term power outlook, ING would open the door to methods of electrical breeding of fissile material and, with development of efficient accelerators and associated technology, promises a radical new approach to economic power*".

Later studies (1975-88) on the Fertile-to-Fissile Conversion (FERFICON) [Gilm88] Program - a collaborative effort with various laboratories - investigated the energy dependence, up to 800 MeV, of the fertile-to-fissile conversion efficiency using standardised target materials and geometry's.

The Zangger Committee was formed in the early 1970s to establish guidelines for implementing export controls of the Nuclear Non-proliferation Treaty[7]. Basically it covered special fissionable material and technology for the production of this material. The list of controlled items developed by this committee became known as the Trigger List since exports of such items triggers IAEA safeguards. Agreements accepted by member states are published in the IAEAs Information Circular (INFCIRC) 209 Series.

The Nuclear Suppliers Group (NSG) [Mult96] formed in 1974, went a step further in its guidelines to ensure that nuclear co-operation did not contribute to proliferation. For Trigger List exports, NSG guidelines required further restrictions than those imposed by the Zangger Committee. In 1992, the NSG extended its controls to dual use goods (i.e. goods which could be used for both civil and military activities. Hence the NSG guidelines control technology included in the Trigger List

and Dual-Use Goods. These guidelines are also published in the IAEA Information Circular Series. INFCIRC/254 Part 1[Guid96a] covers Nuclear Transfers and INFCIRC/254 Part 2 [Guid96b] covers Dual-Use equipment, Material and Technology. The screening limit used in the above is a capability to produce 100g Pu per year.

The Accelerator Transmutation of Waste (ATW) programme [Over1, Taki95] started around 1990 and is mainly concerned with destroying rather than producing material. Both the United States and France are currently considering programs for the Accelerator Production of Tritium (APT) [APT1].

5.2 Fissile Material Production Rate

5.2.1 An Estimate of the Neutron Intensity from Spallation

Denote the accelerator current and proton energy as I and E respectively. The rate at which protons are emitted from the accelerator R_p is given by

$$R_p = I/e = 6.25x10^{15}.I(mA) \quad (protons/s) \tag{1}$$

where e is the electronic charge. Through the spallation process, each proton gives rise to S neutrons such that the rate of neutron production is given by

$$R_n = S.R_p = 6.25x10^{15}.I(mA).S \quad (neutrons/s) \tag{2}$$

The spallation multiplication factor depends on the proton energy, target geometry and material. For a cylindrical target, 10 cm in diameter and 60 cm in length [Vaz95] we have

$$S = C_M.(E-0.12) \ \ for\ E \geq 0.12\ GeV \tag{3}$$

where the materials constant C_M = 22.7 for Pb and 36.7 for depleted uranium.

5.2.2 Fissile material production in the blanket

We consider the device composed by a spallation target that converts the ion beam into neutrons and a converting blanket producing the fissile material by neutron capture in a proper material. For simplicity here, we consider a blanket composed only of a single fertile material, ^{238}U or ^{232}Th metal.

We assume that the dominant reactions in the blanket are radiative capture and fission. Of the neutrons absorbed, a fraction $\sigma_c/(\sigma_c+\sigma_f)$ will lead to fissionable atom production by radiative capture. For every neutron absorbed by fission, $1/(1-k_{eff})$ neutrons will result in multiplication in the blanket medium. Hence for every neutron entering the blanket, the total rate of fissionable atoms R_{fa} which result is given by

$$R_{fa} = R_n\,.\,\eta = R_n.\ 1/(1-k_{eff}).\ \sigma_c/(\sigma_c+\sigma_f)$$

or

$$R_{fa} = R_n.(1-k_{eff}/\nu)/(1-k_{eff}) \tag{4}$$

where ν is the number of neutron produced by fission. The efficiency factor η depends strongly on the energy of the neutrons emerging from the spallation target. The formula reported in the previous section gives the average number of neutrons produced by the spallation target but does not give any information about the energy distribution of these neutrons. We estimate that the average energy is between 0 and 10 MeV.

On this basis we have performed some neutron diffusion calculations to evaluate the efficiency term as a function of the neutron energy. We have used a 1-D neutron transport code: the XSDRNPM module from the SCALE [Petr1] system.

We have considered a sphere of radius of 50 cm, to ensure neutron losses by leakage are very low, and supposed a point-wise mono-energetic neutron source located at the centre of the sphere. The code can compute the space and energy distribution of neutrons in the medium and the reaction rate. Table VIII shows the resulting reaction rates normalised to one source neutron. The results agree with the simple formula given in relation 4.

Table VIII. Reaction rates normalised to a source neutron

Target	E(MeV)	n, 2n	fission	capture
^{238}U	10	0.28	0.50	2.24
"	6	0.01	0.43	1.75
"	3	-	0.32	1.49
"	1	-	0.02	0.99
^{232}Th	10	0.63	0.17	1.91
"	6	-	0.08	1.09
"	3	-	0.05	1.04
"	1	-	-	0.98

The efficiency term coincides with the last column. We see that it is almost close to one and increases to two when the neutron energy approaches 10 MeV due to the multiplication effect caused by fission. Of course this is true for a quasi-infinite pure homogeneous medium. In a finite medium and in the presence of other materials (as happens in practice) these values are reduced due to leakage and parasitic capture. The calculation of efficiency needs a correct description of the geometry and composition of the assembly and is beyond the scope of the present work.

5.2.3 Most Effective Irradiation Time

What is the optimum time for irradiation from the standpoint of maximum fissile material production? For very short irradiation times, the amount of fissile material produced is directly proportional to the irradiation time. For long irradiation times, a steady state is reached whereby the fissile material production and loss (e.g. due to fission, capture etc.) rates balance exactly. At this point, increasing the irradiation time further will not result in an increase in the amount of fissile material. This latter effect can be avoided by continuously removing the irradiated material through the use for example of liquid recycling. Alternatively, one can ask the question how long can a target block be irradiated in the 'linear growth' regime before the steady state value is reached. To investigate this problem we must consider the reaction kinetics in more detail.

Irradiation of a uranium target with neutrons gives rise to the following reactions (we assume again that the neutron energies are below a few MeV so that capture reactions play a significant role):

$$^{238}U \rightarrow {}^{239}U$$
$$\downarrow$$
$$^{239}Np \rightarrow {}^{240}Np$$
$$\downarrow \qquad \downarrow$$
$$^{239}Pu \rightarrow {}^{240}Pu \rightarrow \ldots\ldots \qquad (5)$$

In steady state, the concentrations of ^{239}Np and ^{239}Pu are given by

$$^{239}Np(\infty) = s_c(^{238}U).f/[l(^{239}Np) + s_a(^{239}Np).f]$$
$$^{239}Pu(\infty) = {}^{239}Np(\infty).l(^{239}Np)/[s_a(^{239}Pu).f] \qquad (6)$$

where ϕ is the neutron flux, σ_c and $\sigma_a = (\sigma_c + \sigma_f)$ the radiative capture and absorption cross sections, and ∞ denotes the value in steady state. Assuming the neptunium instantaneously reaches its steady state value, the build-up of plutonium arises from the decay of the neptunium i.e.

$$d(^{239}Pu)/dt \; @ \; [d(^{239}Pu)/dt]_{t=0} = l(^{239}Np).{}^{239}Np(\infty) \qquad (7)$$

It follows that the time required for the plutonium to reach its steady value is given by:

$$t = {}^{239}Pu(\infty)/[d(^{239}Pu)/dt]_{t=0}$$
$$= {}^{239}Pu(\infty)/[l(^{239}Np).{}^{239}Np(\infty)] = [s_a(^{239}Pu).f]^{-1}$$

or

$$t(y) = [7x10^{-17}.f(cm^{-2}\,s^{-1})]^{-1} \qquad (8)$$

hence for $\phi = 10^{17}$ cm^{-2} s^{-1}, τ = (1/7)y = 1.7 months!, for $\phi = 10^{14}$ cm^{-2} s^{-1}, τ = 143y! Another possibility, of course, is to irradiate only until the steady ^{239}Np concentration is reached. After this time the uranium containing neptunium is removed and the neptunium decays with a half-life of 2.35 d to ^{239}Pu. The time dependent build-up of ^{239}Np is given by:

$$^{239}Np = {}^{239}Np(\infty).(1-exp(-at)) \qquad (9)$$

where $a = [\lambda(^{239}Np) + \sigma_a(^{239}Np).\phi]$. The time required for the neptunium to reach its steady value is given by

$$t = {}^{239}Np(\infty)/[d(^{239}Np)/dt]_{t=0} = 1/a$$
$$= [l(^{239}Np) + s_a(^{239}Np).f]^{-1} \; @ \; [l(^{239}Np)]^{-1} = 3.4d \qquad (10)$$

Notice, however, that the steady state value ^{239}Np(∞) is sensitive to the flux as shown in Table IX.

Table IX. Uranium target / blanket. Equilibrium concentration of ^{239}Np and time τ required to reach this value.

ϕ (cm^{-2} s^{-1})	τ (days)	$^{239}Np(\infty)/^{238}U$ (%)
10^{14}	3.4	0.0009
10^{15}	3.4	0.009
10^{16}	3.3	0.09
10^{17}	3.2	0.8
10^{18}	2.0	5.4

Similarly, the reaction path for thorium is:

$$\begin{array}{ccc} ^{232}Th & \rightarrow & ^{233}Th \\ \downarrow & & \\ ^{233}Pa & \rightarrow & ^{234}Pa \\ \downarrow & & \downarrow \\ ^{233}U & \rightarrow & ^{234}U \rightarrow \ldots\ldots \end{array} \qquad (11)$$

with the results shown in Table X.

Table X. Thorium target/blanket. Equilibrium concentration of ^{233}Pa and time τ required to reach this value.

ϕ (cm^{-2} s^{-1})	τ (days)	$^{233}Pa(\infty)/^{232}Th$ (%)
10^{14}	38.9	0.01
10^{15}	38.8	0.1
10^{16}	37.6	1.0
10^{17}	29.0	7.7
10^{18}	8.7	23

Clearly, clandestine irradiation of thorium is the more serious problem. The amount of fissionable material which is generated is a factor ten higher than through the irradiation of uranium.

5.3 Accelerators for Nuclear Applications

In Table XI we list some present and future accelerator systems.

Table XI. Present and future accelerators systems

Accelerator (Organisation)	Status	E (MeV)	I (mA)	Yield (n/s)
CYCLONE (IBA s.a.) [Jong95, Cohi96, Jong1, Jong94]	commercial	30	0.5	-
ADONIS (IBA s.a.) [Jong95, Cohi96, Jong1, Jong94]	commercial	150	1.5	$9x10^{15}$
SINQ (PSI) [SINQ]	in operation	590	1.5	$6x10^{16}$
Moscow Meson Factory [MMF]	in operation	600	0.5	$3x10^{16}$
ISOLAB [Vaz95]	design	800	< 1	$< 1x10^{17}$
Rubbiatron- Linac [Rubb96]	design	1000	30	-
Rubbiatron-Cyclo-Linac [Rubb96]	design	2500	10	-
ATW, ABC	design	1600	100	$3x10^{19}$
LAMPF/LANSCE [APT1]	in operation	800	<1	-
OMEGA [Part95](Japan)	design	1500	39	-

From the previous section, the relation for the rate of fissionable atom production can be expressed as

$$R_{fa} = \eta.S.R_p = \eta.\ S.\ R_p*(3.15x10^7/6.02x10^{23})*M_{fa}$$

or (12)

$$R_{fa}(g/y) = 5.23x10^{-17}.M_{fa}.\eta.\ S.\ R_p(protons/s)$$

where M_{fa} is the molecular weight of the fissionable atom. It follows that:

ADONIS (I.B.A.): uranium target/blanket, S=1.1, η=1-2, $R_p=9x10^{15}$ protons/s, hence R_{239Pu} = 124g/y

Rubbiatron Linac: uranium target/blanket, S=32, η=1-2, $R_p=1.9x10^{17}$ protons/s, hence R_{239Pu} = 76 kg/y

5.4 Safeguards for ADS

Accelerator driven power units or waste burners will be subject to international safeguards provided any of the following conditions are satisfied:

a) fuel or target materials consist of thorium, uranium, or plutonium, which are already subject to I.A.E.A. or Euratom safeguards,
b) normal operation, misuse, or clandestine operation of the accelerator could be used for the production of significant quantities of fissionable material.

These features are by no means new in nuclear fuel cycle facilities. From the beginning of the peaceful use of nuclear energy, inherent proliferation concerns had to be covered by adequate international safeguards concepts and implementation.

As far as fresh or irradiated fuel is concerned, new verification techniques may need to be developed in order to permit verification of receipts to the ADS and shipments of nuclear material from the ADS. If the nuclear material becomes difficult to access for verification during the annual physical inventory verification, containment and surveillance methods will need to be applied to maintain continuity of knowledge on the inventory. Such systems exist and provide effective and efficient safeguards verification in different reactor types.

It is important, that safeguardability criteria be included in the design of the ADS from the beginning in order to assure cost effectiveness.

The production of fissionable materials, either during normal operation or by clandestine operation, is a feature which has to be covered already now in existing reactors. Particular cases are powerful research reactors or fast breeders, where fissionable material could be produced by the use of special fuel pins or blanket materials.

In such cases - and this will be the case also for ADS- a detailed diversion analysis is performed based on the design parameters and the layout of the system. Following this analysis, measures will be identified and implemented, which would assure the detection of misuse with a very high detection probably within the relevant detection time.

The most important safeguards measures for ADS would be containment and optical surveillance devices and monitoring systems. These systems allow one to "freeze" parts of the ADS such that any access for misuse or reconfiguration would be detected. Highly tamper resistant monitoring devices permit real time observations of important operational or system control data and would therefore indicate any deviation from normal operational practices.

The fact that the neutron source in the ADS is outside the reactor is a new feature but does not present a particular problem. It just requires that the neutron source is included in the safeguards system such that any attempt to misuse or re-direct the beam to a non-controlled location of targets would be detected. During the shutdown period of the ADS, assurance of "non-breeding" could for example be obtained by a tamper -resistant control of the power of the accelerator.

A first analysis of potential diversion paths for accelerator driven systems therefore shows, that many of the features developed and implemented for various nuclear reactor types could be applied. The safeguards concept for an accelerator driven system could therefore rely on the following basic elements:

-- verification of the design information
-- verification of fuel receipts and shipments
-- verification of the physical inventory
-- containment and surveillance measures to maintain continuity of knowledge
-- verification of nuclear material accountancy system
-- monitoring of essential system parameters

Major inspection activities would be related to the verification of the fuel receipts and fuel discharges, the physical inventory and the evaluation of containment and surveillance measures.

Depending on the detailed layout and operational characteristics of such a facility, and the relationship with the fuel fabricator or spent fuel receiver, the safeguards effort could be comparable to that of certain critical reactor types.

5.5 Conclusions

The number of fissile atoms which can be produced by a spallation neutron is given by equation (4) i.e.

$$\textit{fissile atoms per spallation neutron} = (1- k_{eff}/\nu)/(1-k_{eff})$$

which depends only on k_{eff} and ν the number of neutrons produced in fission! Hence the problem of maximising the fissile material production rate reduces to that of maximising k_{eff} and ν. In the calculations present here, we have considered only the simplest possible diversion scenario in which the proton beam is dumped into blocks of denatured uranium or natural thorium. Even in this case, 1-2 fissile atoms per spallation neutron can be obtained (from Table VIII). A further increase of a factor ten can be obtained by suitable design of the blanket (pin diameters, lattice pitches) by, for example use of natural uranium and a water moderator. An optimally moderated system with such materials can result in a k_{eff} in excess of 0.95.

Further optimisation can be obtained by maximising ν as the above relation shows. This could be achieved by clustering the rods closer (less moderator) immediately around the target. The higher the neutron energy, the higher the number of neutrons released in fission. Further from the target the rod spacing is increased to thermalise the neutrons and thereby increase the value of k.

At present, commercially available machines (ADONIS, I.B.A. Belgium) with proton energies around 150 MeV and currents of 1.5 mA (power 225kW), are at the limit of the technology threshold (capacity to produce 100g Pu per year) laid down by the I.A.E.A in their INFCIRC documents. It appears that next generation machines must be specified in the Trigger List and Dual-Use Goods.

In the future, large powerful accelerators (such as the Rubbiatron Cyclo-linac) may be used for power production and waste transmutation. Because of the size of these machines, they will automatically fall under I.A.E.A. safeguards. It has been shown that during the down time for such systems (e.g. required for fuel reloading), the accelerator beam current can be used for clandestine activities in which significant amounts of weapons grade material can be produced on a timescale of a few days to one month. Steps have to be taken to ensure that this does not occur (for example through the use of power monitors).

Another fundamental difference between a critical reactor and an accelerator driven sub-critical assembly is that the ADS can be used for "isotopic enrichment" and for "fissile material conversion". In the former process, the spallation neutrons can be surrounded by a multiplying medium such as spent reactor fuel ($k_{inf} \approx 0.9$) containing poor grade plutonium to "amplify" the neutron flux. This can then be used to breed pure Pu in the outer blanket. In the latter process, an enriched uranium blanket (containing for example 20% ^{235}U) can be used to amplify the neutron flux. These neutrons are captured by ^{238}U to produce ^{239}Pu. Because the Pu is a different element, it can easily be separated by standard chemical processing.

V. SPALLATION NEUTRON TARGET STUDIES

The spallation target being an interface module between accelerator and subcritical reactor is one of the most important components of ADS and may easily be a technological show-stopper for further development. Consequently, some efforts were put in the IABAT-project to assess the simulation tools for spallation targets and to propose solutions, which may mitigate some of the serious problems arising on merging accelerator and nuclear technologies.

Most calculations concerning spallation target were performed with high-energy transport codes: LAHET [Prae89], HETC [Arms72] and FLUKA [Fass93]. Some of the investigations have also been carried out with the beta test version 2.1.5 of MCNPX [Hugh97].

1. Basic Simulations and Benchmarking of Spallation Codes

1.1 Spallation Neutron Yields

The high-energy transport calculations were focused primarily on the spallation neutron yields and optimization of the target dimensions. Fig. 1 presents the spallation neutron yield for different target materials (Pb, W and Pb/Bi eutectic) as a function of the incident proton energy. Fig.2 shows the number of spallation neutron yield per proton and GeV (Pb, W and ^{238}U). Target length for this analysis has been chosen to 100 cm (close to the optimal length, see Figs 3 and 4) and diameter - only 25 cm. 25 cm diameter for a spallation target for protons of 1 to few GeV is not an optimal size (see Figs 3 and 4) and it has been chosen to simulate experimental target being under construction in the frame of the project 559 of the

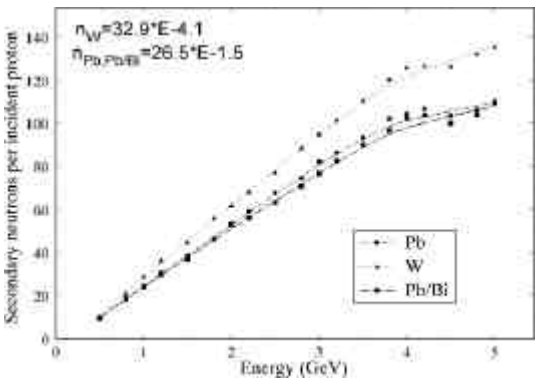

Figure 1. Spallation neutron production in different target materials as a function of the incident proton energy. Target diameter 25 cm, length 100cm. The expression for the neutron production (upper left corner) is valid for 0.8 < E < 4 GeV.

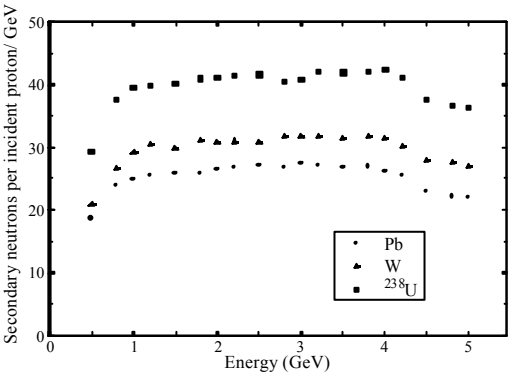

Figure 2. Spallation neutron production per GeV in different target materials as a function of the incident proton energy. Target diameter 25 cm, length 100cm.

International Science and Technology Centre [Yefi99]. It can be concluded that protons of energy between 1 – 2 GeV are most efficient giving the highest neutron yield per proton and GeV [Carl97]. Liquid Pb/Bi target of dimensions mentioned above can give about 25 n/p×GeV.

Figures 3 and 4 show the dependence of the spallation neutron yield for a cylindrical Pb/Bi spallation target as a function of target dimensions: radius and length for 1 and 1.6 GeV

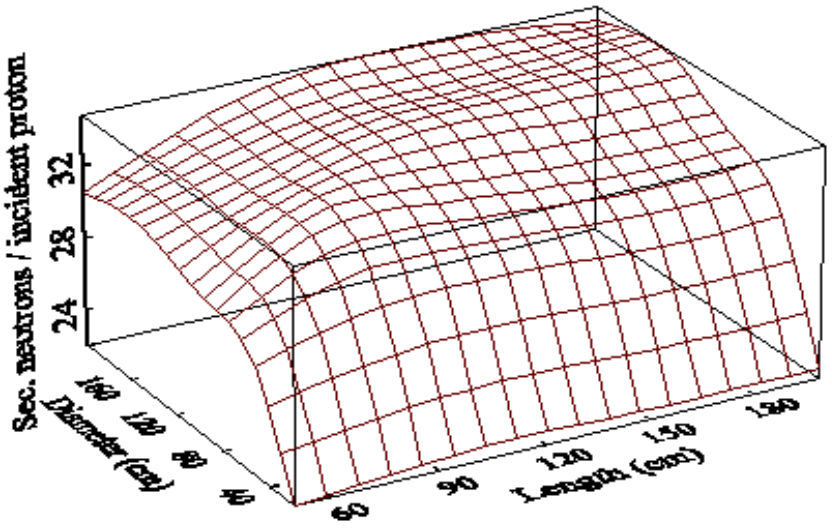

Figure 3. Spallation neutron yield per incident proton as a function of spallationtarget dimensions. Incident proton energy – 1.0 GeV, Pb/Bi cylindrical target.

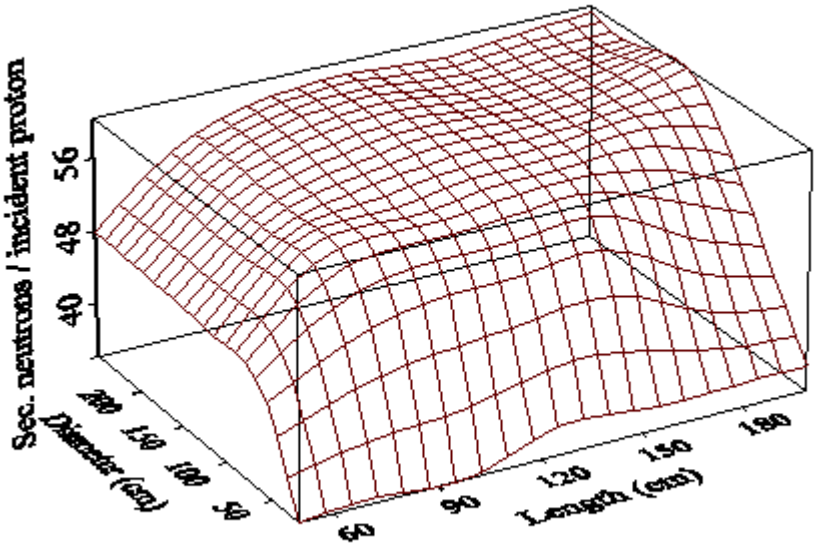

Figure 4. Spallation neutron yield per incident proton as a function of spallation target dimensions. Incident proton energy - 1.6 GeV, Pb/Bi cylindrical target.

protons, respectively. From these pictures may be concluded the optimal size for 1GeV target is 80x100 cm giving about 34 neutrons per proton. For 1.6 GeV protons an optimal size would be around 100x120 giving 56 neutrons/proton.

In order to validate and benchmark high-energy transport codes, simulations of the old Cosmotron experiments [Gibs66] have been performed. Table 1 summarizes LAHET results, corresponding to a proton beam having energy of 960 MeV. Most of the simulation results show an excellent agreement with the experimental data except for Be. The calculations indicate the trend to overestimate slightly the experimental data (with an exception for depleted U results).

Table I. Comparison between experimental and calculated neutron yields. Ep = 960 MeV. LAHET/MCNP calculations

Material	Target size (cm)	Experimental Data	Calculation Results
Uranium	10X60	40.5	39.5
Lead	20X60	20.5	21.5
Lead	10X60	17.2	18.3
Tin	10X60	12.5	12.2
Beryllium	10X10X91	2.7	1.79

For the lead target of different sizes the LAHET simulations have been also performed using Bertini and pre-equilibrium models as presented in Table II. It can be concluded that high-energy transport codes with pre-equilibrium model give reliable results for the spallation neutron yields. This conclusion is very important for ADS simulations because neutron yields is a crucial parameter determining the accelerator power and having a big weight for economical estimation of ADS costs.

Table II Spallation neutron yields for a lead target. LAHET simulations of Cosmotron experiments

Proton Energy (MeV)	Target size(cm)	Experimental Data	Calculation Results	
			Bertini	Preequilibrium
540	10X60	7.90	9.514	7.948
720	10X60	12.05	14.582	12.834
960	10X60	16.82	21.054	18.151
1470	10X60	26.82	31.488	30.136
540	20X60	8.60	10.583	9.037
720	20X60	14.09	16.324	14.288
960	20X60	20.46	22.541	20.979
1470	20X60	31.82	35.213	32.77

Fig. 5 presents FZK benchmark results for LAHET and a test version of MCNPX and demonstrates a very good agreement between these 2 codes for the neutron spectrum calculations from 600 MeV protons in a spallation target of lead.

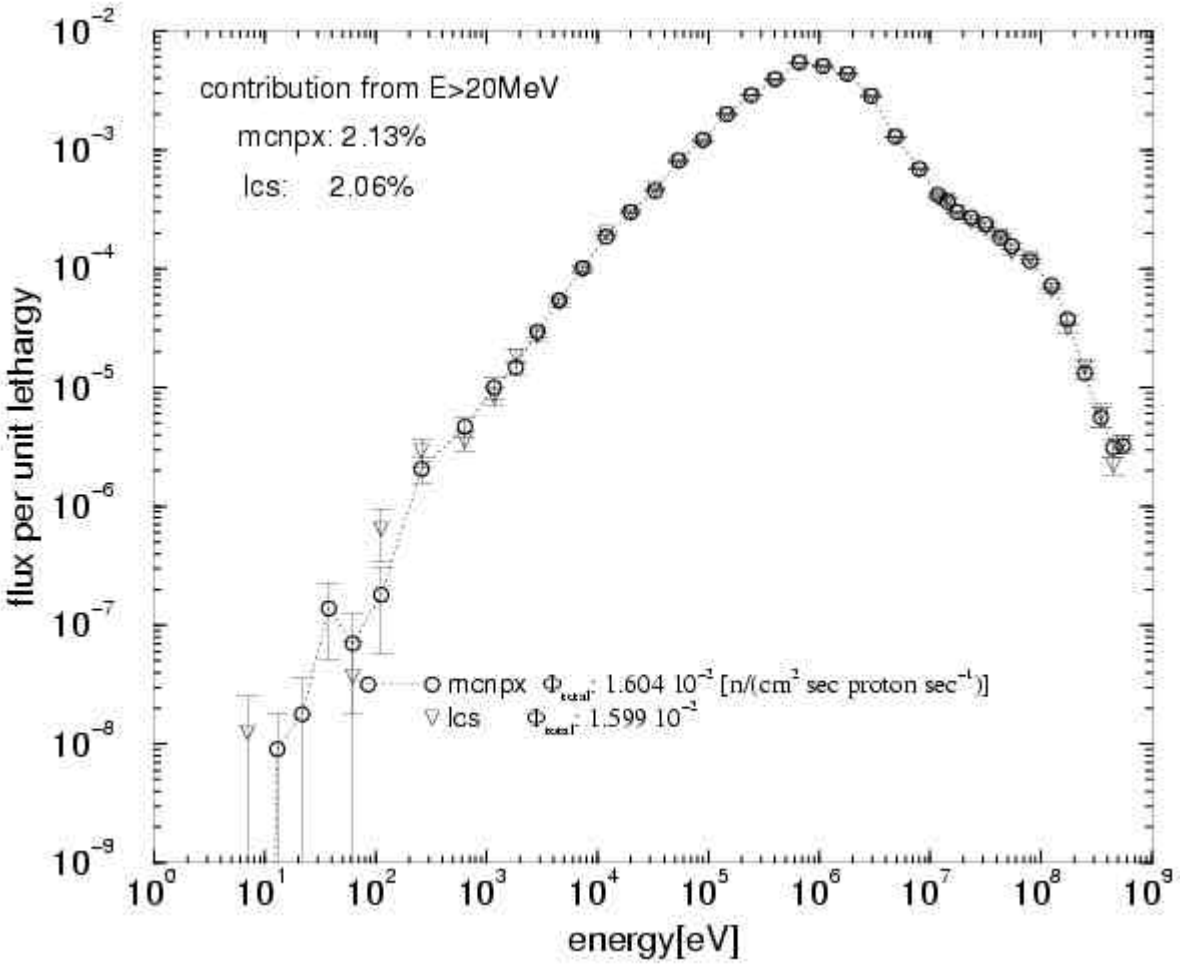

Figure 5. Comparison of neutron spectra from MCNPX and LAHET in a target window.

1.2 Energy Deposition

Thermal hydraulics and thermal stresses in the spallation target, particularly in the target window, have a major impact on the target performance. In this area high power densities may occur and reliable calculation methods are required for the energy deposition in order to be able to design the heat removal facilities. The main goal of the investigation (see also reference [Broe99]) is the determination of the spatial distribution of the energy deposition in the target. Most of the calculations have been carried out with the LAHET Code System (LCS), HETC [Bers96] and with FLUKA. For the nuclear model parameters that have to be chosen by the input of LAHET the default values are used, with the only exception that a pre-equilibrium phase following the intranuclear cascade was specified. For the calculations the following models and methods are used (in parentheses the corresponding LCS input variables):

Table III. Models, methods, parameters and simplifications used in High-Energy Transport

LAHET (corresponding LCS parameter in parenthesis)	HETC
The Bertini model for the simulation of the intranuclear cascade (IEXISA=0)	The recoil of struck nuclei + de-excitation or decay of these nuclides → primary energy deposition to the medium. Recoil corresponds to local energy deposition.
A pre-equilibrium model following the intranuclear cascade (IPREQ=1)	Ionization - secondary process of energy deposition, non-local
The RAL (Rutherford and Appleton Laboratories) evaporation-fission model (IEVAP=0)	The Bethe formula applied to all particles and over the whole geometry of the model
For light nuclei (A<18) the evaporation model is replaced by the Fermi breakup model (IFBRK=1)	Neglected phenomena: ▪ The Bremstrahlung, neither for electrons nor for protons. ▪ The Cerenkov effects for protons ▪ The decay of all activated elements and the transport of consecutive radiation
The Gilbert-Cameron-Cook-Ignatyuk level density model (ILVDEN=0)	
The neutron elastic scattering data file ELSTIN which is part of the LCS system (NOELAS=23)	
The nucleon-pion transport option (NBERTP=1)	
See [Prae94] and references and details	

Fig. 6 gives the geometry model of the targets, on the left- based on preliminary design considerations at FZK [Chen99], on the right –model used at CEA.

1.2.1 CEA Target Models

A simpler 2D-RZ spallation target model embedded in ADS subcritical core was investigated – see Fig. 7. The 2-D RZ geometry seems convenient to ADS' in a first approximation as these systems have a cylindrical symmetry. Moreover, 2D is quite reasonable as it gives a large volume for integration in the meshes where statistics in Monte Carlo calculations is often low

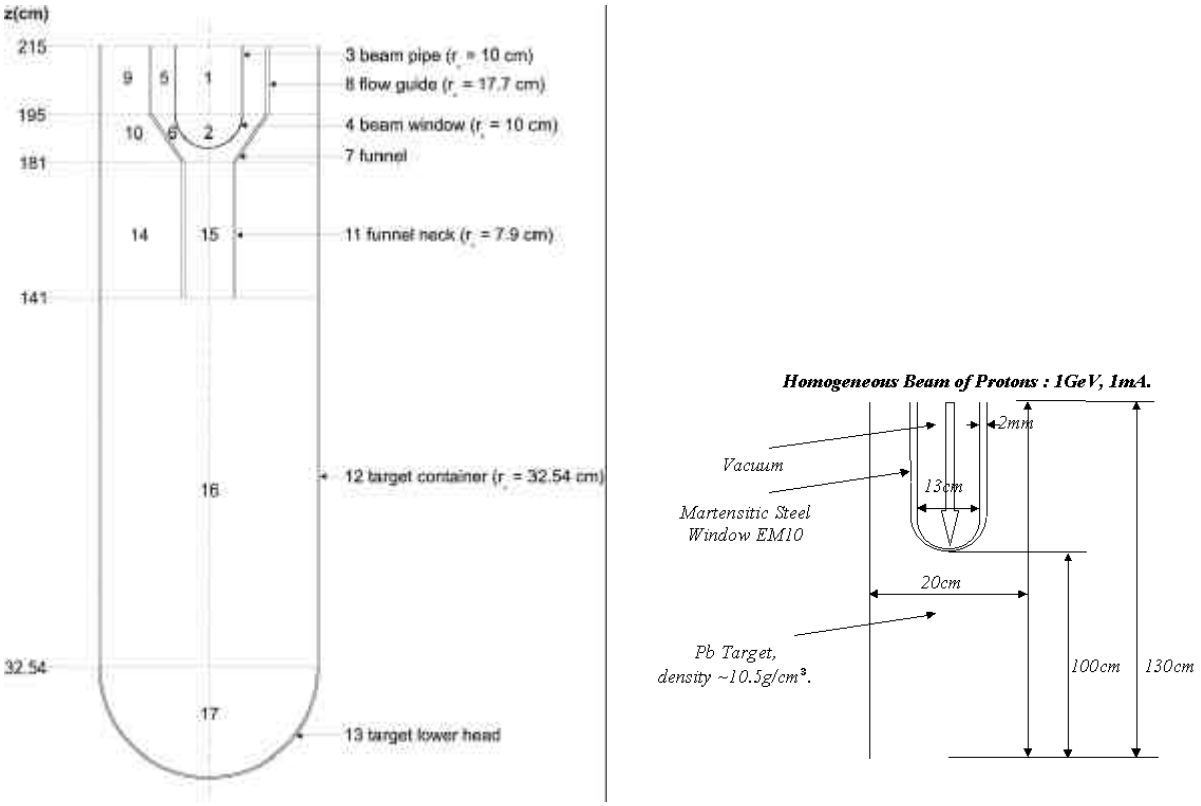

Figure 6. Geometry model of the lead targets used for the energy deposition calculations. On the left FZK-model simulated with LAHET, on the right: CEA-model simulated with HETC.

This model is very flexible giving a user possibility to vary dimensions of the cylinder corresponding and some other parameters important for calculations: Radius, Height, Mesh size on R and Z. The results are given in a 2D matrix, where Q(i,j) is the energy given in ring of radius r_i at height z_j. This includes local and scattered phenomena. The mesh volume is taken into account ($V = \pi(r_{i+1}^2 - r^2{}_i).\Delta z$) and does not depend on Z as the grid is regular $\Delta z = C^{st}$. The units can be either MeV/cm^3/ incident proton or W/mAcm^3. A typical order of magnitude of deposited power rate in a heavy material for 1 GeV protons is ~1 kW/cm^{3}mA.

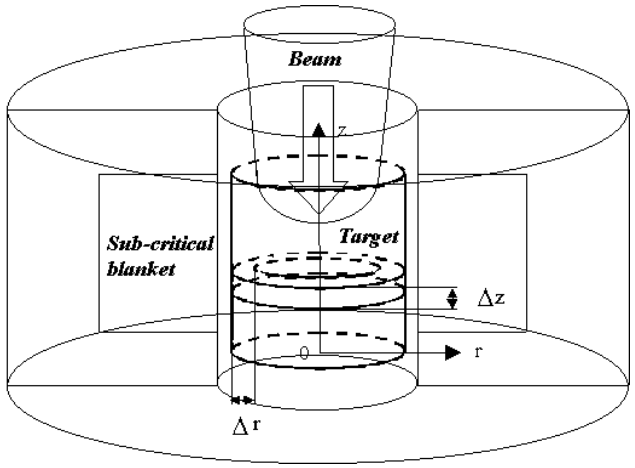

Figure 7. A CEA ADS model for target calculations.

Dimensions for the grid

The grid corresponds to the lattice of R-Z meshes. The dimensions of a singular mesh are given by Δz and Δr.

The size of a mesh must be large enough to collect enough statistics in the region of interest. It must also take into account the important physical parameters, that is why recoil was treated (mean free path ~ μm) as local and contained inside one mesh.

Methodology

There are two options to iterate deposited energy: the first and easiest corresponds to the recoil + deexcitation energy as these events are local (although some corrections may be applied to the deexcitation) and the second is the ionisation which must be treated as a non-local phenomenon.

Recoil

The energy of the recoiled nuclides after an interaction with protons may range from 0 eV to almost proton beam energy i.e. ~ GeV. The mean free path for heavy target nuclides is several tens of μm (1 μm for a 50 MeV Pb nucleus) and depends on the material density. So it is practical to make a grid with meshes larger than 50 μm thus making recoil a local phenomenon.

The grid dimensions are determined so that each local event record in the history file would be stored in the proper mesh. All records including residual nucleus are identified and the corresponding energy is summed and registered in the right mesh.

In this first approach, the recoil energy includes also deexcitation and decay. Actually, all nucleus related loss of energy is initially considered local. For deexcitation and decay, the emitted radiations (photons, β and/or α) are transported in a simplified manner to build the exact map of deposited energy. It is considered that charged particles deposit their energy immediately at the point they emerge but photons are transported (a 5 MeV γ goes up to 10 cm in liquid lead).

Ionisation

In this case, energy is deposited in several meshes along the path of a charged particle e.g. a 1 GeV proton has a penetration depth of ~ 55 cm in lead (see Fig. 15) which covers more than 100 meshes. The deposited energy is calculated by integration of the stopping power dE/ds=f(E) according to Bethe's formula.

Beam

A proton beam profile has been assumed Gaussian (Fig. 8) with a limited gradient of current density at the boundaries to avoid thermal stresses in the window. In the HETC computation, several regions with identical current densities have been defined.

As the regions where the beam is described are discrete, we will see this effect of discretization in the power distribution.

Target dimensions

The axial dimension of the target is determined by the proton beam energy and has been chosen for 1 GeV protons to ~65 cm in liquid lead and ~50 cm for mercury (this length gives about 90% of maximum yield). In the case of solid targets, the thickness of each element (plates, rods) and their spacing is determining the source extension.

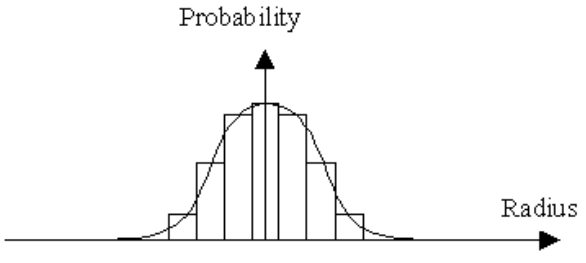

Figure 8. Proton beam profile.

The radial dimension was optimized taking into account constrains on the window (rather than optimal size for containing high-energy particle cascade):

maximum average and peak current densities as a function of the lifetime of the window (35μA/cm² for a maximum 100 dpa/year limit in this case), maximum thermal stress load.

The beam intensity has been determined, a priori, knowing the overall ADS - core characteristics (k_{eff}, φ* [Salv97a], thermal power).

In the case of solid targets the thickness of each element is given by thermal-hydraulics parameters obtained through calculations of a balance between spallation heat generation and cooling for each plate. Table IV summarizes parameters of sodium cooled tungsten target plates.

Table IV. Thermal hydraulic parameters of the tungsten target

Inlet-Outlet temperature	400 - 550	°C
Sodium speed	5	m/s
Specific heat	1.28	J/g.K
Density	0.85	g/cm^3
Exchange surface	4	m²

Spallation neutrons are fast and may require some spectrum modification to limit damages to the materials nearby the target enclosure walls. Thus a buffer zone [Rubb95] is often considered between the actual source region and the core. The thickness of that region has been determined by calculation of necessary spectrum softening (scattering mean free path, lethargy increment) and was set to 10 cm.

Three target types have been investigated:

1. Liquid lead target with a hemispherical window for a proton beam of 1 GeV, 1 mA protons – see Fig. 6;
2. Liquid mercury target with a hemispherical window for a proton beam of 1 GeV, 33 mA protons – Fig. 10.
3. Sodium-cooled tungsten plates with a hemispherical window for a proton beam of 1 GeV, 33 mA protons – Fig. 12.

1.2.1.1 Liquid lead target

The window of this is made of martensitic steel EM10 and its dimensions are adjusted to a 1 GeV Gaussian beam for 1 year of operation (Fig. 6).

The results are presented in Fig. 9 where three 3-D graphs exemplify a distribution of energy deposition. The protons penetrate along the Z-axis from atop. The energy deposition decreases exponentially on the beam axis. The first (upper) graph of this figure shows the sum of local (recoil) + non-local (ionisation) phenomena. The peak of heat deposition, in front of the window is ~ 1.2 kW/cm^3. The straggling in the power distribution is due to a poor statistics (10^4 histories in a validation test case). The Bragg peak, at the end of the path, must be accurately computed; in particular in solid targets as the absolute value of energy deposition is important over a small range. As mentioned before the diameter of this target is

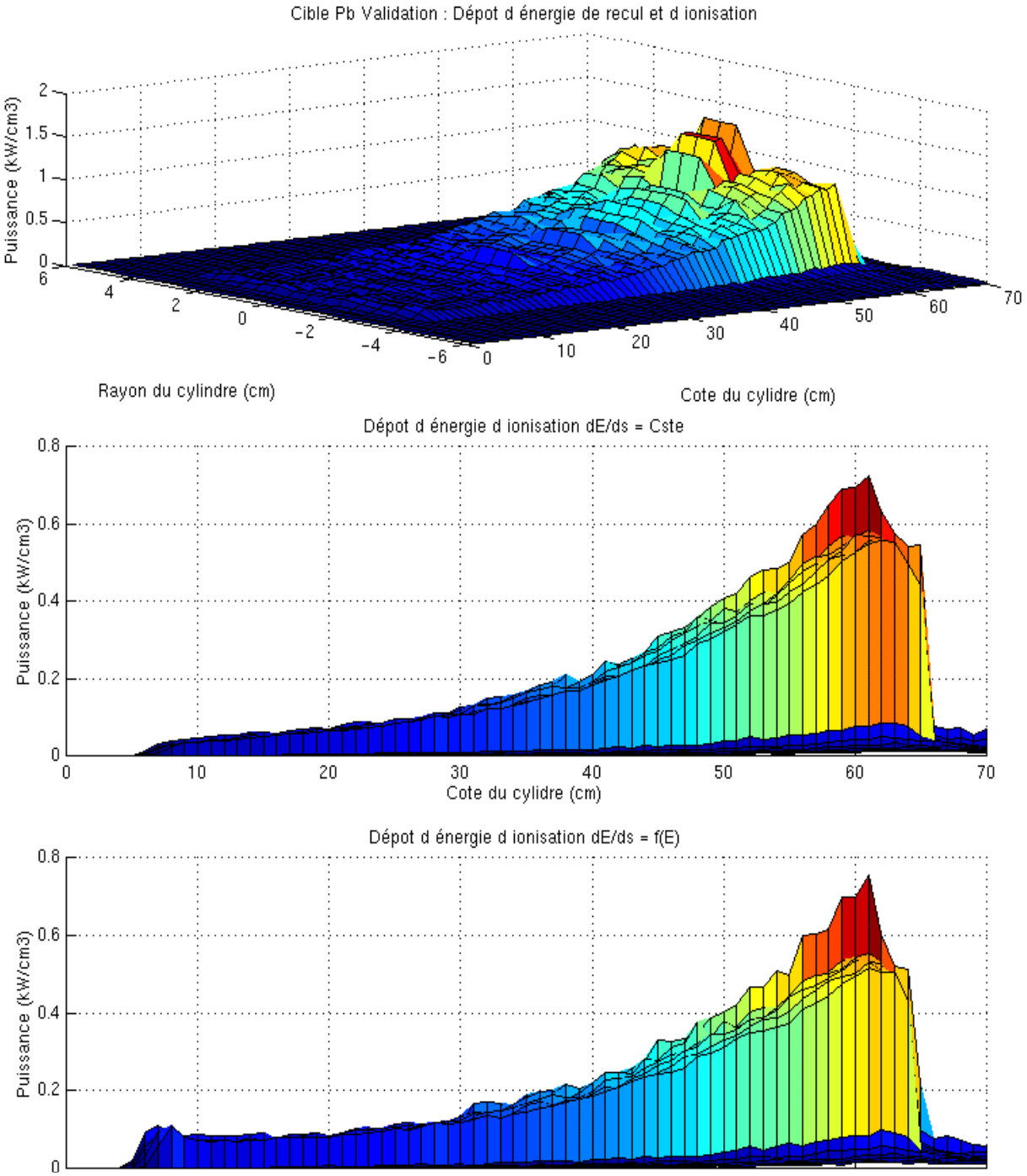

Figure 9. Examples of energy deposition in a liquid lead target.

optimized taking into account the window requirements. If optimized for the neutron yield, the diameter of the target would be much larger (see Figs 3 and 4).

1.2.1.2 Mercury target.

The mercury target presented on Fig.10 is larger than the lead target and can accommodate for 1 year a proton beam of 33 mA with 1 GeV energy.

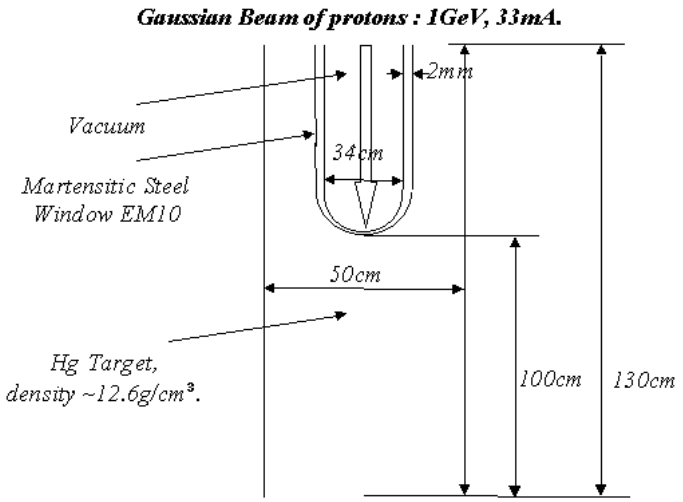

Figure 10. A model of the mercury target.

The beam has a Gaussian current density to avoid excess thermal stresses in the window.

Fig. 11 shows the power distribution due to High Energy interactions. The beam shape is clearly visible, as there is almost no radial dispersion.

Local (*recoil*, decay and deexcitation), and non-local (*ionisation*) energy depositions are presented for the maxima, radially and axially

In mercury, the beam penetration depth is almost 20 % smaller than in lead which makes the source more compact. Mercury does not freeze at room temperature but corrosion problems (dissolution of steel) are very serious.

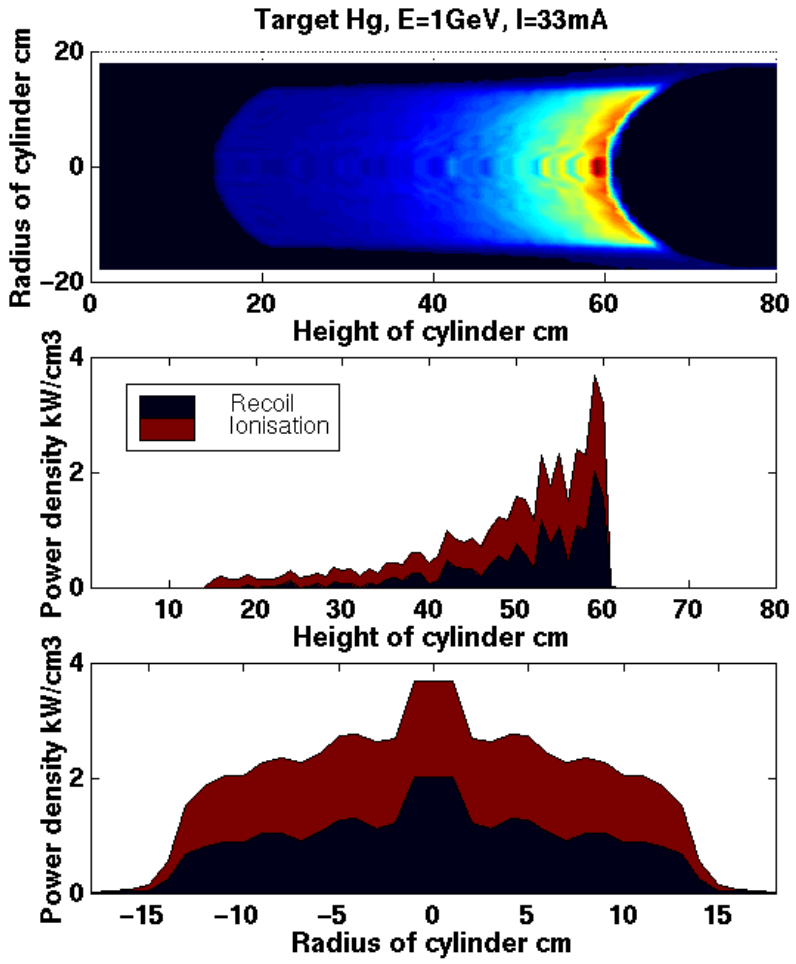

Figure 11. Energy deposition in the mercury target.

1.2.1.3 Solid tungsten target, sodium cooled : ADS burner

This target is directly inspired by the early concept of JAERI [Taki92] considering a pile of solid tungsten plates cooled by sodium – see Fig. 12. This concept avoids the axial peaking factor and increases the source elongation along the beam axis. The tungsten plates are pierced by holes to let the coolant flow through and alternatively positioned so that the hole in an even plate would not face the hole in an odd plate (thereby avoiding the beam to go across). Thickness of the plates and spacing between them vary in order to optimize the axial neutron

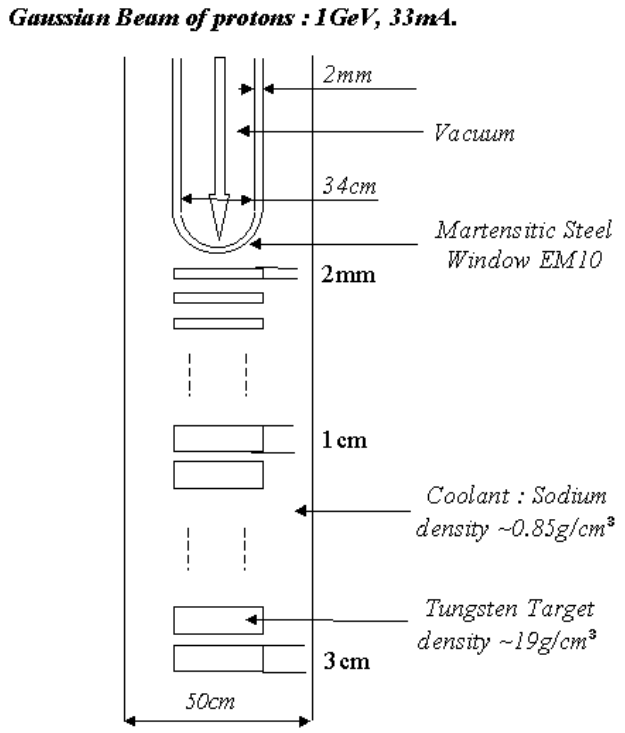

Figure 12. A model of the tungsten target.

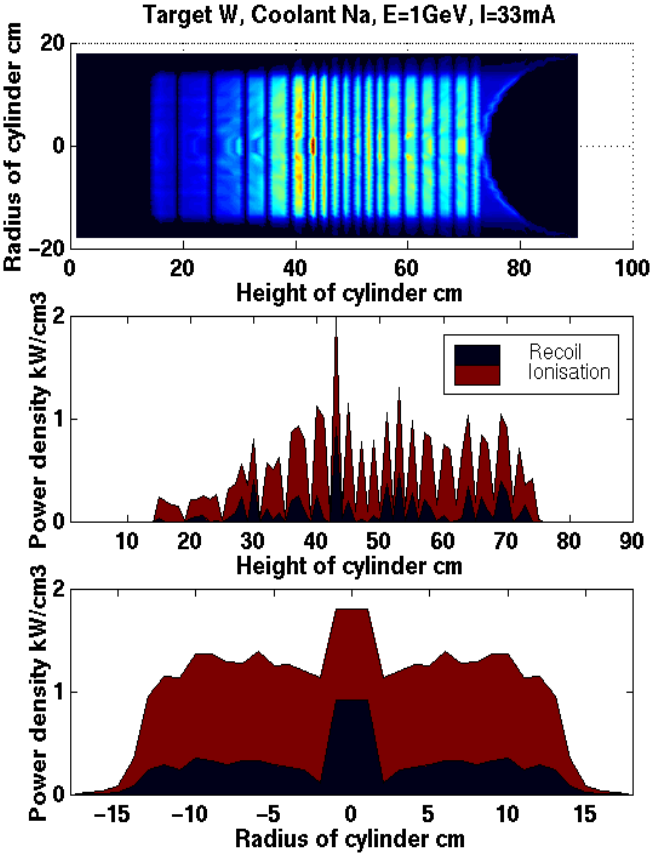

Figure 13. Energy deposition in the tungsten plate target.

distribution.

Energy deposition occurs mainly in the tungsten plates – see Fig. 13. In the sodium coolant, power deposition is due to ionisation (almost no spallation occurs, thus decreasing the overall neutron multiplicities by a factor of 2 as compared to the lead target) and the loss of energy is negligible as compared to the target elements.

The main advantage of this target is more extended neutron source distribution (uniformly shaped over ~ 40 cm), which is difficult to achieve with a liquid metal target. In this case, the plates correspond to a peak of (3.5 MeV isotropic) neutron production, which are scattered in the buffer medium so that the actual source at the target - core interface may be almost linear.

1.2.2. FZK Lead Target

In Fig. 14 a close-up view in the vicinity of the window of FZK model is shown. The shadowed area indicates the arrangement and the shape of the intensity of the proton beam. The proton range in different candidate target materials as a function of the proton energy is given in Fig. 15. It may be observed that the differences are remarkable between lead and HT9 steel on the one hand, and tungsten and rhenium on the other hand. The energy deposition in the target strongly depends on the characteristics of the proton beam.

For the target model as on Fig. 14 and the ADS arrangement of Fig. 2 in Section 4 a detailed analysis of energy deposition was also performed. The final result is shown in the power density distribution in Fig 16. We may clearly recognize the shape of the proton beam intensity. The power

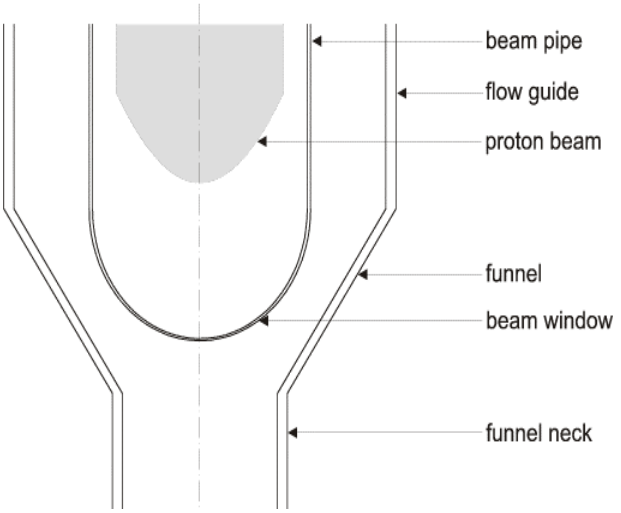

Figure 14. Geometric model of the FZK spallation target in the vicinity of the window.

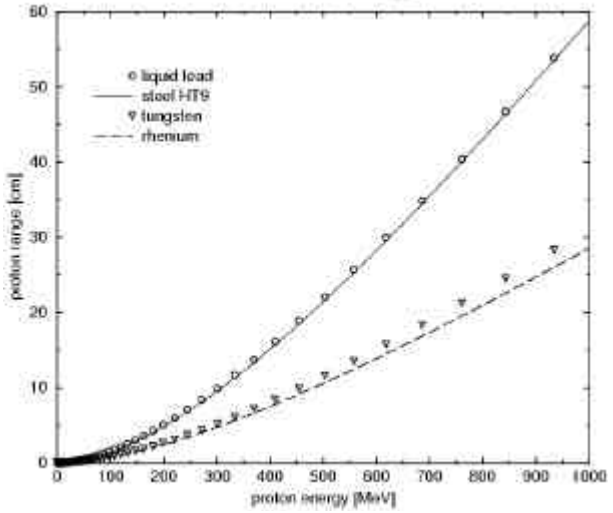

Figure 15. Proton range in different materials for proton energies up to 1000 MeV.

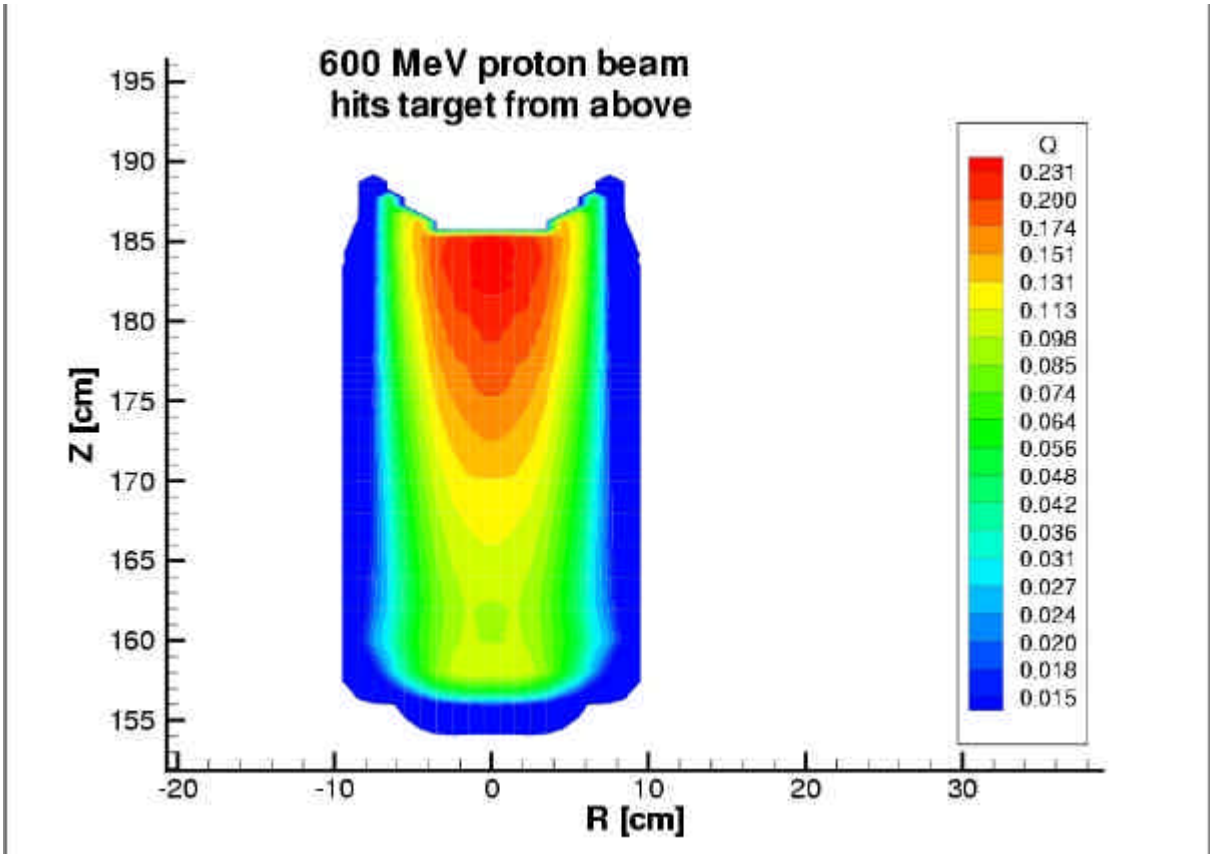

Figure 16. Energy [kW/mA.cm^3] deposited in a liquid lead target by a 600 MeV proton beam.

density varies from 0.230 kW/mA.cm^3 at the hot spot down to 0.015 kW/mA.cm^3 on target boundaries. The next step in this modeling is to couple these *calculations with thermal hydraulic simulations.*

1.3 Target Lifetime

The window of the spallation target is a critical part of this device. It is directly exposed to the proton beam, it must be transparent for protons so it can not be thick and being an interface between accelerator and reactor environment it will most probably be also an interface between low and normal or high pressure. Moreover it will also be exposed to backscattered spallation neutrons and neutrons coming from surrounding subcritical core.

Table V presents the main parameters applied to the assessment of the lifetime of the ***window*** for each of the above-mentioned targets: neutron yield, gas release, interstitials production and displacements.

Table V. Main parameters determining lifetime of the window

	Pb	Hg	W plates	Units
Neutron yield	28.2	24.6	15.5	n / p
Gas release:				
H,D,T	740	790	680	appmH/mA×year.
^{3}He,^{4}He	40	43	39	appmHe/mA×year.
Interstitials:				
Phosphorus	6	5	5	appmP/mA×year.
Sulphur	4	3	4	appmS/mA×year.
dpa	0.92	0.94	0.68	dpa/mA×year

This table shows that lead and mercury suffer to similar damages to the however Hg target has been design for higher power. Interstitial atoms of phosphorus, sulphur migrate towards grain boundaries at high temperatures and might cause local embrittlement. These phenomena still require more investigations from the materials standpoint and should include dynamics analysis of diffusion and migration mechanisms for chemical species as function of the temperature. In the case of a solid target, gas releases in the window are lower because the plates (where intranuclear and internuclear cascades occur) are distant from the window and because a thin layer of coolant makes a limited though observable shielding against secondary particles between both parts.

The lifetime of the window is essentially determined by its mechanical properties. Here, two arbitrary limits prior to the deterioration of the material are used: maximum He production (2000 appm He corresponds to the dose accumulated in the Inconel window tested at LANL) and maximum dpa (100 dpa is twice smaller than the objective for FBR's in order to be conservative).

Table VI indicates the lifetime of the window for a beam current I = 33 mA for different targets.

Table VI. Lifetime of the window for a beam current I=33 mA, E=1 GeV

Limiting factor	**Liquid Pb**	**Hg**	**W plates**	*Units*
^{3}He,^{4}He	1.5	1.4	1.6	years
dpa	3.3	3.2	4.5	years

In all the previous cases the appmHe/dpa ratio is higher than 1, (appmHe/dpa <1 in FBR's) so that the limit in terms of lifetime is set by gas release rather than by the displacements. However, the displacements presented in the previous tables do not include "reactor range" neutrons. These neutrons induce more than 50 % of the overall damages and should therefore be taken into account.

The main conclusion is that our hypotheses (J_{ave}=25μA/cm², J_{max}=35μA/cm²) with two very conservative criteria (2000 appm He & 100 dpa) allow a replacement of the window less frequent than every other year.

2. Radiation Damages to the Window of Spallation Target and Enclosure Walls

This chapter focuses on the damages to the main ADS components i.e. core structure, target container and beam window. It considers contributions from reactor range neutrons with "reactor range energies" and high-energy particles. It was assumed that radiation damages are determined by dpa, specific spallation residuals and gas releases.

The target model for this study - Lead Bismuth Eutectic (LBE) - as well as the beam window were not optimized, assuming that those parameters have a secondary effect on core neutronics.

2.1 Model of the Target

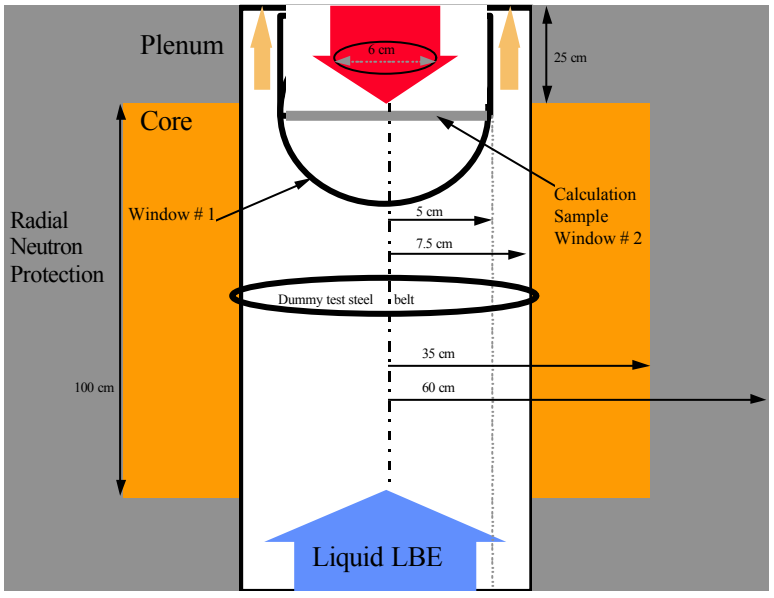

Figure 17. An ADS model for radiation damage simulations.

The target material is flowing liquid Lead Bismuth Eutectic. The beam window material is OPTIFER steel. The target module is surrounded by a subcritical core with MOX-fuel pins (ε_0=37.8% Pu/Heavy Nuclides, 29% ^{239}Pu equivalent) in hexagonal subassemblies cooled by LBE – see Fig. 17. The beam parameters are ∅ = 6 cm and $E_{protons}$ = 1 GeV.

All high-energy transport calculations have been performed with 50,000 histories, leading to 1,500,000

neutrons below the cut-off ($E_{cut-off}$=19.64MeV). The "deterministic" spallation neutron source has been computed in the same geometry model (Fig. 17). In order to refine damage (dpa, gas production) calculations, the hemispherical window (Fig. 17 - #1) has been replaced by a thin plate of OPTIFER steel (Fig. 17 - #2), 1.5 mm thick. As long as surfaces are identical it does not bias damage calculations. In order to improve the investigations of the contribution of high-energy particles to radiation damages in the window, the beam tube and in the core, a dummy test belt of OPTIFER steel, 1 mm thick around the target module, at mid core height (maximum flux level) was introduced. This "dummy" sample will receive the same maximum exposure as the target module enclosure walls.

Table VII gives OPTIFER composition (mass fractions).

Table VII. Composition of OPTIFIER steel (mass fractions)

Fe	Cr	W	Mn	Si	Ta	V	C
88.75	9.3	0.96	0.5	0.06	0.07	0.26	0.1

2.2 Results

2.2.1 Results for High-Energy (20 MeV < E < 1 GeV)

The neutron yield is about 30 neutrons/proton for neutron energy E_n < 20 MeV and 4.8 n/p for 20 MeV<E_n<1 GeV. The spallation source is rather compact - 75% of spallation neutrons are generated within the first 10 cm.

The energy above 20 MeV deposited into the window leads to: 20.93 $dpa_{NRT-steel}$/mA×year.

Table VIII shows the damages induced by high-energy particles into the main system components ($dpa_{NRT-steel}$/mA×year).

Table VIII. Radiation damages to ADS components induced by high-energy particles

Core	Beam Tube	Window-#2	Dummy test belt
0.18 dpa/mA×year	0.66 dpa/mA×year	20.93 dpa/mA ×year	0.51 dpa/mA×year

Table IX gives an evaluation of gas production induced by spallation particles in the main target components. In each case the values are averaged over the component volume.

Table IX. Evaluation of gas production induced by high-energy spallation particles

Component	H - D - T			He		
	appm/mA×d	appm/mA×year	appm/dpa	appm/mA×d	appm/mA×year	appm/dpa
Window #2	53.14	19409.40	927.35	3.36	1127.2	53.86
Beam tube	1,165	425.52	644.73	0,032	11.70	17.27
Core	0,017	6.21	34.50	0,0030	1.10	6.11
Dummy belt	0,56	204.54	401.06	0,022	8.00	15.69

Large gradients of damages into the window are expected due to the brightness of the beam.

We can account for 4.6 nuclear interactions per incident proton, 0.5 % of which take place in the window, 50 % in the liquid target and 37 % in the core (The core volume is 20 times larger than the target module). An upper neutron shielding (4%) is twice as much exposed as a lower neutron shielding. 12.5% of the nuclear interactions take place in axial and radial shielding.

The spallation cascades occurring in the window cause a significant gas release (H & He), corresponding to one of the main de-excitation modes for the nucleus. 1.4 % of primary nuclear interactions (0.95 / incident proton @ 1 GeV vs 0.53 @ 400 MeV) directly occur in the window, the others take place into the target. Most nuclear interactions in the window are due to protons (70%).

Table X summarizes the relative contributions of neutrons and protons to nuclear interactions by ADS-components.

Table X. Neutron and proton contribution to nuclear interactions

ADS-component	Proton	Neutron
Target	0.520	0.480
Upper neutron protections	0.002	0.998
Radial neutron protections	0.007	0.993
Lower neutron protections	0.030	0.970
Core	0.020	0.980
Dummy test belt	0.008	0.992
Beam Tube	0.310	0.690
Window	0.700	0.300

Out of the beam axis most interactions come from neutrons. These interactions generate more dpa than gas release, as indicated in the *appm/dpa* column of the Table IX.

The power deposited into the window #1 is 6.23×10^{-15} J/g×p_{inc}. or 40 W/g×mA or 300 W/cc×mA (current density J = 75 µA.cm²). In the window #2 (1.5 mm thick) the specific power is 1.55 10^{-14} J/g×P_{inc}. or 97 W/g×mA or 750 W/cc×mA. The specific power in the region of the window that is most exposed to the beam is ~ 100 W/g×mA on average and while the power dissipated in the whole volume is 6.3 kW/mA (if k_{eff}=0.945, and the core power = 100 MW_{th} (HADRON [Salv97]) the current must be ~ 2.2 mA).

To exemplify the scale of radiation damages the comparison was made between damages due to a beam with Ep = 1 GeV and 300 MeV into window #2. Table XI shows the figures of merit relative to that study.

Table XI. Comparison of radiation damages in the window #2 - Fig. 17, for different beam energy

Energy	300 MeV	1 GeV
dpa/mA×year	13	21
appmH/mA×year	8460	19410
appmHe/mA×year	316	1130
Neutron yield n/p	4	30

The last line of the Table XI is the most interesting because it gives the relative beam currents (damages @ 300 MeV × 7.5 to compare with damages @ 1GeV). Thus it seems more interesting to use a high energy beam (E_p > 1GeV) in order to minimize radiation damages. However, one must keep in mind that a significant flux at high energy more actively contributes to ground activation and off-core biological exposure, thus there may be a need for an optimisation allowing to minimize damages and radiation protection problems. It would be possible to start operations at 300 MeV and then progressively increase the beam energy. A supplementary study remains necessary to address the issue of vertical *vs* horizontal beam entry.

2.2.2 Results for "Reactor Range" Energy (E < 20 MeV)

These calculations couples a stochastic spallation source $S(\underline{r},E)$ calculated with HETC to a deterministic core calculation with ERANOS (BISTRO S_4P_1 transport module). The core spectrum is similar to a fast reactor like the European Fast Reactor and rather insensitive to the source – see Fig. 18. This can be understood as the source is only a limited fraction of the core neutron population, moreover, it is separated from the core region by a scattering medium (LBE for this application) and eventually the source spectrum itself – see Fig. 19 - is essentially due to evaporation with a peak around 4 MeV which does not make it so hard. Spectrum in Fig. 19 includes neutrons backscattered from the core. Neutron spectrum in the core is essentially determined by the level of enrichment in fissile elements and the fraction of scattering isotopes. The offset in lethargy between the fission spectrum and the actual leakage spectrum is given by the inverse of the coefficient $r = \overline{\nu\Sigma_f} / \xi\Sigma_s$ [Buss].

All these results correspond to a case where k_{eff} (Beginning of Life) = 0.945 and the MOX-fuel pins (ε_0=37.8%Pu/Heavy Nuclides, 29% Pu-9 equivalent) are cooled by LBE in hexagonal subassemblies.

Maximum dpa rates are reached at End of Life when the reactivity is the lowest, thus leading to a larger peaking factor. This effect is hard to compensate because starting at a higher enrichment is equivalent to be further from equilibrium concentrations so that reactivity decreases faster.

σ_{dpa} come from a library corresponding to the NRT [Norg75] model in steel. The elementary data are stored as $\sigma_{dpa}/\sigma_{\infty i}$ where $\sigma_{\infty i}$ corresponds to the infinite dilution cross section of element *i*. This allows to correct (by multiplying it by $\sigma_{cell\ calculation}$) the dpa cross section in core calculations according to some occasional self-shielding effects. The NRT

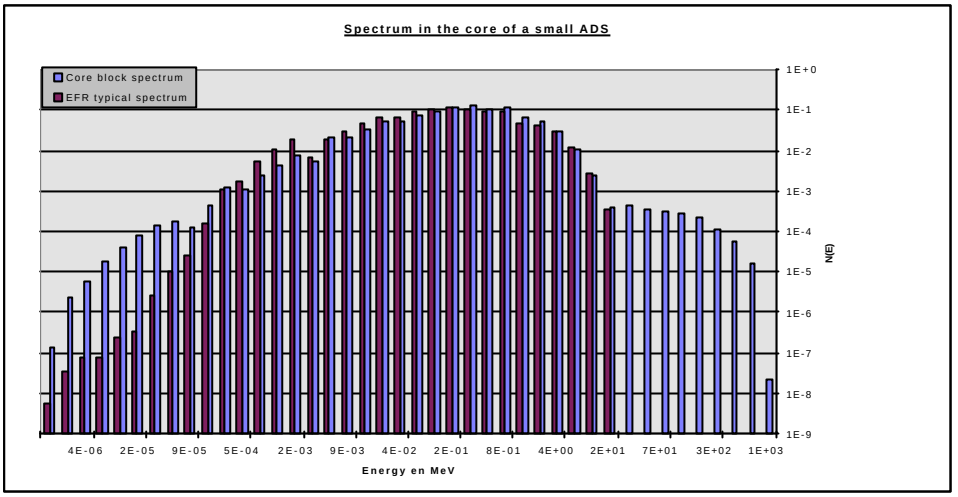

Figure 18. Neutron spectrum in the core of a fast ADS cooled by LBE.

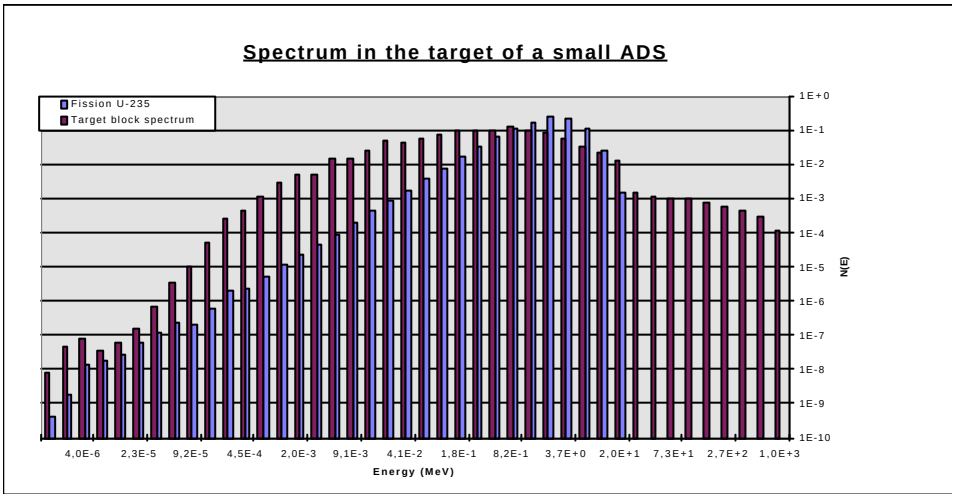

Figure 19. Neutron spectrum in the LBE target of ADS.

model may not be sound for this type of calculations as it neglects contributions from the protons [Leli99].

Table XII gives maximum dpa rates in the core and in the window for $E_n < 20$ MeV.

Table XII. Maximum dpa rates for $E_n < 20$ MeV

	t=0		t=90 FPD*	
Window	0.16 dpa/day	28 dpa/year×mA	0.19 dpa/day	22 dpa/year×mA
Inner core	0.17 dpa/day	29 dpa/year×mA	0.19 dpa/day	22 dpa/year×mA

The peaking factor gets worse as the fuel burns up. It makes the window as sensitive as the core at end of cycle.

Table XIII gives the neutron flux level for $E_n < 20$ MeV.

Table XIII. Neutron flux below 20 MeV

(Flux n/s.cm²)	Window	Inner Core
Max Flux	6.03×10^{15}	5.58×10^{15}
Mean Flux	5.60×10^{15}	3.87×10^{15}

The power peaking factor on the window is relatively small because the source is very compact. The intensity of spallation source (E_n < 20 MeV) at beginning of life (k_{eff}=0.945) is 4×10^{17} n/s.

2.2.3 Final Results for a Whole Energy Range

At beginning of life a maximum 28 dpa/year×mA in the window due to "reactor range" neutrons is to be expected. High energy contribution is estimated to 21 dpa/year×mA. The total is 49 dpa/year×mA for the target window. For E_p=1 GeV and k_{eff}=0.945 beam current reaches I_{beam}=2.16 mA whereas for k_{eff} = 0.97 I_{beam}=1.29 mA. This makes radiation damages in the window ranging from 62 to 105 dpa/year for reactivities 0.97 and 0.95, respectively. High and low energy contributions are fairly close. However, an improved dpa model may be necessary to simulate this phenomenon better.

In the most exposed region in the core radiation damages reach 29 dpa/mA×year at low energy and 0.2 dpa/mA×year at high energy. So damages in the core can range from 37 to 63 dpa/year corresponding to the k_{eff} changes from 0.97 to 0.95. The main conclusion is that the high energy contribution to dpa is negligible (~ 0.6%) in the core with a buffer region 2.5 cm thick.

Gas release in the most sensitive region of the window reaches a level from 25000 to 42000 appm H+D-T/year and 1600 ÷ 2600 appm He/year corresponding to reactivities 0.97 ÷ 0.95, respectively Corresponding current densities are 76.4 μA/cm² for k_{eff}= 0.95 and 45.6 μA/cm² for k_{eff}= 0.97.

As a comparison, we give in the Table XIV the gas releases and dpa rates (for the same current density *j* in μA/cm² and per year) in the tungsten window of the Energy Amplifier [Rubb95].

Table XIV. Comparison of gas release and dpa rates for different ADS models

System	Window	dpa	appm H	appm He	$\sigma_{H(800MeV)}$[barn] *	$\sigma_{He(800MeV)}$[barn]
EA	Tungsten	1.77	116.4	1030	5.13	0.58
This study	Steel	1.224	28.38	488.7	2.52	0.32

* Target materials and engineering by W. Fischer (PSI),

Gas release at high energy comes essentially from spallation. This explains why the figures in the dummy test belt (enclosure wall) are so low (1%) as compared to the window. However, these yields should be compared to (*n,**a**)* and (*n,p)* reactions due to core neutrons.

3. Spallation Product Analysis

During the irradiation of an ADS-target with protons a large number of spallation products are produced. Most of these spallation products have short lifetimes and have no significant impact on the behavior of the system. However, a considerable number of spallation products or their successors have longer lifetimes and must be taken into account with respect to the criticality of the system and to the consequences for the back-end of the system. Recently a Russian study has been published with a comparison of long-lived residual activity characteristics of liquid metal coolants for advanced nuclear energy systems [Ouss99]. In this reference the impact of ^{205}Pb with lead coolant and of ^{210m} Bi with lead-bismuth coolant is pointed out.

The significance of spallation products in a fast spectrum ADS has been investigated in some detail [Sege99]. The study is performed for a lead-cooled sub-critical energy amplifier system, similar to the proposal of Rubbia [Rubb95]. It has been shown that in a fast spectrum the neutron absorption in the spallation products only presents a weak competition to the nuclear decay as long as the half-life is smaller than about 30 days. So tabulations have been made for isotopes with decay times larger than 30 days. In order to reduce the amount of output the printouts are restricted to abundance above 1%. These tabulations are based on decay calculations without competition of neutron interactions utilizing an extensive decay-list of some 3000 isotopes and meta-stable states, compiled in conjunction with the investigations in reference [Sege94]. The most important spallation products in a lead target are summarized in Table XV, including half-life, yield per proton and availability on evaluated nuclear data files. We may observe a quite large number of missing isotopes on the evaluated data files, e.g. Pb^{205} with high yield and long half-life. In Table XVI one-group cross sections of important spallation products in the inner core of a Rubbia-type energy amplifier are compared. The one-group cross sections have been calculated with the processing code NJOY, using the different evaluated data libraries ENDF/B-6, JENDL-3.2 and JEF-2.2. Also given are the corresponding fast spectrum values on the KORIGEN library. The differences between the one-group cross sections from different origins are remarkable, both for KORIGEN and the other calculated values. For the impact of the spallation products on the reactivity of the fast spectrum ADS an educated guess leads to about 1% of the fission product contribution if the sub-criticality level of the system is low (about 0.75). For slightly sub-critical systems the influence may be neglected.

Table XV. Spallation products in the lead target of the Rubbia ADS concept

The list is shortened to include those elements for which
a: half-life > 30 days
b: relative abundance in the target > 1.0%

Isotope	Half life	Yield per proton	Availability of basic neutron X-section data					
			1	2	3	4	5	6
82 Pb 206	s	0.454	+		+	+		+
82 Pb 207	s	0.252	+		+	+		+
82 Pb 205	1.5×10^{7} a	0.228						
82 Pb 204	1.4×10^{17} a	0.150	+					+
81 Tl 203	s	0.143						
82 Pb 208	s	0.139	+		+	+		+
80 Hg 201	s	0.079						
80 Hg 200	s	0.077						
80 Hg 199	s	0.070						
82 Pb 202	$\sim3\times10^{5}$ a	0.064						
79 Au 195	183 d	0.062						
80 Hg 203	46.6 d	0.060						
80 Hg 198	s	0.059						
81 Tl 205	s	0.054	+	+	+	+	+	
79 Au 197	s	0.052						
80 Hg 196	s	0.042						
80 Hg 202	s	0.039						
78 Pt 193	~ 50 a	0.034						
81 Tl 203	s	0.033						
76 Os 186	2.0×10^{15} a	0.030						
80 Hg 194	367 a	0.029						

legend
1 - brond22
2 - cendl21
3 - endfb6
4 - endfb64
5 - jef22
6 - jendl32

Table XVI. Effective one-group cross sections for selected spallation products in the fast neutron spectrum

(the list is arbitrarily shortened to include those elements for which half-life > 30 days)
(relative abundancy in the inner-core > 1.0%)

				KORIGEN LIBRARIES	NJOY-generated, collapsed on the flux-spectrum of the Rubbia-concept inner-core cross sections (barns)		
Isotope	half life days	yield per proton	Reaction type		endfb6	Jendl3.2	jef2.2
6C12	S	0.0293	n,γ n,α	1.56×10^{-3} (both)	2.65×10^{-6} 1.22×10^{-2}	1.79×10^{-3} 1.34×10^{-2}	2.65×10^{-6} 1.31×10^{-2}
7C15	S	0.0140	n,γ n,α		1.19×10^{-5} 3.04×10^{-4}	3.70×10^{-7} 2.94×10^{-4}	3.70×10^{-7} 2.94×10^{-4}
8O16	S	0.0220	n,γ n,α	6.00×10^{-4} (both)	1.34×10^{-7} 1.30×10^{-2}	5.35×10^{-5} 2.32×10^{-2}	1.34×10^{-7} 1.30×10^{-2}
24Cr52	S	0.0113	n,γ n,α	1.53×10^{-3} (both)	6.16×10^{-3} 4.85×10^{-5}	6.36×10^{-3} 4.98×10^{-4}	6.41×10^{-3} 4.74×10^{-4}
25Mn54	312	0.0133	n,γ n,α				
25Mn55	S	0.0170	n,γ n,α	1.93×10^{-2} (both)	3.83×10^{-2} 2.60×10^{-5}	3.83×10^{-2} 2.60×10^{-5}	5.34×10^{-2} 2.24×10^{-5}
26Fe54	S	0.0107	n,γ n,α				
26Fe55	986	0.0203	n,γ n,α				
26Fe56	S	0.0220	n,γ n,α	1.01×10^{-2} (both)	8.43×10^{-3} 1.44×10^{-4}	9.28×10^{-3} 1.29×10^{-4}	8.04×10^{-3} 6.42×10^{-4}
80Hg200	S	0.0143	n,γ				
80Hg201	S	0.0157	n,γ				
81Tl203	S	0.0337	n,γ				
82Pb202	$1.1\times10^{+8}$	0.0180	n,γ				
82Pb204	$5.0\times10^{+9}$	0.0473	n,γ			6.54×10^{-2}	
82Pb205	$5.5\times10^{+9}$	0.0640	n,γ				
82Pb206	S	0.1370	n,γ		1.05×10^{-2}	8.80×10^{-3}	
82Pb207	S	0.0791	n,γ		7.61×10^{-3}	5.95×10^{-3}	
82Pb208	S	0.0458	n,γ		7.66×10^{-4}	6.55×10^{-4}	
90Th228	697	0.0149	n,γ n,fiss	4.00×10^{-1} 4.00×10^{-1}		3.62×10^{-1} 1.59×10^{-2}	
90Th229	$2.7\times10^{+6}$	0.0227	n,γ n,fiss	4.00×10^{-1} 3.00		1.197 7.92×10^{-1}	
90Th230	$2.8\times10^{+7}$	0.0220	n,γ n,fiss	4.00×10^{-1} 4.40×10^{-1}	1.97×10^{-1} 2.81×10^{-2}	3.80×10^{-1} 7.01×10^{-2}	1.97×10^{-1} 2.81×10^{-2}
90Th232	$5.0\times10^{+12}$	0.0164	n,γ n,fiss	4.44×10^{-1} 1.37×10^{-2}	3.64×10^{-1} 2.84×10^{-2}	3.48×10^{-1} 2.53×10^{-2}	3.81×10^{-1} 6.33×10^{-2}
91Pa231	$1.2\times10^{+7}$	0.0157	n,γ n,fiss	8.00×10^{-1} 3.83×10^{-1}	1.01 1.79×10^{-1}	1.37 1.49×10^{-1}	1.01 1.79×10^{-1}

VI. IMPACT ON THE RISK FROM HIGH-LEVEL WASTE REPOSITORIES FROM RADIOTOXICITY REDUCTION USING ADS

1. Introduction

The main objective of accelerator-driven systems (ADS) for transmutation would be to reduce the risks associated with the long-term management of radioactive wastes from the generation of electricity by reducing the long-term radiotoxicity of the wastes. The aim would be to reduce the radiotoxicity of high-level wastes (HLW) and if possible secondary wastes.

There are a variety of proposals for applying ADS, ranging from their use to transmute legacy wastes from existing reactors, to their use as devices whose primary aim would be energy production with lower environmental impact than existing reactors. Between these two concepts lie proposals for applying accelerator-driven transmuters as an integral part of a new fuel cycle involving conventional light-water and possibly fast reactors. In some cases the proposal would be to move from the transmutation of legacy wastes to a new fuel cycle. HLW from conventional reactors includes spent fuel, the by-products of spent fuel reprocessing, and possibly some plutonium.

The assumption has been that HLW would be disposed of in a deep repository, which would provide sufficient isolation from man's accessible environment over the long term. Ideally, the objective of ADS for transmutation would be to remove the need for deep repositories. This would imply the need to transmute virtually all the long-lived radionuclides in all wastes from a fuel cycle to short-lived or stable nuclides. In practice, it is more likely that transmutation could reduce the risk from the disposal of wastes in a deep repository.

The aim of this section is to examine the potential impact on the risk from HLW repositories from radiotoxicity reduction using ADS. The work reported in this section can be viewed as setting the objectives for ADS transmutation of spent fuel.

The risk from a repository would not in general be directly proportional to the radiotoxicity of the disposed wastes. The reason for this is as follows. One pathway along which radionuclides might return to man's environment from a repository is by dissolving in groundwater flowing through the repository and then being carried to the surface. Different radionuclides in the wastes would be affected to different extents by the various physical and chemical barriers to the release of the radionuclides along the groundwater pathway, delaying their release to the surface by different amounts. For example, radionuclides would sorb to varying extents on materials in the repository and on rock. Also, the solubility of some chemical species would limit the rate at which some radionuclides could dissolve into the groundwater and be transported along the groundwater pathway. Relatively short-lived radionuclides would be completely contained by the repository and geosphere; relatively long-lived radionuclides and their decay daughters might be released back to the surface.

To understand the potential impact on the risk from HLW repositories from reducing radiotoxicity using ADS it is necessary to understand which radionuclides could lead to significant risks and the relationship between the inventory of these radionuclides and the risk from a repository. The work reported in this section examines these two factors and considers the implications of the results obtained.

2. Important Radionuclides

A wide range of European risk studies for deep repositories for spent fuel, vitrified high-level wastes (VHLW) from spent fuel reprocessing, and secondary wastes have been reviewed with the aim of showing which radionuclides contribute most to repository risk. This review used as its starting point an earlier review of repository studies [Kane95], but covered a wider range of studies. The results of the CEC PAGIS project for disposal on land were included [Cade88].

The review reported in reference [Kane95] was performed with the aim of examining whether research on partitioning and transmuting radioactive wastes should use the toxicity of the wastes or repository risk as a measure to decide which radionuclides should be transmuted. It was concluded that using repository risk is the most desirable approach because it will be used for decisions on the implementation of partition and transmutation; however, there are problems with using repository risk which suggest toxicity should also be taken into account. The problems relate to the variety of results that can be obtained for different wastes, sites, repository concepts and scenarios and the way results can change as understanding improves. While recognising the difficulties, the view is also taken here that repository risk should be used as the measure to identify which radionuclides would need to be transmuted for ADS to have a beneficial impact on long-term radioactive waste management. Radioactive waste is currently a national responsibility, while a commercial ADS would almost certainly need to have application in a number of countries. The aim of the review was to identify what if any general conclusions can be drawn for developing a commercial ADS from the set of repository risk studies for particular countries, sites etc., producing a variety of results.

The results of the review of repository risk studies are summarised in Table I. For each risk study reviewed, the table shows the country, site/rock type, waste type, scenarios considered and most significant radionuclides. The measure used to judge significance is generally risk or dose to the critical group.

The following fission products appear in Table I:

^{14}C, ^{79}Se, ^{93}Zr, ^{99}Tc, ^{107}Pd, ^{126}Sn, ^{129}I, ^{135}Cs

Radionuclides in all four actinide decay series also appear:

4n	(^{240}Pu, ^{236}U)
4n+1	(^{241}Am, ^{237}Np, ^{233}U, ^{229}Th)
4n+2	(^{242}Pu, ^{238}U, ^{234}U, ^{230}Th, ^{226}Ra)
4n+3	(^{239}Pu, ^{235}U, ^{231}Pa)

The results demonstrate the well-known point that fission products can be the most important contributors to peak risks from repositories even though their collective long-term radiotoxicity is below that of the actinides. The reason for this is the generally greater mobility under repository system conditions of fission products over that of actinides.

The results also demonstrate the difficulties of using repository risk studies to identify the radionuclides to be transmuted by an ADS, or at least an ADS which could be used to transmute wastes from different countries. Actinides of all four decay series appear in Table I Not surprisingly, actinides from the 4n+1 series, particularly ^{237}Np, tend to dominate for VHLW, while radionuclides from the other series also appear for spent fuel; however, the pattern is not always followed for VHLW. Although the number of fission products is low, all the long-lived fission products above a particular activity over repository timescales appear in

Table I: Results of Review of Repository Risk Studies.

Country/ Study	Site	Waste*	Scenarios	Most Significant Radionuclides	Notes	References
Belgium	Mol-Dessel: Boom clay	VHLW (PWR)	Natural discharge and well	^{237}Np, ^{135}Cs, ^{99}Tc, ^{233}U, ^{236}U, ^{107}Pd, ^{235}U, ^{229Th}	Focussed on ^{99}Tc, ^{107}Pd, ^{135}Cs, and 4n, 4n+1 and 4n+3 series. In order of maximum individual dose $>10^{-10}$ Sv yr^{-1}	[Cade88] [Kane95] [Mari88]
			Altered evolutions	Similar		
France	Auriat: granite	VHLW (PWR)	Natural discharge	^{237}Np, ^{229}Th, ^{233}U, ^{135}Cs, ^{99}Tc, ^{93}Zr	^{79}Se, ^{126}Sn, ^{239}Pu and ^{240}Pu neglected, ^{107}Pd and ^{241}Am only considered for human intrusion. For normal evolution, in order of maximum individual dose $>10^{-8}$ Sv yr^{-1}	[Cade88] [Kote88]
			Human intrusion by cavity excavation	^{237}Np and ^{229Th} for miners, and ^{99}Tc and ^{237}Np for surface dwellers (due to contamination)		
Germany	Gorleben: salt dome	VHLW (PWR + BWR)	Subrosion	^{237}Np, ^{234}U, ^{233}U, ^{135}Cs		[Buhm95] [Cade88] [Stor88]
			Altered evolutions	^{135}Cs, ^{237}Np, ^{79}Se, ^{233}U		
			Human intrusion by solution mining	^{237}Np, ^{233}U, ^{229Th}, ^{135}Cs		

UK/ Nirex 97	Sellafield: volcanic overlain by sedimentary rocks	ILW	Natural discharge	^{14}C, ^{36}Cl, ^{99}Tc, ^{129}I, ^{210}Pb, ^{226}Ra, ^{230}Th, U^{234}, ^{237}Np, ^{238}U		[Bake97a] [Bake97b]
			Variants	Plus ^{10}B, ^{229}Th, ^{232}Th, ^{233}U		
			Wells	^{36}Cl, ^{99}Tc, ^{129}I, $^{38}U2$ and daughters		
			Gas	Tritium and ^{14}C		
Sweden/ SKB 91	Granodiorite	SF (PWR + BWR)	Natural discharge and well	^{129}I, ^{135}Cs, ^{226}Ra, ^{231}Pa		[Kane95] [Neal95]
			Altered evolutions	Same		
Sweden/ KBS-3	Notional	SF (PWR + BWR)	Natural discharge and well	^{129}I, ^{135}Cs, ^{226}Ra	-	[Kane95]
			Altered evolutions	^{129}I, ^{135}Cs, ^{226}Ra, ^{231}Pa, ^{237}Np		
Finland	Fennosarmatia	SF (BWR)	Natural discharge and well	^{129}I, ^{231}Pa, ^{94}Nb	Radionuclides listed if one of three most significant for a scenario	[Teol92]
			Altered evolutions	^{14}C, ^{36}Cl, ^{79}Se, ^{94}Nb, ^{99}Tc, ^{129}I, ^{135}Cs, 226Ra, ^{229}Th, ^{231}Pa, ^{237}Np, ^{239}Pu, ^{240}Pu, ^{242}Pu		
Switzerland/ Gewahr	Granite	VHLW	Natural discharge and altered evolution	^{135}Cs, ^{79}Se, ^{237}Np	Radionuclides giving peak annual dose of $>10^{-8}$ mrem yr^{-1}	[Kane95]

Switzerland/ Kristallin-1	Gneiss or granite overlain by sedimentary layers	VHLW (PWR + BWR)	Natural discharge and altered evolution	^{79}Se, ^{93}Zr, ^{99}Tc, ^{126}Sn, ^{135}Cs, 4n, 4n+1, 4n+2, 4n+3 series	Radionuclides giving peak annual dose of $>10^{-9}$ mSv yr^{-1} from all pathways	[Zuid93] [Smit93] [Smit95]
			Geosphere barrier ignored	As above plus ^{59}Ni		
UK/4FP	Hard rock	SF (PWR)	Natural discharge	^{126}Sn, ^{226}Ra, ^{129}I, ^{230}Th, ^{135}Cs, ^{79}Se	-	[Volc98]
			Human intrusion	^{241}Am, ^{238}Pu		
		VHLW (PWR)	Natural discharge	^{126}Sn, ^{233}U, ^{79}Se, ^{226}Ra, ^{137}Cs, ^{129}I		
			Human intrusion	^{241}Am, ^{99}Tc		
Germany/ 4FP	Salt dome	SF + VHLW (PWR)	Subrosion	^{129}I, ^{135}Cs, 4n+1, 4n+2	-	[Volc98]
Belgium/4FP	Clay	SF + VHLW (PWR)	Well	^{129}I, ^{79}Se, ^{126}Sn, ^{135}Cs, 4n+1, 4n+2	-	[Volc98]
			Human intrusion	Similar to UK/4FP results above		

* SF Spent fuel
VHLW Vitrified high-level waste
ILW Intermediate-level (secondary) wastes
PWR Waste from pressurised water reactor BWR Waste from boiling water reactor

Table I. If fission products with a half-life of less than 10^2 years and greater than 10^{10} years and below a particular activity are excluded from the output of a typical calculation of the radionuclide inventory in irradiated fuel from a conventional reactor (like that on which the calculations reported in Chapter 3 are based), then the same list of fission products as that given above is obtained. It should be noted, however, that for repository risk studies prior assumptions are often made about what will be the significant radionuclides and only these are then considered in the studies.

The main general conclusion that can be drawn from this analysis is that the development of ADS should proceed on the assumption that ideally all the fission products listed above should be transmuted along with the actinides (see below in Chapters 3.1 and 4.4 in relation to uranium). Although a smaller number, or even a single radionuclide, may make the dominant contribution to peak risk for a particular repository system taking into account current uncertainties, it would be unwise to base the development of ADS, and particularly a multinational ADS, on such results.

Some activation products are also listed in Table I:

^{14}C, ^{36}Cl, ^{59}Ni, ^{94}Nb

Activation products may need to be transmuted by an ADS. It should be noted that activation products are not always included in the inventories assumed for repository risk studies, for example, if the clad on spent fuel is ignored. In the case of the risk study for ILW in the UK [Bake97a], whose results are summarised in Table I, ^{36}Cl is the dominant contributor to risk from the groundwater pathway. ^{36}Cl has also been shown to be the dominant contributor to risk in calculations for UK spent fuel and HLW [Cumm96a,Cumm96b]. That an activation product can be the dominant contributor to risk has important implications for the design of ADS. This point is discussed further in Chapter 4.2.

Most of the studies whose results are summarised in Table I addressed only the groundwater and in some cases the human intrusion pathways for radionuclides to return to man's accessible environment. A third potential pathway is the gas pathway. A number of processes might lead to the generation of gases in a repository: corrosion of metals of waste containers or in the wastes, microbial degradation of organic wastes, and radiolysis. Radionuclides from the wastes might get incorporated into these gases, or the gases might carry radon from rock more quickly to the surface. The gas pathway is most likely to be of significance for secondary wastes. Such wastes may include operational and decommissioning wastes containing metals and organic materials. Secondary wastes also tend to have a relatively large volume and therefore the waste containers may contribute significant quantities of steel to the inventory of materials in a repository. In the gas pathway, relatively short-lived radionuclides, such as ^{14}C or even tritium, might return to the surface, which might not by the groundwater pathway. In the case of such a relatively short-lived radionuclide as tritium, measures such as extended storage could be used to reduce its impact if necessary.

3. Relationship Between Radionuclide Inventory and Risk

It has already been pointed out in Chapter 1 that the repository risk a given radionuclide would give rise to is not necessarily directly proportional to the inventory of the radionuclide in a repository. An understanding of the relationship between risk and inventory is required in order to know to what efficiency a given radionuclide needs to be transmuted to achieve a given reduction in risk. The

relationship between repository risk and radionuclide inventory is examined in this section. The groundwater and human intrusion pathways are considered.

3.1 Groundwater Pathway

Some calculations for a particular repository system are used to illustrate the relationship between repository risk and radionuclide inventory. The calculations are for the risk from a repository in hard rock containing transmuted waste derived from spent fuel from a PWR. They were performed using the PSA tool MASCOT [Sinc95].

The calculations reported here are based on those for a repository in hard rock containing spent fuel from a PWR or corresponding VHLW reported in references [Volc98,Bush99]. The calculations reported in references [Volc98,Bush99] were performed with the aim of showing the effects of different fuel cycles on repository risk as part of studies of partition and transmutation using conventional reactors. Such calculations can be used to identify which radionuclides should be transmuted to reduce repository risk and the results are summarised along with other studies in Table I. Here the quantitative relationships between risk and inventory are being discussed.

Calculations were performed for a range of different climate states. The risks were greatest for a boreal climate state and results for this state are shown. Calculations were also performed for different repository conditions: neutral pH, which might result from the use of bentonite as a backfill; and high pH, which would be the case in a cementitious repository.

The calculations, with some exceptions, used the same data and models as the earlier calculations. Revised biosphere factors for ^{90}Sr, ^{137}Cs and ^{126}Sn were applied. This means that the relative importance of different radionuclides in the base cases with no transmutation is different in the two sets of calculations. A different assumption about the inventory of ^{129}I in processed wastes was also made (see below). The initial inventory was based on the results of a calculation of the irradiation of UO_2. Quantities of ^{14}C and ^{36}Cl were added to the calculated inventory to account for activation.

Figures 1 and 2 show the risks over time calculated for the spent fuel from a PWR disposed of in either a neutral or high pH repository. Figures 3 and 4 show the risks from the same waste, but with most of the uranium and plutonium removed for recycling. Residual quantities of uranium (7×10^{-4}) and plutonium (4×10^{-5}) were assumed to be left in the processed waste. For the purposes of this application, all the ^{129}I was assumed be in the processed waste. (For the calculations reported in references [Volc98,Bush99], it was assumed that most of the ^{129}I would be removed by the processing, as happens currently in spent fuel reprocessing.) The figures show the radionuclides which at some time make at least a 5% contribution to the total risk. The risks shown are for a single borehole containing either spent fuel equivalent to 15 teU or HLW equivalent to 27 teU. The results can be scaled for larger quantities of wastes.

The Table II shows by what factors the different radionuclides in the processed wastes would have to be transmuted to achieve either a reduction in the risk or dose (risk is directly proportional to dose) from the repository by a factor of 10 or a 100 for the waste with the uranium and plutonium mostly removed. It has been assumed that the uranium and plutonium would either be recycled or dealt with by some other waste management procedure (see below in this section and in Chapter4.4). in the risk or dose (risk is directly proportional to dose) from the repository by a factor of 10 or a 100 for

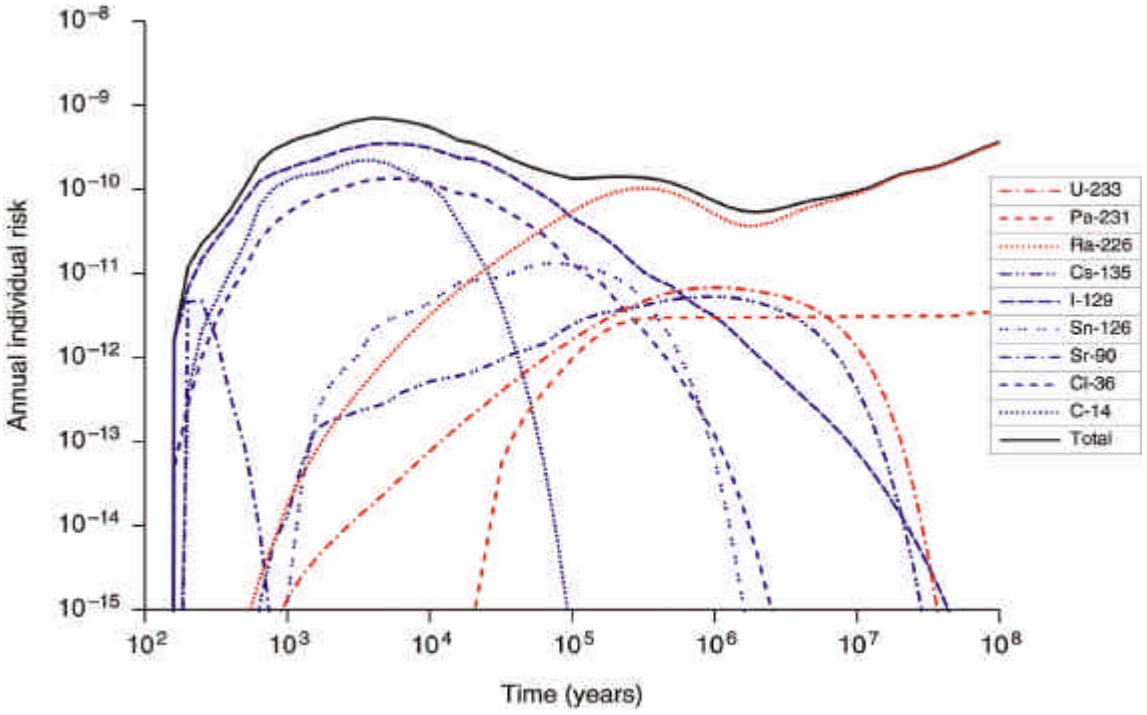

Figure 1. Risk from Groundwater Pathway for Spent Fuel in Neutral pH Repository.

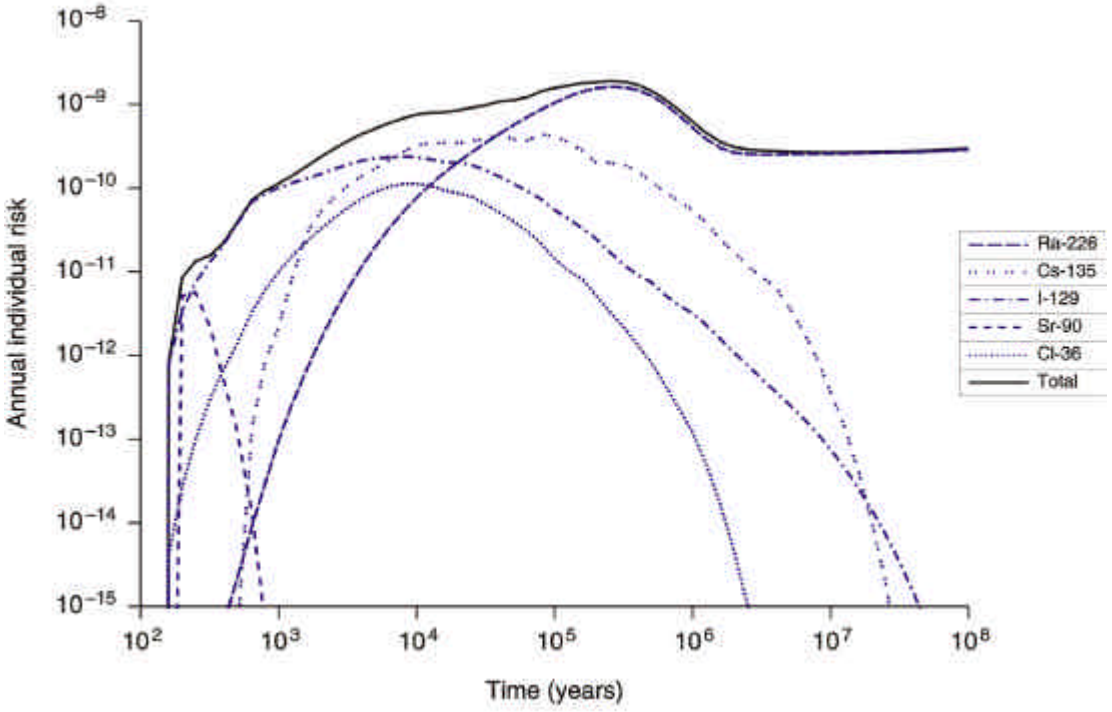

Figure 2. Risk from Groundwater Pathway for Spent Fuel in Neutral pH Repository.

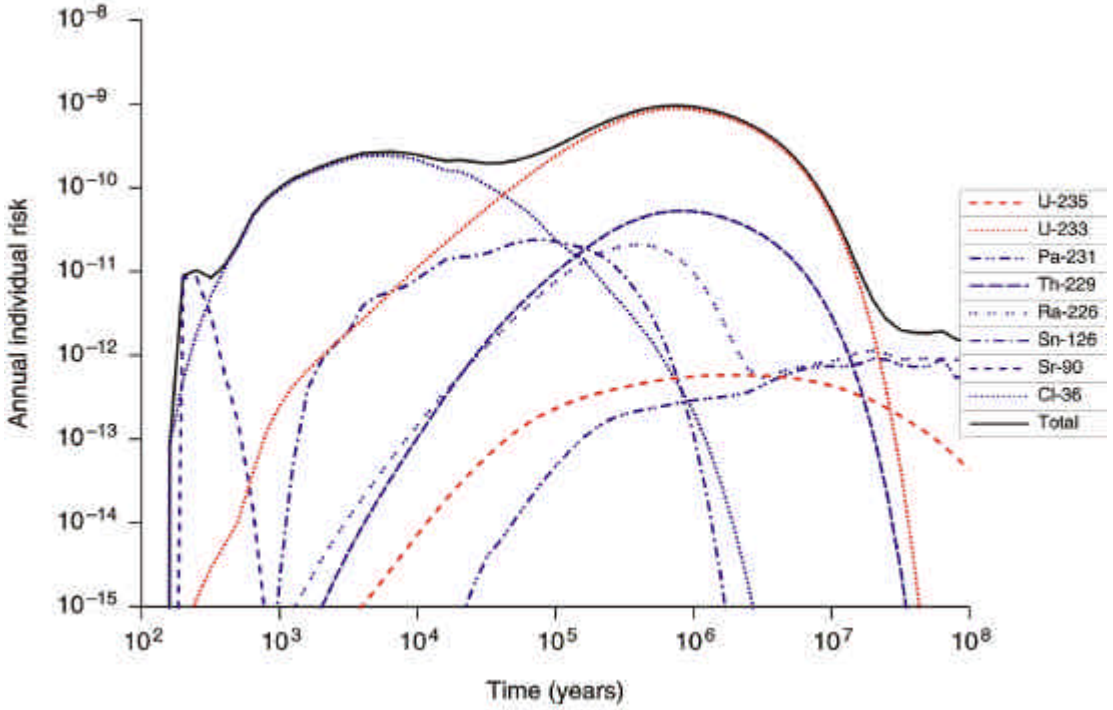

Figure 3. Risk from Groundwater Pathway for Processed Waste in Neutral pH Repository.

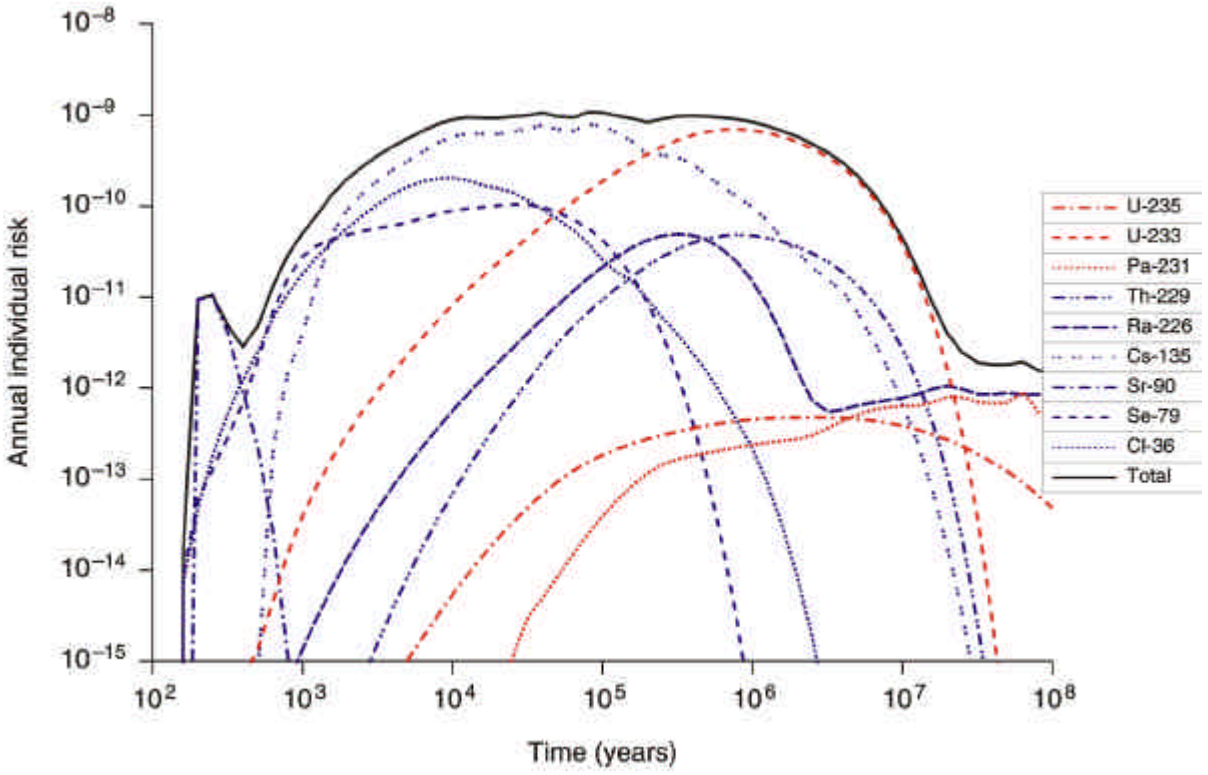

Figure 4. Risk from Groundwater Pathway for Processed Waste in High pH Repository.

Table II. Required transmutation factors for 10/100 dose reduction.

		10	**100**
Neutral pH	^{36}Cl	5	50
	^{126}Sn		4
	^{129}I	12	120
	^{135}Cs		2
	^{237}Np	12	500
	^{238}Pu		6
	^{241}Am	12	500
	^{242m}Am		6
High pH	^{36}Cl	6	60
	^{79}Se	3	50
	^{126}Sn		3
	^{129}I	12	120
	^{135}Cs	18	180
	^{237}Np	12	150
	^{238}Pu		8
	^{241}Am	5	60
	^{242m}Am		8

Figures 5 to 8 show the risks from the wastes with these reductions in inventories.

Note that these results are not unique. For radionuclides making a significant contribution to risk at any time, different combinations of reductions in inventory will lead to the same reduction in total impact. Also, reducing the inventories of different precursor radionuclides in a decay chain by different amounts can give the same overall effect on the risk from a nuclide lower in the chain.

A simple model is available which can be used to understand these results and could be used to perform further calculations for different repository systems. In this model the peak risk from a radionuclide, *R*, is calculated as follows:

$$R = \frac{rBSM}{\sqrt{\sigma_r^2 + \Sigma \sigma_g^2}} \qquad (1)$$

where r is the risk per unit annual individual dose;

B is the dose per unit radionuclide flux from the geosphere;

S is the shape factor of the flux curve;

M is the inventory of the radionuclide;

σ_r^2 is the spreading time from the repository;

Σs_g^2 is the sum of the squares of the spreading times in each of the geosphere units.

The peak risk is, according to this model, inversely proportional to the total spreading time, resulting from spreading of the peak in the radionuclide flux from the repository and the various rock

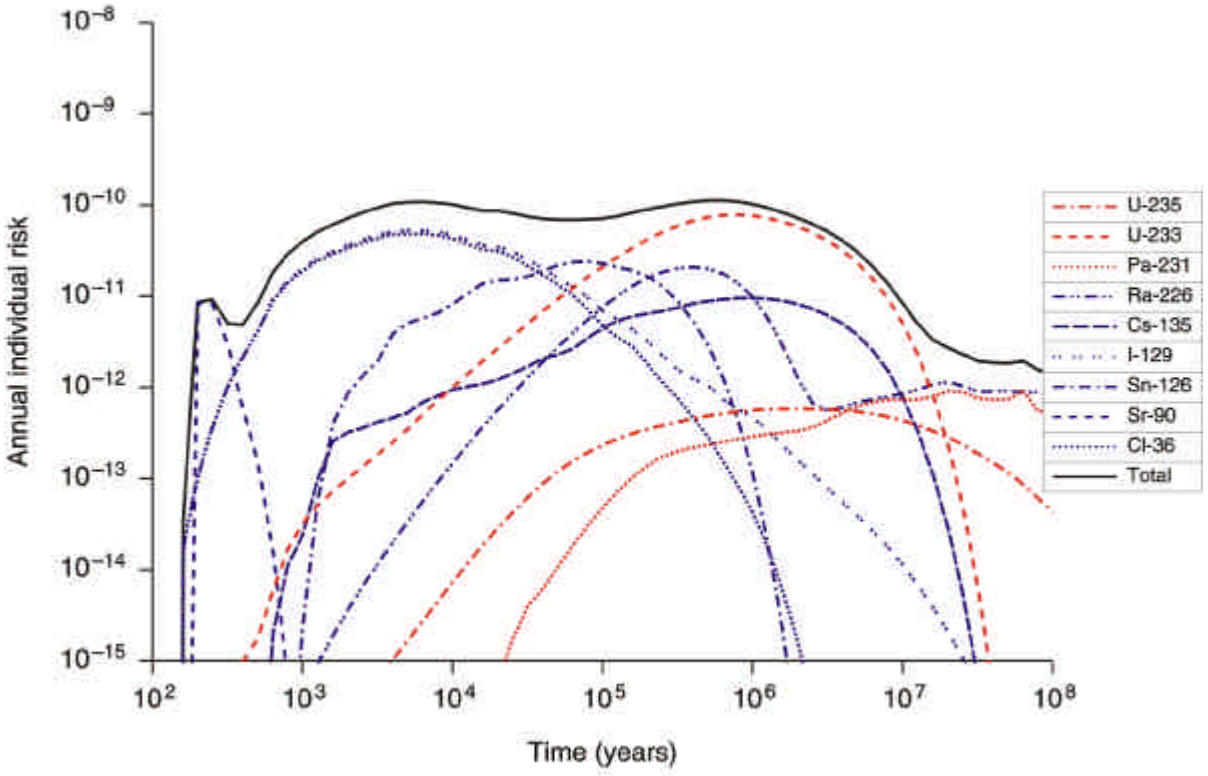

Figure 5. Risk from Groundwater Pathway for Processed Waste in Neutral pH Repository - Risk Reduced by Factor of 10.

units the radionuclide would have to pass through to reach the surface. Expressions for the spreading times are discussed below. The shape factor is dependent on the nature of the release, but does not vary much; for example, a Gaussian has a shape factor of 0.40 and decaying exponential has a shape factor of 1.

The model assumes that the release of a radionuclide from the repository would be limited by the rate groundwater flowed through the repository, any solubility limitation and sorption on repository materials (see below), and not by any other limitations such as the dissolution rate of the waste. A derivation of this expression and the others quoted in this section can be found in reference [Bake95].

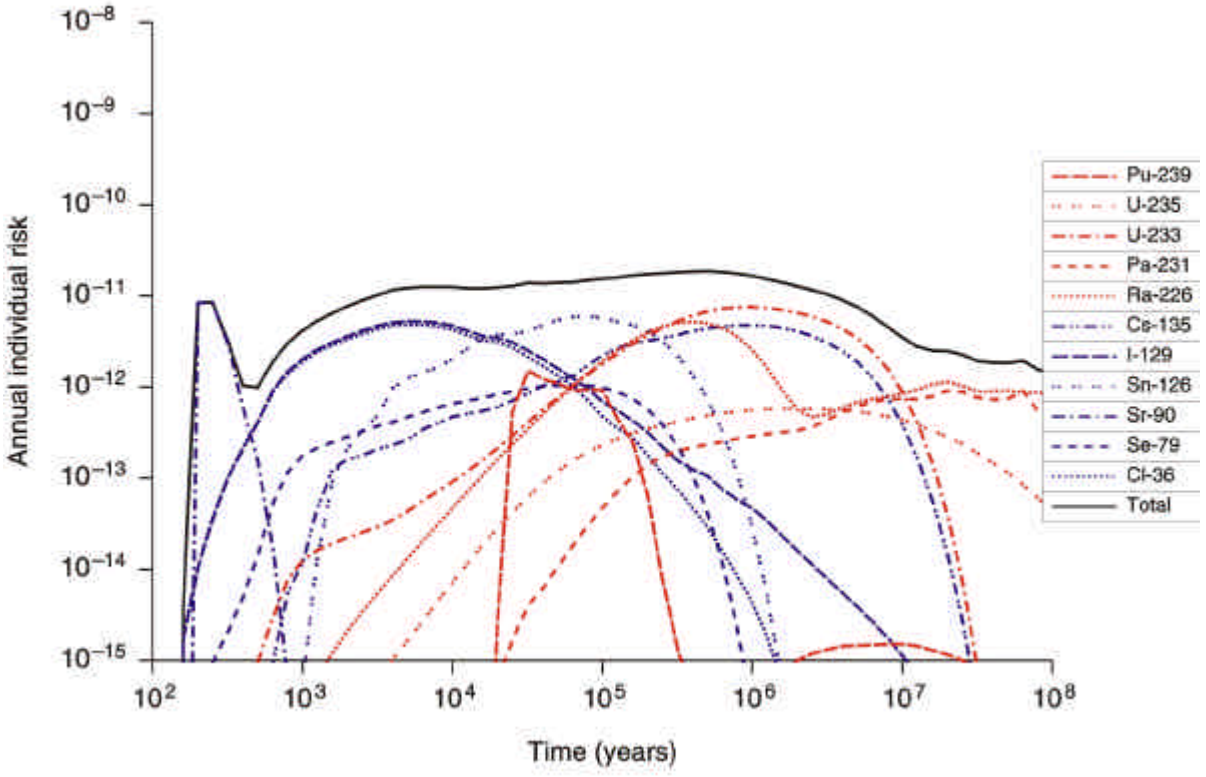

Figure 6. Risk from Groundwater Pathway for Processed Waste in High pH Repository - Risk Reduced by Factor of 10.

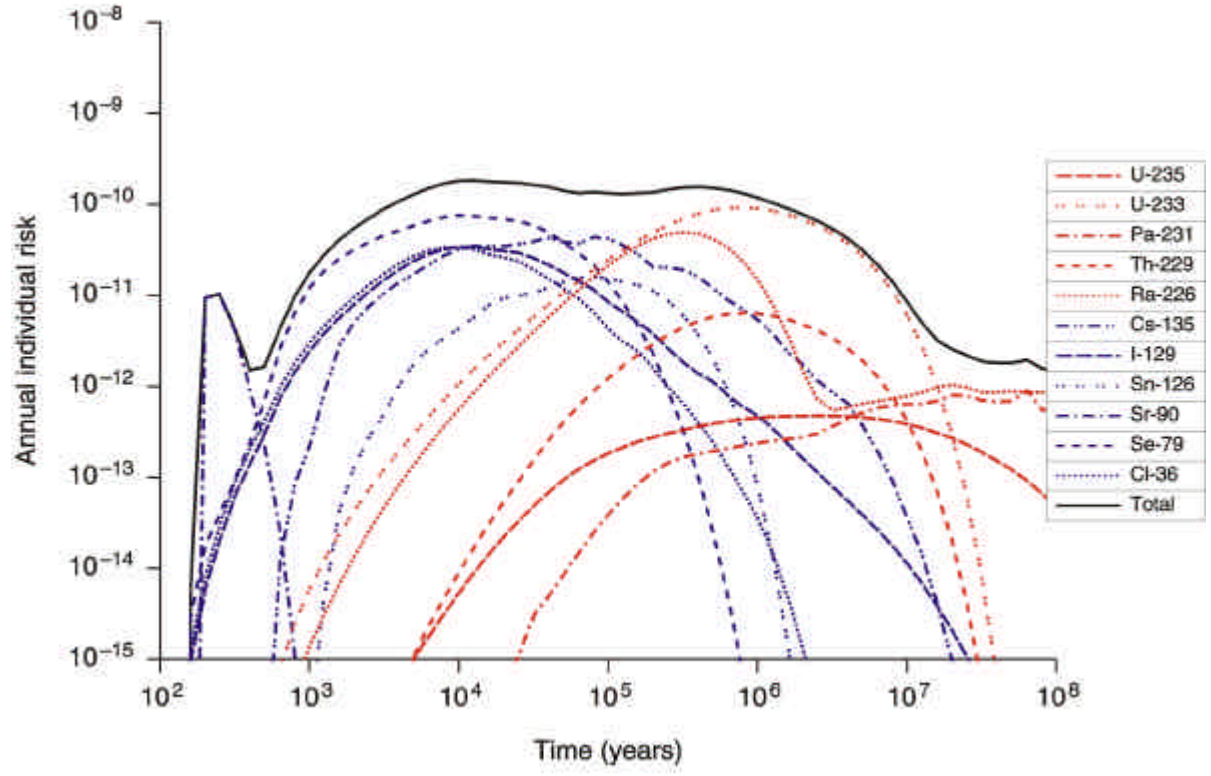

Figure 7. Risk from Groundwater Pathway for Processed Waste in Neutral pH Repository - Risk Reduced by Factor of 100.

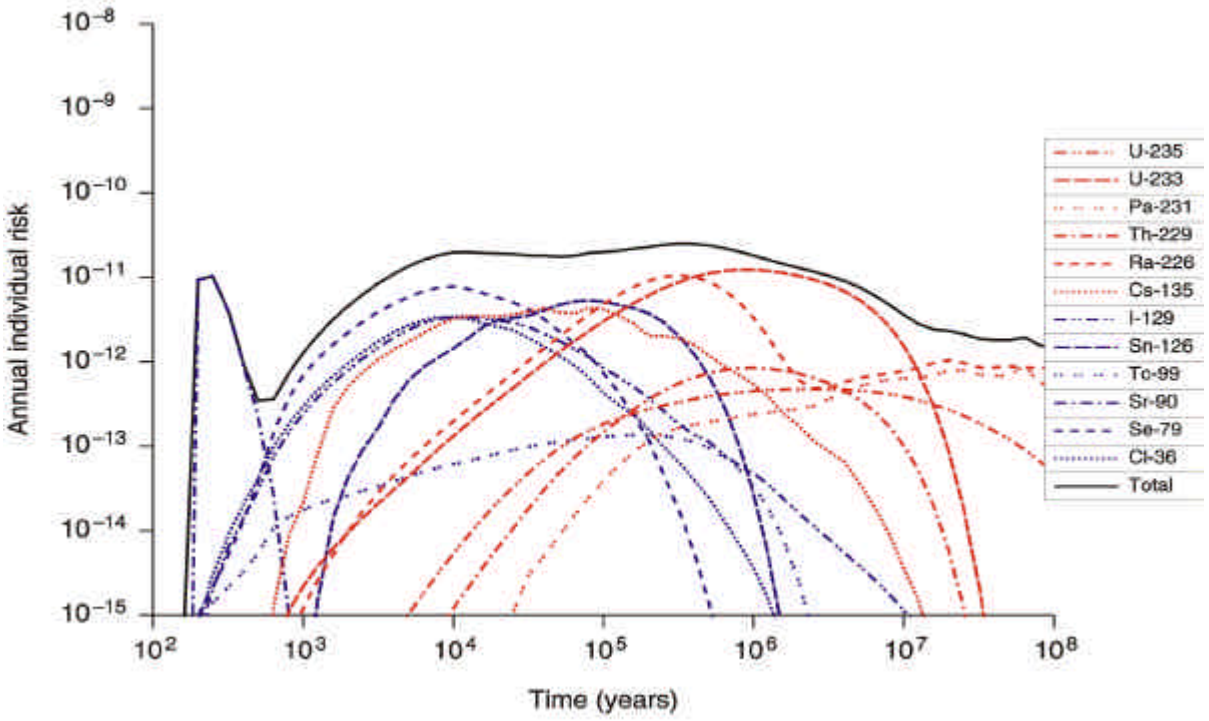

Figure 8. Risk from Groundwater Pathway for Processed Waste in High pH Repository - Risk Reduced by Factor of 100.

The version of the model described here conservatively ignores the effects of radionuclide decay on peak risk. A more sophisticated version of the model that does account for radionuclide decay is described in reference [Bake97a]. The model has been found to accurately reproduce the results of deterministic calculations using the MASCOT computer model used to calculate the (PSA) results described above, if there is not a very large dispersion in the geosphere and no ingrowth.

The peak risk given by Equation 1 assumes natural discharge of groundwater. An expression of similar form can be derived for the peak risk from the extraction of contaminated groundwater from wells.

The spreading time from a repository will depend on whether or not the solubility of the radionuclide is limited. If the solubility of a radionuclide is limited, the quantity of the radionuclide that can dissolve in the groundwater saturating the repository and hence be released from the repository over some period will be limited. The rate of release will depend on the groundwater flux through the repository and the solubility limit of the radionuclide. If the solubility of the radionuclide is effectively unlimited, the release rate will depend on the groundwater flux through the repository and the amount of sorption on repository materials.

For a radionuclide whose release is solubility-limited, the spreading time is given by:

$$s_r = k_1\left(\frac{M}{QC_s}\right) \qquad (2)$$

where k_1 is a constant;

Q is the groundwater flux through the repository;

C_S is the solubility limit of the radionuclide.

For a radionuclide whose release from a repository is not solubility limited:

$$\sigma_r = \frac{V(\phi + \rho K_d)}{Q} \tag{2}$$

where V is the repository volume;

ϕ is average repository porosity;

ρ is the mass of backfill per unit volume;

K_d is the sorption distribution coefficient of the radionuclide on the repository backfill.

The spreading time in a geosphere unit is given by:

$$\sigma_g = \sqrt{\frac{2R^2DL}{u^3}} \tag{4}$$

where R is the retardation factor of the radionuclide;

D is the dispersion coefficient;

L is the path length;

u is the transport velocity.

For a simple porous unit, R is given by:

$$R = 1 + \rho K_d / \phi \tag{5}$$

where K_d is the sorption distribution coefficient of the radionuclide on the rock.

For a unit in which the flow is in fractures, an additional term must be added to R to account for the effects of radionuclide diffusion from the fractures into the matrix porosity of the rock.

The expressions above show the main factors affecting risk from an individual radionuclide in the model. An examination of these expressions shows that whether or not the risk from an individual radionuclide is directly proportional to its inventory depends on whether or not the release of the radionuclide from the repository is solubility limited, because Equation 2 contains the radionuclide inventory, but Equation 3 does not. Note, however, that whether or not the risk from an individual radionuclide is directly proportional to its inventory will also depend on the relative magnitudes of the spreading times in the repository and geosphere. If,

$$s_r << s_g \quad (6)$$

then the exact nature of the release from the repository will not be significant and the risk from the radionuclide will be directly proportional to the inventory of the radionuclide. Where the risk from the radionuclide is affected by its solubility, dilution of a radionuclide by other nuclides which are isotopes of the same element may be important because the solubility limitation will apply to all the isotopes collectively. If the radionuclide potentially giving rise to the risk is very diluted, it can be shown that the risk is approximately proportional to inventory.

It has already been mentioned that the simple model discussed above assumes that the release of a radionuclide from a repository would be controlled by the rate groundwater flowed through the repository, any solubility limitation and sorption on repository materials, and not by any other limitations such as the dissolution rate of the waste. If the dissolution rate of the waste prevented solubility limitation of a radionuclide occurring, again this would remove any nonlinearity in the relationship between risk and inventory.

It follows that only under a particular set of circumstances would the risk from a radionuclide not be directly proportional to its inventory; however, if this were the case, a radionuclide might have to transmuted with great efficiency to produce any reduction in risk. Figure 9 illustrates this point. The figure shows the peak risk from ^{79}Se against initial inventory, calculated using the simple model above with the data for a high pH repository used to calculate the results given above obtained using the MASCOT PSA program. Where the line is horizontal, a large decrease in inventory would be required to have any affect on the risk. In fact, for the particular inventory and data in this case, the source term spreading for Se-79 is not significant, even though its release is solubility limited, and the risk is proportional to inventory.

Of the fission and activation products listed above in Chapter2, Se, Zr, Tc, Pd, Sn, Nb and Ni have relatively low solubility limits under repository conditions and there is the potential for their release from a repository to be solubility limited. Among the actinides, Th, Np, Pu, Am and Cm have relatively low solubility limits. The solubility of U is higher than the other actinides listed, but its release would still be solubility limited if large quantities of uranium were present.

In the calculations reported above, of the elements whose isotopes are listed in the table of transmutation factors required, the releases of Se, Np, Pu and Am were solubility limited in both types of repository, while the release of Sn was limited in the high pH, but not the neutral pH, repository.

The simple model described above also shows the reasons why particular radionuclides give the peak risks from a repository. The main radionuclide dependent parameters in the model are solubility limitation and sorption in the repository and sorption on the rocks. Radionuclides with high solubility limits and low sorption coefficients, coupled with long half-lives and depending on inventories, give the highest releases and generally highest risks, depending on their biosphere factors.

Figures 1 and 2 for the spent fuel in the two different types of repository show the peak risks coming from a decay daughter of the natural ^{238}U, although in the case of the neutral pH repository the peak risk occurs after a very long period when quantitative predictions are probably not meaningful. The implications of this are discussed below in Chapter 4.4.

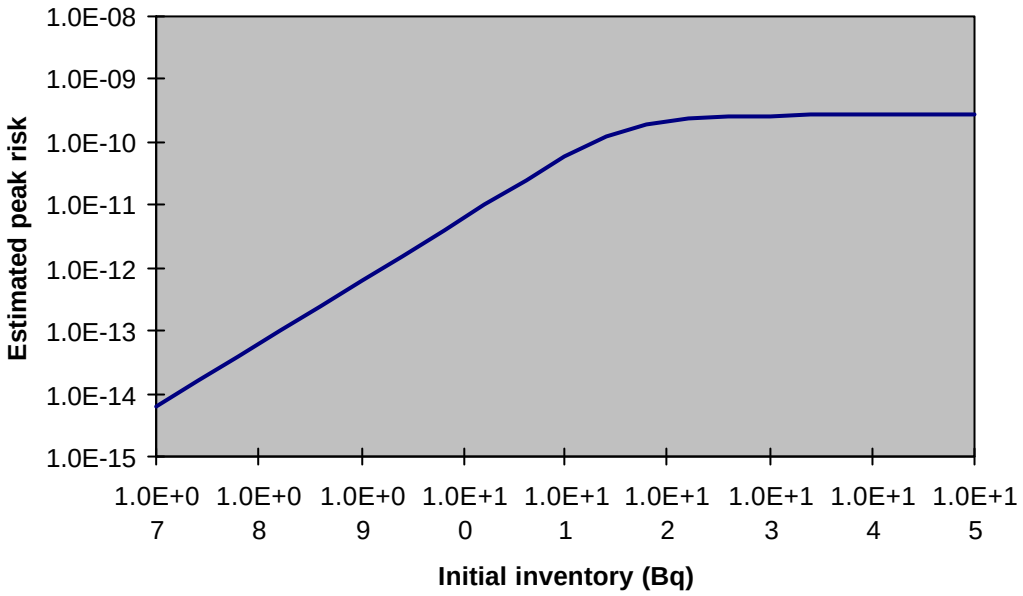

Figure 9. Peak Risk from Groundwater Pathway for Se-79 vs. Inventory.

3.2 Human Intrusion Pathway

The second pathway for the release of radionuclides from a repository is inadvertent human intrusion. The most likely way in which an intrusion would occur, for a repository in hard rock, would be the drilling of a borehole. This might lead to the exposure of geotechnical workers ("core examination scenario") and the later exposure of others due to spoil being left on the ground at the drilling site ("site occupation scenario").

Example calculations are again used to illustrate the relationship between radionuclide inventory and risk and the factors by which the inventories of specific radionuclides would have to be reduced to decrease the total risk by given factors. The calculations are again based on those reported in references [Volc98,Bush99] for PWR spent fuel. The calculations have been made for the processed waste with most of the uranium and plutonium removed.. Figures 10 to 13 show the base case results from references [Volc98,Bush99]. The risks over time from the core examination and occupation scenarios for the PWR spent fuel and processed wastes are plotted. The results are plotted in terms of risk here, rather than dose as in references [Volc98,Bush99], and show the significant individual radionuclide contributors to total risk. Note that the risk from an individual radionuclide can increase with time in the occupation scenario, even if its inventory is not increasing through ingrowth, because of accumulation of spoil.

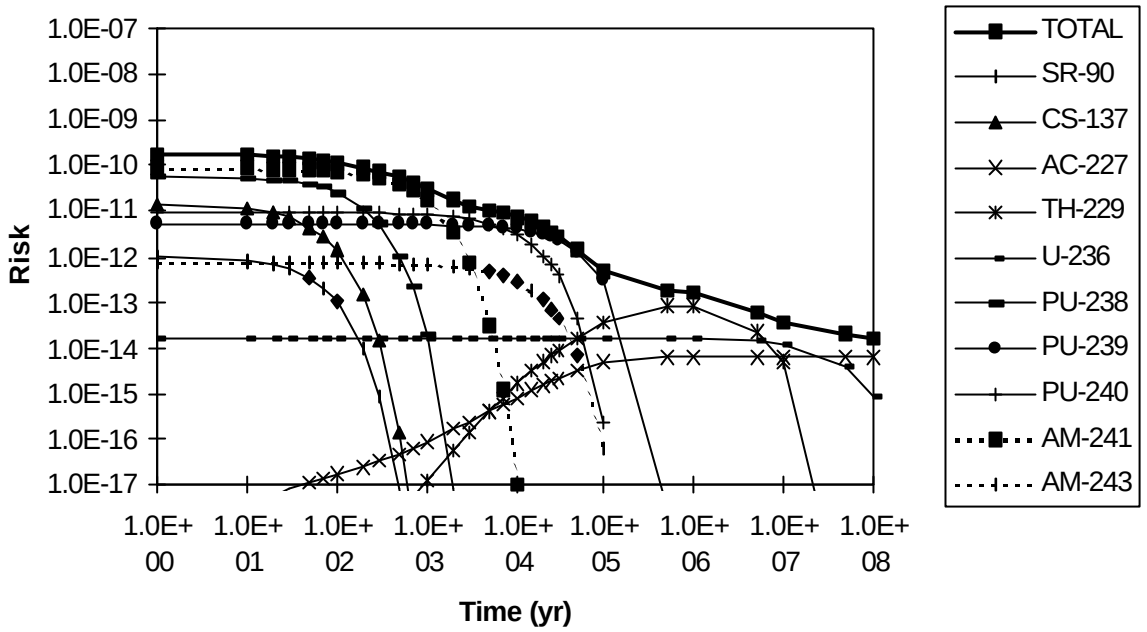

Figure 10. Risk from Human Intrusion Pathway for Spent Fuel - Core Examination Scenario.

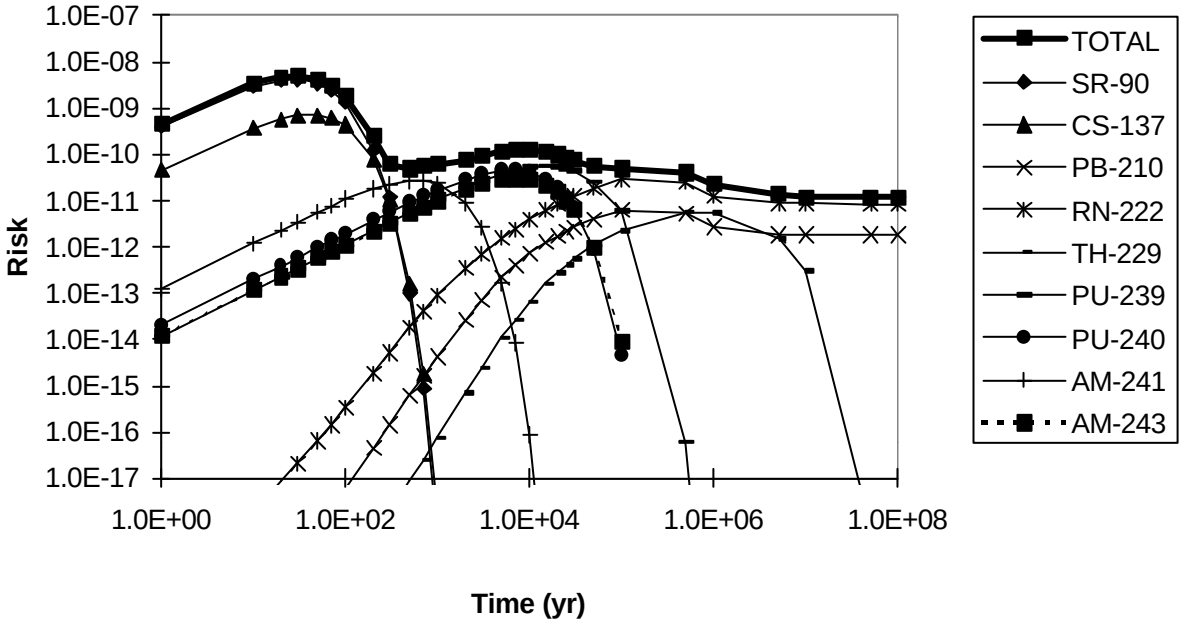

Figure 11. Risk from Human Intrusion Pathway for Spent Fuel - Occupation Scenario.

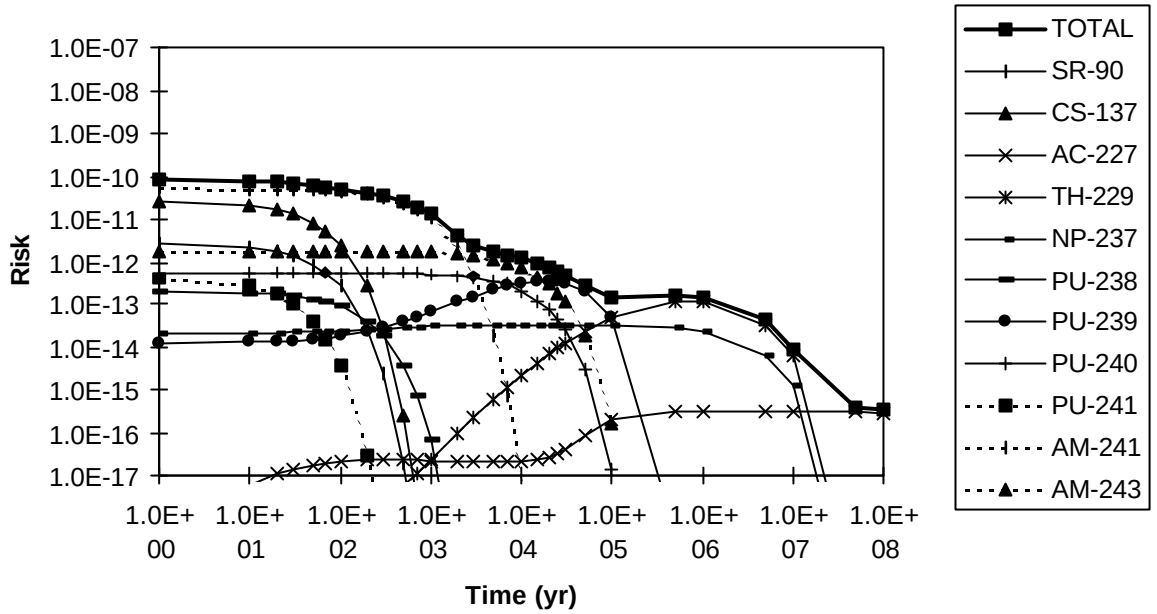

Figure 12. Risk from Human Intrusion Pathway for Processed Waste - Core Examination Scenario.

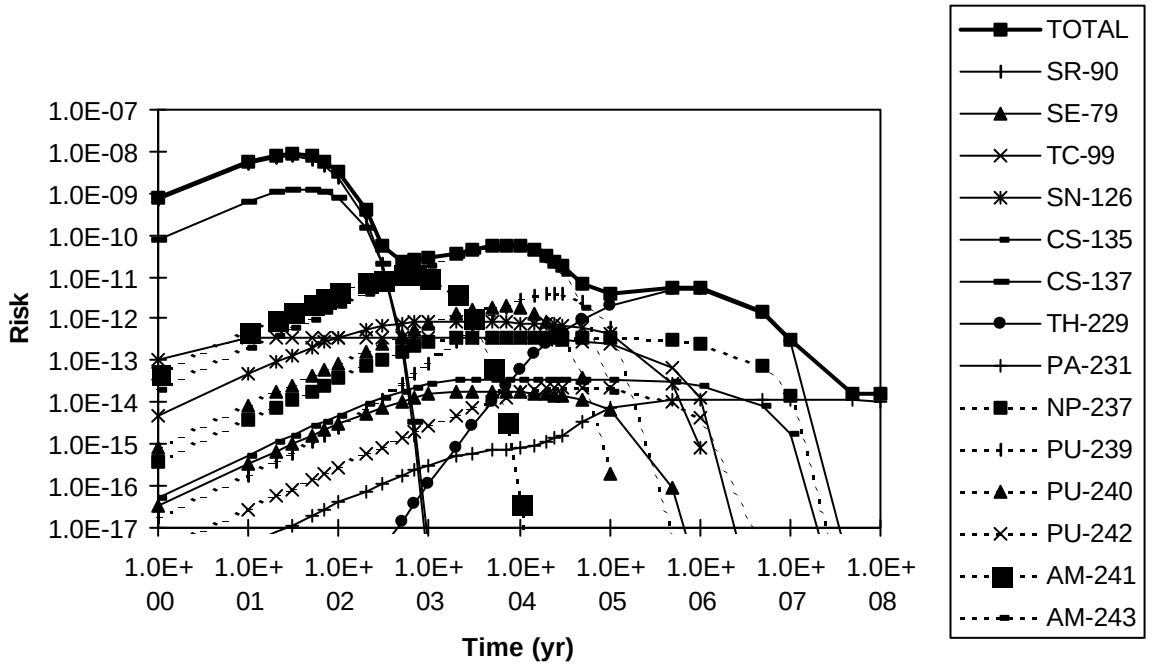

Figure 13. Risk from Human Intrusion Pathway for Processed Waste - Occupation Scenario.

The Table III shows the factors by which the inventories of individual radionuclides would have to be transmuted to reduce the overall risk by 10 and 100 (to an accuracy of 5%). In this case, risk reduction over different time periods is considered, because the early risks are highest but can result

Table III. Factors by which the inventories of individual radionuclides would have to be transmuted to reduce the overall risk by 10 and 100 (to an accuracy of 5%).

	Timescale (years)	Radio-nuclides	10			100		
Core examination scenario	0 - 3×10^2	^{90}Sr		7	10	200	100	
		^{137}Cs	30	12	10	200	100	
		^{238}Pu			10	200	100	
		^{240}Pu			10	200	100	
		^{241}Pu					100	
		^{241}Am	30	12	10	200	100	
		^{243}Am		7	10	200	100	
	3×10^2 - 10^5	^{238}Pu					100	
		^{240}Pu			10	115	100	
		^{241}Am	30	12	10	115	100	
		^{243}Am		10	10	115	100	
Site occupation scenario	0 - 3×10^2	^{90}Sr		11	10	110	100	
		^{137}Cs		7	10	80	100	
	3×10^2 - 10^5	^{79}Se					100	
		^{99}Tc		10		120	100	
		^{126}Sn		10		120	100	
		^{135}Cs					100	
		^{237}Np		10		120	100	
		^{239}Pu					100	
		^{240}Pu		10		120	100	
		^{242}Pu					100	
		^{241}Am	23	10		120	100	
		^{243}Am	23	10		120	100	

from relatively short-lived radionuclides. Again, the results are not unique and, in this case, different combinations of reductions for different sets of radionuclides are shown by way of example. In each case, a combination is shown which minimises the number of radionuclides which would have to be transmuted to achieve the given reduction in risk.

In the case of the core examination scenario, the early risks, over the first 300 years, result from ^{241}Am and ^{137}Cs, and to a lesser extent ^{90}Sr and ^{243}Am. In this case, a reduction in risk by a factor of 10 could be achieved by reducing the inventories of ^{241}Am and ^{137}Cs. Reducing the risk by a factor of 100 would require the inventories of plutonium isotopes to be reduced. If the likelihood of inadvertent intrusion in the first 300 years can be discounted, a reduction in risk by a factor of ten could be achieved by reducing the inventories of only the americium isotopes, or a reduction in risk by 100 by also reducing the inventories of some of the plutonium isotopes. Note that reducing the inventories of ^{241}Am and ^{243}Am would reduce the later ingrowth of ^{239}Pu and ^{237}Np respectively. Reducing the inventory of ^{241}Am would also reduce the ingrowth of ^{229}Th, which makes the dominant contribution to risk after 10^5 years.

The results are different in the case of the site occupation scenario. The risks in the early period are dominated by ^{90}Sr and ^{137}Cs. In the later period, a reduction in risk by a factor of ten could be achieved by reducing only the inventories of the americium isotopes; however, to achieve a reduction in risk by a factor of 100 would require some of the longer-lived fission products, as well as actinides, to be transmuted.

The relationship between risk or dose from an individual radionuclide and its inventory is more straightforward for this human intrusion pathway than the groundwater pathway considered in Section 3.1. In the absence of any change in repository volume or area, risk and dose are directly proportional to inventory. The dose scales with the volume or area of the repository, but the risk remains constant (see Chapter 4.3).

If the first few hundred years can be discounted, where the effects of ^{90}Srand ^{137}Cs dominate, the risk from the human intrusion pathway could be significantly reduced by transmuting only actinides, in contrast to the groundwater pathway, where fission products would have to be transmuted; however, if large decreases in risk were required, by a factor of at least 100, some fission products would also have to transmuted.

It is worth noting that the risks calculated here for the human intrusion pathway are lower than those for the groundwater pathway, by approximately an order of magnitude, if the effects of ^{90}Sr and ^{137}Cs over the first few hundred years are discounted; otherwise, the risks calculated are approximately an order of magnitude greater. The calculated doses from an intrusion event, however, are high.

4. Discussion

4.1 Using Repository Risk to Set the Objectives

The objectives of ADS have been examined from the perspective of reducing the risk from deep repositories for HLW. An alternative view would be that uncertainties in the estimates of long-term risks from repositories are such that they cannot be relied on and ADS should have the objective of reducing long-term total radiotoxicity. The uncertainties about estimations of risk can be exaggerated. Risk studies consider alternative evolution scenarios and pessimistic assumptions can be made about aspects such as land being used for subsistence farming where a community takes all

its food from a contaminated area. In the case of human intrusion scenarios, to calculate risks, probabilities have to be estimated for future human actions. In the case of the scenario considered here there seems no reason to attach a high probability to intrusion into a deep, hard rock. Historical data are available on the frequency of such borehole drilling. Likely locations of natural resources, such as oil, would be a factor in the choice of a repository site and therefore the likelihood of intrusion would be minimised. Even if the view point is adopted that reducing overall radiotoxicity should be the main aim, repository risk still needs to be considered, unless radiotoxicity could be reduced to such an extent that long-term radiotoxicity would be reduced to effectively zero. Otherwise there would the possibility of reducing overall radiotoxicity, but having no practical impact on risk.

4.2 Activation Products

That ^{36}Cl is the dominant contributor to risk from the groundwater pathway in studies in the UK was noted in Chapter 2. ^{36}Cl is an activation product that can arise from neutron capture in stable ^{35}Cl as well as in other ways. The main source of ^{36}Cl in UK wastes is waste derived from the first generation gas-cooled Magnox reactors. Nevertheless, that a radionuclide created by the activation of nuclides present at low concentrations in materials can be a dominant contributor to the risk from a repository has important implications for the design of ADS. It is quite conceivable that with the use of inappropriate or badly specified materials, in terms of repository risk, the positive benefit of transmutating actinides and fission products could be negated by the creation of activation products.

^{36}Cl is an important contributor to risk in the UK studies because it would have a high solubility and would not sorb strongly in a repository or a geosphere. ^{129}I is sometimes predicted as a peak contributor to risk for the same reasons. Note that ^{129}I can also be an activation product. Other activation products which have more limited solubilities or higher sorption coefficients have still been shown to make a significant contribution to risk in some studies, as shown by Table III. An ADS should be designed, and the materials from which they are constructed should be specified, to minimise the creation of activation products, particularly those with high solubilities and low sorption coefficients like ^{36}Cl and ^{129}I.

Salts containing chlorine and fluorine have been suggested for use in ADS. Fluorine would be expected to behave similarly to chlorine in a repository system, but it has no long-lived radioisotopes.

Lead and lead/bismuth eutectics are being widely considered for use as targets or for cooling in ADS. Both lead and bismuth have long-lived isotopes, but only bismuth has a long-lived isotope with higher mass than the stable isotope or isotopes of the element. Both lead and bismuth can have high solubilities, but are relatively highly sorbing.

It is noted that the chemical toxicity, as well as the radiotoxicity, of wastes disposed of in a repository needs to be addressed. If it were necessary to disposed of large quantities of lead from an ADS in a repository, this potential impact would need to be considered.

4.3 Secondary Wastes

Any additional process in a fuel cycle will produce some secondary wastes, including both operational and decommissioning wastes. Wastes may be activated or contaminated. Activation has already been discussed above, in Chapter 4.2. The level of contamination would depend on the

efficiency of the process. Low contamination would imply high partition efficiencies in the application of ADS.

It should be noted that a given amount of activity in secondary wastes might have greater impact than in spent fuel or VHLW. Secondary wastes would generally have relatively greater volume, which might lead to larger groundwater fluxes through them in a repository (see Equations 2 and 3). For the human intrusion pathway, the risk will generally be unaffected by a change in waste nature or volume. This is because the frequency of intrusion will increase with increasing volume, as the concentration of activity in the waste reduces; the dose will, however, decrease with increasing volume.

Radionuclides might not be so well contained in secondary wastes for other reasons. Their greater volume might affect the feasibility of different packaging options. Also, organic materials in secondary wastes can degrade to produce products that can complex radionuclides, potentially increasing their solubilities, and hence the rate at which they would be released from a repository, by orders of magnitude. Alternatively, the introduction of partition technologies might allow different wastes to be conditioned in different ways which would improve their containment in a repository (see the discussion below on optimisation, in Chapter 4.6).

4.4 Uranium and Thorium

That the natural ^{238}U in spent fuel can cause the highest peak risks from a repository was observed in Chapter 3.1. Although ^{238}U is naturally occurring, the risks from the material cannot be ignored once a large quantity is accumulated. In terms of transmuting legacy wastes to reduce repository risk, uranium does present a problem. It would be present in spent fuel and there would be large quantities of by-product depleted uranium from fuel manufacture. Only some of this uranium could be recycled in a fuel cycle. It could not be transmuted. An acceptable waste management solution would have to found both for applying transmutation to legacy wastes and in new fuel cycles (see Chapter 4.6).

The risk from thorium fuels has not been calculated in the same way as for the uranium fuels, but an examination of the data on solubility limits, sorption coefficients and biosphere factors suggests that the use of thorium fuels could have the same implications as using uranium fuels.

4.5 Reducing the Number or Cost of Repositories

The discussion so far has been in terms of reducing the risks from a repository by reducing the radionuclide inventory in the repository. In practice, repositories are not designed to present as low a risk as possible; but against regulatory guidance, which varies from country to country, as to what would present an acceptable risk. Effectively this limits the inventory of radionuclides that could be put into a particular repository. If ADS could reduce the number of repositories needed, this would have a significant impact on the costs of disposal and possibly on public acceptability. The reduction in inventories of particular radionuclides needed to achieve a significant impact from this perspective might be relatively small. In simple terms, a reduction by a factor of two might half the number of repositories needed, although the accuracy with which estimates of repository risk can be made needs to be borne in mind. If transmutation could be used to reduce the number of repositories, this would be likely to have a greater impact than reducing the risks of single repositories (which are calculated to be low).

Another way in which costs might be reduced would be to reduce the depth of a repository while keeping the risk constant. An expression for the relationship between risk, repository depth, *h*, and inventory can be derived from the simple model described in Chapter 3:

$$R = rBMS\sqrt{\frac{u^3}{2R^2Dk_2h}} \qquad (7)$$

where k_2 is a constant.

This expression assumes that the path length is directly proportional to depth and the source term can be neglected. It suggests that a decrease in inventory from transmutation by some factor would allow a decrease in depth by the same factor squared to give the same risk. In practice, it is not likely that such a large decrease in depth would be possible: the dispersion coefficient, *D*, would be related to the path length and hence depth in this model; the effects of the source on spreading and radioactive decay would complicate the relationship between risk, inventory and depth; and, at a specific site, the relationship between depth and risk would depend on the local hydrogeology where there might be a number of rock layers with different properties. Nevertheless, it might be possible to reduce the depth and therefore cost of a deep repository.

To produce a qualitative difference in repository type, i.e. a surface or shallow repository rather than a deep repository, implies very great reduction in inventory. For example, in the UK, low-level waste (LLW), at least some of which will go to surface repository, is defined as waste with a beta/gamma activity of 400 to 12 MBq kg^{-1} and an alpha activity of 400 to 4 MBq kg^{-1}. The activity in UO_2 spent fuel after 50 years of cooling would be approximately 4×10^6 MBq kg^{-1} for beta activity and 4×10^5 MBq kg^{-1} for alpha activity. It has been suggested that ADS could produce only LLW [Rubb97].

4.6 Optimisation

This and other similar studies [Kane95,Volc98,Bush99] have discussed the objectives for partition and transmutation based on the results of existing studies and models of radioactive waste disposal. Existing repository concepts have been optimised for the disposal of spent fuel and other wastes derived from fuel cycles involving conventional reactors. Given that the application of ADS is still in the research phase, with the long-term objective of developing new fuel cycles with reduced environmental impact, the approach from now on should be to develop ADS such that whole fuel cycle, including waste management, is optimised from point of view of risks and costs. ADS should be developed taking into account what it is possible to achieve using repositories. Consideration should be given to whether different repository concepts would be optimal for wastes derived from fuel cycles involving ADS. Given that the introduction of ADS implies the use of novel partition technologies, there would seem to be potential in new waste disposal concepts to, for example, condition different waste streams in different ways or create chemical conditions in different repositories or repository vaults which minimised the release of particular radionuclides. The management of uranium might be part of this process (see Chapter 4.4).

5. Conclusions

The following conclusions can be drawn from the analysis in this section.

- A wide-ranging review of repository risk studies has used to identify which radionuclides would need to be transmuted to reduce risk from a repository. Specific examples have been used to show by how much the inventory of different radionuclides would have to be transmuted to produce reductions in repository risk by factors of 10 and 100.
- The studies reviewed show the importance of reducing inventories of fission products as well as actinides to reduce repository risk. Even with the human intrusion pathway, where there is a closer relationship between risk and radiotoxicity than with the groundwater pathway, reductions in risk or dose of two of orders of magnitude would need some reduction in fission product inventories.
- In reported repository risk studies there is a wide variation in what are the most significant radionuclides and by how much the inventories of these radionuclides would have to be transmuted to decrease the risk. Variations arise from different assumptions about scenarios, repository design and siting, and other data. Radioactive waste management is a national responsibility, while the development of a commercial ADS would in all likelihood be international. It would be unwise to develop ADS based on the results of a single scenario or repository study for one country. If the objective is to reduce repository risk, ADS should ideally be developed to retain the flexibility to transmute as wide a range as possible of the long-lived fission products and actinides given here.
- It is conceivable that with the use of inappropriate or badly specified materials, in terms of repository risk, the positive benefit of transmutating actinides and fission products could be negated by the creation of activation products. ADS should be designed, and the materials from which they are constructed should be specified, to minimise the creation of activation products, particularly those with high solubilities and low sorption coefficients under repository system conditions like ^{36}Cl and ^{129}I.
- The decay daughters of uranium can make a significant contribution to repository risk over long timescales. Significant quantities of uranium could not be transmuted. The waste management of uranium (or thorium) needs to be addressed in a fuel cycle involving ADS.
- The impact of introducing ADS on the number of repositories required or depth might be more significant than the straight forward reduction in the (low) risk from a single repository.
- The optimisation of fuel cycles involving ADS should include waste management aspects, e.g. waste conditioning and repository design.

VIII. ASSESSMENT OF ACCELERATOR TECHNOLOGY AND ACCELERATOR RELIABILITY STUDIES

1. Introduction

The applicability of accelerator technology in future fuel cycles depends on a number of factors, including technical feasibility and cost. The high-power accelerators proposed for transmutation of radioactive wastes and plutonium require a high level of capital investment and carry high operational costs. It is therefore important to be able to identify the most cost effective system. AEA Technology has developed two costing models to evaluate the different accelerator options available and has applied the models to some of the accelerator systems that have been proposed.

The models are in the form of spreadsheets: the first covers linear accelerators, such as that proposed by Los Alamos National Laboratory (LANL) [Venn98a], and the second covers circular accelerators, such as that proposed by Rubbia et al., as the driver for the Energy Amplifier [Fern96]. Despite similarities in the costing methods, the constructional differences between linear and circular machines required separate models to be created.

The models have been used to investigate the effects on cost of varying a number of parameters for each type of accelerator. An equivalent baseline specification for both linear and circular machines was established by working at constant neutron flux and this proved to be the pivotal parameter for all the costing exercises. The required neutron flux assumed was based on the proposed systems studied.

It is not possible to establish a cost for an accelerator system to within an accuracy of approximately ±20% without a detailed technical design for the system. The models developed are intended to provide a relatively simple way of comparing the costs of different system options (linear and circular) and the effect on cost of varying system parameters. The example costings presented here should only be regarded as indicative.

A very important issue for ADS is the reliability and availability of the accelerator. Coupling of an accelerator to a nuclear installation like a subcritical core of ADS puts new requirements on high availability, reliability and maintainability of accelerators. Moreover, persistent beam power fluctuations will certainly have a negative influence on ADS. In collaboration with Los Alamos National Laboratory a reliability study of the LANSCE accelerator have been performed [Eric98] in order to estimate and improve the availability and reliability of future accelerator designs. The accelerator facility at Los Alamos Neutron Science Center (LANSCE) offered enough operating history to supply meaningful reliability data.

2. Survey of Proposed Accelerator Schemes

The development of accelerator-based transmutation technology has been led by Los Alamos National Laboratory (LANL), although several other nations now have R&D programmes of some form in this area. At LANL, the Accelerator Treatment of Waste (ATW) programme has run in tandem with the Accelerator Production of Tritium (APT) programme, which proposes the use of either a 1.7GeV/100mA cw superconducting or a 1.3GeV/134mA cw normal linac. The reference design for ATW is a 1GeV/40mA cw linac which would drive up to five waste burners [Venn98a]

and produce electricity. In Europe there are programmes in France (HADRON & IPHI) and the Energy Amplifier proposed by Rubbia using a 1GeV/12.5mA circular accelerator [Fern96]. The latter device has evolved through several different configurations involving linear and circular machines. A linear accelerator based 1GeV/30mA system is under consideration in Italy. In Japan, the JAERI has proposed the OMEGA machine, a 1.5GeV/39mA (5mA cw) linac, and, in Korea, the HYPER project has proposed a 1GeV/20mA linear accelerator.

It is clear from this brief survey that most proposals assume a beam energy of 1GeV or more to be necessary and that linear machines are the favoured option. There are technical reasons for preferring the linear option based upon a fundamental limit of operation for isochronous cyclotrons. In the normal cyclotron with D-shaped magnets, the field and accelerating gradient are nominally constant with radius. As the proton energy increases with each orbit, the mass increases due to the relativistic motion and the separation of each successive orbit is reduced. Eventually the penultimate and ultimate orbit are so close that the protons cannot be extracted without disturbing the orbital motion. An additional problem is the phase slippage of the particles as the outer orbits bunch, so that eventually no accelerating field is seen by the particles and the energy limit of the cyclotron is reached.

It is possible to avoid the energy limitation by designing the cyclotron to operate with an energy gain per turn which increases with radius and by simultaneously increasing the magnetic field with radius such that each successive orbit is separated by the same radial distance. The particles are thus maintained in synchronous motion with the accelerating fields and higher energies can be obtained. The separated sector cyclotron (SSC) and the closely related separated orbit cyclotron (SOC) are such devices. There are several of these machines in use, e.g. at PSI in Switzerland, TRIUMF in Canada and TUM Garching in Germany. Although economic considerations favour cyclotron designs, as will be shown in Section 3, the relatively wider experience with linacs is probably a major contributing factor to the greater number of linac based proposals.

3. Modelling

In order to compare the linear and circular machines, a common baseline specification of a 1GeV/10mA cw proton beam was used. Assuming a beam radius at the target of 10cm, and a neutron yield Y_n per proton on a lead or lead/bismuth target given by [Gudo97]:

$$Y_n = 26.5E(GeV) - 1.5$$

a cw beam of 1GeV/10mA would produce 5×10^{15} n cm^{-2} s^{-1}. Most of the proposed systems discussed above produce fluxes of the order 10^{15} - 10^{16} n cm^{-2} s^{-1}.

An exchange rate of 1€=£0.8=US$1.28 has been used to compare different schemes. The costs are presented in € at 1996 values.

3.1 Linear Accelerator Cost Model

The linear accelerator cost model is based upon a spreadsheet originally provided by LANL and modified by AEA Technology to incorporate costs appropriate to the EU. The model assumes a series of linear accelerators as shown in the schematic diagram of Fig. 1. There may be one single

injector or two which are merged in a funnel and these can be accommodated by using the total beam current in the spreadsheet.

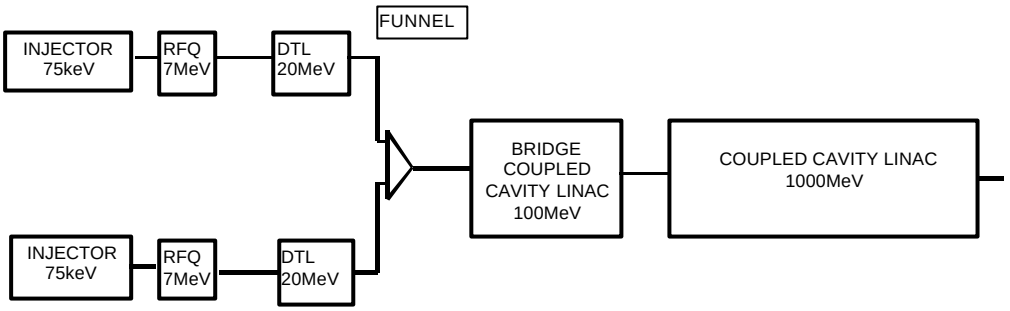

Figure 1. Schematic Diagram of Baseline Linear Accelerator.

3.1.1 Spreadsheet

The methodology is to establish capital costings for the three major parts of the highest energy linac, viz. RF power supplies, cavities and vacuum system and then multiply their sum to account for the costs the rest of the device, of design, administration, staff, construction and buildings. This establishes the capital cost of the accelerator and its associated buildings and construction. The costs of operating the accelerator are then calculated from the cost of electrical power used, the cost of maintaining the RF power supplies and the cost of operating staff per annum. If desired, the repayment of the capital costs over a given period can also be included. The costs of operating over extended periods can then be obtained from the annual cost, with interest paid on the capital if desired. Finally, in order to compare the linear and circular machines the cost of producing a unit of 10^{18} neutrons is calculated over a 10-year and 40-year period.

The RF power absorbed in the coupled cavity linac (CCL) cavity walls is determined by the structure length and the shunt impedance of the cavities. The structure length, L, is obtained from the equation:

$$L = \frac{\Delta U}{G_{str} \cos \phi}$$

where U is the beam energy, G_{str} is the accelerating gradient and ϕ is the phase angle between beam and RF power. The shunt impedance, Z, of a cavity characterises its efficiency, i.e. the ratio of power transferred to the beam to that absorbed in its walls. The effective shunt impedance is obtained by multiplying the shunt impedance by the square of the transit time factor, T. The values used in the spreadsheet are calculated using the equation:

$$ZT^2 = (0.0029\, I_b + 4.24)\ln U + 9.30 - 0.046\, I_b$$

where I_b is the beam current in mA and U is in MeV. This expression was obtained by parametric fit to data generated by the code SUPERFISH. In the linac, as the beam energy increases with distance traversed, the shunt impedance also varies. The average value is used by the spreadsheet. The RF power absorbed by the cavity walls is given by the equation:

$$P_{rfcav} = \frac{LG_{str}}{ZT^2}$$

Table I shows the spreadsheet data input and output page; the parameters are described in detail below. Essentially, the upper part of the spreadsheet consists of input data (such as cost per unit of RF power and cavities), whilst the lower part of the spreadsheet calculates the shunt impedance, ZT^2, power requirement and length of the linac for the given baseline specification of a 1GeV/10mA cw proton beam. These are combined to obtain the RF capital and operating costs as described above.

Linac Total Length. The total length of the CCL including the intercavity tanks, which are estimated to be 40% of the structure length.

Prf(total)-Linac. The total RF power requirement of the linac including the RFQ (radio frequency quadropole), DTL (drift tube linac) and funnel (Pbeam Total + Prf(cav) CCL +Pcon)

Total Linac AC. The total AC line power for the linac, including the non-RF elements.

Annual AC Costs. The cost of providing AC power for one year operation.

Annual Staff Costs. Cost of staff for one year estimated at 70,000 €/person

Annual M&S Cost. The annual cost of maintenance and spares. It is assumed that this is dominated by the replacement cost of the klystron tubes. A klystron tube lifetime of 4500 hours is assumed and the cost of replacement is calculated from this, the number of klystrons and the number of working hours assuming 100% availability.

Linac Cap Cost. The capital cost of the linac, which is comprised the RF power supplies, the construction of the cavities, and the construction of the vacuum system.

Linac Cap Cost x Mult. The adjusted capital cost of the linac to include design, assembly, administration and buildings. The contribution of the non-linac items is obtained from an estimate for the cost of building a 250mA/100MeV system and scaled according to beam power.

Annual Cost. The annual operating cost, the sum of the AC power, staff and M&S costs.

Ann Cost Discounted. The annual cost including repayment of the capital costs over 10 years.

10 Year Cost. The cost over 10 years of operation and repayment of the capital at an interest rate of 5% per annum.

40 Year Cost. The cost over 40 years of operation and repayment of the capital over 10 years at 5% interest per annum.

10 (or 40) Year Cost per 10^{18} Neutrons. The cost of producing each unit of 10^{18} neutrons based on the discounted cost over 10 or 40 years.

RF cost. The capital cost of the RF power supplies required calculated from the total RF power and the cost per watt of RF supplies (5.85 **€**/W).

Table I. Spreadsheet for the Linear Accelerator Model

Data input Sheet

Baseline: 5x10^{15}n/cm^{2}s ~ 1GeV/10mA in 10 cm radius target footprint				
Calculation Parameters	**Value**	**Units**	**Spreadsheet Parameter**	**Description**
Output energy	1000	MeV		
Injection energy	0.05	MeV	Gstr	Structure gradient
RFQ1 output energy	2.00	MeV	CCL Energy Gain	Energy gain in CCL (MeV)
RFQ 2 output energy	5.00	MeV	Avg CCL ZT2	Average shunt impedance
DTL output energy	70.00	MeV	Beam Current	Average beam current
Cos(phi) RF phase	0.906		Pbeam RFQ1	Beam power in RFQ1
Capital RF unit cost	5.85	euro/W	Pbeam RFQ2	Beam power in RFQ2
CCL structure cost	0.055	euro/m	Pbeam FUNNEL	Beam power in funnel
RF Cu power RFQ to CCL	12.0	MW	Pbeam CCL	Beam power in CCL
Construction cost 250mA100MeV	1250	Meuro	Pbeam Total	Total beam power
AC/RF conversion efficiency	0.7		Structure Length	Length of CCL
Balance accel AC power	1.0	MW	Linac Tot Length	Total length including inter-cavities
Availability	1.00		Prf(cav) CCL	RF power in CCL cavities
Klystron tube cost	0.20	Meuro	Prf(total) Linac	Total linac RF power inc RFQ's etc.
AC power cost	0.08	euro/kW hr	AC Power for RF	AC power required for RF power
RF power per klystron	2.00	MW	Total Linac AC	Total AC power required by linac
No operating staff	117		Annual AC costs	Annual cost of AC power
Average klystron life	4500	hours	Annual Staff Costs	Annual cost of operating staff
Duty cycle	0.05		Annual M&S Cost	Annual cost of maintenance & spares
Depreciation rate	0.05		Linac Cap Cost	Capital cost of linac components
			Linac Cap Cost x Mult	Cost of linac including non capital items
			Annual Cost	Annual operating cost
			Ann Cost Discounted	Annual cost with total cost discounted at Rate
			10 Year Cost	Total cost of operating with capital discounted over 10 years
			40 Year Cost	Total cost of operating with capital discounted over 40 years

Data Output Sheet

E_{out} (MeV)	**G_{str} (MV/m)**	**CCL Energy Gain (MeV)**	**Avg CCL ZT2 (MW/m)**	**Beam Current (A)**
1000	1	930	38.3	0.01
Pbeam RFQ1 (MW)	**Pbeam RFQ2 (MW)**	**Pbeam FUNNEL (MW)**	**Pbeam CCL (MW)**	**Pbeam Total (MW)**
0.0195	0.03	0.8	9.3	20.15
Structure Length (m)	**Linac Tot Length (m)**	**Prf(cav) CCL (MW)**	**Prf(total) Linac (MW)**	**AC Power for RF (MW)**
1026.5	1487.1	1.34	33.49	47.84
Total AC Linac (MW)	**Annual AC Costs (M€)**	**Annual Staff Costs (M€)**	**Annual M&S Costs (M€)**	**Linac Cap Costs (M€)**
48.84	34.23	8.19	6.52	314.88
Linac Cap Cost x Mult (M€)	**Annual Cost (M€)**	**Ann Cost Discount (M€)**	**10 Year Cost (M€)**	**40 Year Cost (M€)**
814.87	48.94	130.42	1369.45	2837.55
10 Year Cost per 1E18 Neut (€)	**40 Year Cost per 1E18 Neut (€)**	**RF Cap (M€)**	**Cav Cap (M€)**	**Vac Cap (M€)**
2.78	1.44	195.91	81.79	37.18

Cav Cost. The capital cost of the RF cavities of the CCL calculated from the total linac length and the cost per metre of cavity of 55k€/m. This allows for additional beam handling equipment between the cavities.

Vac Cost. The capital cost of the vacuum system calculated from the total structure length multiplied by 25k€ per metre.

3.1.2 Results

The spreadsheet was benchmarked against the costing given in the European Synchrotron Source Report [ESSC96] and a breakdown is shown in Fig. 2. The ESS, being a much larger installation than the accelerator alone, includes costs for items which are not relevant in this context; it was therefore necessary to modify the costs in the report to obtain estimates for those elements pertaining to the accelerator system alone. The spreadsheet reproduced the modified costs of the ESS report to within the quoted ±20% with a reasonable match in the capital cost distribution. Having established confidence in the updated spreadsheet, it was used to investigate the effect of varying several parameters.

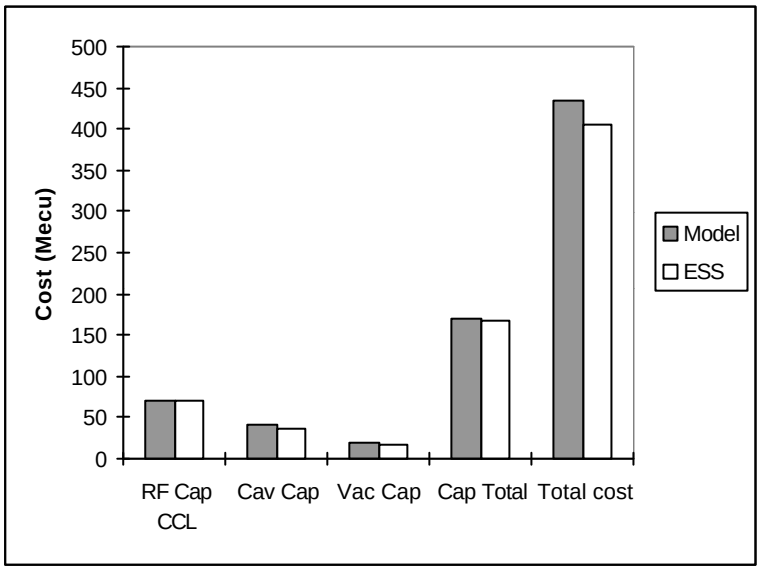

Figure 2. Cost Distribution for ESS Benchmark.

Parameter Survey

The results of varying the beam energy, accelerating gradient and duty cycle for constant neutron flux are shown in Figs 3 to 5. Fig. 3 shows the beam energy variation, which in order to maintain constant neutron flux requires the beam current to vary between 39mA at 300MeV to 6.1mA at 1.6GeV. Due to the improved neutron yield at higher beam energies, the beam current required to maintain a constant neutron flux drops non-linearly so that the beam power decreases slightly more rapidly than the beam energy increases. The RF cavity power requirement increases with beam energy and the two combine to create a clear minimum in the total RF power requirement as manifested in the RF capital cost. At a higher neutron flux the minimum would shift to higher energy.

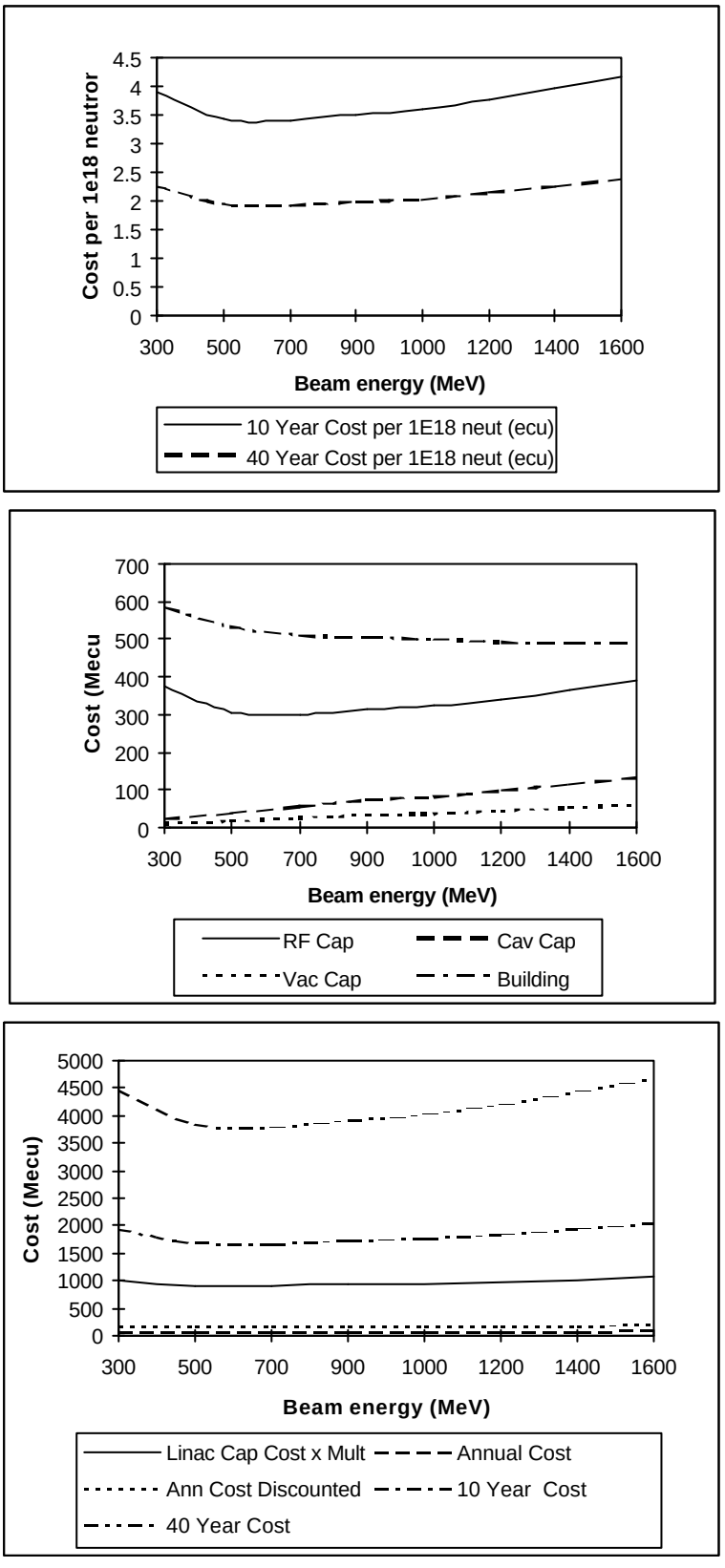

Figure 3. Variation of Beam Energy at Constant Neutron Flux.

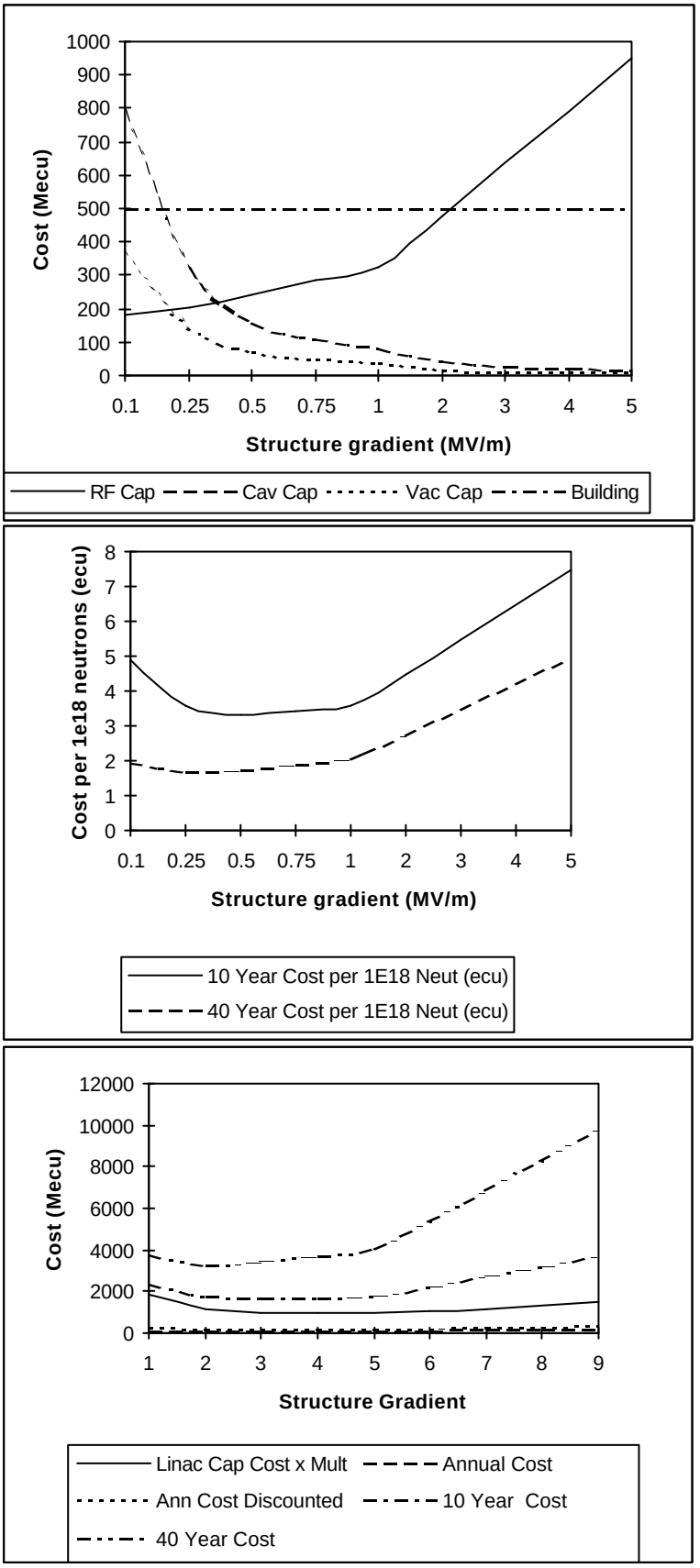

Figure 4. Variation of Structure Gradient.

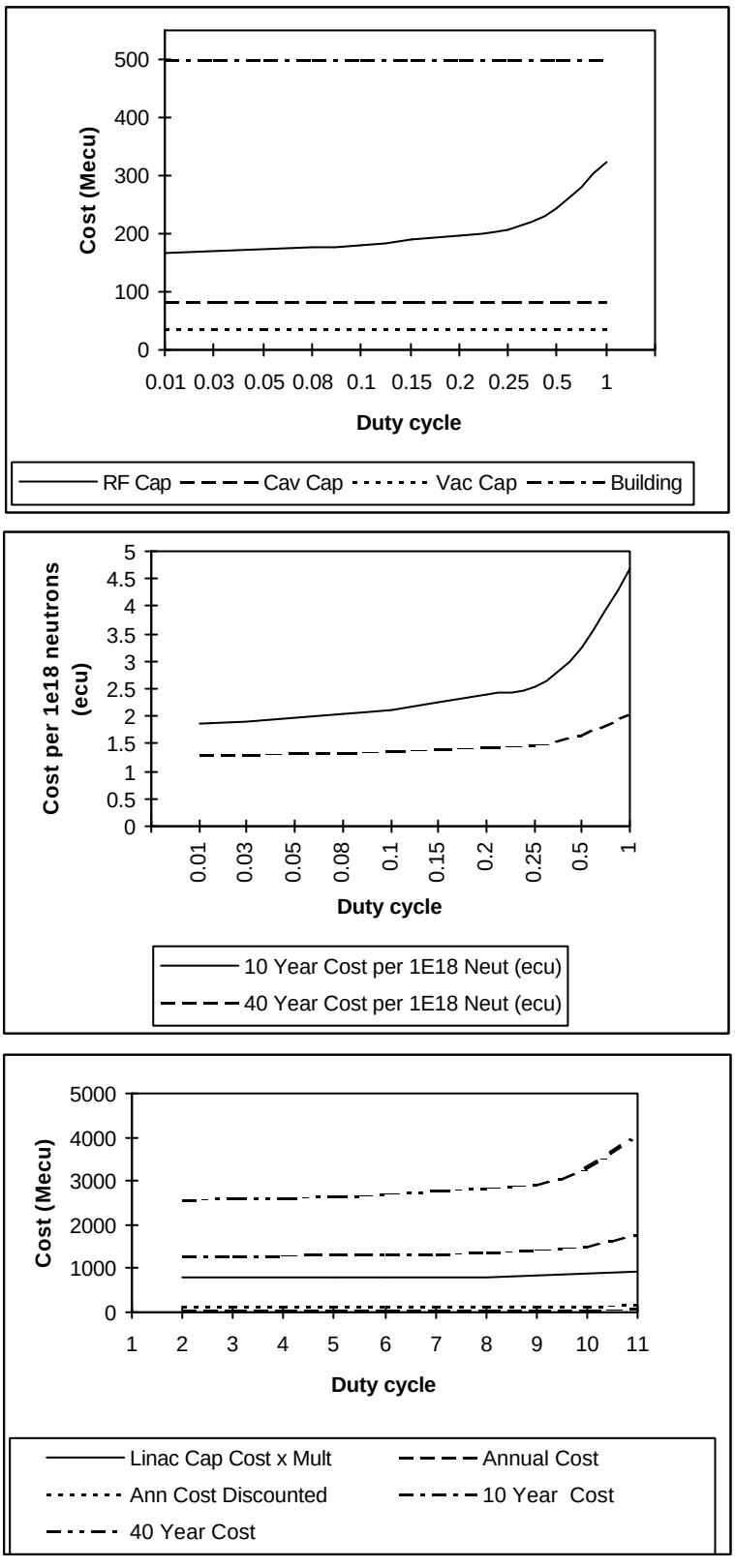

Figure 5. Variation of Duty Cycle.

Fig. 4 shows the effect of the structure gradient at constant beam power. In this case, the linac length decreases with increasing accelerating gradient so that the cavity and vacuum capital costs fall. The RF capital costs rise, however, giving a minimum at around 1MeV/m in this case. Note that the relative unit costs of the cavities and vacuum and the RF power influence the position of this minimum.

Fig. 5 shows the effect of duty cycle on the costs. Note that this is for constant average current of 10mA; hence the peak current increases from 10mA at 100% duty cycle (unity on the graph) to 1000mA at 1% (0.01 on the graph). The results show that in order to minimise the RF capital cost, as high a current and low a duty cycle as possible should be used.

Fig. 6 shows the effect of increasing the beam current at constant energy. In this case, the neutron flux is not constant but varies from $5x10^{14}$ n cm^{-2} s^{-1} at 1mA to $2x10^{16}$ n cm^{-2} s^{-1} at 40mA. The production cost of neutrons drops sharply as the current increases up to 6mA and then begins to flatten.

It is emphasised that all the costs shown are dependent on the selected neutron flux.

3.2 Circular Accelerator Cost Model

A new model for costing circular machines has been developed by AEA Technology. It is based on a similar methodology to that for linear machines. There are a number of differences however, because cyclotrons are intrinsically more complex than linacs, the specifications of their components parts being interdependent. The model assumes a series of cyclotrons, as shown in the schematic diagram of Fig. 7. Again, there may be a single injector, or two which are merged and these can be accommodated by using the total beam current in the spreadsheet.

3.2.1 Spreadsheet

The philosophy of calculating the capital costs from the power requirement and size of the machine is maintained in the new model, although the calculation now involves the magnet volume and the DC power component in addition to cavities, vacuum and RF power. Modelling the cost of a cyclotron is further complicated by the interdependence of many of the parameters, for example the Larmour radius, magnetic field magnitude, final energy, accelerating gradient and machine size are all connected by the physical principle of operation. To simplify matters, the parameter survey using the model was carried out with a constant number of proton orbits.

There are four basic capital items calculated in the spreadsheet: the cost of RF power, the cost of cavities, the cost of the magnet and the cost of the DC power. The concept of shunt impedance has not been used because the design of the cavities varies considerably from that of the CCL. Instead, the RF power absorbed in the cavity walls is calculated from the fundamental expression for a rectangular cavity of dimensions a, b, d with peak electric field strength E_0:

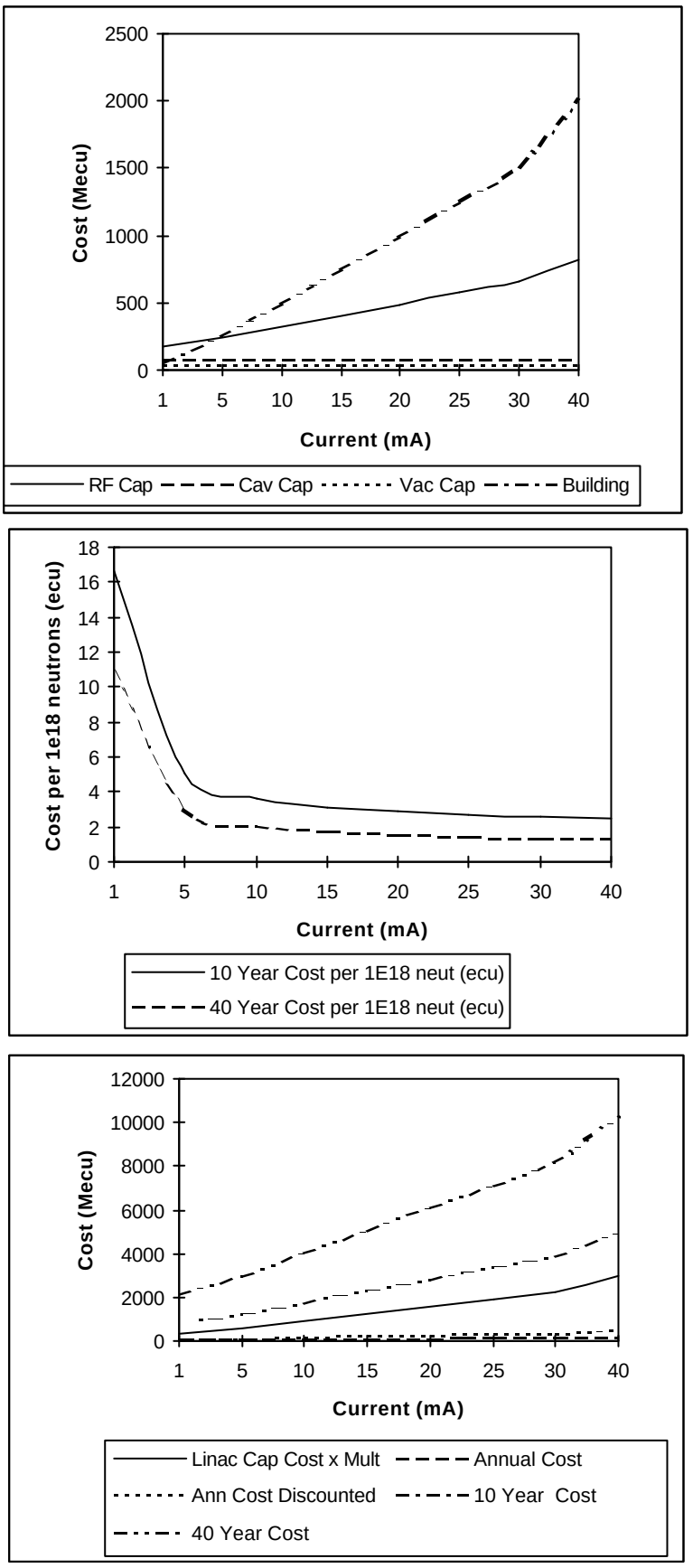

Figure 6. Variation of Beam Current at Non-constant Neutron Flux.

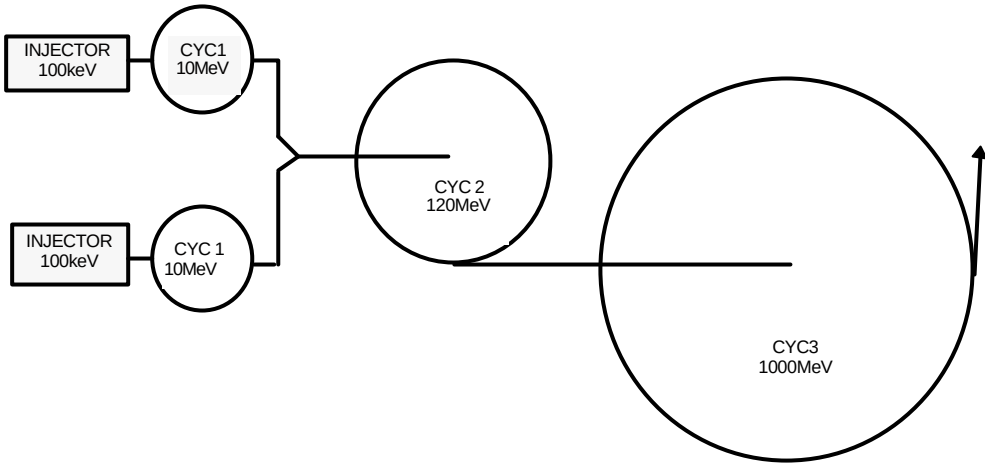

Figure 7. Schematic Diagram of Baseline Circular Accelerator.

$$P_{ab} = \left(\frac{pE_0}{d}\right)^2 \frac{ab}{\sqrt{2s}} \frac{1}{(wm_0)^{3/2}}$$

$$P_{ad} = \left(\frac{pE_0}{b}\right)^2 \frac{ad}{\sqrt{2s}} \frac{1}{(wm_0)^{3/2}}$$

where σ is the conductivity of the wall and $\omega=2\pi f$ is the angular frequency of the RF power.

The Larmour radius, ρ, is calculated from the relativistic equation of motion for a proton of energy U (eV) in a uniform magnetic field, B:

$$r = \frac{\left[(U-U_0)^2 - U_0^2\right]^{1/2}}{Bc}$$

where U_0 is the proton rest mass (983 MeV).

The magnet parameter, Parmag, is defined as:

$$Parmag = (N \cdot I_{mag} \cdot B \cdot K)$$

where $N \cdot I_{mag}$ is the number ampere turns in the magnet coil of circumference K. This is used to calculate the power requirement of the magnet in the output stage of the spreadsheet.

The cost of building the cyclotron and providing services is related to the machine size. The expression given in the Intense Neutron Generator (ING) report [Bart66] has been used in modified form to obtain a cost that varies with Larmour radius:

$$Ccon = 2.16 \cdot 10^5 + 1.82 \cdot 10^3 \left(\frac{400\,r}{30.5}\right) + 72.72 \left(\frac{400\,r}{30.5}\right)^2$$

Table II gives the input data for the baseline specification of a 1GeV/10mA machine. The organisation of the spreadsheet is the same as for the linear accelerator, with the input data at the top and the output powers and costs below. The powers and costs are essentially calculated in the same manner as the linear case, with the following details.

Pmag. The DC power requirement of the magnet obtained from the expression:

$$P_{mag} = 45.11 ln(N \cdot I_{mag} \cdot B \cdot K)$$

which was obtained by parametric fit to example data.

Cyc Cap Cost. The capital cost of the cyclotron, i.e. the RF power supplies, the cavities, the magnet and the DC power supplies.

Cyc Cap Cost x Mult. The total capital cost including buildings, assembly, staff, management, etc. obtained by estimating miscellaneous items to be 25% of the component capital cost, the assembly costs to be 12.5% of the total capital cost and adding the construction cost C_{con}. The cost of constructing the two smaller injector cyclotrons is included as 40% of the capital cost of the high energy machine.

Cav Cost. The cost of the cavities calculated from the total wall area of the cavity and the cost per square meter of 900k€ m^{-2}.

RF Cost. The cost of RF power units obtained from the total RF power requirements and the cost per watt (0.9€/W).

Mag. The capital cost of the magnet obtained from the magnet volume, V, and the parametric fitted expression $C_{mag}=0.076V+0.29$.

Vac Cost. Capital cost of associated vacuum equipment parametrically scaled with the Larmour radius, ρ, as $Cvac=0.104\exp(1.2\rho)$.

3.2.2 Results

The spreadsheet was benchmarked against the costing given in the ING Report [Bart66] and a breakdown of the results is given in Fig. 8. The costings in the ING report are relevant to 1966 Canadian Dollars and so the unit costs are not those given in Table II, which are recent European derived values. Overall, the agreement was good. An unexplained discrepancy in the costs for the smallest cyclotron is not significant in terms of the total cost. The spreadsheet was used to perform a parametric survey for a limited number of variables, as with the linear case.

Parameter Survey

The inter-dependency of the components of the cyclotron creates a more complex relationship between the different capital items. Assuming a constant neutron flux of $5x10^{15}$ n cm^{-2} s^{-1}, as for the linear accelerator, the beam energy and cavity number were varied. There are two possible ways of dealing with a variation in beam energy, arising from the effect of proton energy on the Larmour radius. As the beam energy is varied the Larmour radius of the proton changes if the magnetic field is maintained constant, in which case the size of the machine varies (as the magnets must be at least the same value as the Larmour radius of the final orbit). The effect of this on costs is shown in Fig. 9, where the increasing capital cost of the magnet, vacuum system and cavities reflect the increase in machine size. The alternative strategy, to keep the machine size constant and vary the magnetic field

to give the correct Larmour radius, results in much less variation of costs with energy, as is shown in Fig. 10. As in the linear accelerator case, there is a minimum cost as a result of the increased beam current required to maintain constant neutron yield at lower beam energies.

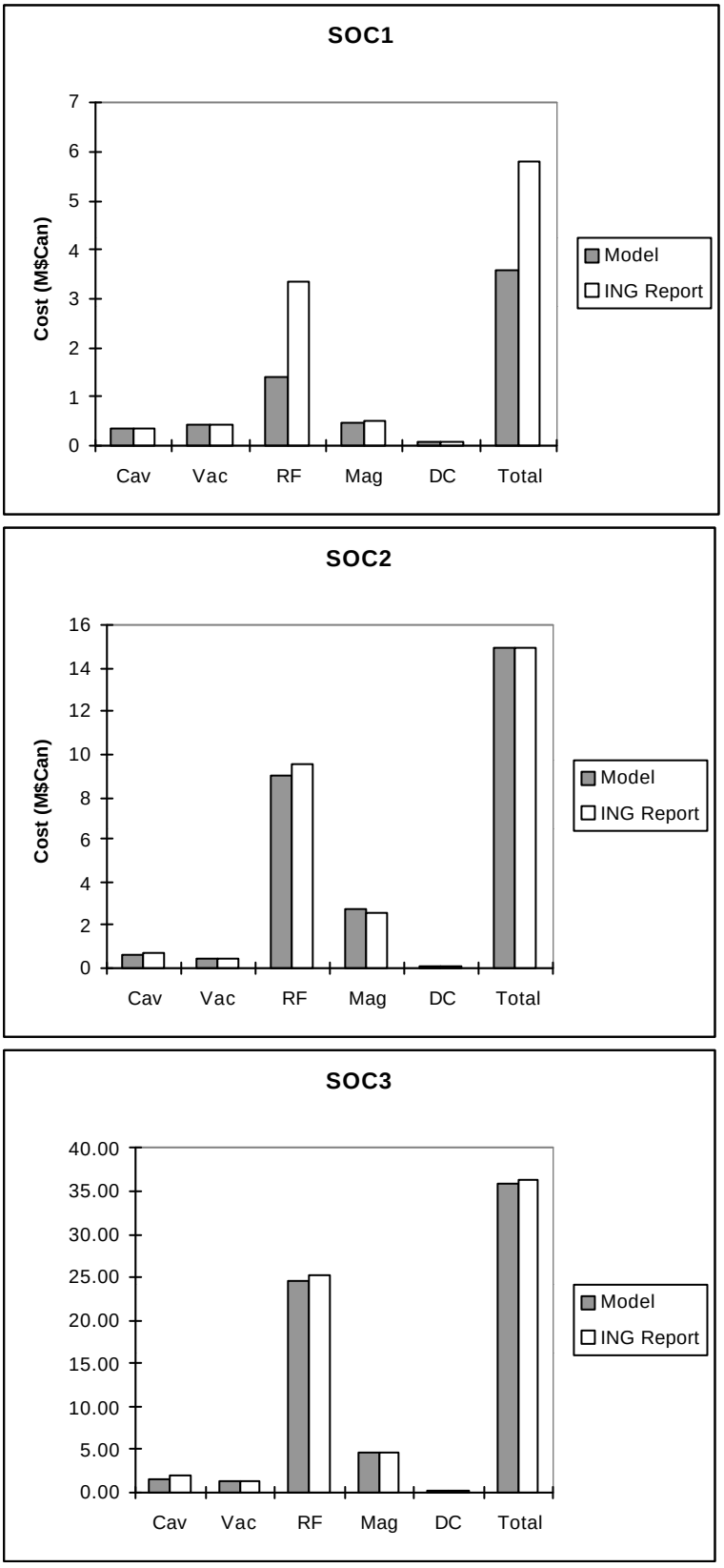

Figure 8. Cost Distribution for ING Benchmark.

Table II. Spreadsheet for the Circular Accelerator Model

Data input Sheet

Baseline: 5x10^{15}n/cm^{2}s ~ 1GeV/10mA in 10 cm radius target footprint				
Calculation Parameters	**Value**	**Units**	**Spreadsheet Param.**	**Description**
Output energy	1000	MeV		
Injection energy	120	MeV		
Number cavities	6		E0	Maximum accelerating field
Cavity gap	0.10	m	Cyc Energy Gain	Energy gain in cyclotron
Cavity height	4.30	m	Beam Current	Average beam current
Cavity width	0.43.	m	Pbeam Cyc	Beam power in cyclotron
Final beam Larmour radius	4.28	m	Pcav Pab	RF power in cavity wall axb
Capital RF unit cost	0.90	€/W	Pcav Pad	RF power in cavity wall axd
Cavity structure cost	0.90	€/m^2	Pcav Tot	Total RF power in cavity wall
RF frequency	42.0	MHz	Pbeam Total	Total beam power
Magnet volume	360	m^3	Bmag	Average magnetic field
Cost of magnet	27.65	€/m^3	Pmag Total	Total DC power for magnet
Capital DC cost	3.0	€/W	AC Power for RF	AC power required for RF power
Building cost	5.5	M€	Ptot cyc	Total power for cyclotron.
AC/RF Conversion efficiency	0.70		Annual Power costs	Annual cost of AC power
Balance accel AC power	5.91	MW	Annual Staff Costs	Annual cost of operating staff
Availability	1.0		Annual M&S Cost	Annual cost of maintenance & spares
Klystron tube cost	0.01	€/yr/W		
AC power cost	80	€/MWhr		
RF power per klystron	2.00	MW	Cyc Cap Cost	Capital cost of cyclotron components
No operating staff	117		Cyc Cap Cost x Mult	Cost of cyclotron including non capital items
Average klystron life	15000	hrs	Annual Cost	Annual operating cost
Depreciation rate	0.05		Ann Cost Discounted	Annual cost with total cost discounted at Rate
			10 Year Cost	Total cost of operating with capital discounted over 10 years
			40 Year Cost	Total cost of operating with capital discounted over 40 years

Data Output Sheet

E_{out} (MeV)	**E_0(MV/m)**	**Cycl Energy Gain (MeV)**	**Beam Current (A)**	**Pbeam Cyc (MW)**
1000	2	880	0.01	8.8
Pcav Pab (kW)	**Pcav Pad (kW)**	**Pcav Tot (MW)**	**Pbeam Total (MW)**	**Prf Total (MW)**
1.175	1175	7.05	10	17.06
Bmag (T)	**Pmag (kW)**	**AC Power for RF (MW)**	**Ptot Cyc (MW)**	**Annual Power Cost (M€)**
1.2	1366	24.37	33.10	23.18
Annual Staff Costs (M€)	**Annual M&S Costs (M€)**	**Cyc Cap Costs (M€)**	**Cyc Cap Cost x Mult (M€)**	**Annual Cost (M€)**
8.19	0.09	78.46	159.95	31.46
Ann Cost Discount (M€)	**10 Year Cost (M€)**	**40 Year Cost (M€)**	**10 year Cost per 1E18 Neut (€)**	**40 year Cost per 1E18 Neut (€)**
47.48	498.32	1442.24	1.01	0.73
RF Cap (M€)	**Cav Cap (M€)**	**Vac Cap (M€)**	**Magnet Cap (M€)**	**DC Cap (M€)**
15.35	13.62	17.14	27.65	4.10

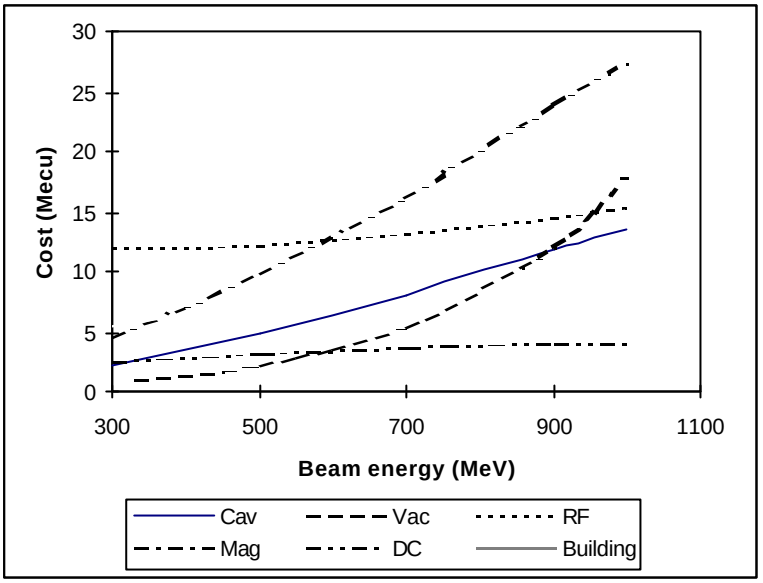

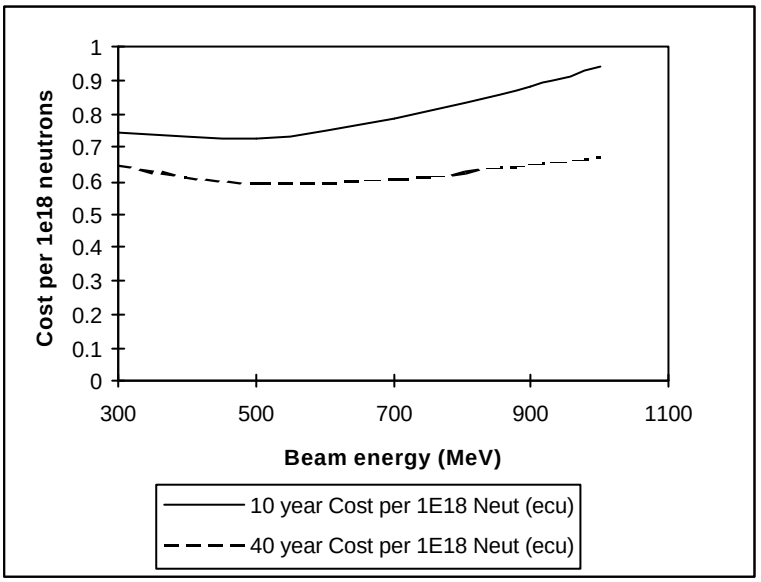

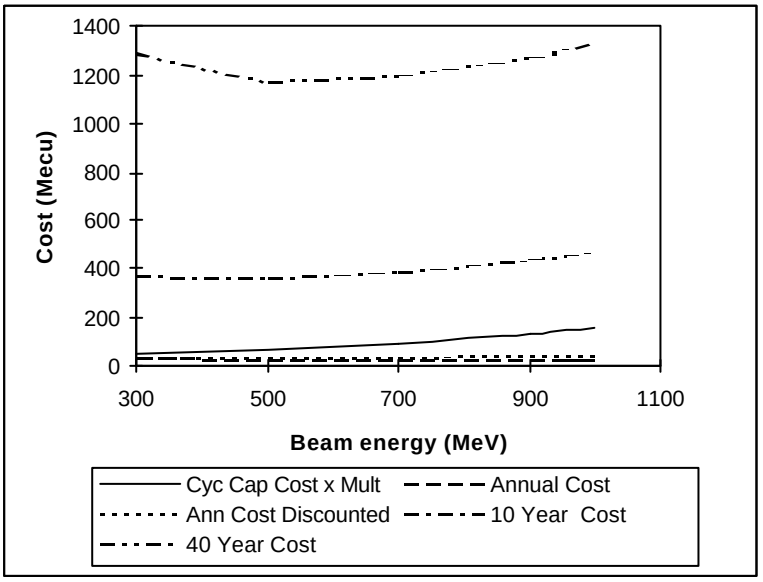

Figure 9. Variation of Beam Energy at Constant Magnetic Field.

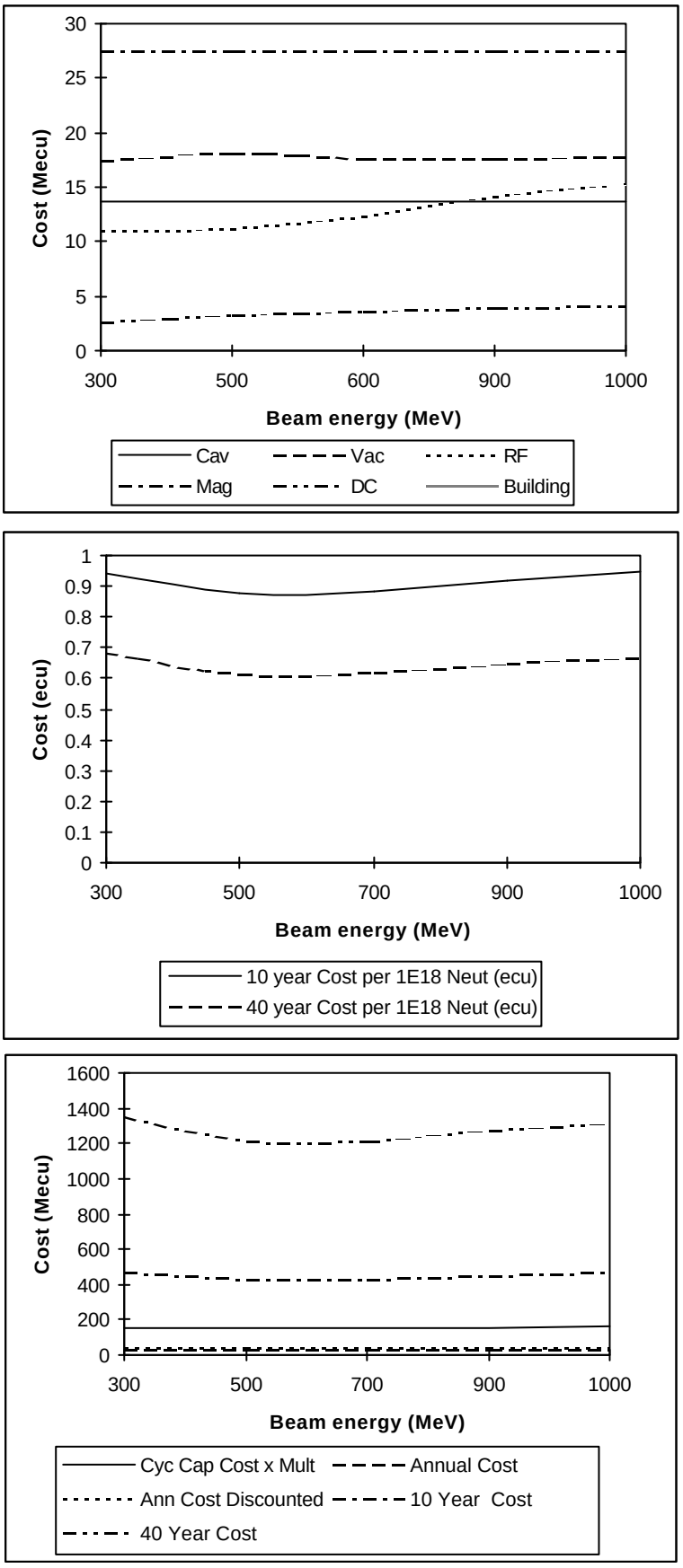

Figure 10. Variation of Beam Energy at Constant Larmour Radius.

Fig. 11 shows the effect of changing the number of cavities. This is equivalent to changing the structure gradient in the linear accelerator as the accelerating field is allowed to vary with cavity number so that a constant number of turns is executed. Using more cavities allows the electric field to be reduced, thus reducing the RF power absorbed by the cavities. However, the capital cost of the cavities increases with number, resulting in the minimum shown in the graph.

Fig.12 shows the effect of increasing current at constant reference energy; as for the linear accelerator, the neutron flux is not constant in this case, but varies from 5×10^{14} n cm^{-2} s^{-1} at 1mA to 2×10^{16} n cm^{-2} s^{-1} at 40mA. Although the current and energy are limited in a conventional cyclotron, the theoretical limits for the SSC/SOC are similar to those for the linac. As for the linear machines, the highest current gives the most economical operation.

3.3 Costs for Development

It has already been mentioned that it is not possible to estimate very accurately the capital and running costs of an accelerator system without a detailed design specification. The same is true of the research and development costs of a new system. The 1GeV/10mA+ machine that would be required is well beyond the specification of any that has been built. Clearly the length and cost of any research and development programme would depend upon the novelty of the design and in this respect linear machines are probably closer to operating at the required power and energy than circular machines. The ESS report estimates the R&D costs to be approximately 15% of the construction cost of the linac.

The fundamental problem associated with accelerating protons beyond 1GeV in a standard cyclotron was discussed in Chapter 3.2. The SSC/SOC prevents the bunching of successive proton orbits by arranging increasing electric and magnetic fields with radius. This requires individual magnet and cavity sectors for each orbit of the protons. In essence these cyclotrons operate rather like a linac wound into a spiral and hence the theoretical current limits are similar. However, this is relatively new technology and does not have the maturity of the linear accelerator, so that development times would be expected to be greater. An experimental, low power, SOC, the TRITON, has been successfully operated at TUM Garching [Cuza98] and a 0.9MW SSC operated at PSI [Stam94], where a 10MW, 1GeV cyclotron is now proposed [Schr95]. It is clear that demonstration of 10MW beams with losses at a level commensurate with safe operation would require considerable R&D.

3.4 Discussion

The results of the spreadsheet calculation show that the circular machines have lower costs associated with both the capital and operational aspects. This is primarily due to the much cheaper cost of RF power supplies at the lower frequency of operation and lower losses in the cavity. It should be noted that these calculations are based upon an assumed neutron flux of $5\text{x}10^{15}$ n cm^{-2} s^{-1} from a 10cm beam radius and that any changes to these parameters, such as higher flux or larger beam, would result in a different set of costs. In addition to costs, the limits to accelerator technology would also influence the choice of an accelerator system and this is addressed below.

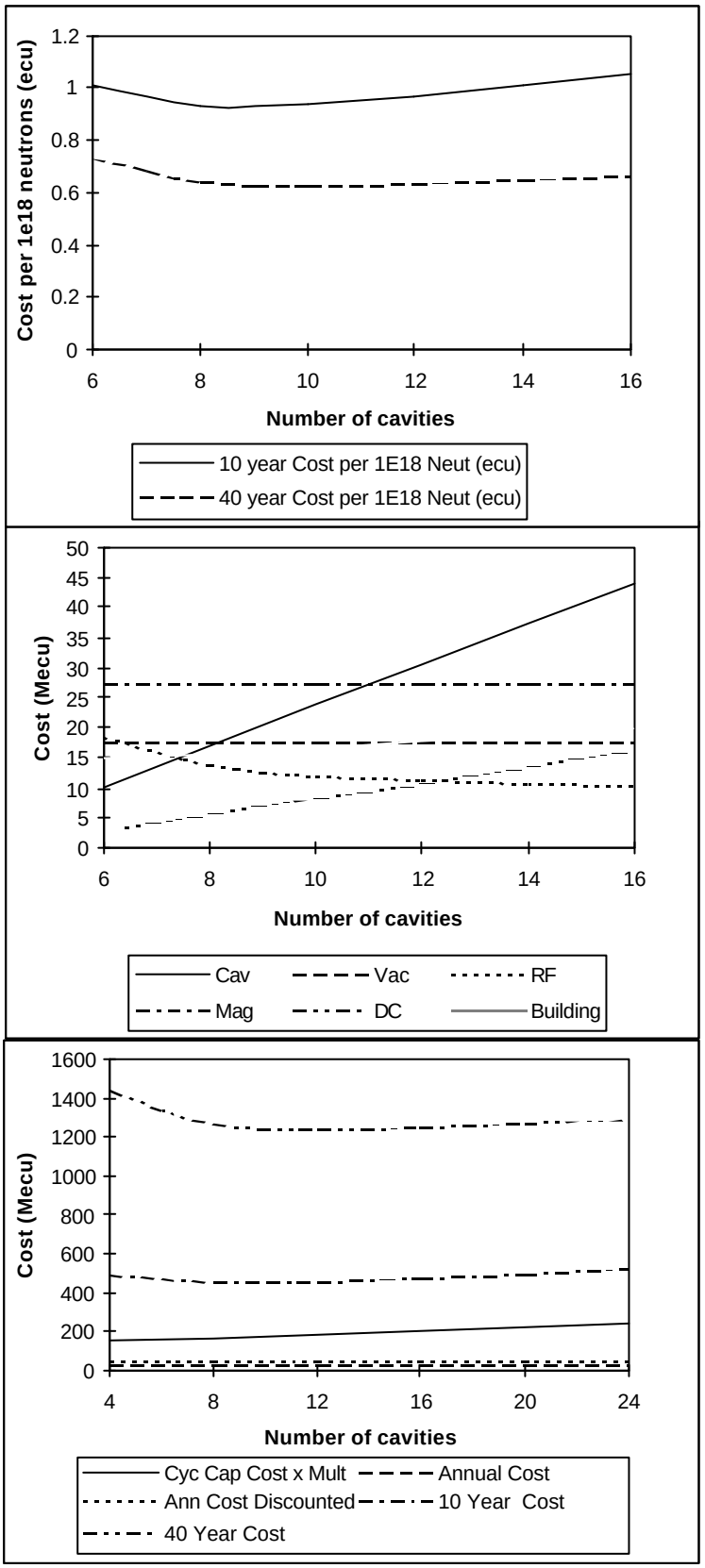

Figure 11 Variation of Number of Cavities at Constant Energy Gain per Turn

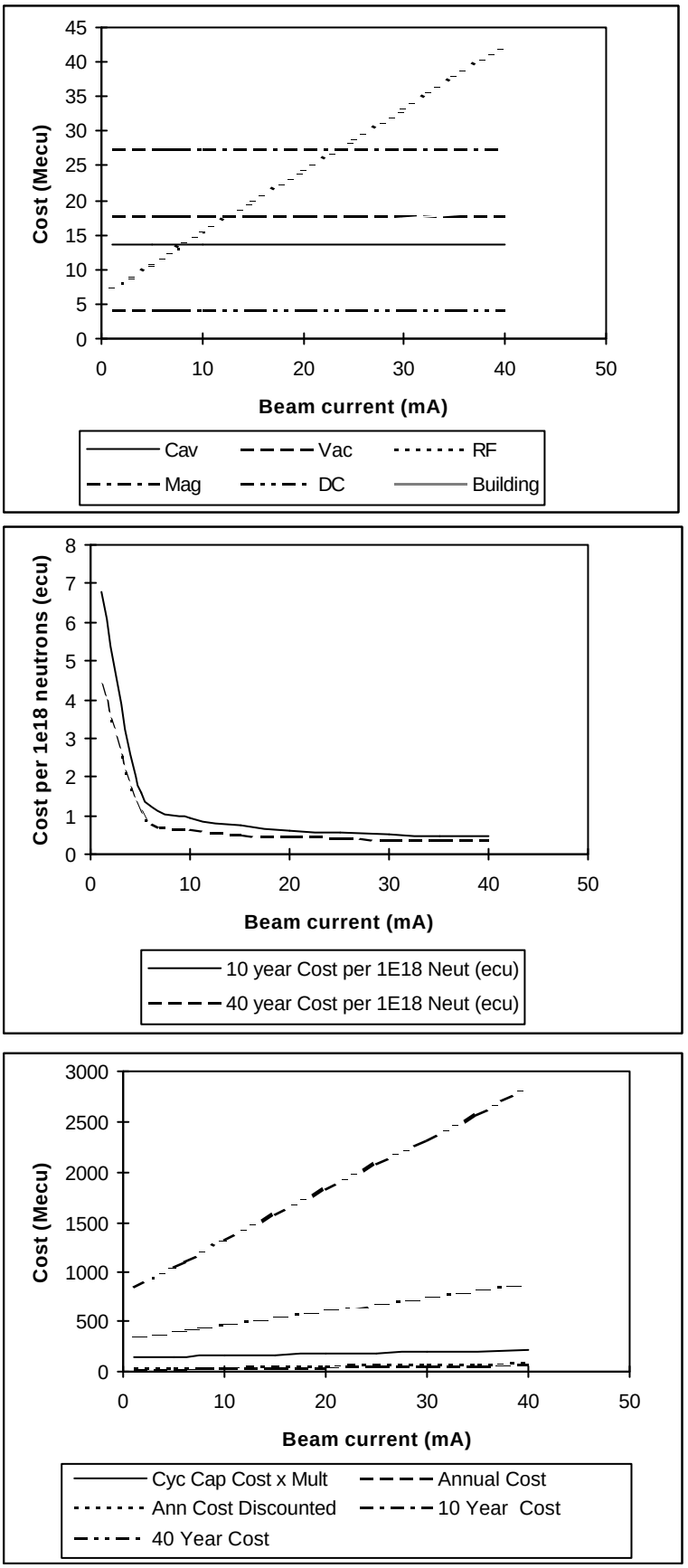

Figure 12. Variation of Beam Current Non-constant Neutron Flux.

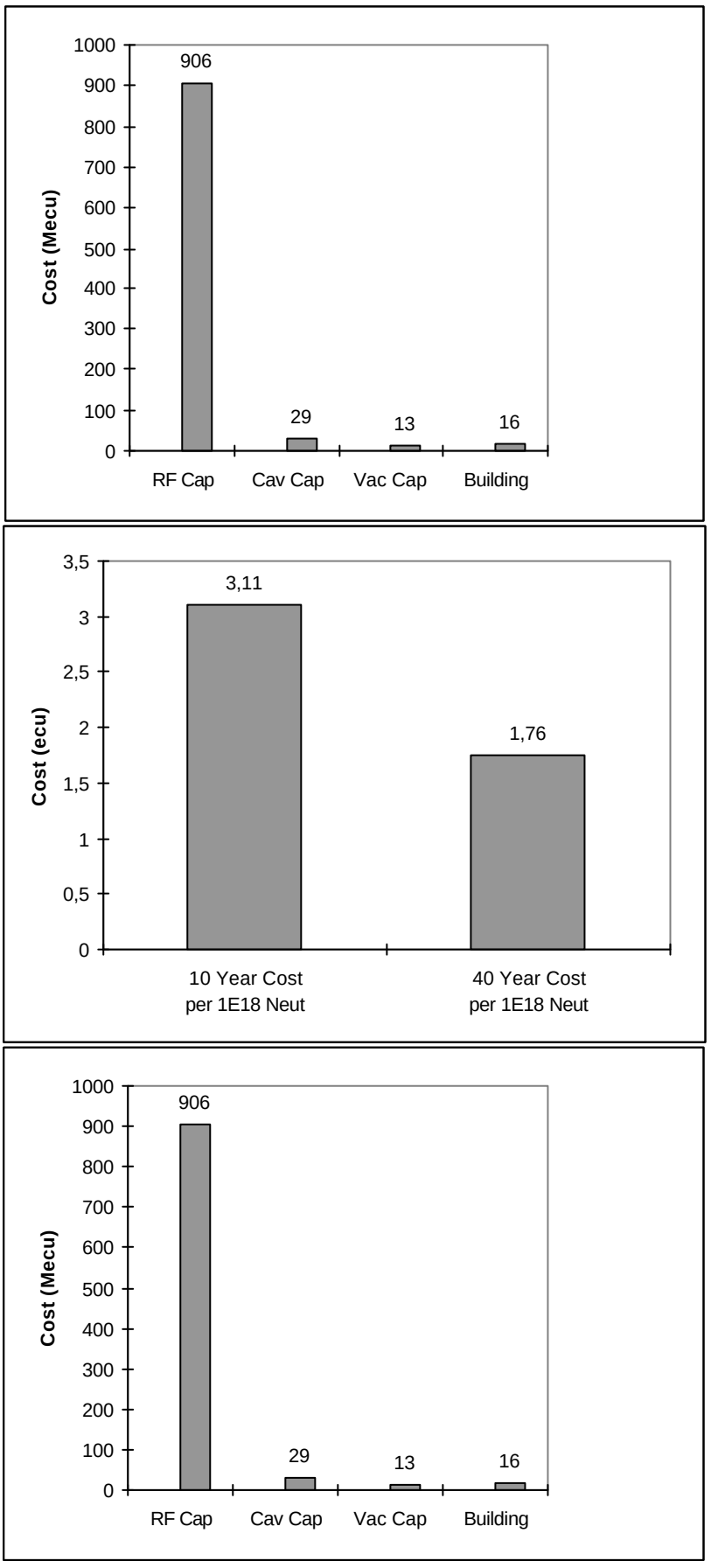

Figure 13. Costings for the Baseline US System.

3.5 Example Calculations

To demonstrate the application of the spreadsheet, calculations of the cost of building two systems that have been proposed were carried out. The baseline ATW system proposed by LANL (1GeV/40mA) was taken as the example of a linear accelerator, whilst that proposed by Rubbia to drive the Energy Amplifier (1GeV/12.5mA) was used as the example of a circular accelerator system. The results are shown in Figs13 and 14.

The figures show the total costs for complete systems, i.e. including two injectors where appropriate, construction and operation. In addition, the cost of generating a unit of 10^{18} neutrons is given, calculated over a 10 and 40 year period. It is assumed that the systems are cw and available 100% and that the capital costs are discounted over 10 years at 5% per annum.

The details of the ATW system are taken from the Jason Review [Jaso94] and Venneri, et. al. [Venn98a]. Unfortunately, a full specification is not available and there are discrepancies between the two references. Where possible the model defers to reference [Venn98a], and the system length given in this work has been used to obtain an estimate of the structure gradient. The capital costs (in particular the RF capital costs) are based on those determined for the ESS Design Report and do not necessarily reflect US costs. Thus, the model shows an estimate of the cost of building the equivalent system in Europe based on 1996 Euro. No detailed costs for the US system are available, but a construction cost of US$50B has been published [Venn98b]. This figure includes all of the ATW system (i.e. multiple burner units, facilities, construction, etc., so that the cost of the accelerator system is some fraction of this value. Fig. 13 shows a construction cost of 2448M€ for the accelerator, which, using the exchange rate of Section 3 gives US$3.06B. However, it is not clear from Reference [Venn98b] whether any discounted capital is assumed over the 5 year construction period, nor what fraction of the total is represented by the accelerator system.

The Energy Amplifier proposed by Rubbia [Fern96] is more fully specified in the literature and the results from the circular model are shown in Fig. 14. Two injector cyclotrons have been included in the costs. It is immediately obvious that the circular machine is a more economical option. The total cost of construction of the accelerator system is given by the model as 201M€, a figure which includes assembly, installation and buildings for the accelerator. These items are not individually identified in Reference [Fern96], but can be estimated from the accelerator capital cost (US$184.45M), assembly (US$23M), Instrumentation & Control (US$14.91M) and building (US$29.17M). These values were obtained from the report by estimation, given the relative sizes of the individual components. Thus the instrumentation and control budget for the primary system, accelerator and EGU, is given as 65% of $35M and it has been assumed that half of this is used by the accelerator. Converting to € using the rates in Chapter 3.3 gives a total accelerator construction cost of 196M€.

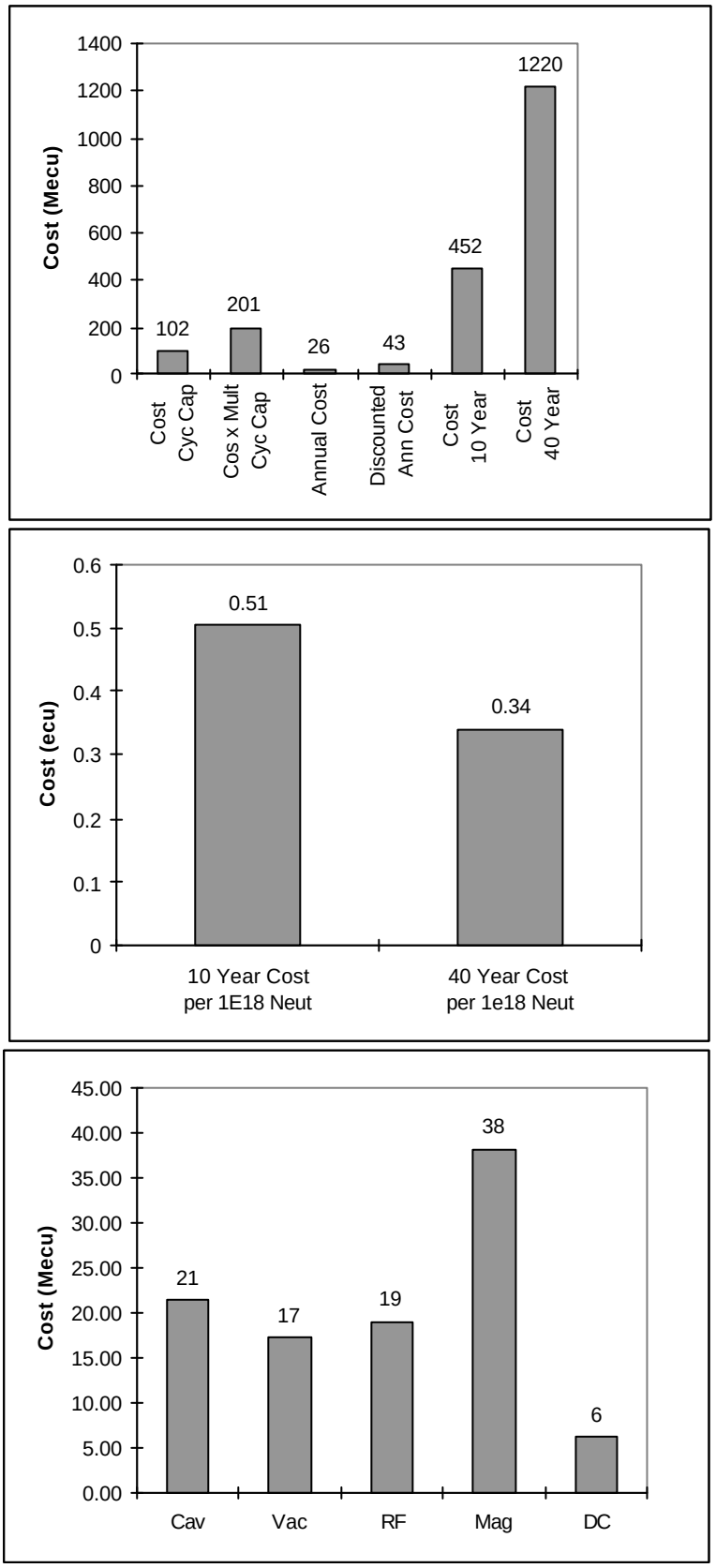

Figure 14. Costings for Energy Amplifier System. Upper picture: total costs; middle picture: costs per 10^8 neutrons; lower picture: distribution of capital costs.

4. Technical considerations

The discussion so far has not included any technical issues which might restrict the choice of accelerator power and type (circular or linac). The most obvious restriction is the technical feasibility of operating any particular accelerator at high power. There is a general consensus in the community that 1GeV high current linacs with a beam power limit of 100MW are feasible, but these are still in the developmental stage. There is, however, considerable scepticism as to the feasibility of operating cyclotrons with currents higher than approximately 10mA, due to the inherently weaker focusing of the channels [Bowm97]. In theory the SSC and the SOC should both be capable of transporting the necessary cw current, but it has yet to be proven as, indeed, is also the case for the linac.

The results of Section 3 indicate that to reduce costs the highest current possible should be used. For example, Fig. 3 shows that operation at lower energy and higher current is the optimum and this was originally proposed in the US for the plutonium conversion process. However, the power deposited in the window material that separates the beam pipe from the target is energy dependent. In most designs this is tungsten and the stopping power of tungsten to a 1GeV proton is 2.32 MeV/mm, whereas at 300MeV proton energy it is 3.67 MeV/mm. Thus a 3mm thick window would extract ~70kW from a 1GeV/10mA beam and ~430kW from a 300MeV/39mA beam (giving the same neutron flux) so that the heating of the window is a factor of six higher in the case of the low energy proton beam. The ability of the window material to tolerate the beam power and the required neutron energy spectrum are the major drivers towards higher energy.

Considerable cost savings can be achieved by running superconducting cavities. The ESS report estimates a saving of 27% on capital and 48% on operational costs for a superconducting version of that linac. This considerable advantage is obtained by operating the linac at the much higher structure gradient permitted by superconducting systems. The length of the accelerator is approximately halved, although increased complexity offsets some of the 50% saving gained on the number of cavities. Superconducting technology applies equally to linear and circular machines and progress at DESY, PSI and Garching should help to indicate the possible benefits to be gained.

The capital cost of the linear accelerator is dominated by the cost of the RF supplies and this is exacerbated by operation at frequencies of hundreds of MHz. Development of the Inductive Output Tube (or Klystrode) has provided a cheaper alternative to the klystron, although the peak power is lower. Further developments may reduce the cost of high frequency modules, making the linear accelerator options more economic.

5. Accelerator Reliability Studies

In collaboration with Los Alamos National Laboratory and Christopher Piaszczyk from Northrop Grumman Corporation, USA, a reliability study of the LANSCE accelerator has been performed [Eric98]. The reliability and availability of the accelerator in accelerator driven systems is an important issue. Taking into account the fact that proton beams from existing high power proton accelerators trip (suddenly stop) very frequently, it is indispensable to understand the effects of such beam trips on different subsystems, especially a subcritical reactor. Temperature fluctuation caused by power change in the accelerator beam enforces thermal transients to reactor structures and beam window, where thermal fatigue or creep-fatigue damage will be accumulated during lifetime. When large number of severe thermal stress cycles is enforced, there is a possibility of crack initiation and propagation at structural walls.

The first step towards a more reliable accelerator is to study the operational experiences of the existing high power proton accelerators, paying special attention to the beam trip records. The accelerator facility at Los Alamos Neutron Science Center (LANSCE) offers enough operating history to supply meaningful reliability data of relevance for high-power accelerators..

5.1 The LANSCE Accelerator Facility

The LANSCE accelerator delivers two proton beams at 800 MeV: the H^+ and the H^- beam. The H^+ beam may deliver 1.25 mA current (routine operation is at 1 mA) and the H^- beam delivers 70 μA. Each injector system includes a 750 keV Cockcroft-Walton type generator. Both ions are accelerated simultaneously in one and the same structure. After acceleration the H^+ and H^- beams are separated. The H^- beam is injected into a Proton Storage Ring for accumulation and delivery to the neutron scattering center or weapons neutron research. Table III summarizes LANSCE beam data.

Table III. The LANSCE accelerator delivers two ion beams

Beam line	**Energy**	**Current**	**Injector (High Voltage Generator)**	**Proton Storage Ring**
H+ beam	800 MeV	1.25 mA	Cockcroft-Walton	No
H- beam	800 MeV	70 μA	Cockcroft-Walton	Yes

The low energy section of the accelerator is an Alvarez Drift Tube Linac (DTL). The drift tube linac accelerates protons from 750 keV to 100 MeV. The high-energy section is a Side Coupled Linac (SCL). The SCL may accelerate protons up to 800 MeV. Different RF systems are used for the drift tube linac and for the side coupled linac. In the DTL, triode power tubes are used for the generation of RF power while in the side coupled linac klystrons are used. The RF system for the DTL is sometimes referred to as the 201 system since the RF frequency in the drift tube linac is 201.25 MHz. The RF system for the SCL is called the 805 RF system since the RF frequency is 805 MHz. Table IV

Table IV. Different RF systems are used in the DTL and the SCL

Linac Section	**Energy region**	**RF Power**	**RF Frequency**
Drift Tube Linac	750 keV-100 MeV	Triode power tubes	201.25 MHz
Side Coupled Linac	100 MeV-800 MeV	Klystrons	805 MHz

Scheduled operation at LANSCE is divided into run cycles. During scheduled operation, the accelerator is operated almost 24 hours per day for an entire run cycle with only a few scheduled breaks. A run cycle is maintained for approximately 5-6 weeks (800-1000 hours). A large fraction of the year the accelerator is not scheduled due to maintenance activities. Scheduled operation is usually in the region of 2000-3000 hours per year, which is about 30 % of the year. In reliability assessment of LANSCE the total scheduled beam time is an important factor - *beam trips have been analyzed only if they occurred within scheduled accelerator operation.*

5.2 Input Data

Current monitors near the targets have measured beam delivery. If the beam current for some reason has been **below half the scheduled current** the beam has been considered as interrupted. This event/trip generates loss of scheduled beam time, commonly called down time.

A large amount of operational data was collected including:
1) Operational data records
2) Central Control Room Logbook
3) Operations Shift Supervisor's Summary Reports
4) Beam Monitor data for 1997

5.3 Overall LANSCE Reliability

The analysis has considered scheduled accelerator operation of the H^+ beam for 1997 and of the H^- beam for 1996 and 1997. The H^+ and the H^- beams have been investigated separately. All calculations are based on operational data records or indirectly accelerator logbook data. A histogram of beam trips that occur in the H^+ and the H^- beam is presented in Fig 15.

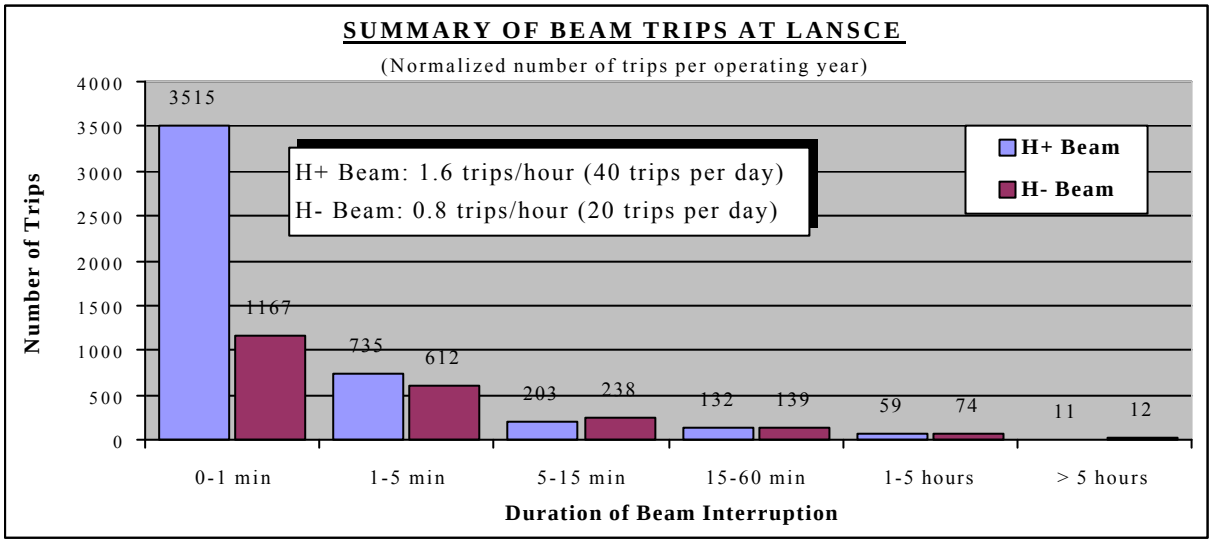

Figure 15. Beam failure statistics of the LANSCE accelerator facility.

One can see from Fig. 15 that the H^+ beam suffers of many trips with short duration. 76% of all trips in the H^+ beam are 0-1 minute long. When comparing the total number of trips in the H^+ and H^- beams, the conclusion is that twice as many trips have occurred in H^+ beam. When operating, the H^+ beam has exhibited 1.6 trips/hour and the H^- beam 0.8 trips/hour. The H^+ beam has tripped 3 times more frequently for short down times. For long down times (> 5 minutes), almost the same number of trips has occurred in the H^+ and the H^- beams. This is not surprising since both beam lines utilize, for most of their length, the same accelerating structure. A slightly larger number of long trips for H^- beam has been caused by the fact that the H^- beam line is more complex. It includes the Proton Storage Ring and hence more components have been subject to failure.

In Fig. 16, the most frequent reasons for beam failure and beam downtime in the H^+ beam are presented. Two columns are displayed for each individual system. The leftmost column shows the fraction of total number of H^+ trips the system is responsible for. The rightmost column shows the

equivalent fraction of total downtime. Trips affect beam stability and generate power fluctuations, downtime degrades the overall beam availability.

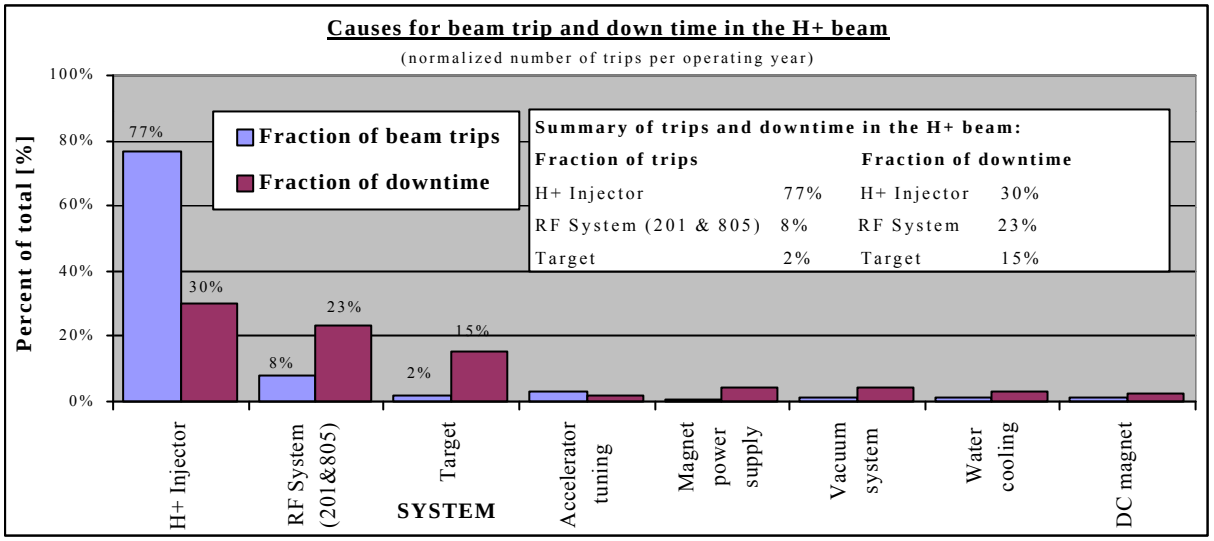

Figure 16. Systems responsible for trips and downtime in the H^+ beam.

As seen on Fig. 16, an injector failure is the most frequent cause for beam trips. In the H^+ beam 77% of all trips have originated from a failure in the H^+ injector. The injector failure initiated usually beam interruptions of one minute length or even shorter, of the order of 15-20 seconds, the time necessary to reset the trip and re-energize the Cockcroft-Walton generator. An injector failure has been usually caused by electric breakdown in the high voltage column. Since a typical injector failure is short, the injector failures do not contribute dominantly to downtimes. While the H^+ injector is responsible for 77% of the trips it is only responsible for 30% of the downtime. So the injector being the main reason for beam current fluctuations does not deteriorate the overall beam availability to the same extent. The RF system, including the RF system for the DTL and the SCL, has generated 8% of the trips but is accountable for 23% of the downtime. Hence, a failure in the RF system usually results in a long downtime (> 5 minutes).

In Fig. 17 historical data on overall beam availability and beam schedule for the years 1979-97 is presented. The line graph represents scheduled beam availability and the column bars represent the scheduled beam time.

Fig. 17 shows also the relation between beam availability and the length of the operating period. Since a short scheduling period is usually followed by a longer maintenance period Fig. 17 gives also information on the affect of accelerator maintenance on overall availability.

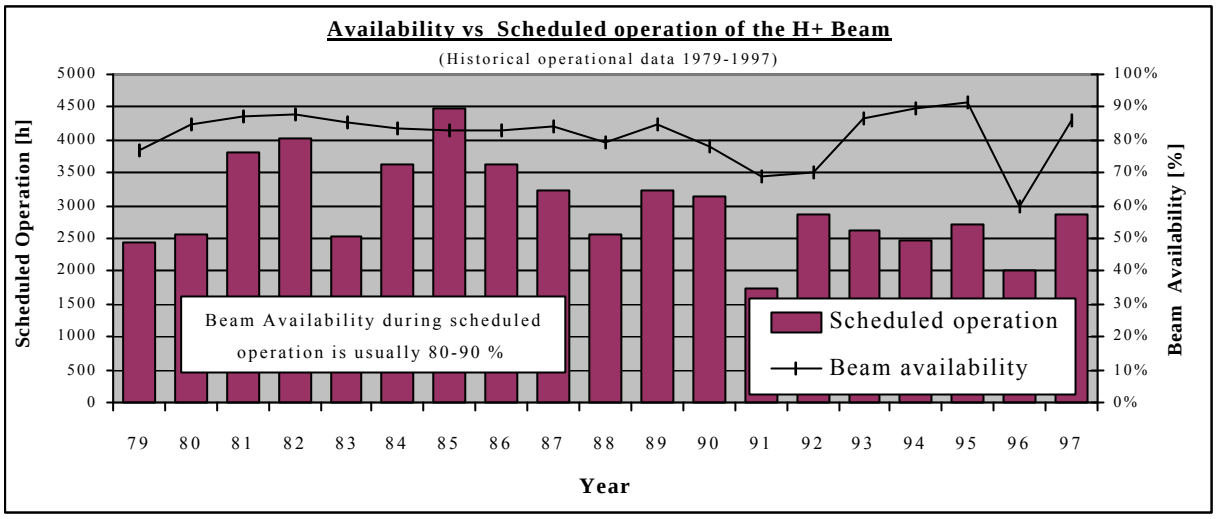

Figure 17. Historical availability and scheduled beamtime of the H^+ beam.

5.4 Analysis of Beam Current

Calculations and diagrams presented in the Chapter 5.3 are all based on data originating from the accelerator logbook. Similar beam reliability analysis has been performed for data collected from beam current monitors. The H^+ beam current has been analyzed during scheduled operation of 1997. The beam current at the end of the H^+ beam line has been monitored and interruptions have been registered. A total of 163.000 beam current records are included in the analysis. This current analysis verifies previous results and it represents the "true" beam performance. When analyzing beam current data it is impossible to investigate the cause of failures. Results of the beam current analysis are presented in Fig. 18. The histogram includes the total number of beam trips detected in the beam current and the corresponding down time. For comparison, the total number of trips registered in the logbook during the same time period is also included in the histogram.

The trips occurred during scheduled operation of the H^+ beam for 1997. A total number of 6914 beam trips has been detected. This number is larger than the number of trips recorded in the logbook (4655 trips) under the same period of time. Fig. 18 indicates that a large number of short interruptions (15-20 seconds) in the beam current which have been not registered in the logbook.

For trips with long downtime (>5 minutes) the results between these two sources agree well. From the analysis of the beam current it is evident that practically no interruptions with downtime shorter than 10 seconds have occurred. In other words, if an interruption occurs it is likely it will last for at least 10 seconds.

5.5 Reliability of the Accelerator Subsystems & Components

Mean Time Between Failure (MTBF) and Mean Down Time (MDT) for individual subsystems have been studied to obtain input data for accelerator reliability modelling (RAMI). Individual failures have been thoroughly investigated with the help of logbooks, operational reports, operators and maintenance personnel.

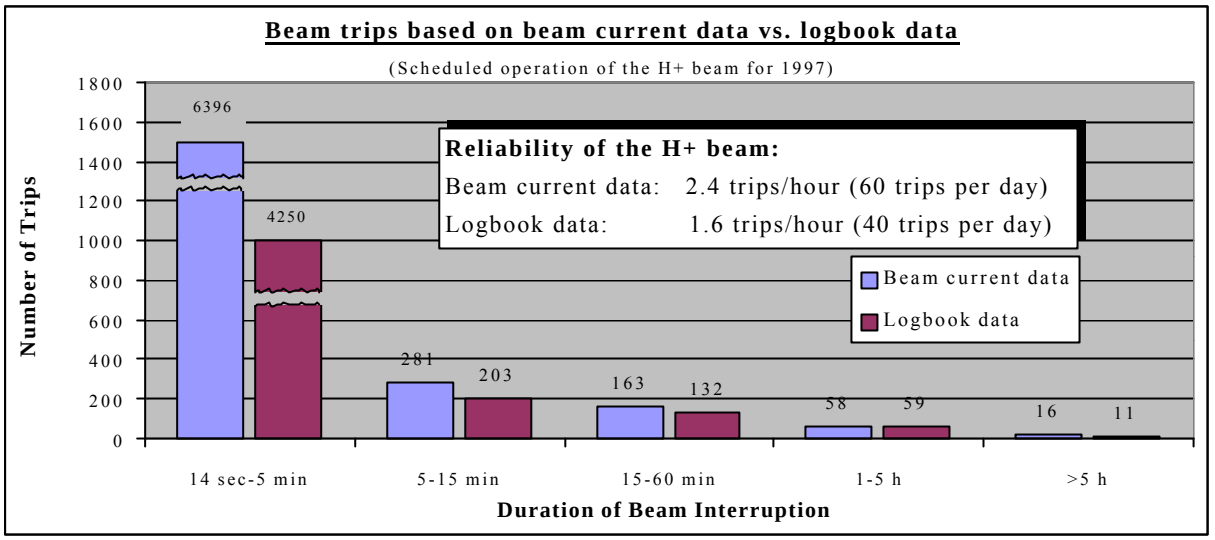

Figure 18. Reliability of the H^+ beam at LANSCE from monitoring records.

The main objective of the analyses was to obtain estimates for the MTBF and MDT for typical accelerator components, such as RF amplifiers, HV power supplies, magnets, magnet power supplies, vacuum system components, or water-cooling components. For illustration the mean downtime estimate as a function of time for the magnet power supplies is presented in Fig. 19. Each dot marks a failure in the magnet power supply. Spaces in between dots correspond to the time between failures. The diagram shows the Mean Down Time estimate at a certain number of failures. The final Mean Down Time estimate for the magnet power supplies is obtained at the last failure in the diagram.

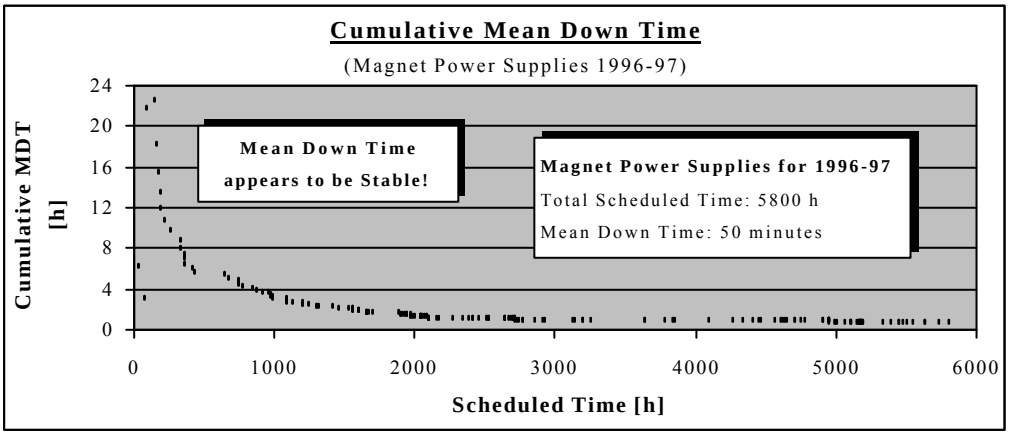

Figure 19. Cumulative Mean Down Time for Magnet Power Supplies.

The asymptotic behavior of the statistical estimators for the desired quantities, such as the Cumulative Mean Downtime is a good indicator of statistical reliability of the data. The Cumulative Mean Downtime has been calculated as the ratio of the cumulative downtime to the cumulative number of events as shown in Fig. 19. The conclusion in this case is that further data collection is not necessary, Mean Down Time estimate appears to be stable at approximately 50 minutes. A similar plot is made for the cumulative Mean Time Between Failure in Fig. 20.

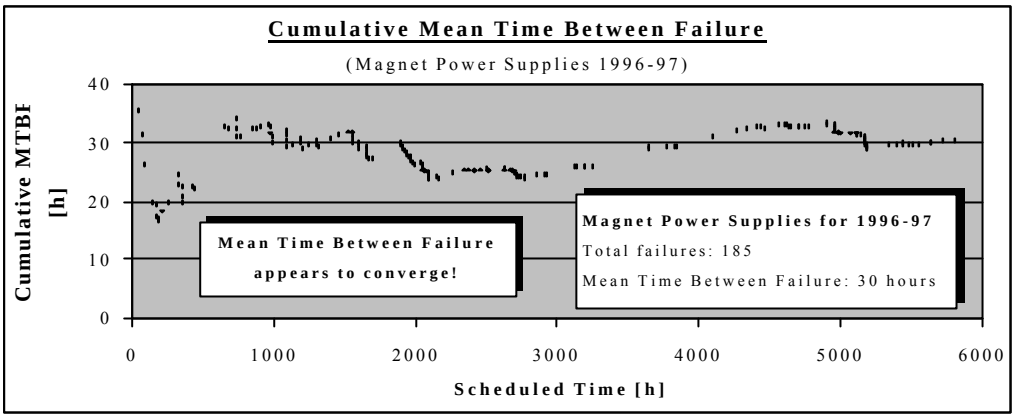

Figure 20. Cumulative Mean Time Between Failure for a single Magnet Power Supply.

Cumulative Mean Time Between Failure has been calculated as the ratio of the cumulative number of failures to the cumulative up time (scheduled time - downtime). As illustrated in Fig. 20, the MTBF behavior for the magnet power supplies is not as smooth as for the cumulative downtime but it appears to converge somewhere in the region of 30 h. With 278 magnet power supplies total in the system, the MTBF estimate for an individual magnet power supply is 8445 hours, assuming that all supplies have the same failure rate and can be treated as a series system of independent power supplies.

The results obtained via similar analyses for the other subsystems at LANSCE are summarized in Table V.

Table V. Some results of the reliability investigation of subsystems and components.

RESULTS OF RELIABILITY STUDY AT LANSCE				
Main System	**Subsystem**	**MDT** [h:mm]	**MTBF for all devices** [h]	**MTBF for a single device** [h]
805 RF	Klystron Assembly	0:44	262	11560
	High Voltage System	0:18	137	960
DC Magnets		0:53	290	232280
Magnet Power Supplies		0:50	30	8445
Pulsed Power	Harmonic Buncher	0:09	44	44
	Chopper magnet	0:08	291	291
	Deflector magnet	0:10	342	684
	Kicker magnet	1:58	185	557
Water System		1:20	120	
	Water pump	0:29	245	29506
Vacuum System		0:48	77	
	Ion pump	0:29	101	25308

The MTBF for the klystron assembly calculated from the raw data corresponds to the entire 805 RF system consisting of 44 klystron assemblies. An estimate of the MTBF for an individual klystron assembly was obtained by multiplying this value by 44 as 11560 hours. This value is reasonable when compared with the 20-50,000 hours commonly quoted for the typical klystron tube by itself. A total of 800 dc magnets exist in the LANSCE facility. MTBF for a single magnet is

232280 hours (.26 years). The dc magnets at LANSCE are very reliable. 50% of the magnet failures have been caused by water cooling problems inside the magnet. The most frequent failure cause in a magnet power supply is malfunctioning electronic equipment. Most of the power supplies at LANSCE are controlled by manual electronics. Modern power supplies are computer controlled and proves to be much more reliable. MDT for a water pump is 29 minutes and MTBF is 29500 hours (.3 years). MDT for an ion pump is 29 minutes and MTBF is 25300 hours (.3 years).

5.6 Failure Analysis

Analysis of failure causes has been performed for all major systems, however here only an example of failure analysis for the RF system is presented. Fig. 21 presents the distribution of trips in the RF system.

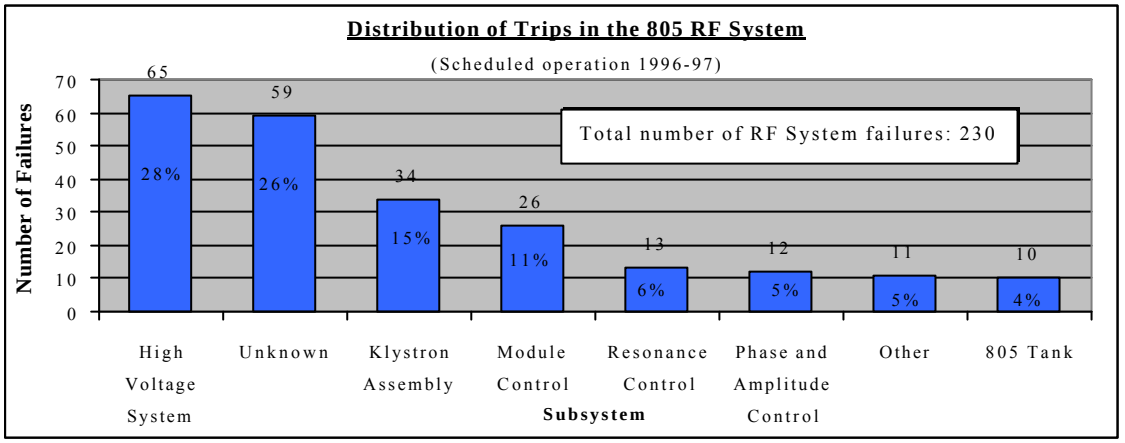

Figure 21. Distribution of trips in the 805 RF system.

All subsystems of the 805 RF system are represented in Fig. 21. The High Voltage System causes many short interruptions. Usually the High Voltage system causes phase or amplitude disturbances to the beam. 26% of the failures in the RF system are unknown. Sometimes when a failure occurs in the RF system it is not possible to point out any specific subsystem (but it is known that the failure occurred in the RF system!). The klystron assembly causes 15% of the failures in the RF system.

6. Conclusions

Costing models have been created that allow the circular and linear accelerator options to be compared and the effect of parameter variations examined. Whilst accurate costs can only be obtained from a detailed system design specification, the costing models allow indicative costs to be estimated in a relatively straightforward way. The calculations reported show that cyclotron systems would be more economical, due mainly to the advantage of the cost of RF power supplies. However, it should be noted that many in the accelerator community regard with scepticism the possibility of transporting and extracting more than a 10mA beam current from a 1GeV cyclotron and therefore technical factors may limit the application of cyclotrons.

For accelerator reliability studies an operational statistics of the powerful 1.25 mA H^+ beam at LANSCE has been obtained using the accelerator logbook and beam monitor data. Over a long period of time (2800 hours), on average 2.4 trips/hour or 60 trips per day are registered. Approximately 75% of all trips are 0-1 minute long. The typical down time of these beam trips is 15-20 seconds.

In the overall reliability balance of the entire LANSCE accelerator, the injector is responsible for most of the trip events. The injector is accountable for 77 % of all trips in the H^+ beam. The injector is primarily generating short trips. For long down times (>5 min) the RF system is the main cause of trips. Upgrading the injector would result immediately in a more stable beam with fewer interruptions, particularly short ones. Upgrading the RF system would result in a better beam availability.

IX. BASIC NUCLEAR DATA FOR ACCELERATOR-DRIVEN SYSTEMS

1. Introduction

The starting point of serious computational modeling of a realistic accelerator-driven system is basic nuclear reaction information. Feasibility calculations of such systems, which include items such as neutron and energy balance, the radiotoxicity of spallation products, damage and activation, rely critically on well-tested nuclear data. It is the task of a nuclear data evaluator to provide this information to the engineering community in a form that enables macroscopic transport and activation calculations. In the IABAT-project, we aimed at classifying the basic nuclear research that is required to fulfill this needs and to demonstrate how such basic nuclear data is connected with an accelerator-driven application. The emphasis will be on measurements and nuclear model calculations for thin targets that will have direct influence on thick target work.

In the second half of this century, many intermediate energy (E > 20 MeV) nucleon-induced reaction experiments have been performed. The main goal of these experiments has usually been to enhance our fundamental knowledge of direct reactions, nucleon-nucleon interactions and nuclear physics in general. With the various new accelerator-based concepts that have emerged in the past decade, there is now suddenly an additional field of relevance for such measurements. A proposal for prioritizing experiments, from the point of view of accelerator-driven systems, will be given in this report.

The actual provision of intermediate energy nuclear data to the users, which provides a justification for the aforementioned experiments that can hardly be overemphasized, is developing rapidly. There are basically two ways to provide a link between thin target nuclear reaction measurements and applied analyses. The first method, which is traditionally linked with high energies, is to perform the calculation of both microscopic nuclear reactions and macroscopic transport processes by the same computer code. HETC, LAHET and FLUKA [Nead94] are well-known examples of intranuclear cascade codes that work according to this principle. Quality statements about such codes can be obtained by comparison of the results with available thin-target experimental data. Then, after choosing geometry specifications for the accelerator, target and/or the reactor, the code could be set in "production mode" to predict processes that take place in a realistic device. Additional validation is possible using integral experiments, in which the neutron flux and other macroscopic quantities of interest can be measured for a thick target.

The alternative method, nuclear data evaluation, is more modular, not only in a computational sense but also from the point of view of human expertise. It is based on the benchmarking of one or more designated scattering and reaction model codes against available experimental data and subsequent storage of the calculated data into evaluated data files [Lanl96, Koni93] in a well-defined manner: the Evaluated Nuclear Data Format version 6, in short the ENDF6-format [Endf90]. Whenever measurements are too difficult to predict, e.g. in the case of residual production cross sections, one can also directly include experimental data in the data file. Hence, since one is in the position to use the best available code or experimental data for each partial nuclear reaction channel, as long as certain sum rules are obeyed, the data evaluation method arguably allows the closest possible connection between nuclear reaction physics and practical applications. After processing, the data libraries can serve as input for deterministic or Monte-Carlo nuclear transport codes. For a

few decades evaluated data files have served as crucial ingredients of fission and fusion reactor research. The same situation is ahead of us for accelerator-driven systems.

At present, the intranuclear cascade and data evaluation methods are regarded as complementary valuable approaches for analyses of accelerator-driven systems. The aforementioned effort in fission and fusion reactor studies has resulted in well-benchmarked data files that cover nuclear reactions up to ~20 MeV. However, the matching energy between the two methods should be around 150 MeV. There are several reasons for this particular energy. First of all, below 150 MeV the predictive power of several pre-equilibrium/statistical model codes (such as GNASH [Gnas96] or ALICE [Blan96]) is superior [Nead94] to intranuclear cascade codes for continuum reactions. Also, individual reaction mechanisms (giant resonances, direct collective reactions, etc.) constitute a relatively larger fraction of the reaction spectrum and require an individual, more sophisticated treatment. When results from such detailed reaction mechanisms are collected and included in a data file, they form a data source that in quality can never be matched by one single computer code. A completely different argument in favor of data files is that quality assurance, which has become quite an important issue in any working process, is more easily guaranteed for data libraries than for intranuclear cascade codes, which allow much freedom with input parameters. Though not directly crucial for pure research, this may prove to be important when eventually nuclear industry desires data for accelerator-driven systems.

An obvious follow-up question after this enumeration of advantages is: Why should nuclear data files stop at 150 MeV and not go all the way up to the incident energy of the proton beam of an accelerator-driven system? At this point, there are several reasons in favor of intranuclear cascade codes at energies above 150 MeV. Above 150-200 MeV, pion production becomes important and the present low-energy codes (and the ENDF6-format) do not yet cover such reactions. Also, above about 150 MeV new physics for reliable optical model parameterizations that should have predictive power in regions where there is no experimental data is required. A major deficit is that the deterministic nuclear model codes that are successfully used up 150-200 MeV cannot handle more than two fast particles in the outgoing channel. Neglect of such multiple particle emission at high incident energies has a significant effect on calculated outgoing particle spectra and a drastic effect on the prediction of residual production cross sections. Another type of problem is that the present transport codes have not yet the capability to transport charged particles. Clearly, here intranuclear cascade codes that handle both the cross section generation and the transport part for various types of particles are still preferable. Summarizing, we argue that a global calculation scheme for accelerator-driven systems should consist of a combination of intranuclear cascade codes above 150 MeV and evaluated data libraries for energies up to 150 MeV. A recent promising development is the integration of the two nuclear data methods (intranuclear cascade + data files/transport) into one code system (MCNPX) [Chad98]. This allows maximal flexibility concerning the choice of intranuclear cascade models and data files.

It is evident that the total nuclear data task is quite sizeable: one has to keep track of nuclear processes starting from 1-1.5 GeV incident protons down to the final reaction stages with thermalizing neutrons and gamma-ray cascades for a large number of residual nuclides. Along this trajectory, a whole panoply of different appropriate nuclear models applies, each with their own validity range. In addition, the required physical methods may differ from nuclide to nuclide. With regard to the tractability of the work, it is important to observe that certain parts of the accelerator-driven system may depend more critically on the quality of nuclear data, and therefore deserve more attention, than other parts [Salv94]. In addition, the data requirements may differ per material. It can easily be imagined that for a target material like tungsten or lead, the number of produced neutrons per incident proton is a key quantity,

whereas for a shielding material like iron, the secondary particle energy-angle distribution is more relevant (for economical aspects of the shielding) as well as activation cross sections. These simple considerations show that sensitivity studies for the different parts of the whole device are indispensable as a parallel area of research in the field of intermediate energy nuclear data. They may provide a valuable guideline for isotopes and reactions to be measured and evaluated.

This section is divided into several parts. The emphasis will be on energies up to about 200 MeV, i.e. covering more or less the energy region for which nuclear data libraries are being produced.

First, we will classify the important aspects of nuclear reaction research that are necessary to maintain a serious data evaluation program. As a particular topic, we report on the status of the international collaboration on intermediate energy nuclear data, as for example covered by subgroup 13 of the Nuclear Energy Agency (NEA)/Nuclear Science Committee (NSC) Working Party on International Evaluation Coordination. The basic purpose of this working group is to investigate:

(a) the most urgent data needs as requested by the ADS applications,

(b) future and existing experimental data,

(c) nuclear model codes,

(d) methods to provide the users with nuclear data in the form of data formats as well as transport and activation data libraries.

Second, we describe the fission yields experiments that were part of this project. These experiments were aimed to provide further basic data on the fission processes of primary interest with respect to ADS nuclear fuel cycles based on thorium.

Next, we give an outline of the whole route from basic nuclear reaction physics to macroscopic calculations. New phenomenological optical models for the whole energy range 0-200 MeV have been constructed, which we will discuss in some detail. The resulting parameterizations have been applied not only directly in the data files but also in a theoretical analysis of the Fe(n,p) and Pb(n,p) reactions. This reaction has been analyzed with the multi-step direct approach of Tamura-Udagawa-Lenske and will be reported in a subsection.

As a central point of our contribution, we present 150 MeV neutron and proton transport data files for iron, nickel, lead, ^{232}Th, ^{238}U and ^{239}Pu. The Fe- and Ni-isotopes are included because they, apart from their relevance in shielding materials, can be validated against an existing integral benchmark. Hence, all data format and processing aspects of the data file have first been tested with these isotopes, with a comparison with a macroscopic experiment as a result. For the lead isotopes such a comparison is not available. However, its importance as target material justifies the evaluation for Pb. The high-energy part of the data files consists completely of results from model calculations, which have been benchmarked against available experimental data. For the Fe, Ni and Pb isotopes, all required nuclear models are used in a code system built around the nuclear reaction codes ECIS96 [Rayn94] and GNASH. In this code system, the process from basic nuclear reaction physics up to the creation of transport libraries is automatically performed. Apart from the optical model and the MSD model which, as previously mentioned, will be discussed more extensively, we will give a short outline of the other nuclear models used in the code system. For neutrons, the calculated high energy data are automatically merged with an existing data file up to 20 MeV. For protons, we construct completely new data files. In this report, we compare the cross sections of the evaluated data files with the few existing experimental data sets. As a recent addition, the neutron file for Th, U and Pu has been extended to 150 MeV.

Finally, the results of our combined HETC/MCNP and MCNPX calculations, on the basis of the new 150 MeV neutron data files, immediately demonstrate the relevance of well-tested nuclear reaction mechanisms below 150 MeV for calculations related to accelerator-driven systems. Comparison with an integral transmission experiment shows a drastic improvement over the older, intranuclear cascade-based, calculation method.

2. Status of Basic Nuclear Data Research

For an important part, the work on basic nuclear data is driven by a few (national) laboratories that have started extensive programs for various accelerator-driven projects. There is however also a more worldwide effort going into transmutation related data. One may distinguish between conventional nuclear data, below 20 MeV, and intermediate energy nuclear data, above 20 MeV. A contribution to the first class, fission yields experiments, will be discussed in the next section. First, we will highlight some ongoing activities, accomplishments and further needed actions in the field of intermediate-energy nuclear data.

2.1 Data Needs and Relevant Experiments

An important task is to investigate the nuclear data requirements from the point of view of applications. As follow-up of the study made in Ref. [Koni92], Kikuchi and Fukahori [Kiku94] have made a systematical inquiry on the type of incident particle, target nuclei and physical quantities. This study is not only aimed at nuclear energy applications, but also serves medical and astrophysical purposes. For accelerator-driven systems, the requested data comprise transport libraries, activation and damage cross sections of accelerator components, double-differential light-particle cross sections and spallation product yields for a whole spectrum of nuclides and recoils. To connect to these requests, a high priority request list has been defined which may serve as a guideline for necessary measurements for accelerator-driven system research. This list is updated regularly and the present version is given in Table I. We stress that the list has already been significantly reduced as compared with the version given in the Kalmar proceedings [Koni96]. The latest proposal is to include 10 nuclides in the list, which cover both the periodic table and various applications. They are the most abundant isotopes of:

(i) one material for medical purposes (O),
(ii) three structural materials (Al, Fe and Ni),
(iii) one fission product (Mo),
(iv) one "nuclear model" material (Zr),
(v) two target materials (W and Pb),
(vi) three actinides (Th, U and Pu).

As an additional comment on Table I we mention that residual production cross sections and deuteron to alpha production cross sections are equally important, but apply to almost every nuclide on the list. Hence they have not been included explicitly. Furthermore, neutron total cross sections have been left out since Los Alamos National Laboratory (LANL) has recently completed a very extensive experimental program for high precision neutron total cross section measurements in the 5-600 MeV region [Diet97] and thereby practically covers this particular need. As stated in the introduction, results of sensitivity calculations are needed to narrow down the high-priority request list. Also, some experimental groups are already taking items of this list into account in their program, e.g., IPN in Louvain-la-Neuve where (n,xp) cross sections for various isotopes in the 25-65 MeV region are being measured. Accordingly, a revised request list is expected before long.

Table I. High priority request list for intermediate energies.

Nuclide	Cross section	Energy (MeV)	Purpose
^{16}O	(p, reac)	10,15,20,30,40,60,80,100,150,200	O,M,A
	(n, xn)	27,41,61,70	M,A,N
^{27}Al	(p, p), (p, p') ,A_y, (p, reac)	20,30,40,50,60,80,100,150,200	O,A,F
	(n, n), (n, n') ,A_y' (n, reac)	40,50,60,70,80,100	O,A,F
	(n, xn)	25,45,80	A,F,N
^{56}Fe	(p, reac)	10,15,20,30,40,60,80,100,150,200	O,A,F
	(n, xn), (n, xp)	25((n, xp)only),45,80	A,F,N
^{58}Ni	(p, xn)	80,160	A,F,N
	(p, xp)	25,45	A,F,N
	(n, xn), (n, xp)	25,45(n, xn only),80	A,F,N
^{90}Zr	(n, xn), (n, xp)	25,45,80	N,A,F
	(p, xp)	25,45	N,A,F
^{100}Mo	(p, p), (p, p'), A_y, (p, reac)	20,30,40,50,60,80,100,150,200	O,M,A
	(n, n), (n, n'), A_y, (n, reac)	20,30,40,50,60,70,80,100	O,M,A
	(n, xn), (n, xp)	25,45,80	M,A,N
	(p, xn)	25,45,60,80,160	M,A,N
^{184}W	(p, p), (p, p'), A_y, (p, reac)	20,30,40,50,60,80,100, 150,200	W,O,A
	(n, n), (n, n'), A_y, (n, reac)	15,20,30,40,50,60,70,80,100	O,A
	(n, xn), (n, xp)	25((n, xp) only),45,80	N,A
	(p, xn)	25,45,80,113,160	N,A
	(p, xp)	25,45,80,160	N,A
	(p, f), (n, f)	50,100,150,200	A,N
^{208}Pb	(p, reac)	40,60,80,100,150,200	O,A,M
	(n, n), A_y	60,70,80,100	O,A,M
	(n, xn), (n, xp)	25,45,80	A,M,N
	(p, xp)	25,45,160	A,M,N
	(p, f), (n, f)	50,100,150,200	A,M,N
^{232}Th	(p, p), (p, p'), A_y, (p, reac)	20,30,40,50,60,80,100,150,200	O,A
	(n, n), (n, n'), A_y, (n, reac)	6,8,10,15,20,30,40,50,60,70,80,100	O,A
	(n, xn), (n, xp)	25,45,80	A,N
	(p, f), (n, f)	50,100,150,200	A,N
^{238}U	(p, p), (p, p'), A_y, (p, reac)	20,30,40,50,60,80,100,150,200	O,A,M
	(n, n), (n, n'), A_y, (n, reac)	6,8,10,15,20,30,40,50,60,70,80,100	O,A,M
	(n, xn), (n, xp)	25,45,80	A,N,M
	(p, f), (n, f)	50,100,150,200	A,N,M

A: Accelerator-Driven Systems, F: Fusion (E_n < 50 MeV), M: Medical, N: Nuclear reaction models, O: Optical models, A_y: Analyzing power

2.2 Compilation of Experimental Data

Computational documentation of experimental nuclear reaction data is extremely important. It will assist nuclear scientists in choosing new experiments and benchmarking model codes. At the NEA Data Bank, the collection of intermediate-energy experimental data has been significantly extended in the past years. At the moment, the total charged-particle EXFOR database contains about 20 MB of relevant data. Updating EXFOR with charged-particle induced data is a relatively new activity and consequently there is still a considerable gap between the data measured in the past and the data actually stored in EXFOR [Koni92]. As a probably redundant statement, *we strongly recommend continuation of updating the*

EXFOR database[1]. Accelerator-driven system research requires a charged-particle database that is as comprehensive as the neutron database that has been maintained by the National Nuclear Data Centers over the years.

2.3 Nuclear Model Parameter Database

A database with nuclear model parameters may be just as important as the aforementioned experimental database. A sound, centralized parameter collection will remove a lot of unnecessary overhead for code developers, and general use of these parameters will narrow down possible differences between model codes. Important components would be:

1. **Optical model parameters**. A compilation of optical potentials for: (a) all energies, (b) neutrons up to alpha particles, (c) spherical and deformed nuclei, (d) global and local optical potentials, (e) dispersive optical model and (f) Dirac phenomenology.
2. **Discrete level file**. Current discrete level files such as the Evaluated Nuclear Structure Data File contain levels which are characterized by energy, spin, parity and gamma branching ratios. Additional parameters that should be included, when available, are the cutoff level to be used in level density matching problems, deformation lengths δ_L and a designator for the collective mode (vibrational/rotational) of the nucleus. The latter two parameters would enable automatic calculation of direct reaction cross sections. This does currently not exist in automatic form.
3. **Level density parameters**. Level density models of varying sophistication are in use (backshifted Fermi gas model, Gilbert and Cameron, Ignatyuk, exact models, etc.). For each model, a parameter set should be provided.
4. **Other parameters**. Nuclear masses, γ-ray strength function parameters and fission barrier parameters.

The IAEA is coordinating the construction of an extensive database that covers a significant part of the aforementioned list. It will be called the Reference Input Parameter Library (RIPL), and the first official version has been released in 1998.

2.4 Computer Code Developments, Benchmarks and Meetings

With the increasing interest in intermediate-energy applications, various low-energy-directed model codes have been extended to higher energies to meet the data requirements. These codes, together with intranuclear cascade programs that were already suitable for high energies, have been compared with each other and with experimental neutron and proton reaction cross sections and spectra in the NEA Code Comparison Meeting [Nead94]. Rather large predicted differences were observed which, not surprisingly, has led to further research recommendations. Perhaps the most conspicuous problem that was revealed in the comparison was an unacceptable spreading (up to 50%) of the predicted proton reaction cross sections. To discuss and solve these problems, an NEA Specialists' Meeting on the Nucleon-Nucleus Optical Model up to 200 MeV [Opti96] was organized in November 1996, in Bruyères-le-Châtel. One of the conclusions was that old, global optical models were no longer suitable to satisfy intermediate energy nuclear data needs. Improved parameterizations, which

[1] The cost of a single update in EXFOR is negligible compared to the total cost of the associated experiment, while general availability and easy retrieval of the data is, next to the actual scientific publication, the most important manifestation of any experiment!

can arguably only be obtained with the inclusion of more advanced physics, are required. Also, as a follow-up of Ref. [Nead94], a benchmark of codes for residual production cross sections [Mich97] has been organized by the NEA, under coordination of R. Michel (University of Hannover) and P. Nagel (NEA, Paris). These quantities turned out to be among the most difficult to predict in nuclear reaction physics. Codes that predict the data, on average, within a factor of 2 of the experimental data *are considered good*. The reason for this large discrepancy is not yet known, although it is clear that the effects of different optical models, level densities and mechanisms like high-energy fission and multiple pre-equilibrium emission have a drastic influence on the predictions. It seems that a sensitivity study on this topic would be very useful.

2.5 Data Formats and Evaluated Data Libraries

Several format proposals for high-energy evaluated data files have been considered [Koni93], all based on ENDF6 rules [Endf90], and there is now reasonably good agreement on the format from the evaluators' point of view. Data files in the ENDF6-format contain blocks of nuclear reaction information that are stored according to so-called files (MF-numbers) and sections (MT-numbers). The MF-numbers contain general types of quantities, such as general information (MF1), resonance parameters (MF2), reaction cross sections (MF3) and energy-angle distributions for emitted particles (MF6). The MT-numbers describe different partial reaction channels, such as the total cross section (MT1), the total elastic cross section (MT2), the total reaction cross section (MT3) or, e.g., the cross section to the first excited state (MT51). By combining MF and MT one can store the information is a compact way. For the construction of a high energy data file, procedures different from those used in the low energy files have to be employed, since it is no longer possible to store all reactions that describe different sequential particle emissions in separate MT-numbers. On the other hand, for accelerator-driven system calculations detailed low energy neutron data are as important as they are in normal reactor calculations. Therefore, as a general rule, the detailed representation of cross sections below 20 MeV should be left untouched as much as possible. For energies above 20 MeV, the detailed information concerning each individual excited state of the target nucleus and each particular sequential reaction chain are somewhat less important than for low energy neutrons. The general advice is as follows: it is appropriate to lump almost all reaction information in MT5, which comprises all non-elastic processes that are not explicitly considered in other MT-numbers (such as fission). The particle and product yields and the outgoing energy-angle distributions can then be stored in MF6/MT5.

Besides consisting of reliable cross sections, the quality criterion for a nuclear data file is a successful check by the standard ENDF-utility codes CHECKR, FIZCON and PSYCHE [Dunf95] and successful processing by the code NJOY [Macf94] into both multi-group format for deterministic codes and a continuous-energy MCNP-library. In another recent NEA document [Koni97], a set of special rules and recommendations for an evaluated nuclear data file are given, such that the above processing conditions are obeyed.

At the time of this writing, there are a few collections of transport data files that: (a) exceed 20 MeV, and (b) have proven to be applicable in transport calculations:

- A collection of 150 MeV neutron and proton data files has been created, and is being extended, at LANL for their H^3-production program [Lanl96, Chad98]. Presently, files exist for all isotopes of H, C, N, O, Al, Si, P, Ca, Cr, Fe, Ni, Cu, Nb, W, Pb [Chad98],

- Several 50 MeV files for fusion research, ^{12}C, ^{16}O, ^{23}Na, ^{28}Si, ^{39}K, ^{51}V, ^{52}Cr, ^{56}Fe and ^{208}Pb, from a Research Centre Karlsruhe (FZK) - Institute for Nuclear Power Engineering (INPE) Obninsk collaboration [Fisc97],
- The BRC/NRG files for ^{54}Fe, ^{56}Fe, ^{58}Ni and ^{60}Ni [Nead97] as described in this report.
- The NRG files for ^{206}Pb, ^{207}Pb, and ^{208}Pb as described in this report.
- The IPPE/Obninsk file for ^{232}Th, ^{238}U and ^{239}Pu as described in this report.

In addition, there is the upcoming, but unreleased, JENDL high-energy file (up to 50 MeV) from the Japan Atomic Energy Research Institute (JAERI) [Fuka97].

3. Fission Yields Experiment

3.1 Introduction and Background

The Th fuel cycle has long been considered attractive for future energy production systems due to the high abundance of Th in the Earth's crust. More recently, the expected low content of actinide activities in the final end products of the fuel cycle has also been considered as an attractive feature. Many aspects of the Th cycle are presently poorly known, however. These include the distributions of products following the fission reactions in the main members of the cycle. The experiments on fission yields were proposed primarily to obtain data for fission of ^{232}Th in the fast flux component in a reactor spectrum. Later, this proposal was extended to also include a study of the fast neutron fission yields of ^{233}U. Such experimental determinations are important due to the lack of accurate theoretical predictions of the product yield distributions. The experimental work has been carried out at the OSIRIS mass-separator facility at Studsvik. This facility has been used for several years for research on various properties of fission products, which are mainly obtained using fission targets of ^{235}U. The Th cycle fission yields experiments had to be specially scheduled since they required "custom made" targets and provisions for filtering out the slow neutron components of the reactor spectrum. The experiments are performed by gamma-spectroscopic assay of each mass-separated isobaric chain, and are therefore rather time consuming. The methodology of fission yields determinations using OSIRIS [Ruds90] is based on the use of standard ^{235}U targets, which required that additional calibrations and control measurements were performed on the specially made targets. All together, these requirements made the scheduling of such extensive experiments more difficult with respect to other users and the available beam time. It was therefore a great disappointment that the first set of measurements on ^{232}Th, in April of 1996, failed due to technical problems. It took about two years until a new experiment could be scheduled and conducted during 1998. The resulting data were of good quality, but has not yet been analyzed in any detail.

The experiments on the fast neutron fission of ^{233}U were performed during 1997, with additional control measurements conducted in early 1998. The individual yields of about 180 fission product nuclei were determined, including the yields of some tens of isomeric states. The new data more than triples the known data base of the yields in the $^{233}U(n_f,f)$ reaction.

3.2 Experimental Procedures and Analysis.

The fission target of the OSIRIS facility is placed in a channel close to the core of the Studsvik R2-0 reactor, and kept at a high temperature of 2300-2400°C to permit a rapid release of most of the fission products. These are subsequently ionized by electron

bombardment and mass-separated with a resolution of about 700. This resolution permits separation of the isobaric chains, but not of individual isobars in the chains. The abundances of specific nuclides are determined by gamma-ray spectroscopy on the mass-separated samples, using a technique, which allows to also determine the half-lives of the observed gamma-ray peaks. The raw experimental results from an experiment of this type consist of well over 1000 gamma-ray spectra to be analyzed semi-automatically with respect to the characteristic gamma-rays of the nuclides present in the samples. The method has a good sensitivity, which makes it possible to routinely study also rare fission products having yields in the range of ppm per fission. Although such low yield products in general are of little interest for reactor applications, they give important information on the shapes of the product yield distributions and hence on the applicability of models for such distributions. The data obtained do not cover the entire range of fission products, however, since the isotopes of a few refractory elements (Zr-Rh) cannot be released from the fission targets. Another limitation is that the method has to rely on the existing gamma-ray data in the nuclear data libraries. There are reasons to believe that such data are not entirely reliable in several cases. Even with these limitations, we find that the number of derived individual yields vastly exceeds what can be obtained using other experimental methods. In the special case of the ^{233}U fast fission, the main experimental problem was that the fission cross section for thermal neutrons is about two orders of magnitude larger than for fast neutrons. It was thus necessary to shield the fission target carefully using a filter arrangement of B_4C to absorb the slow neutron component of the spectrum. An initial study by deterministic and probabilistic neutron transport calculations showed that a filter thickness of about 2 cm should give nearly optimum conditions. The calculations suggested that more than about 80% of the fission reactions then should be induced by fast neutrons. These calculations were subsequently verified by experimental studies of the filtered neutron spectrum, using the threshold activation technique.

An extensive discussion of the present results, including comparisons with systematics and theoretical models, is given in [Galy99]. An overview of the individual product yields is shown in the Fig.1.

4. Nuclear Models and Code Development

Concerning the development of theoretical nuclear models required for this work, we will highlight two important cases: the optical model and the multi-step direct nuclear reaction model.

4.1 Optical Model

For high-energy data evaluation, the optical model is of central importance. In the context of the present work, it has two purposes:

1. A “direct” application: It generates the total, total elastic and the total reaction cross sections as well as the elastic angular distributions (and the polarization, but that is of less relevance to nuclear data evaluation).

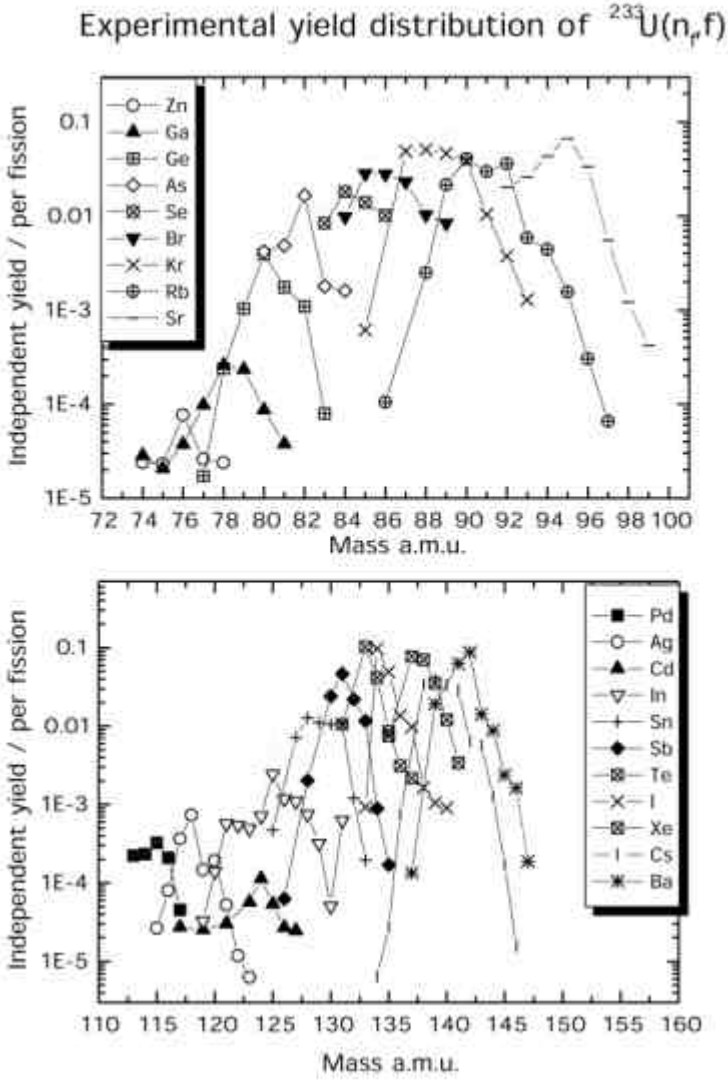

Figure 1. The independent yields of individual fission products as derived from the present experiments. Different symbols are used to designate short-lived isotopes from different elements. The connecting lines are to guide the eye only.

2. An "indirect" application: It is used for direct reaction calculations for discrete states, which can be performed with the Distorted Wave Born Approximation (DWBA) for the (near-) spherical nuclei we are studying here, and it also generates the transmission coefficients that are used in the statistical model (Hauser-Feshbach) calculations. In the next subsection we demonstrate the impact of new optical model parameterizations on multi-step direct calculations.

In order to perform calculations without any unphysical discontinuities, optical models for the whole energy range of the data file should, preferably, be used. Although we are primarily interested in incident energies above 20 MeV, optical potentials for low *outgoing* energies are required for spectrum calculations at any incident energy. When we have one optical model parameterization for the whole energy range, we can obtain total and elastic scattering cross sections that vary smoothly with incident energy as well as smoothly varying results from codes like GNASH.

We have constructed new phenomenological proton and neutron optical models for the energy range 0-200 MeV for all nuclei under study here. We obtain our final parameterization with our interactive optical model tool ECISVIEW [Koni96b]. ECISVIEW is a graphical interface built around ECIS96. The basic purpose of ECISVIEW is the possibility to change optical potential parameters interactively, with the keyboard or the mouse, and to display the calculated results immediately on the screen. This enables us to obtain conveniently the optimal optical potential parameters for a given nucleus over the whole energy region of interest. ECISVIEW makes it possible to simultaneously study the dependence of all calculated polarizations, differential elastic and total cross sections on optical model parameters. The phenomenological optical model potential U has the following form:

$$U(r) = -Vf_v(r) - iWf_w(r) + 4ia_{w_D}W_D \frac{df_{w_D}(r)}{dr} - \left(\frac{\hbar}{m_p c}\right)^2 \vec{L}\cdot\vec{s}\,(V_{so} + iW_{so})\frac{1}{r}\frac{df_{so}(r)}{dr} \tag{1}$$

where the form factors of each component are Woods-Saxon type

$$f_i(r) = \frac{1}{1 + \exp((r - R_i)/a_i)} \tag{2}$$

where a_i is the diffuseness and the radius is given by $R_i = r_i A^{1/3}$.

For all nuclei, we attempt to use the same functional form for the parameterization, in which we try to minimize the number of adjustable parameters and avoid energy-dependencies for which we have no physical justification. Such conditions are important, since they should protect us from unwanted anomalous predictions in energy regions where no data exist. We adopt an exponential decrease of the real central and spin-orbit potential depths, an imaginary volume potential depth of the form proposed by Jeukenne and Mahaux [Jeuk83] and an imaginary surface potential depth of the form proposed by Delaroche et al. [Dela89]. All geometries are energy independent (apart from an energy dependence that we will discuss shortly) and we impose as further constraints equal real and imaginary volume geometries and equal real and imaginary spin-orbit geometries. Finally, we take a linear decrease of the imaginary spin-orbit potential. Summarizing, we have

$$
\begin{aligned}
V(E) &= V_0\, exp(-l(E-E_f)) \\
r_v &= r_w - l_1 \sin\left(\frac{3p}{\frac{E}{l_2}+2}\right) \\
a_v &= \text{constant} \\
W_v(E) &= a_1 \frac{(E-E_f)^m}{(E-E_f)^m + b_1^m}, \qquad \text{where} \quad m=4 \\
r_w &= \text{constant} \\
a_w &= a_v \\
W_D(E) &= d_1\, exp(-d_2(E-E_f))\frac{(E-E_f)^n}{(E-E_f)^n + d_3^n}, \quad \text{where} \quad n=4 \qquad (3) \\
r_{w_D} &= \text{constant} \\
a_{w_D} &= \text{constant} \\
V_{so}(E) &= V_0^{so}\exp(-l_{so}E) \\
r_{v_{so}} &= \text{constant} \\
a_{v_{so}} &= \text{constant} \\
W_{so}(E) &= W_0^{so} - c_{wso}E \\
r_{w_{so}} &= r_{v_{so}} \\
a_{w_{so}} &= a_{v_{so}} \\
r_c &= \text{constant}
\end{aligned}
$$

where E_f is the Fermi energy and E the incident energy.

In conventional phenomenological optical models, straight line segments are often used to represent the absorption potentials. Here, the smooth functional forms for W_V and W_D incorporate essentially the same number of parameters but provide more flexibility. They help to attain a parameterization over the whole 0-200 MeV range, without any discontinuity. This is very important for nuclear model calculations that take the optical model as a starting point. The problem one generally faces is that for complete spectrum calculations reliable optical potentials for all outgoing energies are required, but a complete parameterization is usually missing. Typically, one is forced to take optical model potential A in the first energy region, optical model potential B in the second energy region, etc., which leads to undesired discontinuities, not only for the predicted standard observables, but also for other outgoing channels. The parameterization of Eq. (3) cures this problem. A final comment on the parameterization concerns r_V: The theory of the dispersive optical model predicts an energy-dependent radius of the (effective) real central volume potential. The origin of this is a real surface term in the optical potential that is connected, via the dispersion relation, with the imaginary surface term. The functional form for r_v simulates this effect. In Table II, the obtained parameters for both neutrons and protons incident on ^{54}Fe, ^{56}Fe, ^{58}Ni and ^{60}Ni are given. Both the neutron and proton

TABLE II. Optical model potential parameters for 0-200 MeV nucleons incident on the major Fe- and Ni-isotopes. Preliminary results.

	^{54}Fe		^{56}Fe		^{58}Ni		^{60}Ni	
	N	P	N	P	N	P	N	P
V_0	56.5	65.54	55.0	67.30	56.3	65.30	56.0	67.30
λ	0.0067	0.0076	0.0067	0.0076	0.0067	0.0076	0.0067	0.0076
r_v	1.191	1.157	1.191	1.157	1.191	1.157	1.191	1.157
λ_1	0.03	0.	0.03	0.	0.03	0.	0.03	0.
λ_2	15.	|	15.	|	15.	|	15.	|
a_v	0.63	0.70	0.63	0.70	0.63	0.70	0.63	0.70
a_1	14.0	14.1	14.0	14.1	14.0	14.1	14.0	14.1
b_1	75.0	75.0	75.0	75.0	75.0	75.0	75.0	75.0
d_1	15.0	17.5	15.0	18.0	15.0	17.5	15.0	20.0
d_2	0.026	0.024	0.026	0.024	0.026	0.024	0.026	0.024
d_3	11.6	18.0	11.6	20.0	11.6	18.0	11.6	22.5
$r_{\omega D}$	1.29	1.29	1.29	1.29	1.29	1.29	1.29	1.29
$a_{\omega D}$	0.58	0.58	0.58	0.58	0.58	0.58	0.58	0.58
V_0^{s0}	6.00	6.00	6.00	6.00	6.00	6.00	6.00	6.00
λ_{s0}	0.0050	0.0050	0.0050	0.0050	0.0050	0.0050	0.0050	0.0050
r_{vs0}	1.017	1.017	1.017	1.017	1.017	1.017	1.017	1.017
a_{vs0}	0.60	0.60	0.60	0.60	0.60	0.60	0.60	0.60
W_0^{s0}	0.2	0.2	0.2	0.2	0.2	0.2	0.2	0.2
$c_{\omega s0}$	0.011	0.011	0.011	0.011	0.011	0.011	0.011	0.011
r_C	0.	1.238	0.	1.238	0.	1.238	0.	1.238
E_f	-11.40	-7.83	-9.14	-9.15	-10.47	-8.53	-9.50	-9.80

optical models incorporate relativistic kinematics. Figs 2-3 show a comparison of the neutron optical model for ^{54}Fe with elastic scattering angular distributions and the total cross sections. The figures are in fact snapshots of ECISVIEW and display the end result of the interactive parameter fitting procedure. We note that our results are preliminary and that Table II does not yet represent the final answer. This comment is also relevant for the nucleon-^{90}Zr study presented in [Koni96b]. Future fine-tuning of the parameters is foreseen, including dispersion relations, as soon as the new total cross section measurements from Los Alamos [Diet97] become available.

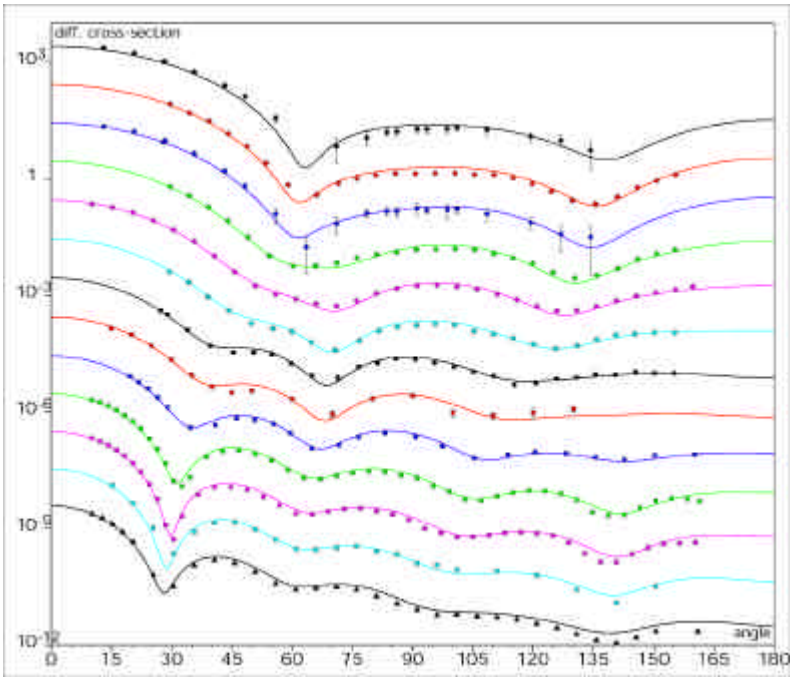

Figure 2. Differential elastic scattering for neutrons incident on ^{54}Fe using the optical model of Table II. The energies of the angular distributions are 7, 8, 8.5, 10, 11, 12, 14, 14.7, 17, 20, 22, 24 and 26 MeV (from top to bottom). All values are given in the center-of-mass system. The symbols represent the experimental data and the continuous curves are the results from ECIS96 calculations.

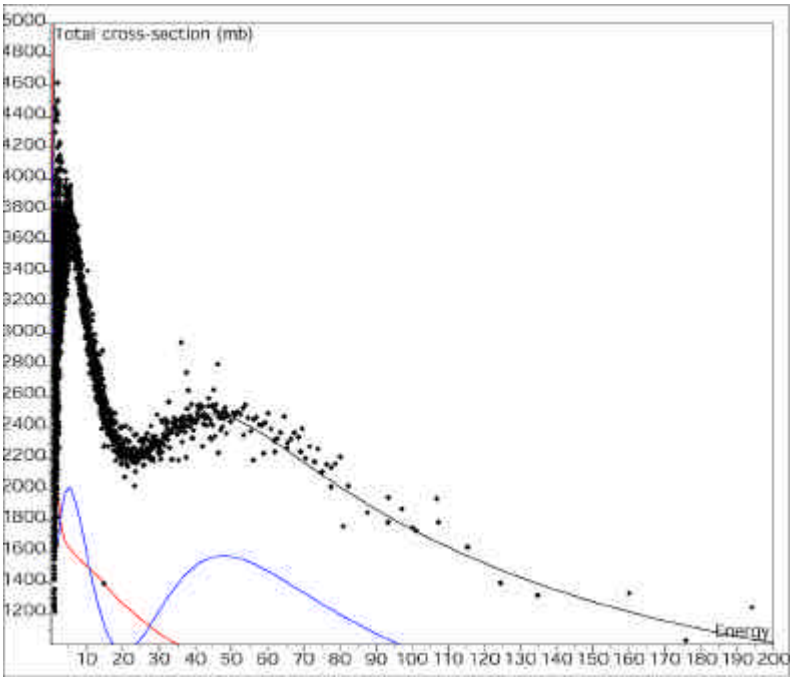

Figure 3. Total neutron cross section for ^{54}Fe up to 200 MeV using the optical model potential of Table II. The symbols represent the experimental data and the continuous curve is the result from ECIS96. The total elastic cross section (with the same shape as the total cross section) and the total reaction cross section can be seen in the bottom left corner.

The optical model parameterization for Pb is similar to that of Eq. (3) and will be published before long. The elastic scattering and total cross sections for Pb are shown in Figs.4-7.

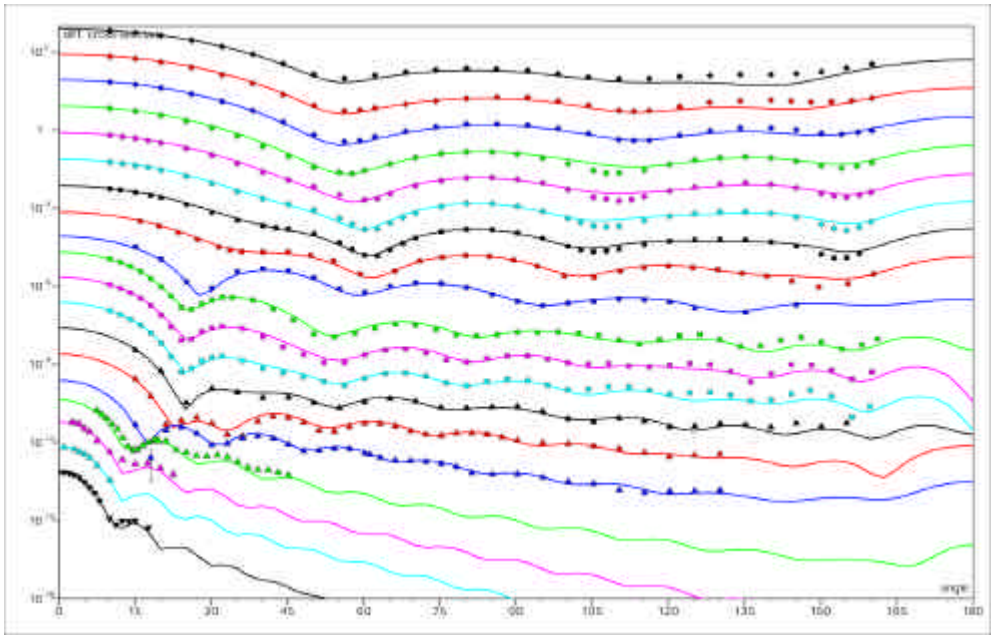

Figure 4. Differential elastic scattering for neutrons incident on ^{208}Pb.The energies of the angular distributions are 4, 4.5, 5, 5.5, 6, 6.5, 7, 8, 11, 20, 22, 24, 26, 30.3, 40, 65, 84, 96 and 136 MeV (from top to bottom). All values are given in the center-of-mass system. The symbols represent the experimental data and the continuous curves are the results from ECIS96 calculation.

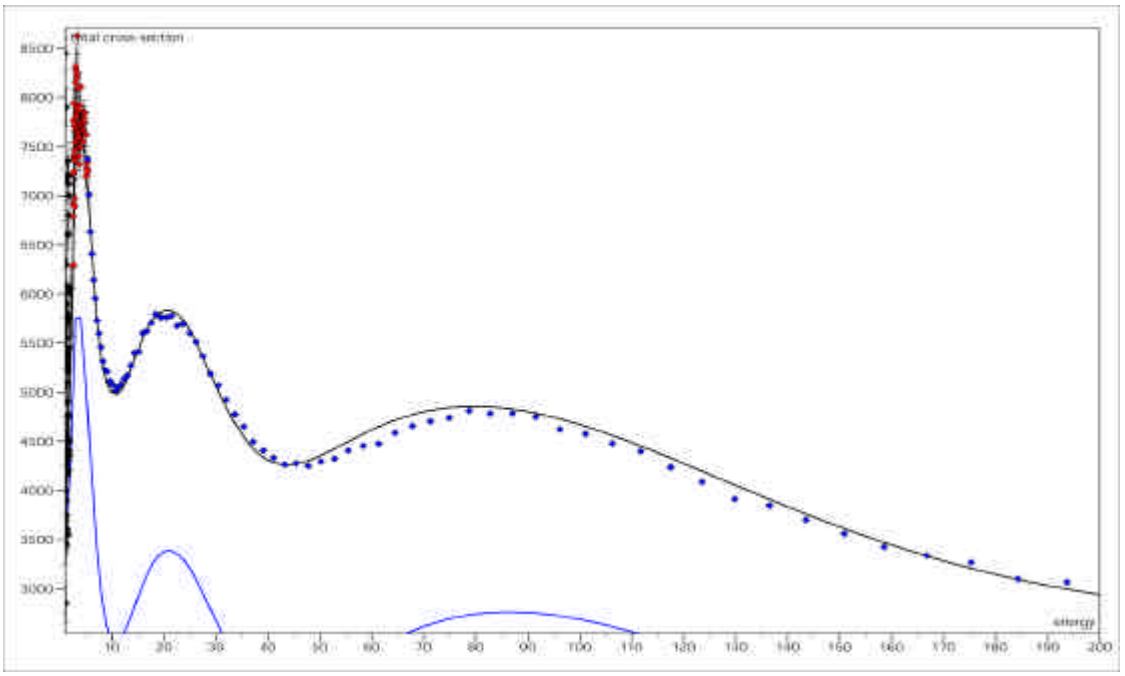

Figure 5. Total neutron cross section for ^{208}Pb up to 200 MeV. The symbols represent the experimental data and the continuous curve is the result from ECIS96. The total elastic cross section (with the same shape as the total cross section) and the total reaction cross section can be seen in the bottom left corner.

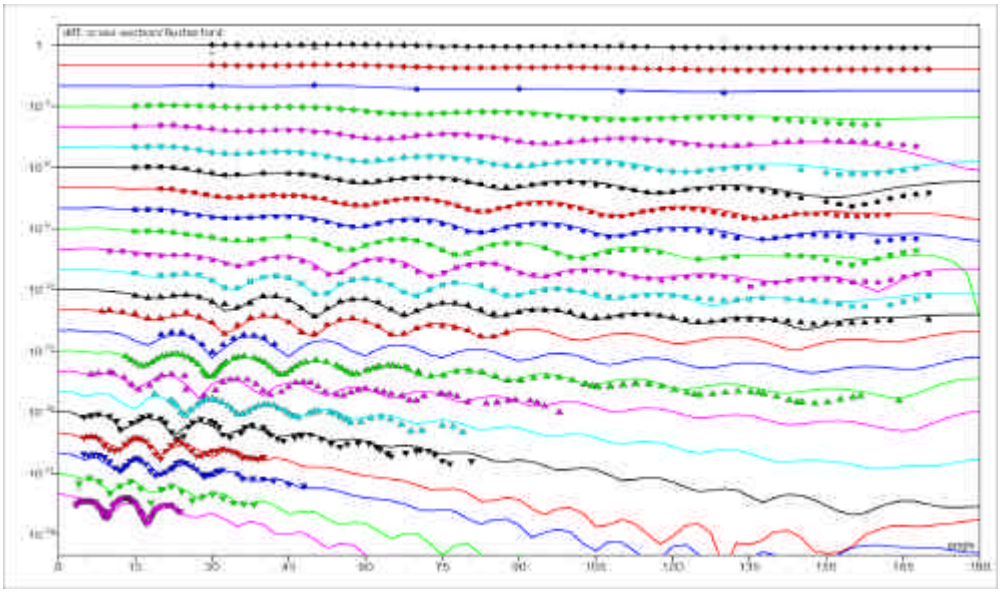

Figure 6. Differential elastic scattering for protons incident on 208Pb The energies of the angular distributions are 11, 12, 13, 16, 21, 24.1, 26.3, 30.3, 30.5, 35, 40, 45, 47.3, 49.4, 61.4, 65, 79.9, 100.4, 121.2, 156, 160, 185 and 200 MeV (from top to bottom). All values are given in the center-of-mass system. The symbols represent the experimental data and the continuous curves are the results from ECIS96 calculations.

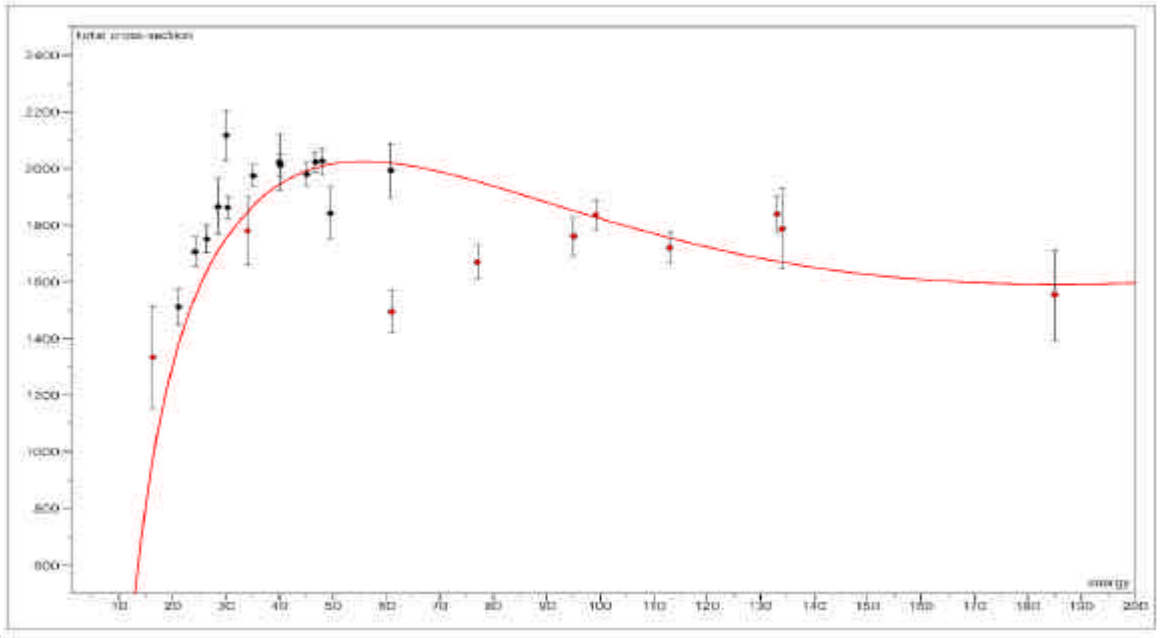

.

Figure 7. Total proton reaction cross section for ^{208}Pb up to 200 MeV. The symbols represent the experimental data and the continuous curve is the result from ECIS96.

4.2 MSD

As stated above a global calculation scheme for accelerator driven systems should consist of a combination of intranuclear cascade codes above 150 MeV and evaluated data libraries for energies up to 150 MeV. Well benchmarked evaluated data files covering nuclear

reactions up to 20 MeV have been constructed earlier in connection with fission and fusion reactor studies. To enable the production of such evaluated data libraries at higher energies there is a strong need of developing scattering and reaction theoretical models and testing them on existing experimental data.

The pre-equilibrium reaction mechanism can be looked upon as the conceptual link between the two extremes of nuclear reaction models, i.e. the compound nucleus reaction model and the direct reaction model. Accordingly that must be the most appropriate approach to use for the description of nucleon induced reactions in the energy region 100-200 MeV. With few exceptions, calculations of the multistep processes for nucleon induced pre-equilibrium reactions have up to now been carried out using two approaches: the Feshbach, Kerman, and Koonin (FKK) theory [Fesh80] and that of Tamura, Udagawa, and Lenske (TUL) [Tamu82, Lens92]. A third approach by Nishioka, Weidenmüller, and Yoshida (NWY) [Nish88] relaxes some of the statistical assumptions in FKK and in TUL but is more difficult to implement. The differences and similarities between the FKK model, which is by far the up to now most commonly used model in applications, and the TUL model were discussed in detail at a workshop in Trento, July 27-August 1, 1998 [Chad99]. Among other things the importance of choosing a proper optical potential in the calculations was pointed out. Furthermore it was stated that the type of effective interaction used is essential. For applications these problems have to be solved properly.

Experimental information on reactions in the continuum region for incident energies in the 20 – 250 MeV range, which are necessary for the development and testing of the different direct reaction theories have so far been provided from a number of experimental programs at different laboratories around the world, such as the National Accelerator Centre (South Africa), Indiana University (USA), Los Alamos National Laboratory (USA), the University of Maryland (USA) Oak Ridge National Laboratory (USA), Ohio University (USA) , Tohoku University (Japan), Kyushu University (Japan), Milan University (Italy), Osaka University (Japan), Louvain-la-Neuve (Belgium) and Uppsala University (Sweden). However additional experiments will be needed to advance developments in the theory. A complete set of double-differential emission spectra including complex particles for the same target and incident energy both for proton and neutron induced reactions would in this connection be very valuable.

The present work is mainly based on the quantum-mechanical statistical direct reaction multistep model according to Tamura, Udagawa and Lenske (TUL) [Tamu82, Lens92] and experimental work from the The Svedberg Laboratory in Uppsala, Sweden. Thus at the intermediate energy neutron facility in Uppsala several neutron-induced reactions, viz. the ^{12}C(n,p), the ^{54,56}Fe(n,p), the ^{90}Zr(n,p) and the ^{208}Pb(n,p) reactions, have been studied experimentally at an incident energy of 100 MeV. The measurements have been performed in the angular range 0^{o}-30^{o} for excitation energies of the residual nuclei up to 40 MeV. The experimental double-differential cross sections have been compared with theoretical calculations using the TUL model. A report has been published in Nucl. Phys. A [Ring97], in which the experimental data for the ^{208}Pb(n,p) reaction are published and compared with theoretical calculations. The results of the same type of calculations for all the studied reactions are planned. Some of these results were presented in a report at the International Conference on Nuclear Data for Science and Technology, May 19-24,1997, Trieste, Italy [Rams97]. In this connection it is important to point out that data for target material (Pb) as well as for structural material (Fe) in a future accelerator-driven system have been included in this work.

As mentioned above the importance of choosing a proper optical potential in the calculations was pointed out at the Trento workshop. In the present work the optical potential according to Schwandt et al. [Schw82], which is the most commonly used in the studied energy range, has been used in the calculations. However, for iron Koning et al [Koni98] have derived a phenomenological optical model potential in the energy range 0.001 – 200 MeV. The same has also been done by Koning for lead (see Figs 4-7) in connection with his work on an evaluated nuclear data file for nucleon induced reactions on this nucleus in the same energy region. These potentials have also been used in calculations with the TUL model for the ^{56}Fe(n,p) and the ^{208}Pb(n,p) reactions, respectively. Discrepancies up to around 20% were found between the cross sections calculated using the two different potentials as shown in Fig. 8. Furthermore it is obvious from the figure that the experimental data are as a whole better described by the calculated cross sections obtained using the Koning potential.

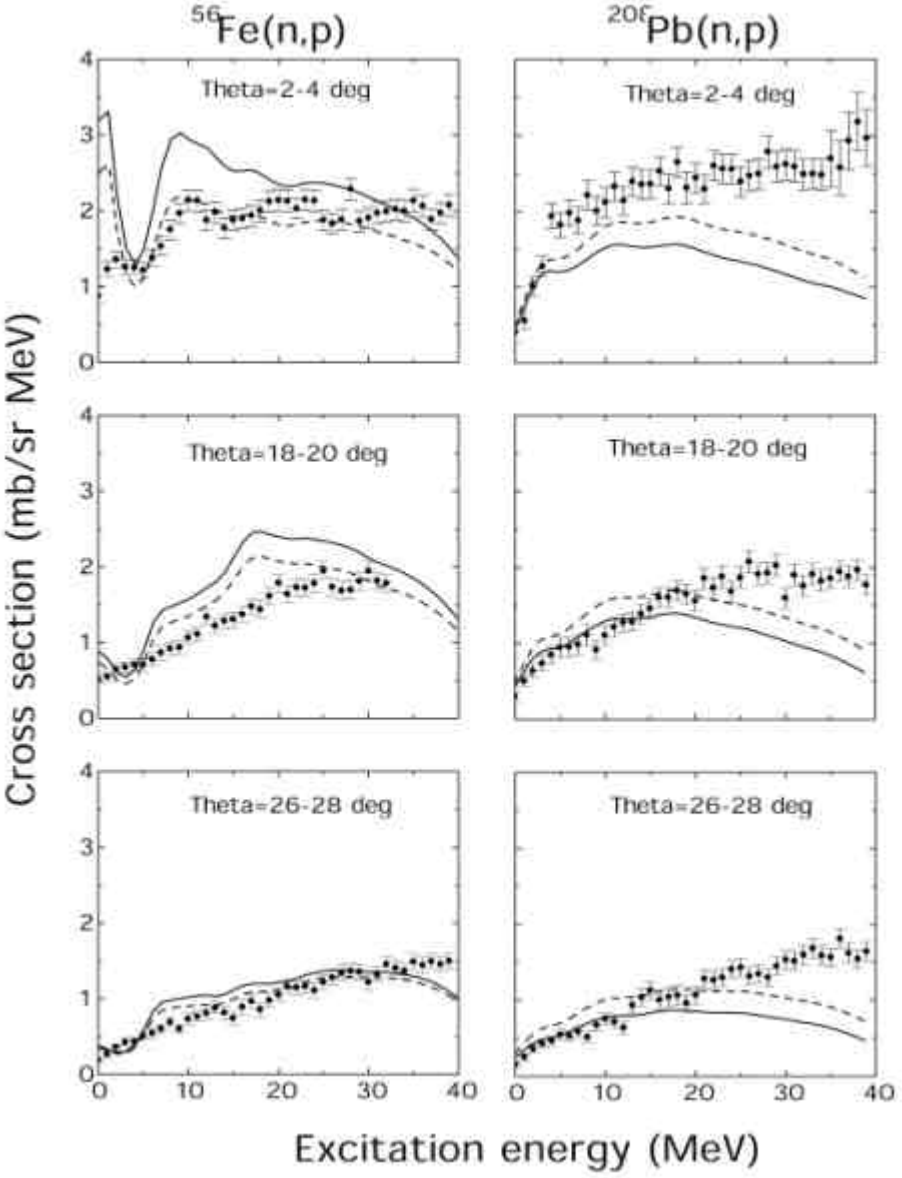

Figure 8. Experimental double-differential cross sections for the ^{56}Fe(n,p) and the ^{208}Pb(n,p) reactions at 97 MeV (filled circles). The different curves represent the cross sections calculated with the TUL model using the Schwandt potential (solid lines) and the Koning potential (dashed lines), respectively.

Since the observables in multistep theories are heavily averaged, the main information is in the magnitude and the energy dependence of the continuum cross sections. In the TUL calculations the magnitude of the cross sections is free of any adjustable parameters, and strictly related to effective interactions and known optical potentials, in a consistent fashion, using RPA and Green function techniques. It is thus a microscopic statistical approach. The FKK approach, however, which has up to now been more widely applied contains variable effective parameters, which makes predictions in connection with different applications more uncertain. Furthermore, even after adjusting these parameters to existing experimental data, it has been shown that this model has difficulties to describe the data both at low and high excitation energies of the residual nuclei. The discrepancies at low excitation energies, especially at small angles, are due to the fact that the statistical assumptions applied in the FKK model are too rough to make the model applicable, where collective phenomena like giant resonances are important. In such cases it is particularly necessary that the statistical approach does not wash out all the microscopic structure of the nuclei involved in a reaction. On the contrary, shell structures such as e.g. irregularities of the mean field spectrum and of the response functions have to survive the averaging process. This is the case in the more quantum-mechanical TUL model , which has been used in the present work.

The TUL model has earlier been shown to give a rather complete description of experimental data at lower energies around 20 MeV. For applications within the ADTT field and also for theoretical reasons, such a unified microscopic statistical multistep description of nucleon induced reactions in the energy range 100-200 MeV would be very useful for the production of the evaluated data files mentioned above. The present work shows that the TUL model gives a good description of the experimental data from Uppsala for charge exchange (n,p) reactions at energies around 100 MeV at small angles and low excitation energies. Two steps have been included in the calculations. The first step was obtained as a direct charge exchange (n,p) reaction. To get the contribution from the second step two different reaction chains were taken into account; first charge exchange (1^{st} step) plus inelastic (2^{nd} step), i.e., (n,p)(p,p) reactions, secondly inelastic (1^{st} step) plus charge exchange (2^{nd} step), i.e. (n,n)(n,p) reactions. Charge exchange and inelastic response functions are described microscopically in the quasiparticle random phase approximation (QRPA).

However, in the studied charge exchange reactions the TUL model found was to underpredict the data at higher excitation energies substantially. Thus to be able to describe the experimental data also at higher excitation energies of the residual nuclei in the investigated energy region, there is a definite need to understand better the mechanisms of additional contributing reactions, in particular the knockout reaction, and to study their relative importance. For that purpose there is a need for a more systematic investigation over a larger energy range of (p,p'), (p,n) and (n,p) reactions for the same target, simultaneously. This will allow to separate the different reaction mechanisms, since different parts of the effective NN force enter in the direct part for those reactions, while the knockout processes are all similar. Thus within the work on developing a unified model for the description of nucleon induced reactions in the energy range 100-200 MeV, an extension of the TUL model to include all reaction mechanisms possible in the studied energy region is necessary.

5. Evaluated Nuclear Data Files

The data files for Fe, Ni and Pb have been created at NRG Petten following one and the same procedure. They will be described first. The files for thorium, uranium and plutonium are reported in a separate section.

5.1 The Evaluation Code System

Here, we will briefly describe our code system that produces the high-energy data files. In our opinion, if one wants to predict all possible nuclear reactions up to 150 MeV, the best working method is to construct a code system that basically consists of two different parts (because they require rather different expertise):

1. A "basic" nuclear reaction code that provides transmission coefficients, total, reaction and elastic scattering cross sections, discrete reaction calculations for both spherical and deformed optical potentials, based on nuclear models that range from very simple to a very high degree of sophistication. The code ECIS96 meets all these requirements and is an obvious choice as backbone for all our calculations.
2. A code that models the reaction mechanisms not covered by ECIS96. To do this, basic reaction information (e.g. transmission coefficients) produced by ECIS96 is read in. The most important components of the second part are pre-equilibrium, multiple Hauser-Feshbach decay and fission. These mechanisms are included in GNASH, which has proven to be one of the multidisciplinary codes with the best predictive power.

We have built a code system around ECIS96 and GNASH that enables massive nuclear model calculations in a relatively simple manner. The initial development was done in collaboration with two of the authors of GNASH, P. Young and M. Chadwick, at LANL [Koni96], and the code system has been further refined at ECN Petten and Bruyères-le-Châtel. The basic philosophy is that all physical information is specified in one basic input file and that, once we have specified our reaction problem, a shell script takes care of the rest. Hence, we automatically perform nuclear model calculations, store the results in an ENDF6 data file, check the data file and process it into multi-group or continuous energy format. The energy region for the nuclear model calculations runs from 20 MeV to 150 MeV for neutrons and from 0 (or, effectively, the Coulomb barrier) to 150 MeV for protons. We note that this set-up may also be suitable for incident neutron energies below 20 MeV. The flow chart of the code system is given in Figs 9-10. For the data files presented in this report, the 20 MeV part of the neutron data files are taken from the ENDF/B-VI.3 library. The quality control of this method is rather rigid: human interference in the calculation process is avoided, which removes the possibility of performing inconsistent calculations at different levels.

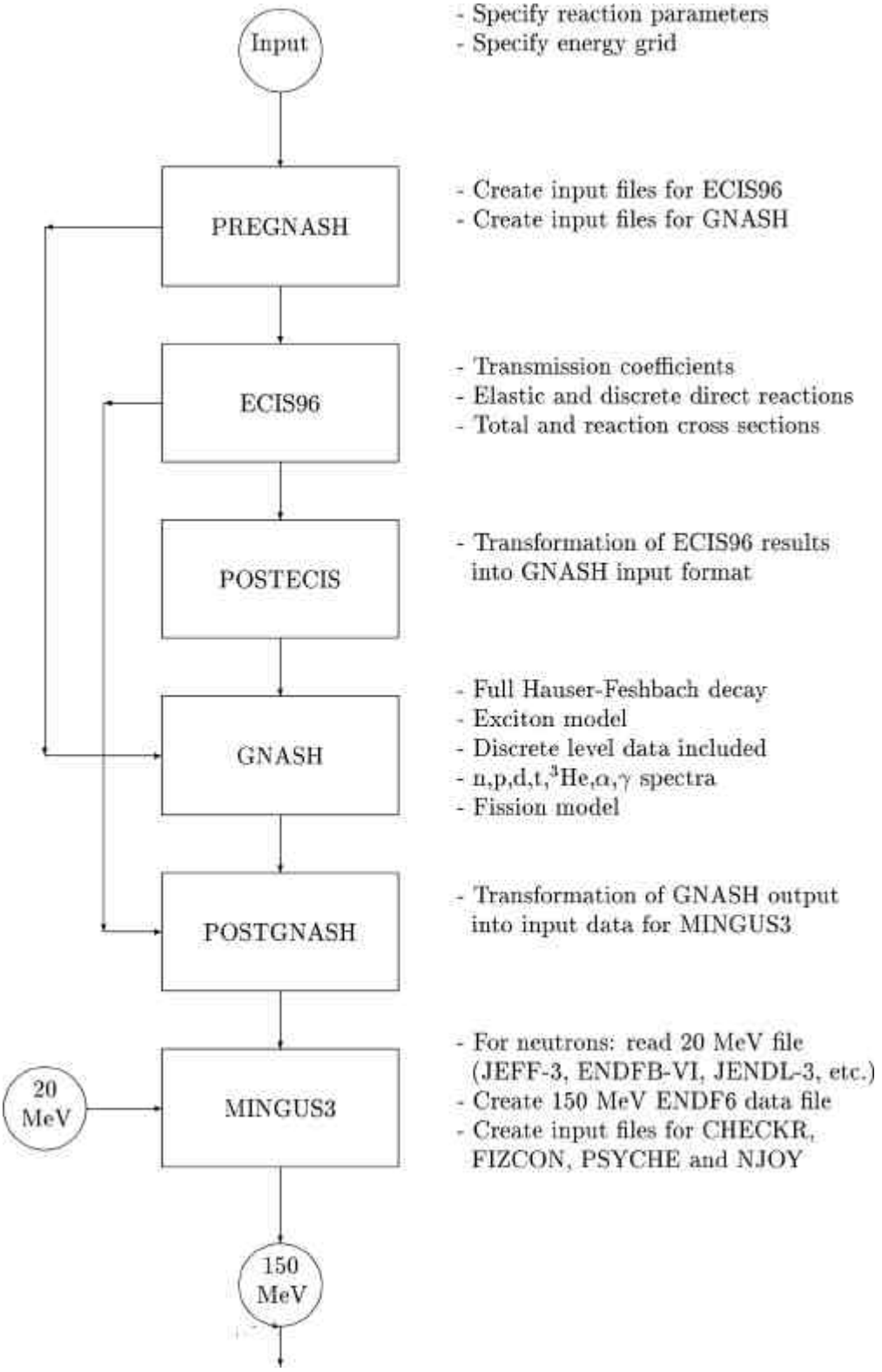

Figure 9. Flow chart of the evaluation code system: Part 1.

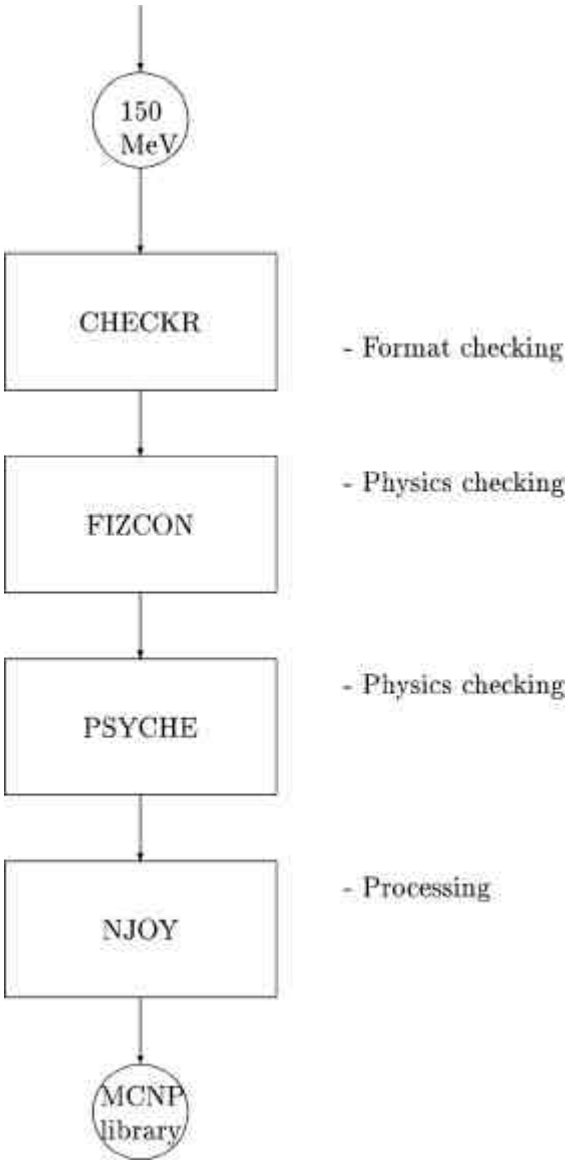

Figure 10. Flow chart of the evaluation code system: Part 2.

5.2 Elastic and Total Cross Sections

5.2.1. Storage in the data file

The technical aspects of storing the data have been described in detail in Refs. [Koni93, Koni97]. Here we restrict ourselves to stating that we cannot avoid some small discontinuities at 20 MeV in the neutron file. This stems from our (provisional) rule that we leave the existing 20 MeV neutron data file untouched and that we have chosen to fine-tune our optical model to the experimental data and not to the low-energy data file. This results in "jumps" in the total cross section of the order of one percent. For the moment, we expect this to be insignificant when the data file is used for applications. Fig. 11 shows the resulting evaluated neutron total cross sections for the four isotopes. We calculate and tabulate the total, total elastic scattering and the total reaction cross section at every 1 MeV of incident energy.

Another point we wish to discuss is the elastic angular distribution. We have used tabular format for the presentation of the data (see [Koni97] for a discussion on the use of tabular

format vs. Legendre coefficients). Since the angular distributions are forward peaked, we use a fine grid at small angles and a wide grid at large angles:

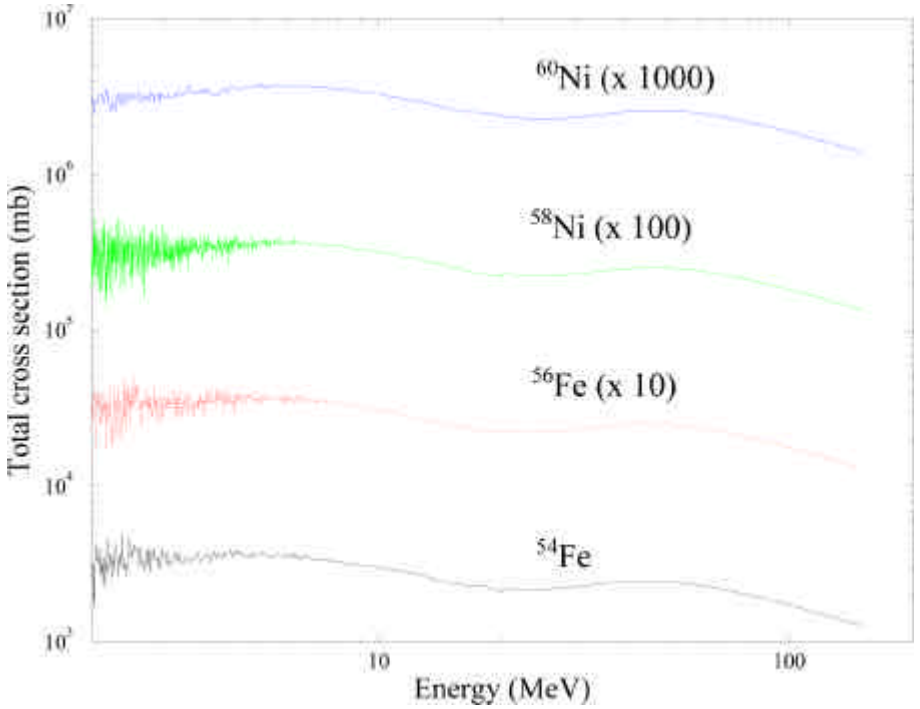

Figure 11. Total neutron cross section for the four isotopes of the BRC/ECN data library.

Angle steps of 1,2,3 and 4 degrees for angles up to 45, 90, 135 and 180 degrees, respectively, a total of 96 angles (the ENDF6-maximum is 100). In Fig.12, the elastic

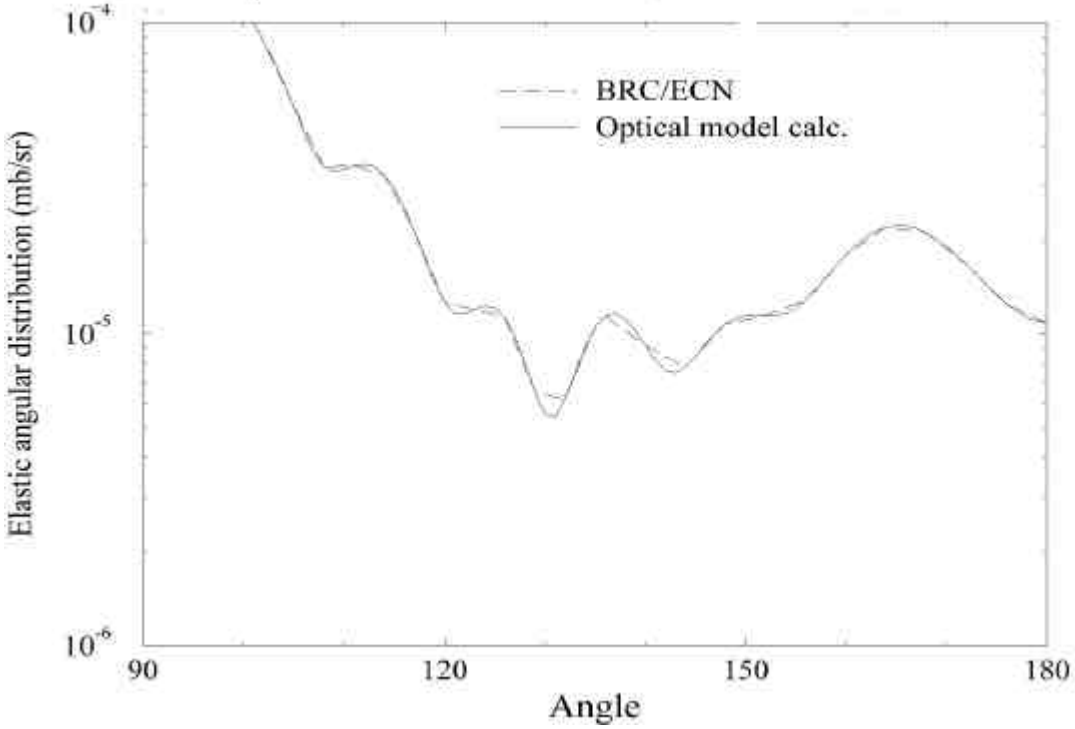

Figure 12. 150 MeV neutron elastic scattering on ^{56}Fe: Comparison between optical model calculation (ECIS96) and the corresponding values as tabulated in the BRC/ECN data file.

angular distribution for the highest incident neutron energy (150 MeV) at backward angles for ^{56}Fe is shown, both for the original ECIS96-calculation (with the cross section calculated at every degree) and the value that is actually tabulated in the data file. It is clear that the difference is very small and that the elastic angular distributions can be accurately represented within the present ENDF6-format. This holds for all the nuclides that we have evaluated. For protons, we use the nuclear + interference expansion as discussed in [Koni93].

5.3 Direct Reactions to Discrete States

5.3.1. DWBA Calculations

Direct reactions to discrete states have been calculated with ECIS96 using DWBA, using the aforementioned neutron and proton optical model potentials. Deformation lengths for the first several MeV have been retrieved from the literature (Nuclear Data Sheets) and are appropriately transformed to deformation parameters, using the potential radius, for each component of the optical potential. The calculated DWBA cross sections are lumped and are included in the continuum spectrum as calculated by GNASH.

5.3.2. Storage in the Data File

The cross sections for the discrete states are included in the continuum spectra for inelastic scattering (MF6/MT5), using the Kalbach systematics [Kalb88] for the angular distributions. A possible future refinement is to store the inelastic cross sections to discrete states separately. This will also remove the problem of using the Kalbach systematics at the highest outgoing energies (where it should not be applied!) instead of the actual discrete angular distribution. Again, sensitivity studies should reveal whether this is a necessity.

5.4. Pre-equilibrium and Compound Reactions

The physics of the GNASH code has been extensively described in [Gnas96] so we do not repeat it here. We briefly mention the main topics of the calculation.

5.4.1. Calculations

- **Pre-equilibrium reactions.** In GNASH, angle-integrated pre-equilibrium cross sections are calculated with the exciton model of Kalbach [Kalb85]. For continuum angular distributions, the Kalbach systematics is used for all outgoing particles. Secondary pre-equilibrium emission is taken into account.
- **Level densities.** We used the standard level density options of GNASH. For the pre-equilibrium part, the particle-hole state density of Williams is used. For compound nucleus reactions, we use the Ignatyuk formula [Igna75], and we account for an appropriate matching of discrete levels and the continuum.
- **Compound reactions.** We include a large number of possible reaction paths and take into account multiple particle evaporation until all final outgoing channels are closed. For the present evaluation, we include residual nuclei that are up to 7 protons and 11 neutrons

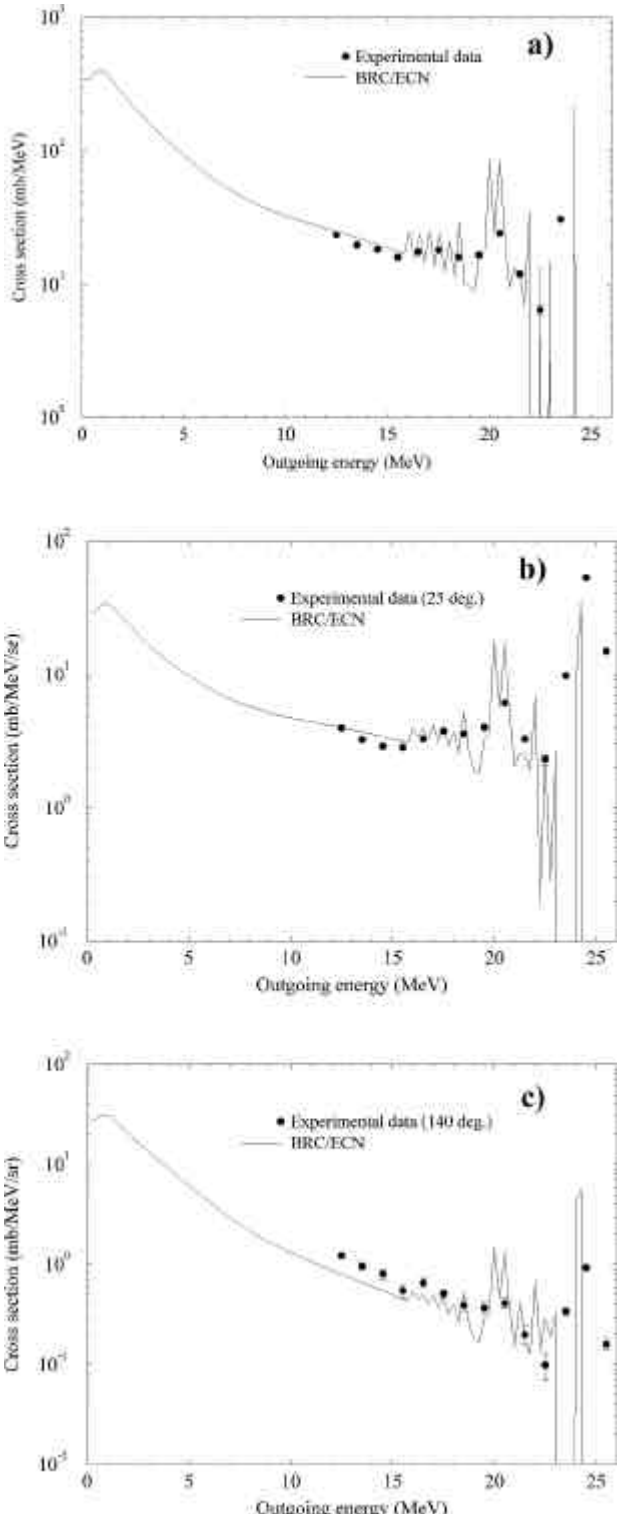

Figure 13. 26 MeV (n,xn) reaction on ^{56}Fe: Comparison between BRC/ECN data file and experimental data [Marc83], (a) Angle-integrated, (b) 25 degrees, (c) 140 degrees.

lighter than the target nucleus. Gamma-ray transmission coefficients were calculated using the Kopecky-Uhl model [Kope90].

5.4.2. Storage in the Data File

The results of all spectrum calculations are stored in MF6/MT5 as yields and energy-angle distributions of outgoing particles (neutrons, protons, deuterons, tritons and alphas) and photons. When combined with the (n(p),x) cross section of MF3/MT5, the double-differential spectra can be recovered. Recoils are not (yet) included, and we realize that this will lead to problems with heat and damage calculations. We tabulate the spectra at incident energy steps of 1 MeV below 30 MeV, 2 MeV steps between 30 and 50 MeV and 5 MeV steps between 50 and 150 MeV. We use an outgoing energy grid of 0.25 MeV for incident energies below 30 MeV, 0.5 MeV between 30 and 50 MeV, 0.75 MeV between 50 and 80 MeV and 1 MeV between 80 and 150 MeV. This gives a sufficiently precise description of the data, enabling reliable interpolations.

5.5 Comparison with experimental data

The total, total elastic scattering and total reaction cross section and the elastic scattering angular distributions that are stored in the data file were automatically benchmarked when the optical model was constructed, see Figs 2-3. All the other comparisons (i.e. of spectra) given in this report are done with results as retrieved directly from the data file, i.e. for absolute safety we check the end product and not the GNASH-output, although they should give the same results. Figs 13-17 present comparisons for several reactions. To get an impression of the difference between data files, we have plotted (n,xn)

and (p,xn) spectra for the four isotopes in Figs 18-19. This demonstrates the well-known simple and weak mass dependence of continuum structureless spectra.

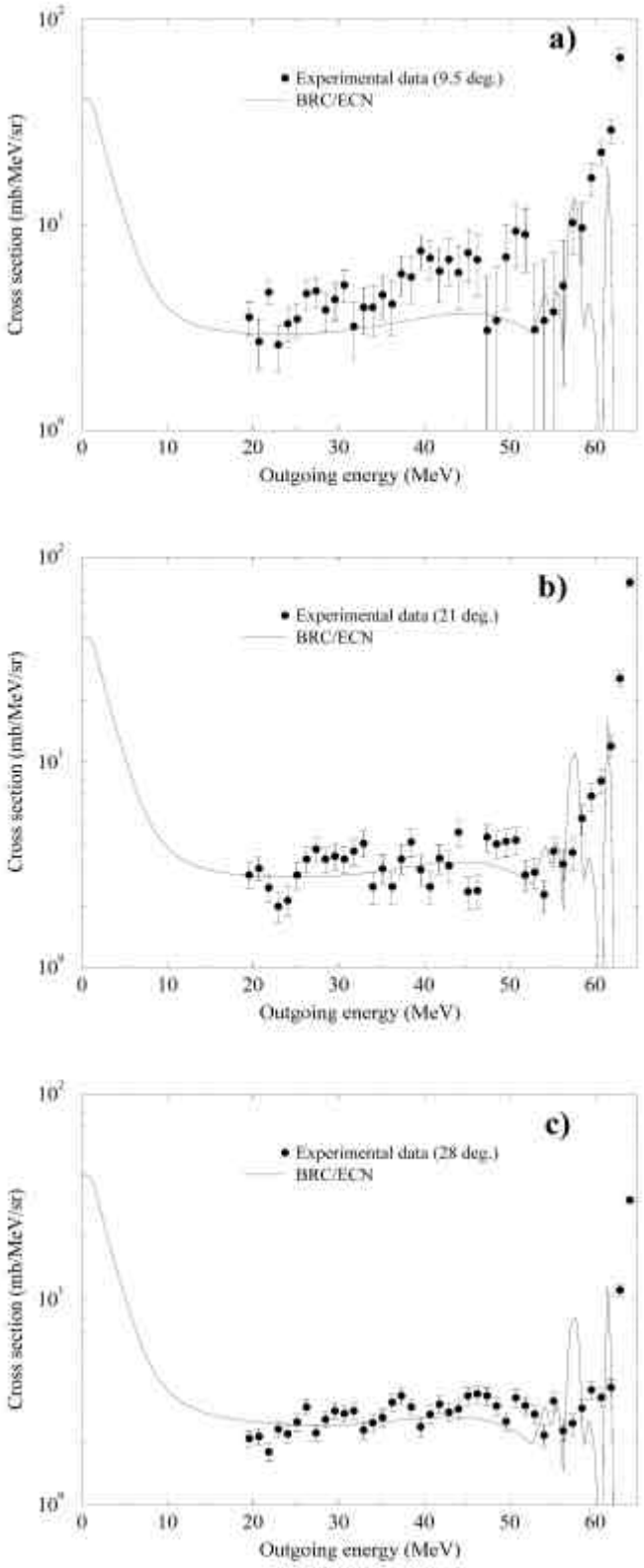

Figure 14. 65 MeV (n,xn) reaction on ^{56}Fe: Comparison between BRC/ECN data file and experimental data [Hjor96], (a) 9.5 degrees (b) 21 degrees, (c) 28 degrees.

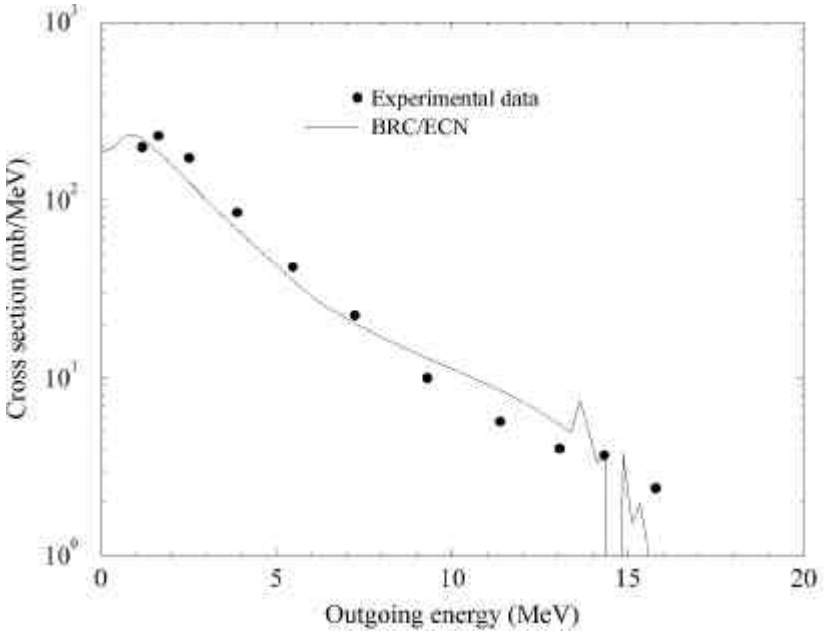

Figure 15. Angle-integrated cross section for 22 MeV (p,xn) reaction on ^{56}Fe: Comparison between BRC/ECN data file and experimental data [Svir83].

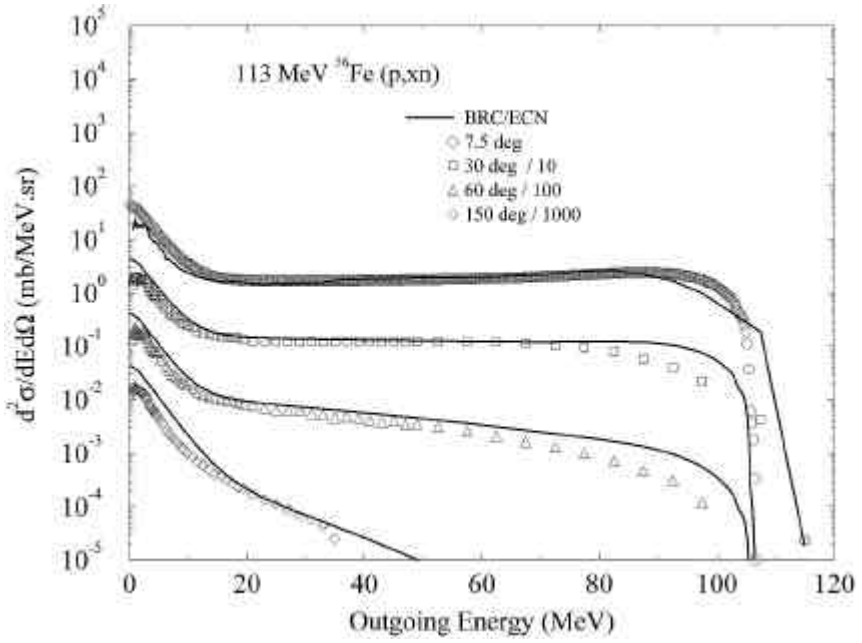

Figure 16. Double-differential cross section for 113 MeV (p,xn) reaction on ^{56}Fe: Comparison between BRC/ECN data file and experimental data [Meie89].

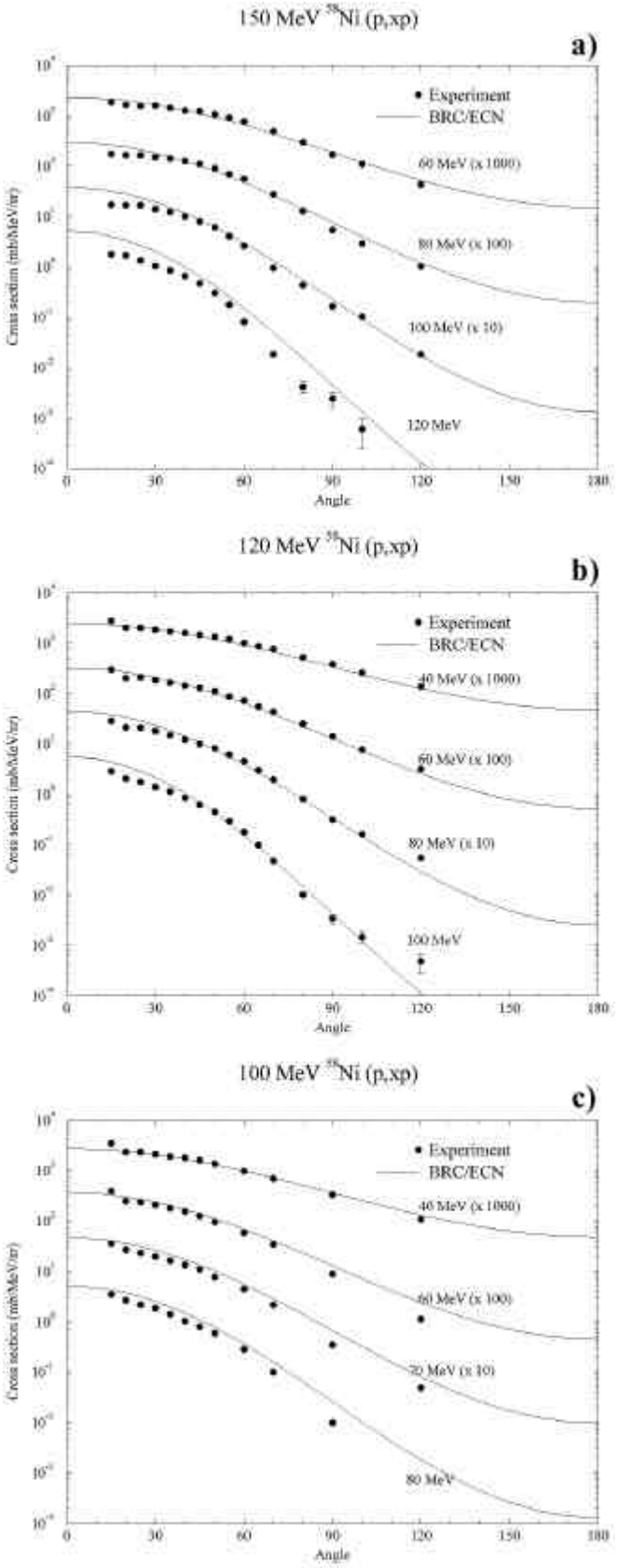

Figure 17. (p,xp) on ^{58}Ni: Comparison between BRC/ECN data file and experimental data [Fort91] for incident energies of, (a) 150 MeV (b) 120 MeV, (c) 100 MeV at several outgoing energies.

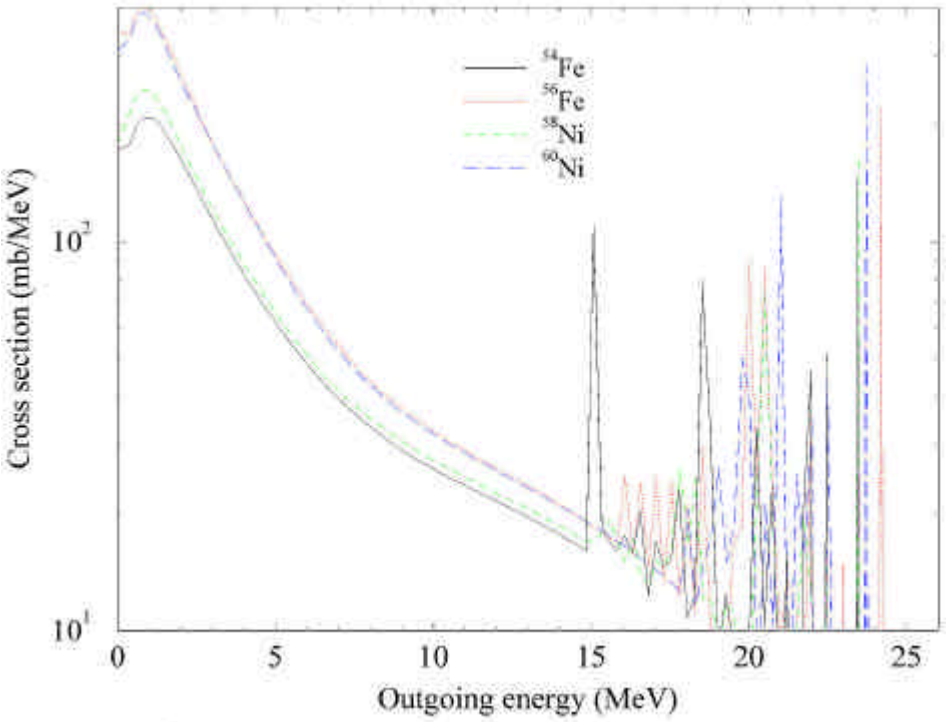

Figure 18. 26 MeV (n,xn) angle integrated cross section: Comparison between the four data files.

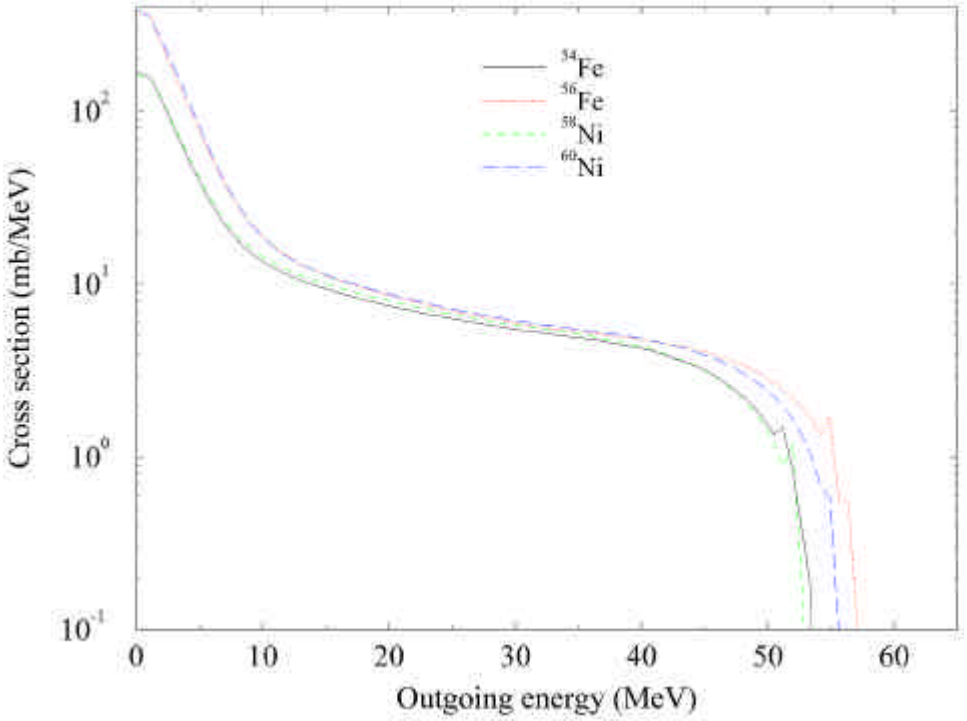

Figure 19. 65 MeV (p,xn) angle integrated cross section: Comparison between the four data files.

5.6 Neutron and Proton Cross-Section Evaluations for ^{232}Th, ^{238}U and ^{239}Pu for Energy Range up to 150 MeV

In collaboration with a Russian group from the Institute of Physics and Power Engineering (IPPE) in Obninsk neutron and proton cross section evalutions have been performed for ^{232}Th, ^{238}U and ^{239}Pu.

5.6.1 Methodology of Neutron Data Evaluations

For the incident neutron energy below 20 MeV the evaluations of ENDF/B-VI, BROND-2 [Mant83] and JENDL-3.2 were used as a rule with an addition of ENDF/B-VI evaluations for the fast neutron inelastic scattering cross sections. The discrepancies between various evaluations are significant but nowadays there are not enough experimental data to improve available evaluations.

Evaluations above 20 MeV have been based on nuclear model calculations fitted to experimental data where available. The coupled-channel optical model has been used to calculate the neutron transmission coefficients and to evaluate the neutron elastic scattering angular distributions [Rayn84]. The GNASH code [Gnas96] was used to calculate the integral and double differential cross sections and to prepare data into the ENDF/B-VI format. The level density description for all channels was obtained on the basis of the Gilbert-Cameron approach fitted to experimental data on the density of low-lying levels and neutron resonances [Igna98]. Neutron and proton transmission coefficients were obtained from the optical potentials [Rayn84], as discussed below. Transmission coefficients for alpha, deuterons and tritons were calculated using spherical optical model.

5.6.2 Total and Scattering Neutron and Proton Cross Sections

Evaluations of neutron total cross sections have been based on the coupled-channels optical model calculations with potential parameters fitted to experimental data. This procedure gives satisfying results for the total neutron cross sections. However, the calculated neutron absorption cross sections show significant discrepancies for various data libraries. These discrepancies are essential at neutron energies above 10 MeV, and their effects appear in the evaluated cross sections of (n,xn), fission and other reactions.

The optimal set of optical model parameters has been estimated from the analysis of experimental data of neutron total cross sections, angular distributions for proton elastic scattering and proton absorption cross sections. These parameters, shown for ^{232}Th, ^{238}U and ^{239}Pu in Tables III, IV and V, respectively, are close to those used for the intermediate energy neutron cross section evaluations of lead isotopes [Vona94, Chad96].

The total cross sections calculated with the parameters given above are compared in Figs. 20,21,22 with available experimental data and other calculations. Below 20 MeV there are many experimental data and only some of them are presented. A reasonable agreement of our evaluation with the Barashenkov's systematics [Bara93] and experimental data is obtained for all energies above 20 MeV.

An example of neutron elastic scattering and absorption cross sections for ^{232}Th is shown in Figs. 23 and 24, respectively. There are no direct measurements of these cross sections at high energies. However, a reasonable estimation of them is given by Barashenkov's systematics, based mainly on proton reaction data [Bara93]. The experimental data available for heavy nuclei are shown in Fig. 25 in comparison with the systematics [Bara93] and our

optical model calculations. The optical model calculations reproduce well the proton absorption cross section in the whole energy region from the Coulomb barrier to 200 MeV, and at high energies they are in reasonable agreement with the Barashenkov evaluations for both protons and neutrons.

TABLE III. ^{232}Th optical potential parameters for neutrons and protons.

Well depth (MeV)	Energy Range (MeV)	Geometry (fm)
$V_R = 53.425 \pm 16\eta - 0.279E + \Delta_C$	$0 < E < 60$	$r_R = 1.183$; $a_R = 0.797$
$V_R = 114.447 \pm 16\eta - 19\ln(E) + 2.$	$60 < E < 200$	
$W_d = 2.694 \pm 8\eta + 0.252E$	$0 < E < 14$	$r_d = 1.273$; $a_d = 0.699$
$W_d = 6.222 \pm 8\eta - 0.0932(E-14.)$	$14 < E < 200$	
$W_V = 0.0$	$0 < E < 14.4$	$r_c = 1.26$
$W_V = -2.6 + 0.18E$	$14.4 < E < 40$	$r_V = 1.373$; $a_V = 0.699$
$W_V = 2.2 + 0.06E$	$40 < E < 100$	
$W_V = 8..2 + 0.018(E-100.)$	$100 < E < 200$	
$V_{SO} = 6.18$	$0 < E < 200$	$r_{SO} = 1.16$; $a_{SO} = 0.667$
Here $\eta = (A-2Z)/A$; $\beta_2 = 0.19$, $\beta_4 = 0.071$ and the scheme of $0^+ - 2^+ - 4^+ - 6^+$ coupled levels is adopted.		

TABLE IV. ^{238}U optical potential parameters for neutrons and protons.

Well depth, MeV	Energy Range, MeV	Geometry, fm
$V_r = 52.33 \pm 16\eta + 0.04306E - 0.02377E^2 + \Delta_c$	$0 < E < 14$	$r_v = 1.185$, $a_v = 0.8$
$V_r = 51.192 \pm 16\eta - 0.2085E + \Delta_c$	$14 < E < 65$	
$V_r = 53.096 \pm 16\eta - 0.2377E + \Delta_c$	$65 < E < 150$	
$\Delta_c = 0.4Z/A^{1/3}$		$r_{coul} = 1.26$
$W_d = 3.082 \pm 8\eta + 0.8477E - 0.01924E^2$	$0 < E < 10$	$r_d = 1.26$, $a_d = 0.52$
$W_d = 11.1232 \pm 8\eta - 0.14882E$	$10 < E < 50$	
$W_d = 8.067 \pm 8\eta - 0.08235E$	$50 < E < 150$	
$W_V = 0.0$	$0 < E < 14.4$	
$W_v = -1.7843 + 0.12745E$	$14.4 < E < 65$	$r_v = 1.26$, $a_v = 0.5 + 0.0125E$
$W_v = 2.9792 + 0.05417E$	$65 < E < 150$	
$V_{so} = 6.18$	$0 < E < 150$	$r_{so} = 1.16$, $a_{so} = 0.667$

Here $\eta = (A-2Z)/A$; $\beta_2 = 0.23$, $\beta_4 = 0.045$ and the scheme of 0^+-2^+-4^+-6^+coupled levels is adopted.

TABLE V. ^{239}Pu optical potential parameters for neutrons and protons.

Well depth, MeV	Energy Range, MeV	Geometry, fm
V_r=51.50 ±16η+0.2420E + Δ_c	0 < E < 40	r_v = 1.21, a_v = 0.7
V_r = 50.58 ± 16η - 0.2190E + Δ_c	40< E < 100	
V_r = 49.34 ± 16η - 0.2066E + Δ_c	100< E < 150	
Δ_c = 0.4Z/A$^{1/3}$		r_{coul} = 1.26
W_d = 3.36 ± 5η + 0.4691E -	0 < E < 5.24	r_d = 1.32-0.0055E, a_d =.63
W_d = 2.079 ± 5η + 0.14882E - 0.0212E^2	5.24 < E < 22	
W_d = 8.067 ± 5η - 0.08235E	22 < E < 35	r_d = 1.2, a_d=0.47-0.008E
W_d = 9.053 ± 5η - 0.0867E	35<E<100	r_d = 1.2, a_d=0.75
W_d = 1.523 ± 5η - 0.01147E	100<E<150	
W_V = -1.708 + 0.122E - 0.000022E^2	0 < E < 100	r_v = 1.26, a_v = 0.35+0.0018E
W_v = -0.408 + 0.107E - 0.0002E^2	100< E < 150	
V_{so} = 6.18	0 < E <150	r_{so} = 1.16, a_{so}=0.667

*Here η = (A-2Z)/A; β_2 = 0.205, β_4 = 0.075 and the scheme of $1/2^+$-$3/2^+$-$5/2^+$-$7/2^+$- $9/2^+$ coupled levels is adopted.

The coupled-channels model makes it possible to calculate also the cross sections and angular distributions for elastic and inelastic scattering of neutrons with excitation of low-lying collective levels in the whole energy range. Experimental data of elastic scattering angular distributions are available only at incident neutron energy up to 14.1 MeV. Our calculations are compared with these data in Fig. 26 for ^{238}U. The contributions of the lowest collective levels, 2^+, 4^+ and 6^+, to inelastic scattering are shown, too. These levels are to be taken into account because their excitation energies are much smaller than the energy resolution in the experimental data of elastic scattering. The quasi-elastic scattering angular distribution including the contributions of the low-lying collective levels is represented by the thick solid curve in Fig. 26. The reasonable agreement of calculations with experimental data allow us to apply the optical model to the evaluation of the elastic and inelastic scattering angular distributions for all higher energies.

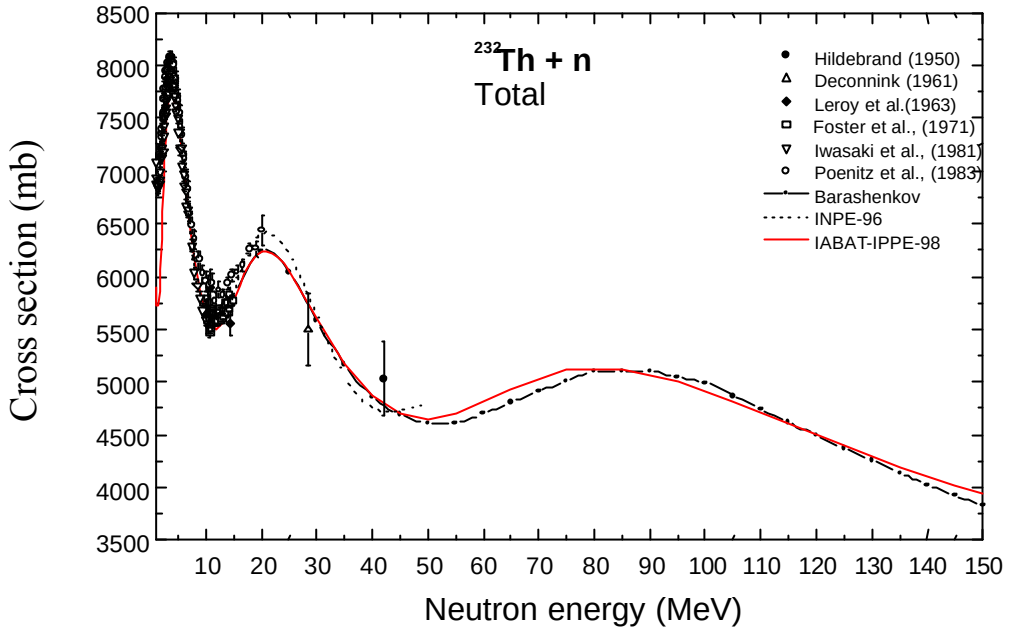

Figure 20. Comparison of different calculations of the ^{232}Th total neutron cross section with experimental data and other evaluations.

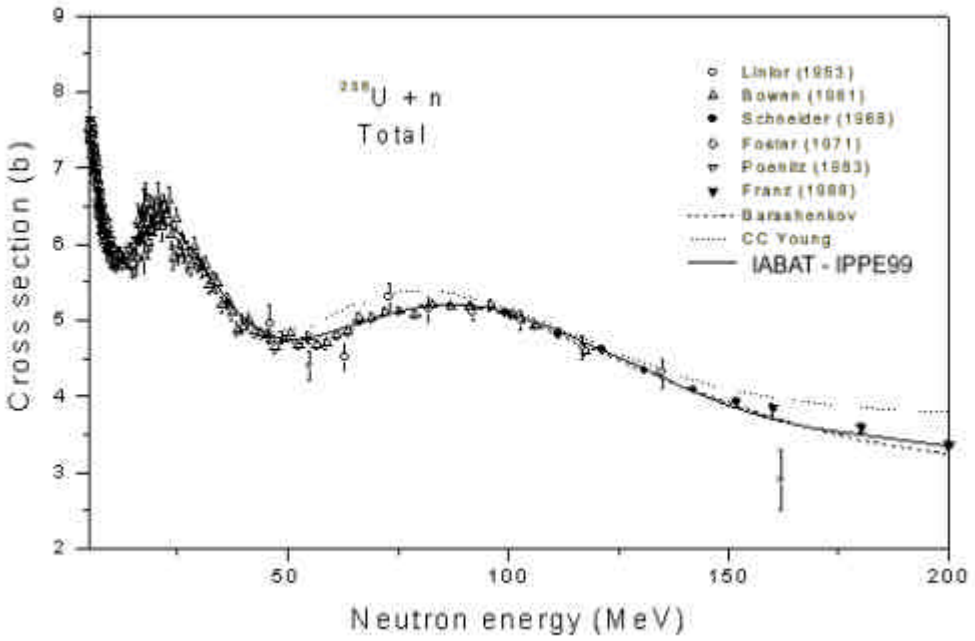

Figure 21. Comparison of different evaluations of the ^{238}U total neutron cross section with experimental data.

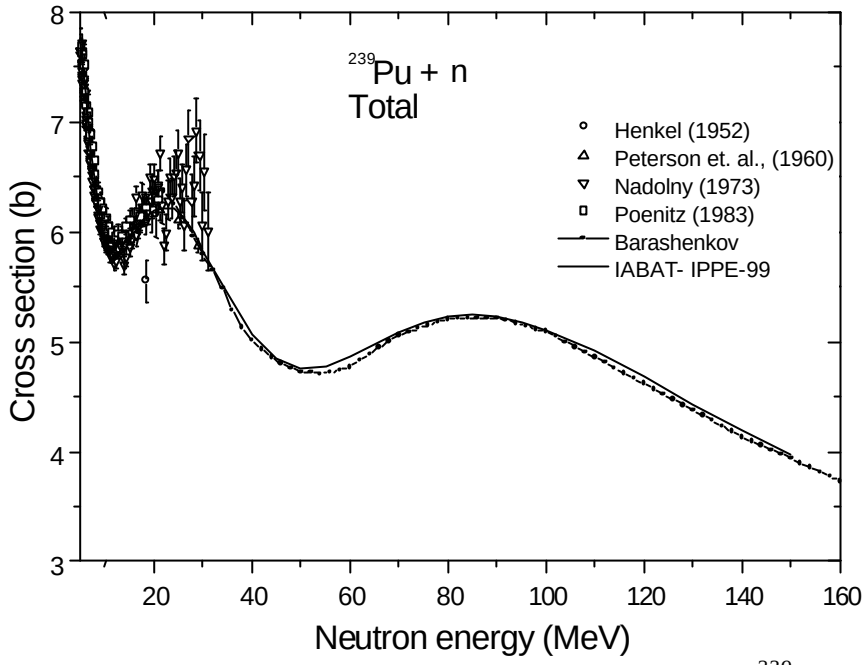

Figure 22. Comparison of different evaluations of the ^{239}Pu total neutron cross section with experimental data.

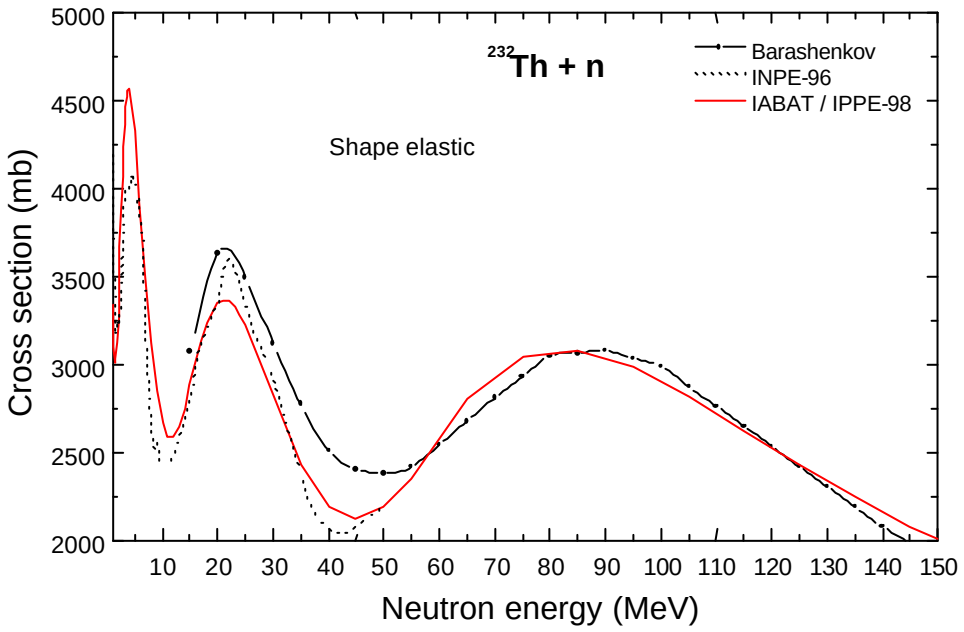

Figure 23. Comparison of the evaluated neutron elastic scattering cross section for ^{232}Th with previous evaluations.

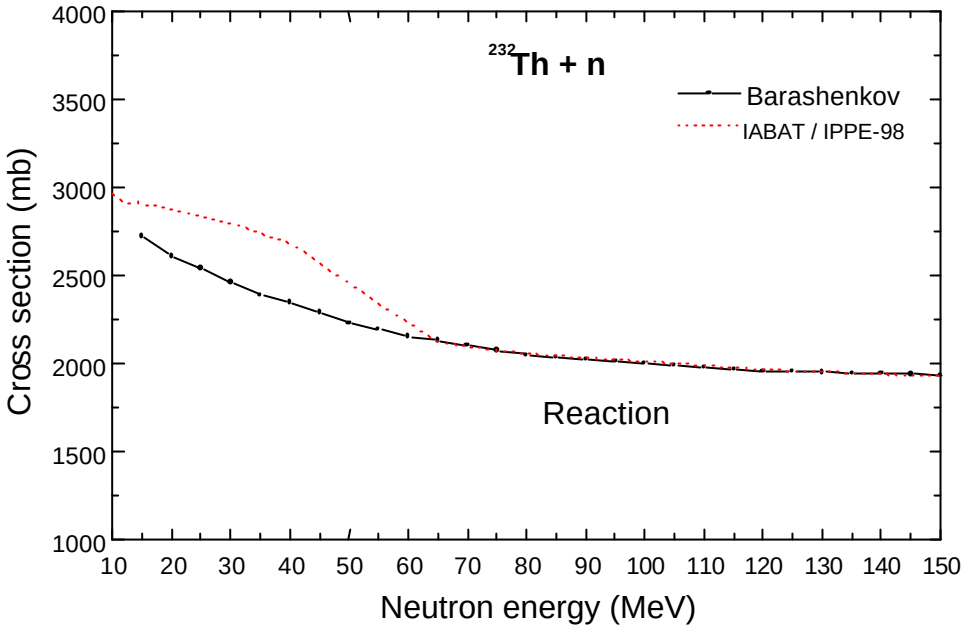

Figure 24. Evaluated neutron absorption cross section for ^{232}Th in comparison with the high energy systematics.

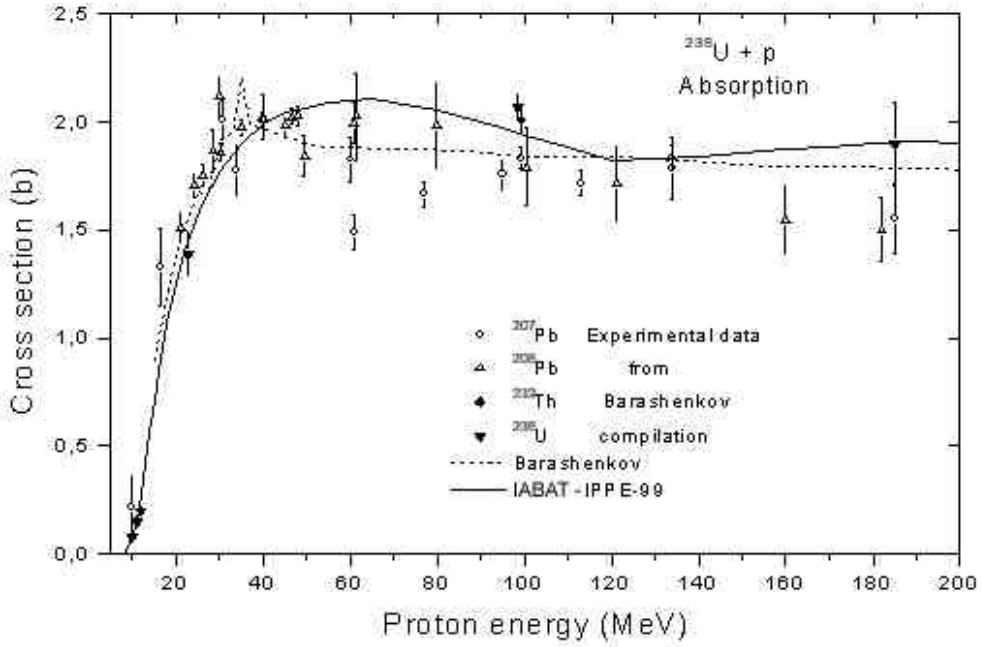

Figure 25. Proton absorption cross section for ^{238}U.

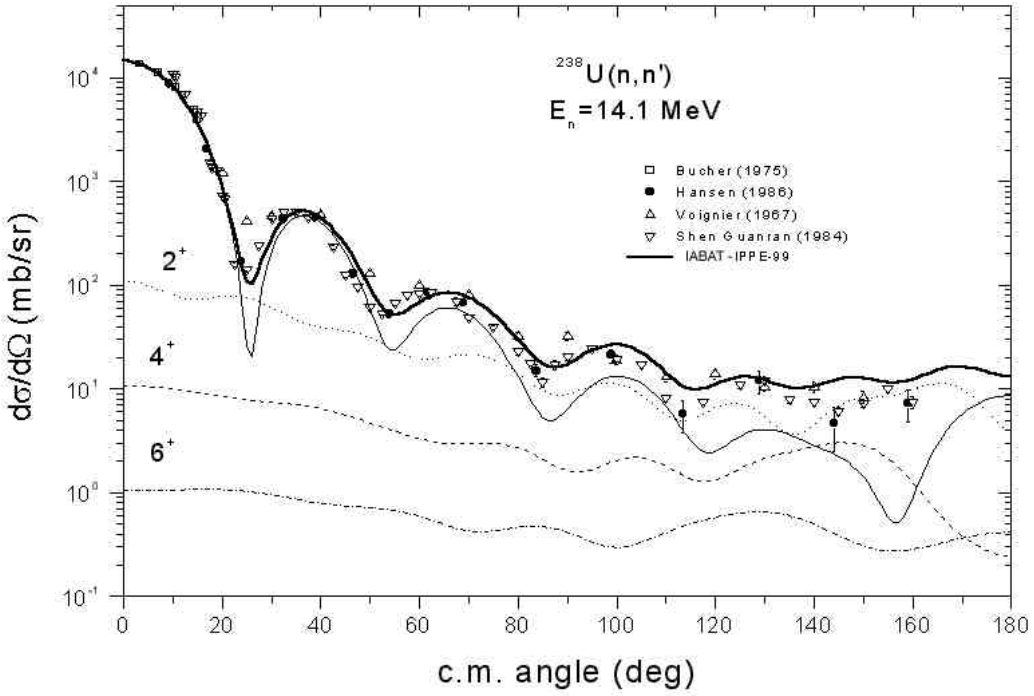

Figure 26. Comparison of the evaluated elastic scattering cross section at 14.1 MeV with experimental data. The scattering cross sections for the ground and collective low-lying levels are shown by solid, dotted dashed and dot-dashed curves respectively. The thick solid curve is the sum of the cross sections for the ground and collective low-lying levels; experimental references: [Voig68; Buch75; Guan84; Hans86].

5.6.3 Fission Cross Sections and Fission Prompt Neutrons

The fission cross section of ^{232}Th, ^{238}U and ^{238}Pu for neutrons and protons with energies above 20 MeV was measured by several research groups [Pank60, Pank63, Liso88, Liso91, Carl96, Eism96, Done99, Smit57, Stap98, Kari78,] and comparisons between different experiments and evaluation data are presented in Figs 27, 28 and 29. Except for some large discrepancies for ^{232}Th [Pank63] and ^{239}Pu [Smit57] older experimental data in the energy range 25 – 50 MeV, the evaluated data fits well into experiments.

For low energy range, up to 20 MeV, the evaluated fission cross sections were fitted to the ENDF/B-VI data in order to obtain fission barrier parameters. For higher energies, the effects of nuclear viscosity were included in the calculations of the fission widths of highly excited compound nuclei [Igna95]. An accurate description of the fission cross sections is very important for consistent evaluation of multiple emission of neutrons and charged particles.

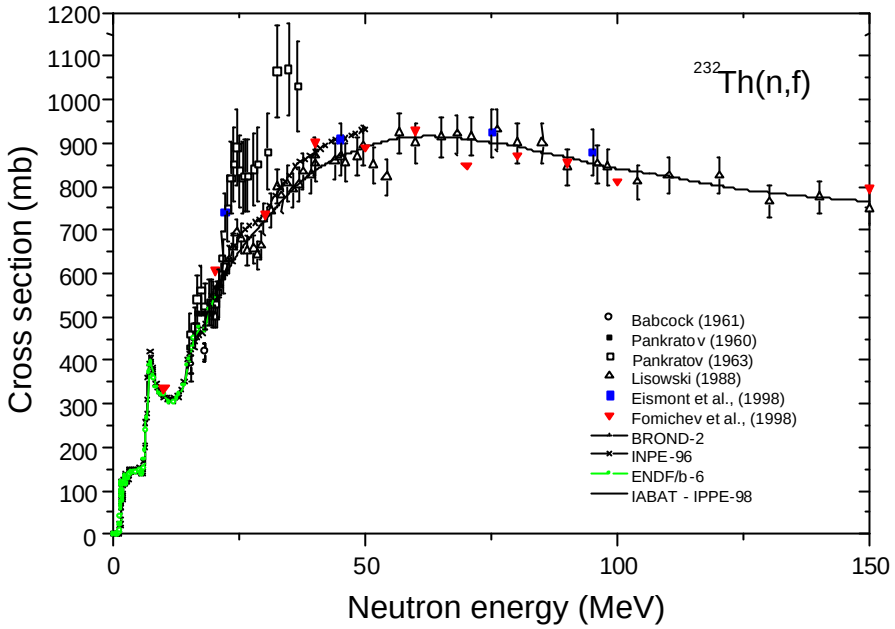

Figure 27. Comparison of the evaluated fission cross section for ^{232}Th with experimental data and previous evaluations.

The result of evaluation for <ν>, the average number of prompt neutrons per fission, is shown in Fig. 30 for ^{232}Th, ^{238}U, ^{239}Pu, in the energy range up to 150 MeV. Scarce, existing experimental data of Fréhaut [Freh76] and of Korovin [INPE96] are also plotted on these figures.

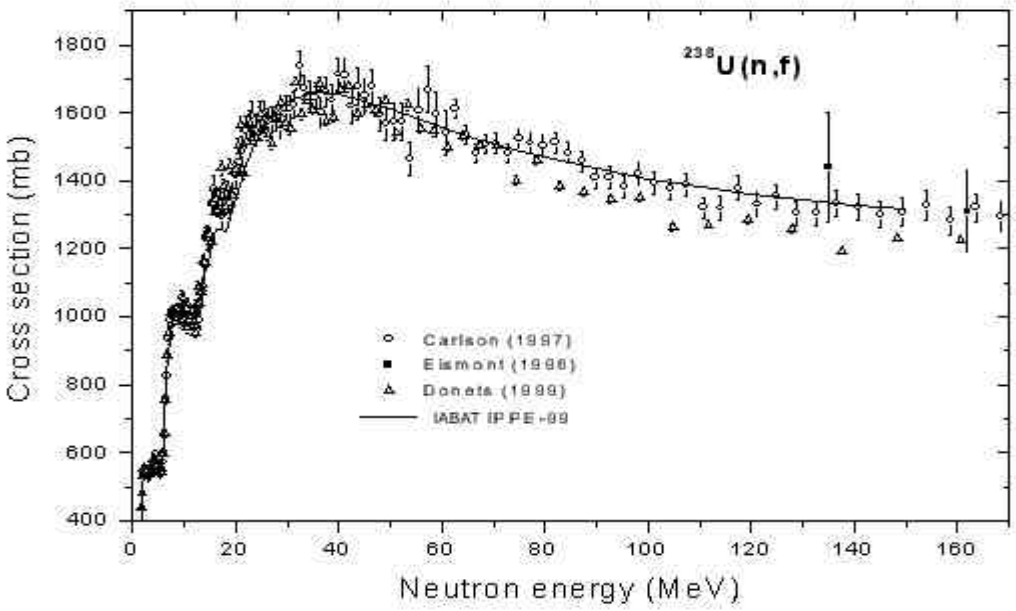

Figure 28. Comparison of the evaluated fission cross section for ^{238}U with experimental data.

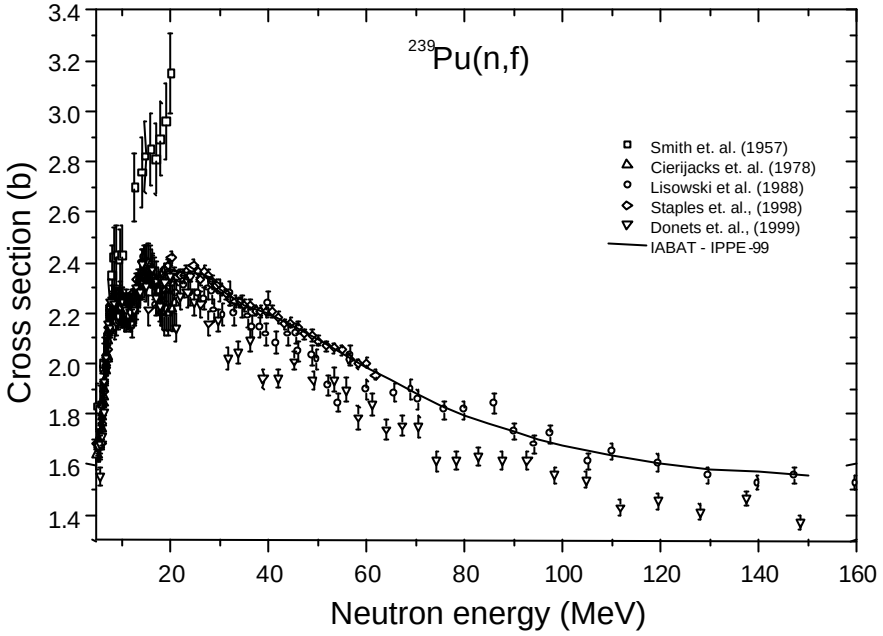

Figure 29. Evaluated and experimental fission cross section for ^{239}Pu.

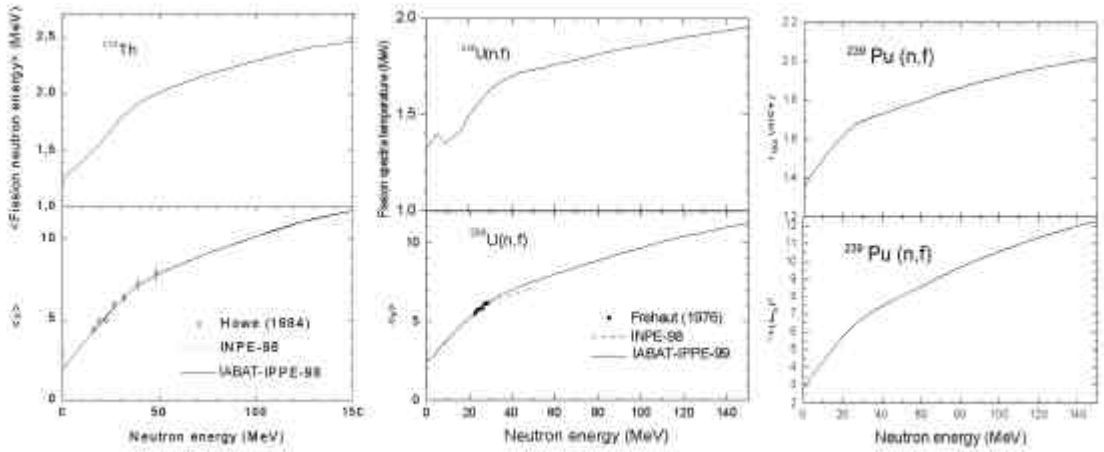

*Figure 30. Average fission neutron energy and number of neutrons <**n**> for ^{232}Th, ^{238}U and ^{239}Pu as a function of neutron energy.*

5.6.4 Neutron Production Cross Sections and Spectra

Evaluations of particle emission spectra and corresponding production cross sections have been performed in accordance with the rules of the ENDF/B-VI format for the double-differential cross sections, by using the Kalbach-Mann representation of such data [Kalb81]. Differential cross sections are described in this approach by the integral production cross section for the corresponding emitted particle multiplied by a normalized angular distribution function of the following form,

$$f(m_b, E_a, E_b) = f_0(E_a, E_b)\left\{\frac{a(E_a, E_b)}{\sinh a(E_a, E_b)}\left[\cosh\left(a(E_a, E_b)m_b\right) + r(E_a, E_b)\sinh\left(a(E_a, E_b)m_b\right)\right]\right\}$$

where E_a is the incident particle energy in the laboratory system, μ_b is the scattering angle cosine of the emitted particle b and E_b is its energy in the center-of-mass system, $f_0(E_a,E_b)$ is the normalized spectrum of the emitted particle, $r(E_a,E_b)$ is the pre-compound fraction of this spectrum, and $a(E_a,E_b)$ is the simple function proposed in [Kalb81], which depends mainly on the center-of-mass emission energy E_b and, to a lesser extent, on particle type and incident energy at higher values of E^a . In accordance with such a description, the two energy-dependent functions $f_0(E_a,E_b)$ and $r(E_a,E_b)$ determine completely the shape of emitted particle spectra and the anisotropy of the corresponding angular distributions, respectively.

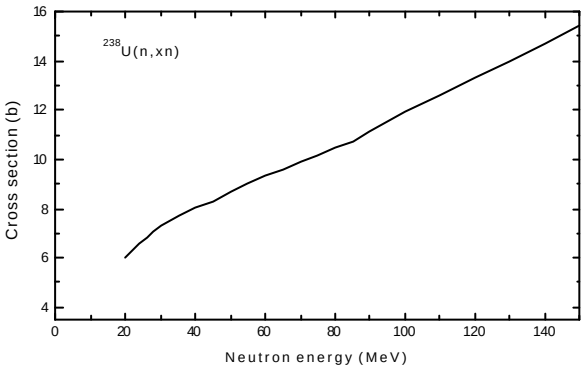

Figure 31. Neutron production cross section for ^{238}U calculated with GNASH.

The neutron emission is a dominant reaction that competes with nuclear fission. The example of neutron production cross section for ^{238}U is shown in Fig. 31. Below 20 MeV these calculations agree well enough with the evaluations of the (n,2n) and (n,3n) reactions based on experimental data and included in the files of BROND-2 or ENDF/B-VI. Above 20 MeV, there are no direct experimental data on neutron emission cross sections or on the multiplicity of secondary neutrons, which can be evaluated as the ratio of the calculated neutron production cross section to the reaction cross section considered above.

5.6.5 Charged Particle Emission Cross Sections and Spectra

In order to calculate the transmission coefficients for protons, the same potential as for neutrons has been used, with the appropriate Lane components. The calculated absorption cross section for such a potential agrees rather well with Barashenkov's systematics of the proton induced reaction cross sections at high energies [Bara93], but, at the present time, the experimental data are not accurate enough to test such calculations for energies close to the Coulomb barrier.

Some deficiency of the pre-equilibrium model used in the GNASH code were demonstrated in the analysis of production cross sections of deuterons and heavier charged particles [Chad96, Iwam82, Dity98]. To get more accurate evaluations of deuteron, triton and α-particle yields the modified ALICE-IPPE code was used. ALICE_IPPE describes the cluster emission on the basis of the Iwamoto-Harada model [Iwam82] with parameters adjusted on the available experimental data of cluster yields and spectra in proton induced reactions [Dity98]. Deuteron emission was calculated using the quasi-direct and pick-up mechanisms. For triton emission the pick-up processes were taken into account, and for α-particles the knock-out, pick-up and multiple pre-equilibrium emission were included into consideration.

The cross sections for the ^{238}U(n,xd), ^{238}U(n,xt) and ^{238}U(n,xα) reactions calculated in such an approach are shown in Fig. 32. The experimental data on the yields of the same charged particles in the proton induced reaction on ^{209}Bi and ^{232}Th, the heaviest studied targets, are shown for the sake of comparison. Undoubtedly, uncertainties of such estimations of light cluster production cross sections are rather large, but we do not have enough experimental data to improve theoretical description essentially at the present time. On the other hand, all of these cross sections are much lower than the neutron production cross section and big uncertainties of less important cross sections seem acceptable for most applications related to the development of accelerator-driven systems.

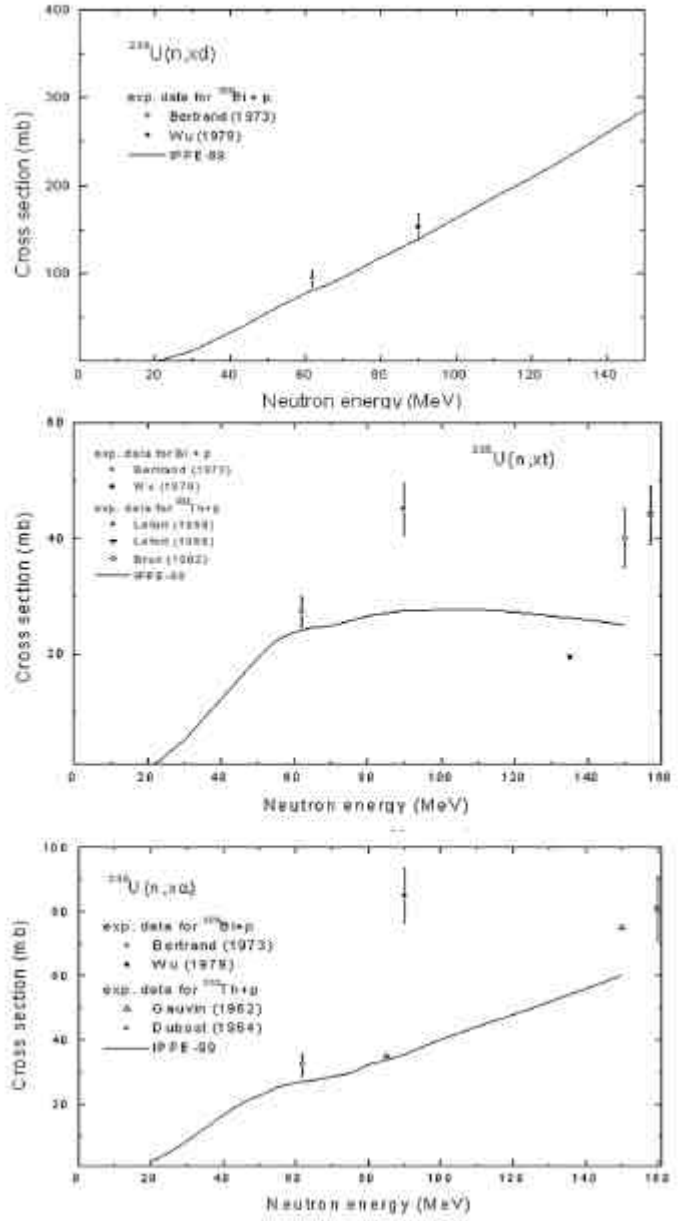

Figure 32. The deuteron, triton and α production cross sections for ^{238}U evaluated on the basis of statistical calculations and experimental data by [Bert73, Wu79, Lefo59, Lefo65, Brun62, Gauv62, Dubo64].

The evaluation of the spectra and angular distributions of emitted charged particles have been done with the GNASH code, however the main parameter of the pre-equilibrium model was changed for each cluster channel to obtain the same production cross sections as with the ALICE-IPPE code.

5.7 Development of Group Neutron Libraries and Evaluated Libraries up to 50 MeV

For the ADS investigations at FZK usually 69 group cross section libraries with the well-known WIMS [Aske66] energy group structure are applied. The upper energy boundary of these libraries is 10 MeV. As a consequence the ADS investigations utilize the formalisms of the high-energy codes above 10 MeV. These formalisms are not well qualified in the energy range up to about 150 MeV. In order to be able to study the influences of these approximations with multigroup calculations, an extended library with energies up to 50 MeV and 6 additional groups above 10 MeV of the WIMS structure has been established.

5.7.1 Calculation Procedures

The nuclear data processing at FZK is based on international standard data formats and calculation codes. The exchange of the basic data occurs with the ENDF/B [Rose90] format. Group constants may be generated by the widely used processing code NJOY [Macf98] in its latest version, at present a slightly modified version of NJOY97.95. For the data verification the ENDFB6 utilities version 6.11 [Dunf95] of CHECKR, LISTEF, PLOTEF and PSYCHE are available. For the KAPROS/KARBUS cross section processing an FZK-own development GRUBA/GRUCAL [Woll75] is applied. Its main characteristics are [Broe92]:

- the multigroup libraries have very flexible data storage on direct access files,
- the data types and structures build a combination of the special features of fast and thermal reactor codes (upscattering, separate treatment of elastic, inelastic, n-2n, .. processes, isotope dependant fission spectrum matrices, etc)
- the cross section calculations are based on arbitrary rules on a so-called control-file,
- data replacements may be easily realized by the so-called secondary input option,
- a refined resonance treatment based on self-shielding tabulations (improved Bell-factor formalism) is applied,
- the code system is well validated for a broad range of applications from heavy water moderated to lead cooled systems.

For the reformatting of the NJOY-results to the special data storage modes a number of local programs are in use.

5.7.2 Development of a 75 Group Library with E_{max}=50 MeV [Broe98]

Since a few years extended nuclear data evaluations up to 50 MeV are established at FZK in a cooperation of the Project Nuclear Safety (ADS studies) and the Project Nuclear Fusion (IFMIF project [Mart96]). The evaluation of the nuclear data files up to 50 MeV has been carried out by the Institute of Nuclear Power Engineering (INPE), Obninsk [Koro97]. Above 20 MeV these cross-sections have been obtained from nuclear model calculations and from available experimental data. Most of the data below 20 MeV have been adopted from evaluated nuclear data libraries (ENDF/B-VI, JENDL3.2). The data for energies from 10-5eV to 50 MeV have been made available in ENDF/B-6 format. From these efforts the following evaluations are available now:

- From the ADS project: ^{16}O, ^{208}Pb, ^{232}Th, ^{233}Pa, ^{233}U, ^{235}U, ^{238}U, ^{239}Pu and ^{240}Pu.
- From the IFMIF project: ^{56}Fe, ^{23}Na, ^{39}K, ^{52}Cr, ^{51}V, ^{28}Si and ^{12}C.

These evaluated data files with ENDF/B format have been processed by the NJOY code to produce adequate input files for the transport calculations. MCNP library generation is in progress within the IFMIF project. For the deterministic calculations, e.g. with the transport code TWODANT, multi-group libraries are required. The generation of a first version of a 75 group library with the Karlsruhe GRUBA format (69 WIMS energy group system, extended above 10 MeV with boundaries at 13.8, 15.0, 20.0, 27.1, 36.8 and 50 MeV) is completed. Some extensive comparisons of the basic data with the calculated group constants have been performed using the standard ENDF-based codes NJOY and PLOTEF and an old local plot program for comparisons of nuclear data from different origins. The pointwise data for (n,ã), (n,p) and (n,á) are compared with the multigroup library data type SCAPT, being the addition of the three reactions mentioned before – see Fig. 33. The nuclear data processing code NJOY

version 94.105 has been applied for the generation of these group constants. The group constants have been calculated for six temperatures: 300, 900, 1200, 1500, 2100 and 3000 K and for the seven values of the background cross section 10^{-3}, 10, 10^{1}, 10^{3}, 10^{4}, 10^{5}, 10^{10} barn. Neutron transfer matrices are given until Legendre order P_5.

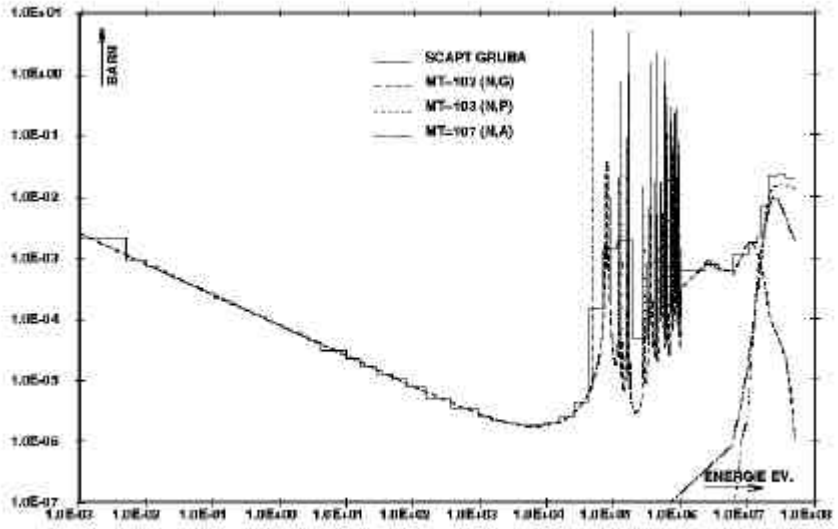

Figure 33. Comparison of point- and groupwise cross-sections of lead.

The GRUBA system had to be extended to take into account reactions typical for energies above 10 MeV as e.g. (n,4n), (n,2n+á), (n,3n+á), (n,2n+p), (n,3n+p), (n,2p), (n,pd). As a typical test case a ^{208}Pb-cylinder has been used with density and geometry corresponding to the lead target in the ADS neutronic benchmark [Sless97], radius: 10 cm, height: 50 cm. In the model for the calculations a spatially homogeneous neutron source within a cylinder of radius 5 cm and height 10 cm in the center of the target was assumed. The energy dependence of the external source is similar to the one given in the benchmark specification. The highest neutron energy of the external neutron source (source 1) is 10 MeV; the lowest energy is 111 keV. Comparisons have been carried out for results obtained from calculations with TWODANT in S16/P3 approximation with the 69 group constant library that has been used for the benchmark calculations and with the new 75 group constants. Results for the total neutron leakage, the neutron flux density and for different reaction rates are shown in Table V. The first 2 columns of Table V show calculations for ^{208}Pb. The ^{208}Pb data from INPE, Obninsk are based on ENDF/B-VI below 20 MeV. In order to eliminate from the comparison differences in nuclear data new ^{208}Pb group constants in the 69 energy group structure have been recalculated. The deviations of the results obtained with the old and with the new group constant set are less than 1% except for a large deviation in the (n,á) reaction rate which is due to different data on ENDF/B-VI and on the Obninsk library. Columns 4 and 5 show calculations with the 75-group set. The energy of the external source neutrons (source 2) is between 50 MeV and 111 keV. Neutron flux density and reaction rates are given for two coarse energy groups: coarse group 1 between 10 MeV and 50 MeV and coarse group 2 between 10-5 MeV and 10 MeV. The contribution of neutrons above 10 MeV to the total neutron flux is about 6 %. The contribution of neutrons above 10 MeV to the total reaction rate, the reaction rates for (n,ã), elastic and inelastic scattering is around 5 %. The contribution of neutrons above 10 MeV to the (n,2n) rate is about 93 %. For other threshold reactions (n, 3n), (n, p), (n, 2p), the contribution of neutrons above 10 MeV is more than 99 %. Column 3

Table V. TWODANT results for ADS benchmark with 69 and 75 group constants. Lead target with external source. TWODANT calculations in S_8/P_3 approximation. Comparison of neutron flux densities and reaction rates from 69 and 75 group constant libraries

Case	75 groups source 1 ^{208}Pb	69 groups source 1 ^{208}Pb	69 groups source 1 ^{207}Pb	75 groups source 2 ^{208}Pb	
	E≤10 MeV			E≤10 MeV	E>10 MeV
net leakage	1.016	1.016	1.021	1.195	1.195
neutron flux	$2.131\cdot10^{1}$	$2.119\cdot10^{1}$	$2.240\cdot10^{1}$	$2.281\cdot10^{1}$	1.523
Reaction rates					
Total	3.873	3.865	4.342	4.142	$2.478\cdot10^{-1}$
Capture	$4.236\cdot10^{-4}$	$4.217\cdot10^{-4}$	$1.850\cdot10^{-3}$	$4.332\cdot10^{-4}$	$7.601\cdot10^{-4}$
(n,γ)	$4.232\cdot10^{-4}$			$4.330\cdot10^{-4}$	$1.475\cdot10^{-5}$
(n,α)	$4.147\cdot10^{-7}$	$1.512\cdot10^{-6}$		$1.973\cdot10^{-7}$	$2.042\cdot10^{-4}$
(n,p)	$4.978\cdot10^{-8}$	$4.969\cdot10^{-8}$		$8.350\cdot10^{-9}$	$4.987\cdot10^{-4}$
(n,2p)					$4.789\cdot10^{-5}$
(n,p d)					$1.053\cdot10^{-5}$
Elastic	3.648	3.637	3.961	3.999	$1.414\cdot10^{-1}$
Inelastic	$2.098\cdot10^{-1}$	$2.111\cdot10^{-1}$	$3.564\cdot10^{-1}$	$1.400\cdot10^{-1}$	$1.017\cdot10^{-2}$
(n,2n)	$1.643\cdot10^{-2}$	$1.641\cdot10^{-2}$	$2.292\cdot10^{-3}$	$2.594\cdot10^{-3}$	$3.618\cdot10^{-2}$
(n,3n)	0.0	0.0	0.0	0.0	$2.393\cdot10^{-2}$
(n,4n)	0.0	0.0	0.0	0.0	$2.156\cdot10^{-2}$

of Table V shows that the capture reaction rate of ^{208}Pb in the spectrum of the lead cylinder is only about 20 % of the capture reaction rate of ^{207}Pb.

As a first application of the new 75 group constant set for a reactor, the fresh core of the ADS neutronic benchmark [Sless97] has been recalculated. The calculations have been carried out with TWODANT in S8/P3 approximation. Table VI shows the results for k_{eff} and k_{source} for different ^{233}U enrichments of the fuel. The ^{233}U enrichment that is necessary to obtain k_{eff}=0.96 is lower (8.722 at %), when the new group constant set is applied. This is mainly due to the difference in the basic nuclear data below 10 MeV. On the Obninsk library the data for ^{233}U and ^{232}Th below 20 MeV are mainly from JENDL-3.2, most of the data for ^{208}Pb below 20 MeV are from ENDF/B-VI. In order to eliminate most of the differences in the data the cross sections for ^{233}U and ^{232}Th in the 69 group constant library were replaced by data from JENDL-3.2 and the cross sections of 208Pb were replaced by group constants obtained from ENDF/B-VI. In Table VI the 69 group constant library with the replacements discussed above is called modified 69 group constant set. The results for k_{eff} calculated with this modified 69 group constant set and with the 75-group constant set differ by about 1 % as is shown in Table VI. For k_{source} a similar difference is found.

Table VI. TWODANT results for ADS benchmark with 69 and 75 group constants. ADS Neutronic Benchmark. k_{eff} and k_{source} calculated with different group constant libraries

A. Criticality calculations		
^{233}U enrichment	75 energy groups from Obninsk data (0-50 MeV)	69 energy groups modified set (0-10 MeV)
9.68	1.0243136	1.01362481
8.72	0.96000698	0.94995146
A. Source calculations		
^{233}U enrichment (atom percent)	75 energy groups source up to 50 MeV	69 energy groups modified set source up to 10 MeV
8.72	0.97643827(1)	0.96300135
	0.97158054(2)	

$$k^{1}_{source} = \frac{R(\acute{\imath}\cdot fiss) + R(n,2\,n) + R(n,2\,n+x) + 2\cdot[R(n,3\,n) + R(n,3\,n+x)] + 3\,R(n,4\,n)}{L + R(abs)}$$

$$k^{2}_{source} = \frac{R(\acute{\imath}\cdot fiss) + R(n,2\,n)}{L + R(abs)}$$

R : reaction rate

$(n,2\,n+x)$: $(n,2\,n+p) + (n,2\,n+\acute{a}) + (n,2\,n+2\,\acute{a})$

$(n,3\,n+x)$: $(n,3\,n+p) + n(3\,n+\acute{a})$

L : net leakag e

5.8 Creation of Temperature Dependent Neutron Cross Section Data Libraries for Energies Below 20 MeV

In order to simulate properly temperature behaviour of ADS and to assess temperature dependent criticality safety margins, temperature dependent neutron cross section data had to be created. It has been done using NJOY-code [Macf94], which performs Doppler-broadening calculations, crucial for creation of temperature dependent cross-sections. Some other important data which can be extracted from data libraries and preprocessed with NJOY for Monte-Carlo simulations include gas-production data, KERMA-factors necessary for radiation damage calculations, gamma heating etc.

Three data bases containing nuclear data necessary for particle transport calculations: JEF2.2, ENDFB6.4 and JENDL3.2 have been processed by NJOY in order to get 6 temperature dependent data sets for 300K, 600K, 900K, 1200K, 1500K and 1800K for each data file. Moreover, same temperature dependent data sets have been produced for activation (transmutation) cross-sections based on EAF3.2 (European Activation File), EAF97 and MENDL-2 [Shub95] in order to enable burnup calculations with MCB-code. EAF data-base contains continuous energy dependent capture (and other transmutation reactions) cross-section data for over 700 isotopes (over 400 isotopes more than in any transport library).

In spite of enormous amount of work which has been put into transport cross section data bases in the last 50 years for the energy range from meV to 20 MeV, there are still significant uncertainties and discrepancies between different data bases and missing data important for transmutation research. Table VII presents discrepancies between JEF2.2, JENDL3.2 and ENDFB6.4 based results of k_{eff} calculations with MCB-code for NEA-reference ADS [Chan99]. The difference of almost 4000 pcm between ENDFB6.4 and JEF2.2 cross-section

data indicates a necessity of scrutiny of some basic nuclear data important for ADS research. In the case presented in Table VII one it was identified that cross sections of Pb are partially responsible for this discrepancy.

Table VII. k_{eff} of NEA reference ADS calculated with different neutron data libraries.

	Start-up core
Data library	k_{eff}
JEF2.2	0.960
JENDL3.2	0.962
ENDFB6.4	0.998

6. Benchmark of the 150 MeV Data Libraries

To our knowledge, a suitable macroscopic experiment for lead that can directly test our Pb-libraries is not available. Fortunately, we can demonstrate the impact of high-energy evaluation by means of an experiment for Fe. First, we will a more isolated example of the difference between intranuclear cascade code and a high-energy library. Next, we will show calculations with the new MCNPX code.

6.1 HETC/MCNP Calculation for Nickel

As a direct application of the 150 MeV ^{58}Ni evaluation we present a calculated result from the TIERCE code system [Bers97], which comprises among others HETC and MCNP. Fig. 34 displays the neutron flux resulting from a 200 MeV proton beam incident on a 50 cm long ^{58}Ni-cylinder. Two calculations were performed: one with HETC and MCNP + 20 MeV data file and one with MCNP + 150 MeV data file. Besides the expected discontinuity at 20 MeV for the case with the conventional 20 MeV cutoff, one can observe an overall difference of up to 40 % in the high-energy region.

6.2 MCNPX Benchmark for Iron

The impact of high-energy data files can be demonstrated more dramatically by comparison with an actual experiment.

A major transport code development effort is underway at Los Alamos National Laboratory, primarily in support of the computational needs of Accelerator Driven Systems (ADS). The main emphases of the project are:

- Merging existing the functionality of the transport code MCNP [Brie97] and the LAHET Code System (LCS) for intranuclear cascade reactions [Prae89].
- Improving the physics capabilities of the merged code.

The resulting code is called MCNPX. MCNPX expands the capabilities of MCNP Version 4B by increasing the standard set of transportable particles (electrons, photons and neutrons), by making use of the newly evaluated high-energy nuclear data files for neutrons, and by incorporating physics models for use where tabular data are unavailable. The cylinder is 50 cm long and has a radius of 20 cm. The mean neutron flux is calculated between 10 and 20 cm. All of the LAHET nuclear physics modules are included in MCNPX, which expands the

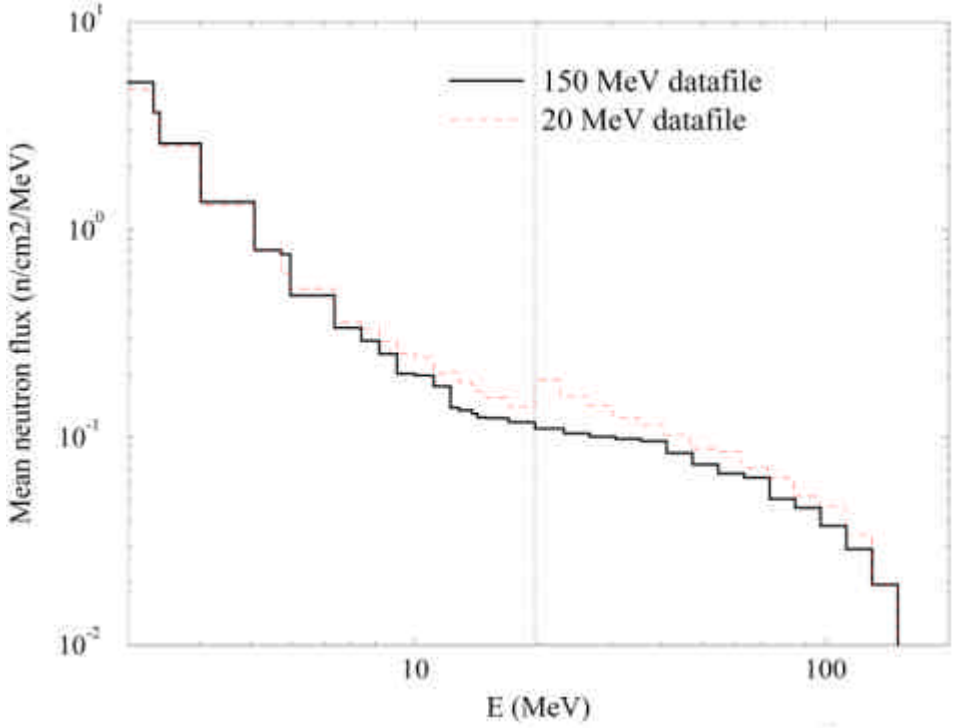

Figure 34. HETC-MCNP4A calculation for 200 MeV protons incident on a 58Ni cylinder with the neutron data file cutoff at 20 vs. 150 MeV.

capabilities of LAHET through the availability of many of the variance reduction methods of MCNP, and through the incorporation of MCNP's very general syntax for specifying geometry, sources, and tallies. Eventually, the result of this project will be a unified, general Monte Carlo transport capability to model a fully-coupled cascade of nuclear particles over a wide energy range.

An important requirement of the current code- and data-development plan is to develop the necessary tools to model transport of coupled neutral and charged particles below 150 MeV based on nuclear-data evaluations. The current version of MCNPX partially meets that requirement. The physics capabilities of MCNP have been upgraded to include the production of secondary charged particles from neutron collisions, using data contained on expanded continuous-energy neutron cross-section tables. Work is in progress on updating MCNPX to utilize the newly evaluated high-energy data tables for incident protons. This will open up huge possibilities in terms of high-energy proton applications.

Calculations with both the 150 MeV neutron data libraries and with the LAHET-option in MCNPX have been performed and are reported here. A number of neutron transmission experiments have been performed [Naka96, Nakb96, Nakc96] at the Azimuthally Varying Field Cyclotron facility at the JAERI Takashi site. Incident 43- or 68-MeV protons impinged on converters consisting of 99.9 % enriched ^{7}Li. The ^{7}Li(p,n) reaction produced nearly monoenergetic neutrons, which were then collimated and allowed to strike iron or concrete targets of various thickness. The neutron transmission was measured at several positions relative to the transmission target. Although the neutrons were initially almost monoenergetic in all cases, their actual spectra were measured in order to allow for more realistic comparison with neutron transport calculations. Details about the geometry can be found in [Hers98].

In this report, we restrict ourselves to the measurements on iron slabs of 40 cm thickness, with the detector placed at centerline, 20 cm and 40 cm off axis, respectively.

In Figs 35-37 we present the MCNPX results for the neutron transmission experiment on iron for the various positions of the detector. There is an overall excellent agreement between the measurements and the data.

With MCNPX, it's easy to perform a calculation with LAHET instead of the 150 MeV libraries. It is obvious from Figs 38-40 that the predictions by LAHET do not have the quality of those using the data libraries. One reason for the deviation from the data is the quality of the elastic scattering model used in LAHET. This is currently under development.

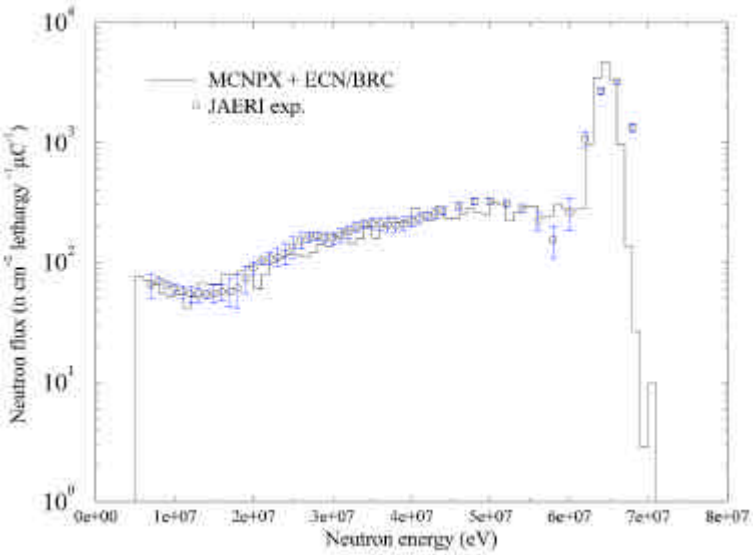

Figure 35. 68 MeV neutrons on 40 cm of iron, detector at centerline: Comparison between experimental data and MCNPX + ECN/BRC data libraries.

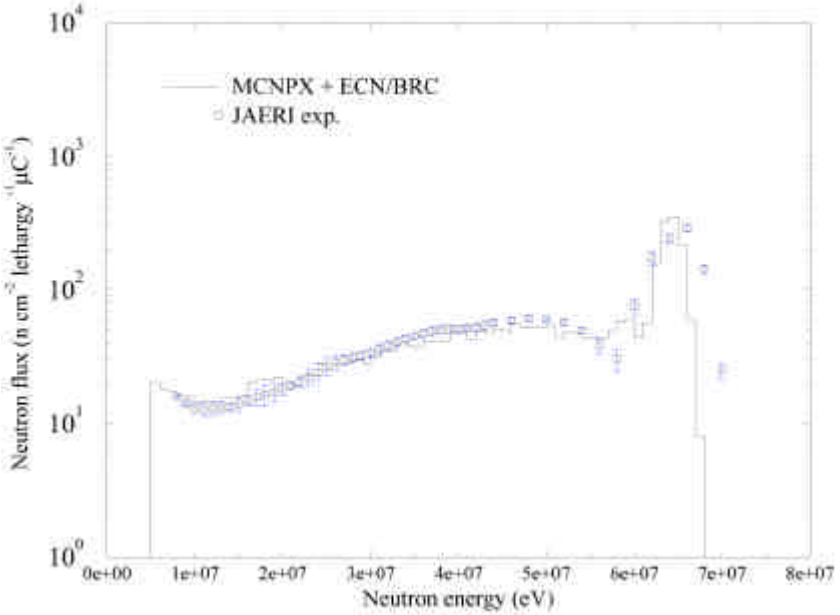

Figure 36. 68 MeV neutrons on 40 cm of iron, detector at 20 cm: Comparison between experimental data and MCNPX + ECN/BRC data libraries.

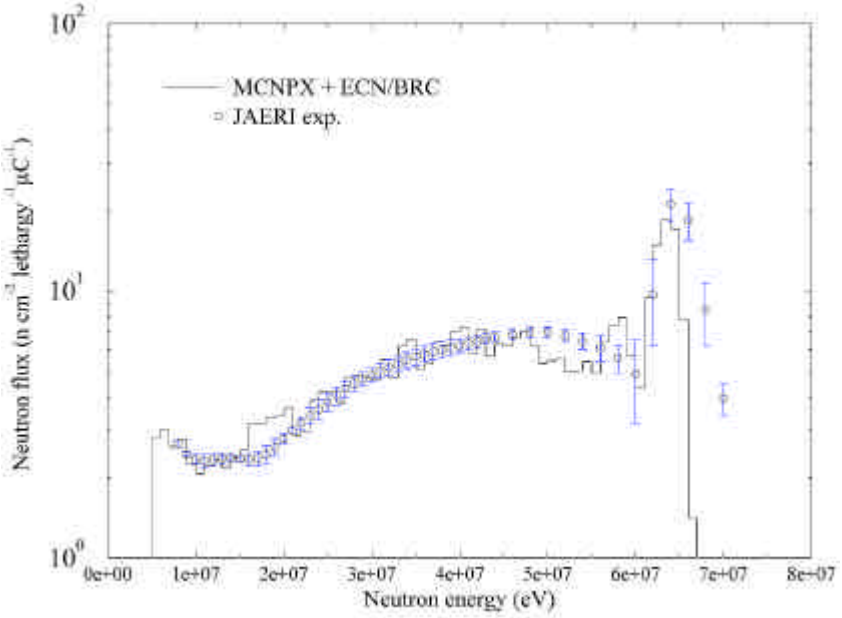

Figure 37. 68 MeV neutrons on 40 cm of iron, detector at 40 cm: Comparison between experimental data and MCNPX + ECN/BRC data libraries.

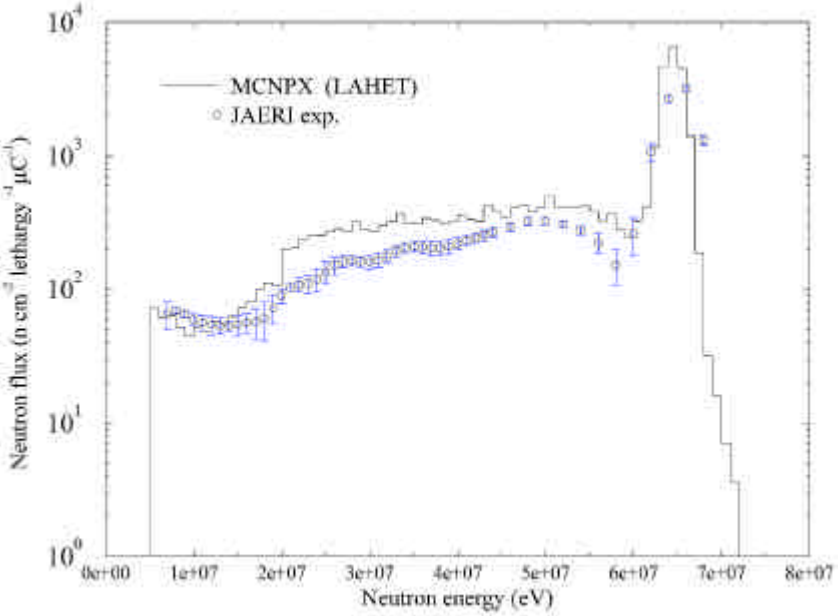

Figure 38. 68 MeV neutrons on 40 cm of iron, detector at centerline: Comparison between experimental data and MCNPX + LAHET above 20 MeV.

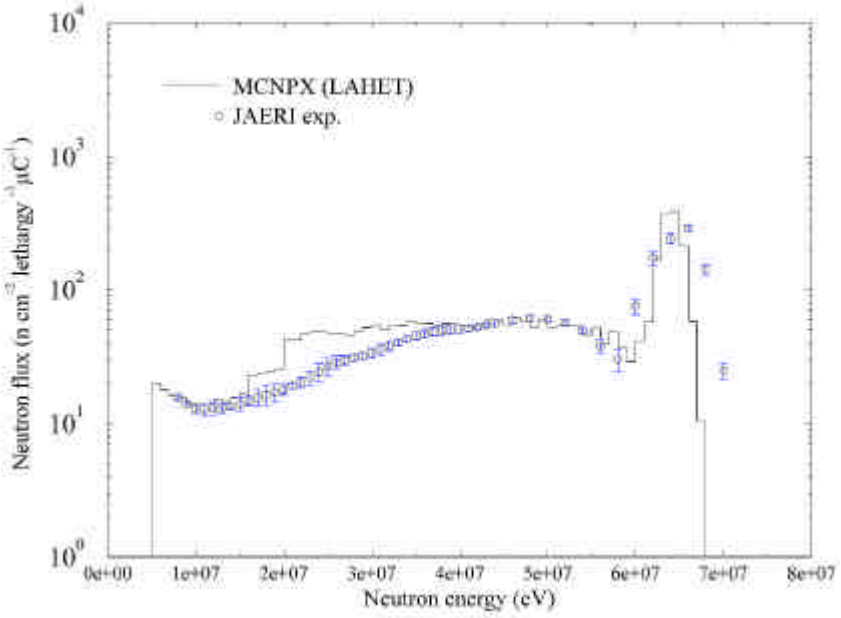

Figure 39. 68 MeV neutrons on 40 cm of iron, detector at 20 cm: Comparison between experimental data and MCNPX + LAHET above 20 MeV.

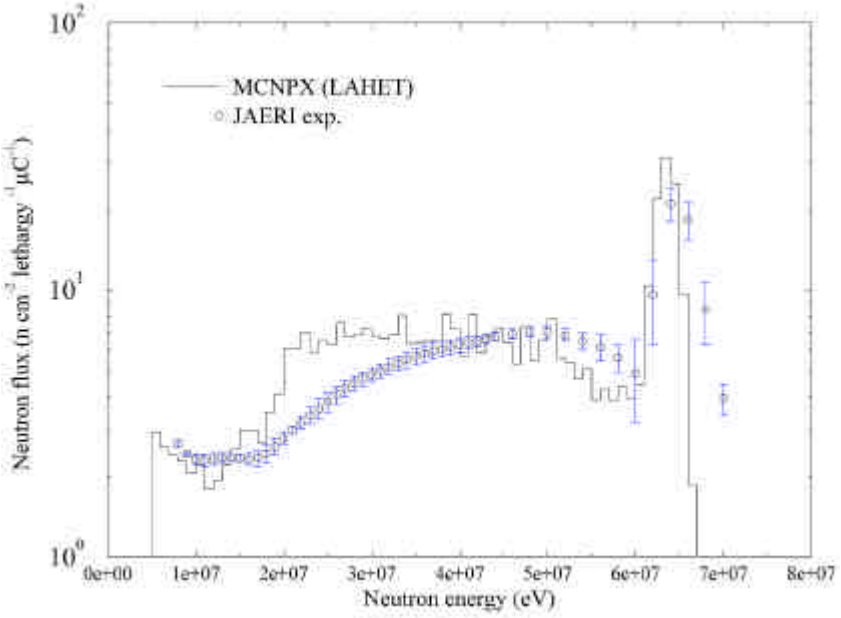

Figure 40. 68 MeV neutrons on 40 cm of iron, detector at 40 cm: Comparison between experimental data and MCNPX + LAHET above 20 MeV.

7. Conclusions

The increasing research on transmutation and energy production methods using a proton accelerator coupled to a subcritical reactor is attended with increasing importance of a systematic evaluation of relevant nuclear reaction information. This workpackage addresses the provision of these nuclear data. Several high-energy transport codes exist which contain an intranuclear cascade model that is mainly successful for the primary stages of the reaction,

including the production of several types of hadrons. For energies below about 150 MeV, when the predictive power of the high-energy transport codes becomes suspect, nuclear data libraries are required.

This report contains a short summary of progress of both low and intermediate energy data evaluation, followed by our specific contribution to the field.

In recent years, progress has been made on the following items:

(1) a more specific survey of data needs for experimental and evaluated data,
(2) consensus on format definition of nuclear data libraries,
(3) significant progress on experimental data compilation,
(4) the collection of starter files,
(5) pilot evaluation projects,
(6) recommendation of, and participation in, specialist meetings and benchmark exercises concerning nuclear reaction models.

The fission product yield distributions have been measured for fast neutron fission of ^{232}Th and ^{233}U which are the main contributors of fission events in systems based on Th fuel. Individual yields of about 180 fission products could be determined. Such data also give a considerably improved basis for predictions of yield distributions using models or systematics.

We have created new phenomenological, spherical, neutron and proton optical model potentials for all isotopes under study here, which are smooth from 0 to 200 MeV.

The potentials are directly applied in multi-step direct calculations to analyze the recent (n,p) measurements at the The Svedberg Laboratory.

With a code system centered around ECIS96 and GNASH we have created 150 MeV neutron and proton transport data files for Fe, Ni, Pb, Th, ^{238}U and ^{239}Pu. The high-energy part of the data files consists completely of results from model calculations, which are benchmarked against the available experimental data. The comparison between the data files and experimental data as given in this report gives an impression of the quality of the evaluations. Although there is obviously future work left regarding fine-tuning of several parts of the data file, we argue that the representation of nuclear reaction information up to 150 MeV is already better than can be attained with intranuclear cascade codes. This is not surprising since we used dedicated model codes for different parts of the calculation and were able to fine-tune the input parameters of the model codes with experimental data. We realize, however, that sensitivity studies and comparisons with integral experiments should help in choosing the right reactions and isotopes to evaluate high-energy data files. The code system presented here is fully automatic, from basic nuclear reaction physics up to the creation of MCNP libraries. This entails that when better nuclear reaction information becomes available (e.g. a dispersive optical model, more precise pre-equilibrium cluster emission data etc.), this will immediately and very simply lead to an updated data file. For neutrons, the calculated high energy data are automatically merged with an existing 20 MeV file. For protons, we have constructed completely new data files. The latter may be used in future transport codes that can handle charged particles.

The impact of using high-energy libraries is quite clear. The ^{58}Ni data file has been used in a combined HETC/MCNP calculation, which shows the effect of using well tested data at energies below 150 MeV. The transport code MCNPX has been installed and tested on a simple iron benchmark experiment with various options for the basic nuclear reaction information. For nuclear applications with nucleon energies below 150 MeV, the calculations

with our new neutron data files suggest a drastic improvement of the description of macroscopic experiments, when compared with the intranuclear cascade code LAHET. This confirms the findings that where reported in [Chad98]. Some discontinuities can still be observed at energies around 20 MeV, although they are no longer as big as in the LAHET + 20 MeV data file calculations. This suggests that for a continuous description the data below and above 20 MeV should preferably be re-evaluated in one and the same working process.

The general recommendation is that for more materials the available data libraries should be extended to 150 MeV. This will require a significant effort from both the experimental and the theoretical nuclear physics community. For consistency, it is important that the part below 20 MeV is of the same quality as that above 20 MeV. It is therefore necessary to revisit the evaluation process over the whole energy range, which should ensure a smooth transition from low to high energies.

X. CONCLUSIONS

Accelerator-Driven Systems open new possibilities to perform effectively transmutation of nuclear waste. It can be concluded that ADS may play an important role in a nuclear fuel cycle as an effective way to transmute the most hazardous isotopes. However, an extraordinary neutron surplus offered by ADS neutronics must be fully utilized in order to enhance ADS transmutation potential over conventional critical reactors. Accelerators and spallation targets make these systems very complex compare to critical reactors and that is why all benefits of theses systems must be very clearly assessed before recommendations are given for their technological development. In the IABAT-project it was not intended to fully assess all the aspects of ADS. Rather, the project should develop the tools and methodology necessary for credible ADS research and stimulate this research field in many European countries. One of the very primary conclusions of this project is that the development of accelerator-driven transmutation technologies requires an extensive research program of interdisciplinary dimension covering nuclear and high energy physics, accelerator technology, nuclear chemistry including partitioning, separation and nuclear fuel development, and also material sciences. Some of the most important topics are:

- Development of nuclear models, creating nuclear data-bases, improving and designing new computer codes for particle interactions in the medium energy range (up to 300 MeV)
- Development and optimization of high power accelerators with exceptionally high reliability, low beam losses and high efficiency
- Development of spallation neutron targets including material compatibility studies
- Material irradiation studies and development of theoretical and computer models for irradiation induced material damages
- New approaches to a nuclear fuel cycle
- Partitioning and separation chemistry, including pyrochemistry and advanced aqueous chemistry

System and fuel cycle studies in the IABAT project were focused on neutronics and transmutation potential. They did not try to address important questions concerning fuel and coolant technologies, partitioning and separation chemistry, or instead attempt an economical assessment.

Four systems have been studied in detail:

- Liquid Lead and Lead/Bismuth Cooled Fast Systems with Solid Fuel
- Liquid Lead Thermal System with Dispersed Fuel (so called Jülicher Transmuter)
- Fast and Thermal (so called superthermal) Molten Salt Systems

Neutronics studies of the **liquid lead (and Pb/Bi) cooled, solid fuel ADS** show that the extraordinary neutron surplus of the ADS would not be a decisive advantage with respect to fast reactor transmutation, if it could not be fully utilized for transmutation purposes in practice. There are several possible options to enhance transmutation potential of ADS:

- Transmutation of the long-lived fission products ^{99}Tc, ^{129}I and ^{135}Cs.

- Use of burnable absorbers to flatten reactivity changes and to block capture in ^{209}Bi (for Pb/Bi cooled systems) and fuel nuclides like capture in ^{241}Am leading to build-up of ^{238}Pu.

ADS with liquid fuel have very appealing features like a very deep burn-up and consequently high transmutation rate, possibilities for advanced fuel feed management etc. The **Jülicher ADS** with a thermal neutron flux and liquid lead as a carrier of a low concentrated TRU fuel offers a lot of advantages. The TRU inventory in the system may be kept very low with a high TRU consumption rate, the k-value can be also kept nearly constant at desired subcriticality and thus the required accelerator power may stay constant. In comparison to other options to burn Pu and/or MA, it is a very efficient system with a high transmutation rate.

The Jülicher ADS is probably the most unusual ADS proposed until now and there are a lot of difficult technological problems to be solved for this system, such as fuel technology, corrosion of liquid lead, high power accelerator, but most of these problems are similar for other ADS-concepts.

Molten salt ADSs share most of the advantages of the Jülicher Transmuter, and feasibility of these systems depends on assessments of other features than neutronics.

The spallation target, being an interface module between accelerator and subcritical reactor, is one of the most important components of ADS and may easily be a technological show-stopper for the further development. An idea of a multiple target system has been investigated order to optimize the radial power distribution in ADS. The 3-spallation target system shows very good power distribution performance at least at beginning of life. However, technical difficulties to design a 3-target (or more) subcritical core make this option unfeasible for the time being.

Radiation damage to the main ADS components i.e. core, target container and beam window have been estimated, including contributions from reactor energy range neutrons + high-energy particles. Damage have been quantified in dpa, specific spallation residuals production and gas releases. Results show that with fairly conservative limits on gas production and dpa, a life time for a target window can be expected to be around 1 year for proton current densities in a range of J_{ave}=25 – 30 μA/cm^2

The IABAT project concludes that **the studies of the impact of ADS on the risk from high-level waste repositories give no crystal-clear benefits**.

- In reported repository risk studies there is a wide variation as to what are the most significant radionuclides and by how much the inventories of these radionuclides would have to be transmuted to decrease the risk. Variations arise from different assumptions about scenarios, repository design and siting, and other data. ADS should ideally be developed to retain the flexibility to transmute as wide a range as possible of the long-lived fission products and actinides given here.
- It is conceivable that with the use of inappropriate or badly specified materials, in terms of repository risk, the positive benefit of transmuting actinides and fission products could be negated by the creation of activation products.
- The decay daughters of uranium can make a significant contribution to repository risk over long timescales. Significant quantities of uranium could not be transmuted. **The management of uranium (or thorium) needs to be addressed** in a fuel cycle involving ADS.

In our **proliferation studies** of ADS we conclude that at present, **commercially available** machines (ADONIS, I.B.A. Belgium) with proton energies around 150 MeV and currents of 1.5 mA (power 225kW), are at the limit of the technology threshold (capacity to produce 100g Pu per year) laid down by the I.A.E.A in their INFCIRC documents. It appears that next generation machines must be specified in the Trigger List and Dual-Use Goods.

In the future, large powerful accelerators may be used for power production and waste transmutation. Because of the size of these machines, they will automatically fall under I.A.E.A. safeguards. It has been shown that during the down time for such systems (e.g. required for fuel reloading), the accelerator beam current can be used for clandestine activities in which significant amounts of weapons grade material can be produced on a timescale of a few days to one month. Steps have to be taken to ensure that this does not occur (for example through the use of power monitors).

Another fundamental difference between a critical reactor and an accelerator driven sub-critical assembly is that the ADS can be used for "isotopic enrichment" and for "fissile material conversion". In the former process, the spallation neutrons can be surrounded by a multiplying medium such as spent reactor fuel ($k_{inf} \approx 0.9$) containing poor grade plutonium to "amplify" the neutron flux. This can then be used to breed pure Pu in the outer blanket. In the latter process, an enriched uranium blanket (containing for example 20% ^{235}U) can be used to amplify the neutron flux. These neutrons are captured by ^{238}U to produce ^{239}Pu. Because the Pu is a different element, it can easily be separated by standard chemical processing.

Assessing accelerator technology, costing models have been created that allow the circular and linear accelerator options to be compared and the effect of parameter variations examined. The calculations reported show that cyclotron systems would be more economical, due mainly to the advantage of the cost of RF power supplies. However, it should be noted that many in the accelerator community regard with skepticism the possibility of transporting and extracting more than a 10mA beam current from a 1GeV cyclotron and therefore technical factors may limit the application of cyclotrons.

The reliability and availability of the accelerator in ADS is an important issue. Generalizing results of LANSCE accelerator reliability studies it is to be concluded:

- An actual beam trip rate of the LANSCE accelerator, constructed for more than 20 years ago, is typically 1.6-2.4 trips/hour or 40-60 trips/day. This is almost 4 order of magnitudes more than acceptable for commercial nuclear power installations. It is believed that improvement in the number of trips by a factor of 100 is achievable with today's technology
- Accelerator trips will be a strongly limiting constraint for a spallation target experiment (e.g. for a liquid Pb/Bi "Obninsk spallation target") due to the load on a target window.

With a code system centered around ECIS96 and GNASH, **150 MeV neutron and proton transport data files for Fe, Ni, Pb, Th, ^{238}U and ^{239}Pu have been created**. The high-energy part of the data files consists completely of results from model calculations, which are benchmarked against the available experimental data. Benchmark calculations show a qualitative improvement of the results using cross-section libraries over the results based purely on intranuclear cascade calculations.

Moreover, the fission product yield distributions have been measured for fast neutron fission of ^{232}Th and ^{233}U, which are the main contributors of fission events in systems based on Th fuel. Individual yields of about 180 fission products could be determined. Such data also give a considerably improved basis for predictions of yield distributions using models or systematics.

The IABAT project has contributed significantly to **development of the tools for ADS simulations and analysis the Accelerator-Driven Systems**. In this field following achievements should be pointed out:

- Development of methodology for monitoring of ADS-subcriticality based on the neutron fluctuation analysis
- Assessment of point reactor models for source injected subcritical reactor dynamics
- Solution of space kinetics in one and two space dimensions for fluid-fuel systems and study of the delayed neutron emission worth
- Assessment of three-dimensional time-dependent computational algorithms
- Development of a Monte-Carlo burnup code

Moreover a number of dedicated code systems for ADS, coupling high-energy transport codes, neutron transport and burnup codes has been set-up and validated giving a good confidence in our simulation tools.

XI. REFERENCES

AEC53 AEC Research and Development Report, Facilities for Electronuclear (MTA) Program, Report LWS-24736, 1953.

Alco90 R.E. Alcouffe, F.W. Brinkley, D.R. Marr, R.D. O'Dell, Users Guide for TWODANT: A Code-Package for Two-Dimensional, Diffusion-Accelerated, Neutral Particle Transport, LA-10049-M, Rev. 1, Manual, October 1984, Revised February 1990.

APT1 Accelerator Production of Tritium, http://www.srs.gov/general/news-notes/tritium_accel/accelerator.html, http://necs01.dne.bnl.gov/atd-mag/acc.html, http://strider.lansce.lanl.gov/apt/how.html

Arms72 T.W. Armstrong, K.C. Chandler, "HETC - A High Energy Transport Code", Nucl.Sci.&Eng. 1972,49.p.110.

Ash65 M. Ash, Nuclear Reactor Kinetics, McGraw-Hill, New York (1965)

Aske66 J.R. Askew, F.J. Fayers, P.B. Kemshell, A General Description of the Lattice Code WIMS, Journal of British Nuclear Energy Society, 5, 564, 1966.

Bach75 H. Bachmann, G. Buckel, W. Hoebel, S. Kleinheins, The Modular System KAPROS for Efficient Management of Complex Reactor Calculations, Proceedings Conference Computational Methods in Nuclear Energy, Charleston, CONF-750413, 1975.

Bake95 A.J. Baker, C.P. Jackson, J.E. Sinclair, M.C. Thorne and S.J. Wisbey, *Post-closure Performance Assessment Nirex 95: A Preliminary Analysis of the Groundwater Pathway for a Deep Repository at Sellafield Volume 3 - Calculations of Risk*, Nirex Science Report S/95/012, 1995.

Bake97a A.J. Baker, A.V. Chambers, C.P. Jackson, J.D. Porter, J.E. Sinclair, P.J. Sumner, M.C. Thorne and S.P. Watson, *Nirex 97: An Assessment of the Post-closure Performance of a Deep Waste Repository at Sellafield Volume 3: The Groundwater Pathway*, Nirex Science Report S/97/012, 1997.

Bake97b A.J. Baker, D.A. Lever, J.H. Rees, M.C. Thorne, C.J. Tweed, and R.S. Wikramaratna, *Nirex 97: An Assessment of the Post-closure Performance of a Deep Waste Repository at Sellafield Volume 4: The Gas Pathway*, Nirex Science Report S/97/012, 1997.

Bara93 Barashenkov, Cross Sections of Particle and Nucleus Interactions with Nuclei (Russian), JINR, Dubna, 1993.

Bart66 G. A. Bartholomew and P. R. Tunnicliffe, The AECL Study for an Intense Neutron Generator, AECL-2600, Atomic Energy of Canada, 1966.

Barth66 G. A. Bartholomew and P. R. Tunnicliffe eds., The AECL Study for an Intense Neutron - Generator (ING) (Technical Details), Atomic Energy of Canada Limited Report AECL 2600, 1966.

Bell73 M.J. Bell, ORIGEN- The ORNL Isotope Generation and Depletion Code, ORNL-4628 UC-32, 1973.

Bers96 O. Bersillon et al. Tierce: A code system for particles and radiation transport in thick targets. Proceedings of the second international conference on

Accelerator Driven Transmutation Technologies and Applications. June 3-7, Kalmar Sweden, 1996.

Bers97 O. Bersillon et al., to be published in the *Proceedings of International Conference on Nuclear Data for Science and Technology*, May 19-24 1997, Trieste, Italy.

Bert73 F.E.Bertrand and R.W.Peelle, "Complete Hydrogen and Helium Particle Spectra from 30 to 60 MeV Proton Bombardment of Nuclei with A=12 to 209 and Comparison with Intranuclear Cascade Model," Phys. Rev. C8, 1045 (1973)

Blan96 M. Blann, Phys. Rev. **C**54, 1341 (1996)

Bowm91 C.D. Bowman et al. "Nuclear energy generation and waste transmutation using accelerator driven intense thermal neutron source", LA-UR-91-2601.

Bowm93 C. Bowman, F. Venneri, High Value use of Weapons Plutonium by Burning in Molten Salt Accelerator-Driven Systems or Reactors, International Seminar on Nuclear War and Planetary Emergencies, 18th Session, pp. 400-411, Erice, Italy, 1993.

Bowm97 C. Bowman, Accelerator Driven Systems in Nuclear Energy: Role and Technical Approach, Report ADNA/97-013, The ADNA Corp., 1997.

Brie97 J.F. Briesmeister, MCNP - A General Monte Carlo N-Particle Transport Code, Version 4B, Report LA-12625-M (1997), Los Alamos National Laboratory (1997)

Broe92 C.H.M. Broeders, Entwicklungsarbeiten für die neutronernphysikalische Auslegung von Fortschrittlichen Druckwasserreaktoren (FDWR) mit kompakten Dreiecksgittern in hexagonalen Brennelementen, KfK 5072, August 1992.

Broe96 I. Broeders, C.H.M. Broeders, Implementation, Development, Validation and First Applications of Different Code Chains for the Investigation of Accelerator-Driven Transmutation Proceedings of ICENES-96, Obninsk, 1996.

Broe97 C.Broeders, I.Broeders, Calculations for the IAEA coordinated ADS neutronic benchmark, FZKA 5963, pages 464 – 472, 1997.

Broe98 C. Broeders, I. Broeders, Generation of a Group Constant Library for Neutron Energy until 50MeV,Tests and Applications, FZKA 6126, pages 580 – 586, 1998.

Broe98a C.H.M. Broeders, A Comparison of Some Neutronics Characteristics of Critical Reactors and Accelerator Driven Subcritical Systems, Proceedings of Fifth International Exchange Meeting Mol, Belgium, 1998.

Broe99 C. Broeders, I. Broeders, Calculations of the Energy Deposition in the Target of an ADS, FZKA 6300, pages 663 – 672, 1999.

Brun62 C. Brun, M.Lefort, X.Tarrago, "Contribution a l'Etude du Double Pick-up Indirect Mesure de la Production de Tritium par des Protons de 82 et 105 MeV dans Diverses Cibles," J. Phys. Radium, 23, 167 (1962)

Buch75 W.Bucher, C.E.Hollandsworth, J.E.Youngblood, "Small-Angle Scattering of Fast Neutrons," Phys. Rev. Lett. 35, 1419 (1975)

Buhm95 D. Buhmann, J. Brenner and R. Storck, *Long Term Safety Assessment of Disposal Concepts for HLW and Spent Fuel in Rock Salt,* 5th International Conference on Radioactive Waste Management and Environmental Remediation, Berlin, 3-9 Sep 1995, p 617.

Bush99 R.P. Bush, *Studies of Partition and Transmutation*, DETR report DETR/RAS/99.011, 1999.

Buss Bussac & Reuss. Traité de neutronique. Hermann Éd. p 558.

Cade88 N. Cadelli, et al., *PAGIS, Performance Assessment of Geological Isolation Systems for Radioactive Waste, Summary*, Commission of the European Communities, EUR 11775 EN, 1988.

Carl96 A.Carlson, "Neutron Induced Fission Cross Sections U-235 and U-238 above 20 MeV", Report to Consultants'Meeting on Nuclear Data Standards for Nuclear Measurements (Vienna, December 1996), IAEA, Vienna, INDC(NDS)-368 (1997)

Carl97 J. Carlsson, MSc thesis, Dep. of Nuclear and Reactor Physics, Royal Institute of Technology, January 1997.

Carm93 F. Carminati et al.,An Energy Amplifier for Cleaner and Inexhaustible Nuclear Energy Production Driven by a Particle Accelerator, CERN/AT/93-47 (ET) (1993)

Chad96 M.B.Chadwick, P.G.Young, "GNASH Calculations of the Neutron and Proton Induced Reactions for Lead Isotopes and Benchmarking of Results," Report T-2-96, Los Alamos National Laboratory (1996).

Chad98 M. Chadwick et al., Nucl. Sci. Eng. **131** 293 1999.

Chad99 M.B. Chadwick et al, Acta Physica Slovaca **49** (1999) 365.

Chan99 B. Chan, P. Wydler, H. takanom "Oecd/Nea Comparison Calculations for An Accelerator-Driven", Second Workshop on Utilisation and Reliability of High Power Proton Accelerators,Aix-en-Provence, France,November 1999.

Chen99 X. Cheng, J.U.Knebel, Private communication, 1999.

Clot88 P. Cloth, D. Filges, R.D. Neef, G. Sterzenbach, Ch. Reul, T.W. Armstrong, B.L. Colborn, B. Anders, H. Brückmann, HERMES- A Monte Carlo Program System for Beam-Materials Interaction Studies, Jül-2203, May 1988.

Cohi96 P. Cohilis, Y. Jongen, G. Lannoye, H. Ait Abderrahim, P. D'Hondt, L. Van Den Durpel, Recent Advances in the Design of a Cyclotron-Driven, Intense, Subcritcal Neutron Source, Proc. of EPAC '96, Sitges, June 1996.

Copp99 G.G.M. Coppa, G. Lapenta, P. Ravetto, M.M. Rostagno, Three-Dimensional Neutron Analysis of Accelerator-Driven Systems, International Conference on Mathematics and Computation, Reactor Physics and Environmental Analysis in Nuclear Applications, Madrid, Spain (1999)

Cumm96a R. Cummings, et al., *An Assessment of Partition and Transmutation Against UK Requirements for Radioactive Waste Management*, DOE Report No: DOE/RAS/96.007, 1996.

Cumm96b R. Cummings, et al., *An Assessment of Partition and Transmutation Against UK Requirements for Radioactive Waste Management: Supporting Studies*, DOE Report No: DOE/RAS/96.010, 1996.

Curi34 I. Curie and F. Joliot, Un nouveau type de radioactivité, Physique Nucléaire, Académie des Sciences, Séance du 15 Janvier, 1934.

Cuza98 A. Cuzan, P. Schutz and U. Trinks, Results of the Triton Project, 1998.

Daga99 R. Dagan, C.H.M. Broeders, Optimization of Multiple Source System for ADS, 20. Conference of Nuclear Societies in Israel, 1999.

Dela89 J.-P. Delaroche, Y. Wang and J. Rapaport, Phys. Rev. **C**39, 391 (1989)

Diet97 F. Dietrich et al., to be published in the *Proceedings of the International Conference on Nuclear Data for Science and Technology*, May 19-24 1997, Trieste, Italy.

Dity98 A.I.Dityuk, A.Yu.Konobeyev, V.P.Lunev, Yu.N.Shubin. "New Advanced Version of Computer Code ALICE-IPPE," Report INDC(CCP)-410, IAEA, Vienna (1998)

Done99 A.Yu.Donets, A.V.Evdokimov, A.V.Fomichev, T.Fukahori, A.B.Laptev, G.A.Petrov, O.A.Shcherbakov, Yu.V.Tuboltsev, A.S.Vorobyev, "Neutron Induced Fission Cross-Sections of ^{233}U, ^{235}U, ^{238}U, ^{232}Th, ^{239}Pu, and ^{237}Np in the Energy Range 1 - 200 MeV," in: Proceedings of VII International Seminar on Interaction Neutrons with Nuclei, (Dubna, 1999, to be publ.)

Dori93 J.Y.Doriath, C.W.Mc Callien, E.Kiefhaber, U.Wehmann, J.M.Rieunier. ERANOS 1 : The advanced European System of Codes for Reactor Physics Calculations. Proceedings : Mathematical methods and supercomputing in nuclear applications. KFK Karlsruhe. 21/04/1993.

Dubo64 H. Dubost, M. Lefort, J. Peter, and X. Tarrago. "4He and 3He Particles from Au, Bi and Th Nuclides Bombarded by 157-MeV Protons," Phys. Rev. 136B , 1618 (1964)

Dunf95 C. Dunford, ENDF Utility Codes Release 6.10, *IAEA report*, IAEA-NDS-29, November 1995.

Eism96 V.P.Eismont, A.V.Prokofyev, A.N.Smirnov et al., "Relative and absolute neutron-induced fission cross sections of 208Pb, 209Bi, and 238U in the intermediate energy region," Phys.Rev. C53, 2911 (1996)

Endf90 P.F. Rose and C.L. Dunford (eds.), Data formats and procedures for the evaluated nuclear data file ENDF-6, *Brookhaven National Laboratory report* BNL-NCS-44945, 1990.

Erik98 Marcus Eriksson and Christopher Piaszczyk, "Reliability Assessment of the LANSCE Accelerator System", Proceedings of the OECD Workshop on Reliability of High Power Accelerators, Mito, Japan, October (1998)

ESSC96 The European Spallation Source Study, Volume 3, ESS-96-53-M, ESS Council, 1996.

Fass93 A. Fassó, A. Ferrari, J. Ranft, P.R. Sala, G.R. Stevenson And J.M. Zazula, Nuclear Instruments and Methods A, 332, 459 (1993)

Fern96 R. Fernandez, P. Mandrillon, C. Rubbia and J. A. Rubio, A Preliminary Estimate of the Economic Impact of the Energy Amplifier, CERN/LHC/96-01 (EET), 1996.

Fesh80 H. Feshbach, A. Kerman and S. Koonin, Ann. Phys. **125** (1980) 429.

Filg95 D. Filges, P.Nagel, R.D. Neef, editors, OECD Thick Target Benchmark for Lead and Tungsten, Report NSC/DOC(95)2 (1995)

Fisc83 U. Fischer, H.W. Wiese,Verbesserte konsistente Berechnung des nuklearen Inventars abgebrannter DWR-Brennstoffe auf der Basis von Zell-Abbrand-Verfahrenmit KORIGEN, KfK 3014, 1983.

Fisc97 The data files are available at *http://maple.fzk.de/IFMIF-n*.

Fort96 Fort et al. "Realisation and performance of the adjusted nuclear data library for calculating fast reactor neutronics". International conference on the physics of reactors. Physor 96,MITO,Japan, 1999.

Fowl70 T.B. Fowler, D.R. Vondy, Nuclear Reactor Core Analysis Code: CITATION, ORNL-TM-2496. Rev. 1, 1970.

Freh76 J.Fréhaut, "Nu-bar Results at Bruyères-le-Châtel", Private communication to EXFOR-21685 (1976)

Fuka97 T. Fukahori et al., Status of JENDL intermediate energy nuclear data files, *Proceedings of the International Conference on Nuclear Data for Science and Technology*, May 19-24 1997, Trieste, Italy.

Galy99 J. Galy, Thesis, Universite de Provence, Aix-Marseille I (to be published)

Gauv62 H. Gauvin, M. Lefort, and X. Tarrago, "Emission d'Helions dans les Reactions de Spallation," Nucl. Phys. 39, 447 (1962)

Gibs66 W.A.Gibson, E.E. Gross, A. Zucker, J.S. Fraser, R.E. Green, J.W. Hilborn, J.C.D. Milton, "Low-energy Neutron Production by High-Energy Proton Bombardment of Thick Targets", pp. 110, 111, ORNL - 3940, Oak Ridge National Laboratory, 1966.

Gilm88 J. S. Gilmore, G. J. Russell, H. Robinson, and R. E. Prael, Fertile-to-Fissile and Fission Measurements for Depleted Uranium and Thorium Bombarded by 800-MeV Protons, Nucl. Sci. Engin. 99 (1988) 41-52.

Gnas96 P.G. Young et al., Comprehensive nuclear model calculations: Introduction to the theory and use of the GNASH code, *Workshop on Nuclear Reaction Data and Nuclear Reactors*, April 15 - May 17 1996, Trieste, Italy.

Goel84 B. Goel, B. Krieg, Status of the Nuclear Data Library KEDAK4, KfK 3838, 1984.

Guan84 Shen Guanran, Huang Tangzi, Wen Shenlin,Yu Chunying, Li Anli,Tang Hongoing, Shen Qingbiao, Zhao Zhixinag, Gu Fuhua, "Fast Neutron Elastic Scattering Differential Cross Sections from U-238," Chinese J. Nucl. Phys. 6, 193 (1984)

Gudo97 W. Gudowski (editor), Accelerator Driven Systems: Energy Generation and Transmutation of Nuclear Waste - Status Report, IAEA-TEC-DOC-985, IAEA, Vienna (1997)

Gudo98 W. Gudowski, Personal Communication, 1998.

Guid96a Guidelines for the Export of Nuclear Material, Equipment and Technology, Nuclear Transfers, INFCIRC/254/Rev.2/Part1/Add.1,7 June 1996, http://www.iaea.or.at/worldatom/infcircs/ inf254r2p1a1.html

Guid96b Guidelines for the Export of Nuclear Material, Equipment and Technology, Nuclear - related Dual-use Transfers, INFCIRC/254/Rev.2/Part 2/Mod.1, 19 March 1996, http://www.iaea.or.at/ worldatom/infcircs/inf254r2p2m1.html

Hans86 L.F.Hansen, B.A.Pohl, C.Wong, R.C.Haight., Ch.Lagrange, "Measurements and Calculation of Neutron Scattering in the Actinide Region," Phys. Rev. C34, 2075 (1986)

Henr75 A.F. Henry, Nuclear-Reactor Analysis, MIT Press, Cambridge, MA (1975)

Herm89 Hermann O.W., Westfall R.M., "ORIGENS, Scale System Module to Calculate Fuel Depletion, Actinide Transmutation, Fission product Buildup and Decay, and Associated Radiation Source Term", NUREG/CR - 0200, Oak Ridge National Laboratory (1989)

Hers98 N.E. Hertel and Evans, "Benchmarking the LAHET elastic scattering model for APT Design applications" ERDA final report, Task order 96-081, Georgia Institute of Technology (1997)

Hils98 D. Hilscher et al., Nucl. Instr. Meth. A 414, 100 (1998)

Hjor96 E.L. Hjort et al., Phys. Rev. **C**53 (1996) 237.

Howe84 R.E.Howe, Measurement of fission neutron multiplicities for Thorium-232 and Uranium-235 with incident neutron energies to 49 MeV. Nucl. Sci. Eng., v.86, (1984) p.157.

Hugh97 H.G. Hughes, R.E. Prael, R.C. Little, MCNPX - The LAHET/MCNP Code Merger,LA-UR-97-4891, XTM-RN(U)97-012, April 22, 1997 and H.G. Hughes,K.J. Adams,M.B. Chadwick, J.C. Comly, S.C. Frankle, J.S. Hendricks, R.C. Little, R.E. Prael, L.S. Waters,, and P.G. Young, Jr., Status of the MCNP™ / LCS™ Merger Project, Proceedings of the Radiation Protection and Shielding Topical Conference, Nashville, Tennessee, April 19-23,1998.

Igna75 A.V. Ignatyuk, G.N. Smirenkin and A.S. Tishin, Sov. J. Nucl. Phys. 21, 255 (1975)

Igna95 A.V.Ignatyuk, G.A.Kudyaev, A.R.Junghans, M.deJong, M.G.Clerc, and K.H.Schmidt, "Analysis of dissipation effects in nuclear fission observed in the fragmentation of 238U projectiles," Nucl. Phys. A593, 519 (1995)

Igna98 A.V.Ignatyuk. Reference Input Parameter Library for Nuclear Model Calculations - Handbook. IAEA - TECDOC, Vienna, 1998, ch. 5.

INPE-96 Yu.A.Korovin, A.Yu.Konobeev, V.P.Lunev, P.E.Pereslavtsev, A.Yu.Stankovski, "Evaluated Data File for U-238," Obninsk, Institute of Nuclear Power Engineering (1996)

Iwam82 A.Iwamoto, K.Harada, "Mechanism of Cluster Emission in Nucleon-Induced Preequilibrium Reactions," Phys. Rev. C26, 1821 (1982)

Jaso94 The Jason Review, La Jolla, 1994.

Jeuk83 J.-P. Jeukenne and C. Mahaux, Nucl. Phys. **A**394, 445 (1983).

Jong1 Y. Jongen, P. D'Hondt, L. van den Durpel, P. Cohilis, , H. Ait Abderrahim, Progress Report on ADONIS: the Proton-Driven, Sub-critical Reactor for Radioisotope Production.

Jong94 Y.Jongen, A Proton-Driven, Intense, Subcritical, Fission Neutron Source for Radioisotope Production, Proceedings of Conference on Accelerator-Driven Transmutation Technologies and Applications p.851-856, Las Vegas, July 25-29, 1994.

Jong95 Y. Jongen, P. Cohilis, P. D'Hondt, L. van den Durpel, H. Ait Abderrahim, A Proton-Driven, Intense, Subcritical, Fission Neutron Source, Proc. of Cyclotrons '95, Cape Town, Oct. 1995.

Kalb81 C.Kalbach, F.M.Mann, "Phenomenology of Continuum Angular Distributions. I. Syste-matics and Parameterization," Phys. Rev. C23, 112 (1981)

Kalb85 C. Kalbach, "PRECO-D2: Program for calculating preequilibrium and direct reaction double differential cross sections", Los Alamos National Laboratory report LA-10248-MS (1985)

Kalb88 C. Kalbach, Systematics of continuum angular distributions: Extensions to higher energies, Phys. Rev. **C**37, 2350 (1988)

Kane95 Kane and Hill, *Comparison of Waste Toxicity Index and Repository Performance Assessment Approaches to Providing Guidance for R&D on Partitioning and Transmutation*, EUR 16167 EN, January 1995.

Kato92 Kato et al. "Accelerator molten salt target system for transmutation of long-lived nuclides". Proceedings "Specialists' meeting on Accelerator Based Transmutation". March 1992. PSI - Villigen. Switzerland.

Kiku94 Y. Kikuchi and T. Fukahori, Result of Inquiry on Intermediate Energy Nuclear Data Needs for Various Applications as Start-up Task of SG13, *JAERI Internal Report*, unpublished 1994.

Koba98 K. Kobayashi, K. Nishihara, Definition of Subcriticality Using the Importance Function for the Production of Fission Neutrons, International Conference on the Physics of Nuclear Science and Technology, Long Island (1998)

Koni92 A.J. Koning, Review of High Energy Data and Model Codes for Accelerator-Based Transmutation, *NEA Data Bank Report* NEA/NSC/DOC (92) 12.

Koni93 A.J. Koning, Requirements for an Evaluated Nuclear Data File for Accelerator-Based Transmutation, *NEA Data Bank Report* NEA/NSC/DOC (93) 6.

Koni96 A.J. Koning, Nuclear Data Evaluation for Accelerator-Driven Systems, *Second International Conference on Accelerator-Driven Transmutation Technologies and Applications*, June 3-7 (1996), Kalmar, Sweden, p. 438.

Koni96b A.J. Koning, J.J. van Wijk and J.-P. Delaroche, ECISVIEW: A Graphical Interface for ECIS95, *Proceedings of the NEA Specialists' Meeting on the Nucleon Nucleus Optical Model up to 200 MeV*, Bruyères-le-Châtel, November 13-15 1996. Avaliable at http://db.nea.fr/html/science/om200/

Koni97 A.J. Koning and A. Hogenbirk, *High-energy nuclear data files: From ENDF-6 to NJOY to MCNP*, NEA Data Bank Report NEA/NSC/DOC (97)

Koni98 A.J. Koning, J.-P. Delaroche and O. Bersillon, Nucl. Instr. Methods **A 414** (1998) 49.

Kope90 J. Kopecky and M. Uhl, Phys. Rev. **C**42, 1941 (1990)

Koro97 Yu.A. Korovin, A.Yu. Konobeyev, P.E. Pereslavtsev, A.Yu. Stankovsky, C. Broeders, I. Broeders, U. Fischer, U. v.Möllendorff, P. Wilson, D. Woll, Evaluation and Test of nuclear Data for Investigation of Neutron Transport, Radiation Damage and Processes of Activation and Transmutation in Materials Irradiated by Intermediate and High Energy Particles,G. Reffo, editor International Conference on Nuclear Data for Science and Technology,Trieste, May 19-24, 1997.

Kote88 F. van Kote, et al., *PAGIS, Performance Assessment of Geological Isolation Systems for Radioactive Waste, Enfouissement dans des Formations Granitiques*, Commission of the European Communities, EUR 11777 EN, 1988.

Kuan99 Kuang Z. F. and Pázsit I. General derivation of the Feynman and Rossi-alpha formulae with multiple emission sources. Submitted to Nuovo Cimento (1999)

Land97 P.A. Landeyro, P. Ravetto, V. Silvani, What Subcriticality Margin is Reasonable for an Accelerator Driven System?, International Conference on Future Nuclear Systems Global '97, Yokohama (1997)

Lanl96 M.B. Chadwick et al., New high-energy evaluated nuclear data libraries for the accelerator production of tritium program, *9th Nuclear explosives code developer's conference*, Oct. 21-25 (1996), San Diego.

Lanl97 The data files are available at http://t2.lanl.gov/data/he.html.

Lape97 G. Lapenta, P. Ravetto, A. Cerrato, A. Roggero, Dynamics of Source Injected Multiplying Systems with Fuel Circulation, International Conference on Mathematical Methods and Supercomputing for Nuclear Applications, Saratoga Springs (1997)

Lape98 G. Lapenta, P. Ravetto, Neutron Model for the Safety Assessment of Actinide Burners with Circulating Fuel, International Conference on Emerging Nuclear Energy Systems ICENES 98, Tel Aviv (1998)

Lape99 G. Lapenta, P. Ravetto, Basic Reactor Physics Problems in Fluid-Fuel Recirculated Reactors, in preparation (1999)

Lawr39 E.O. Lawrence and N.E. Edlefsen, On the Production of High Speed Protons, Science, LXXII, NO. 1867, 376, October 10, 1939.

Lawr60 E. O. Lawrence, E. M. McMillan, and Luis W. Alvarez, Electronuclear Reactor, United States Patent No. 2,933,442 Apr. 19, 1960.

Lebr99 Lebrat et al. Experimental investigation of multiplying subcritical media in presence of an external source operating in pulsed or continuous mode : The MUSE - 3 Experiment. Proceedings ADTTA `99. Praha.

Lefo59 M. Lefort, G.N. Simonoff, X. Tarrago, R.Bibron, " Production de Tritium dans le Thorium par des Protons de 135 MeV," J Phys. Radium, 20 ,959 (1959)

Lefo65 M. Lefort, J.P. Cohen, H. Dubost, and X. Tarrago, "Evidence for Nucleon Clustering from High-Energy Reactions," Phys. Rev. 139B , 1500 (1965)

Leli99 Lelièvre et al. Estimates of radiaition damage induced by a proton beam in the window of an accelerator driven system. Proceedings ADTTA 99'. Prague.

Lens92 H. Lenske and H. Wolter, Nucl. Phys. **A538** (1992) 483c.

Lewi52 W. B. Lewis, The Significance of the Yield of Neutrons from Heavy Nuclei Excited to High Energies, Atomic Energy of Canada Limited Report AECL 968, 1952.

Liso80 P.W.Lisowski et al., Proc. Symp. On Neutron Cross-Sections from 10 to 50 MeV., Upton,12-14 May 1980. v.1 (1980) p.301.

Liso91 P.W.Lisowski et al., in Proc. Symp. on Neutron Cross-Sections from 10 to 50 MeV. Upton, 1980, Vol. 1, p.301; in Proc. Specialists' Meeting on Neutron Cross-Sections Standards for the Energy Region above 20 MeV (Uppsala, May 1991), NEANDC-305/U, p.177 (1991)

Macf94 R.E. MacFarlane, *The NJOY Nuclear Data Processing System, Version 91*, Report LA-12740-M, Los Alamos National Laboratory, 1994.

MacF98 R.E. MacFarlane et. al.Documentation for PSR-368/NJOY97.0 Code Package, 1998.

Mann77 F. M. Mann and R. E. Schenter, Nucl. Sci. Eng. 63 (1977)

Mant83 G.N.Manturov, V.P.Lunev, L.V.Gorbachova, VANT, Yadernye Constanty,1983, v.1(50), p.50

Marc83 A. Marcinkowski et al., Nucl. Phys. **A**402, (1983), 220.

Mari88 J. Marivoet and A. Bonne, PAGIS, *Performance Assessment of Geological Isolation Systems for Radioactive Waste, Disposal in Clay Formations*, Commission of the European Communities, EUR 11776 EN, 1988.

Mart96 M. Martone, editor,IFMIF Conceptual Design Activity, Final Report,ENEA Frascati Report RT/ERG/FUS/96/11 (1996)

Megh60 R.V. Meghreblian, D.K. Holmes, Reactor Analysis, McGraw-Hill, New York (1960)

Meie89 M.M Meier et al., Nuc. Sci. Eng. 102 (1989) 310.

Mich97 R. Michel and P. Nagel, *International codes and model comparison for intermediate energy activation yields*, NEA report, NSC/DOC(97)-1, January 1997.

MMF Moscow Meson Factory : http://www.inr.ac.ru/INR/MMF.html

Mort91 S.V. Fortsch et al., Phys. Rev. **C**43, (1991) 691.

MTA54 Status of the MTA Process, Livermore Research Laboratory Report LRL-102, 1954.

Mult96 Multilateral Nuclear Export Control Regimes, December 17, 1996, http://www.acda.gov/ factshee/exptcon/nuexpcnt.htm

Naka84 M. Nakagawa and T. Mori, MORSE-DD - A Monte Carlo Code Using Multi-Group Double differential Form Cross Sections. JAERI-M-84-126 (1984)

Naka96 Y. Nakashima et al., Nuc. Sci. Eng. 124, 243 (1996)

Nakb96 Y. Nakane et al., ``Neutron transmission benchmark problems for iron and concrete shields in low, intermediate and high energy proton accelerator facilities", JAERI report JAERI-Data/Code 96-029 (1996)

Nakc96 Y. Nakane et al., ``Intercomparison of neutron transmission benchmark analyses for iron and concrete shields in low, intermediate and high energy proton accelerator facilities", OECD proceedings *SATIF-3 Shielding aspects of accelerators, targets and irradiation facilities*, NEA Data Bank (1996)

NEA99 http://www.nea.fr/html/pt

Nead94 *Proceedings of the NEA Specialist Meeting on Intermediate Energy Nuclear Data: Models and Codes*, May 30-June 1 1994, Issy-les-Moulineaux, France.

Nead97 The data files are available at *http://www.nea.fr/dbforms/evatapes.cgi*.

Neal95 F.B. Neall, P. Baertschi, I.G. McKinley, P.A. Smith, T. Sumerling and H. Umeki, *Comparison of the Concepts and Assumptions in Five Recent HLW/Spent Fuel Performance Assessments*, Mat. Res. Soc. Symp. 1995, **353**, 503.

Nish88 H. Nishioka, H.A. Weidenmüller and S. Yoshida, Ann. Phys.(N.Y.) **183** (1988) 166.

Norg75 Norgett, Robinson et Torrens. "A proposed method of calculating diplacements dose rates". Nucl. Eng. and Design 33, 50 (1975).

Opti96 *Proceedings of the NEA Specialists' Meeting on the Nucleon Nucleus Optical Model up to 200 MeV, Bruyères-le-Châtel*, November 13-15 1996. WWW-address: http://db.nea.fr/html/science/om200/.

Ouss99 V.I. Oussanov, D.V. Pankratov, E.P. Popov, P.I. Markelov, L.D. Riabaya, S.V. Zabrodskaya, Long-lived Residual Activity Characteristics of some Liquid Metal Coolants For Advanced Nuclear Energy Systems, Proceedings of GLOBAL-99 Conference, Jackson, WY, USA, 1999.

Over1 Overview of the ATW System, http://neutrino.nuc.berkeley.edu/design/atw/Overview.html

Pank60 V.M.Pankratov, N.A.Vlasov, B.V.Rybakov Cross Sections for the Fission of Th-232, U235 and U238 Induced by 10-22 MeV Neutrons. At. Energy, v.9, (1960) p.399.

Pank63 V.M. Pankratov, "Fission Cross Sections of Th-232, U-233, U-235, Np-237, U-238 for 5-37 MeV Neutrons," Atomnaya Energia, 14, 177 (1963)

Part95 Partitioning and Transmutation Research: http://inisjp.tokai.jaeri.go.jp/ACT95E/11/11-1.HTM

Pazs98a Pázsit I. and Yamane Y. Theory of neutron fluctuations in source-driven subcritical systems. Nucl. Instr. Meth. A 403, 431 - 441 (1998)

Pazs98b Pázsit I. and Yamane Y. The variance-to-mean ratio in subcritical systems driven by a spallation source. Ann. nucl. Energy 25, 667 - 676 (1998)

Pazs99a I.. Pázsit: General backward theory of particle transport with a correlated multiple source. Physica Scripta 59, 344 - 351 (1999)

Pazs99b I. Pázsit and Y. Yamane: Backward theory of Feynman- and Rossi-alpha methods in subcritical systems driven by a spallation source. To appear in Nucl. Sci. Engng (1999)

Pazs99c Pázsit I. and Arzhanov V. Theory of neutron noise induced by source fluctuations in accelerator-driven subcritical reactors. Ann. nucl. Energy 26, 1371-1393 (1999)

Pazs99d Pázsit I. and Sjöstrand N. G. On the significance of the distribution of source neutrons in spallation. To be submitted to Nucl. Instr. Meth. A (1999)

Petr1 L. M. Petrie et al. "SCALE 4.3: modular code system for performing standardised computer analyses for licensing evaluation", (ORNL/NUREG/CSD-2/R4)

Prae89 R.E. Prael and H. Lichtenstein, Users guide to LCS: The LAHET code system", LA-UR-89-3014, Los Alamos National Laboratory (1989)

Prae94 R.E. Prael, A Review of Physics Models in the LAHET™ Code, LA-UR-94-1817 and in Intermediate Energy Nuclear Data: Models and Codes Proceedings of a Specialist's meeting Issy-Les-Moulineaux (France) OECD Documents, 30 May-1 June 1994.

Rams97 E. Ramström, H. Lenske and H. Wolter, Proc. of the International Conference on Nuclear Data for Science and Technology, Trieste, Italy, May 19-24, 1997, ed. G. Reffo, A. Ventura and C. Grandi. (Bologna: Società Italiana di Fisica, Italy, 1997) p.241.

Ruth20 E. Rutherford, Bakerian Lecture: Nuclear Constitution of the Atoms", lecture delivered June 3, 1920.

Rave198 P. Ravetto, Perturbation Theory of Fluid-Core Recirculated Systems, Transactions of the American Nuclear Society, 70, 259-261 (1998)

Rave98 P. Ravetto, G.G.M. Coppa, G. Lapenta, A.M. Larosa, M. Carta, Assessment of Numerical Methods for Time-Dependent Transport Calculations of Subcritical Systems, International Conference on the Physics of Nuclear Science and Technology, Long Island (1998)

Rave99 P. Ravetto, Neutron Amplification in Transport Problems for Multiplying Subcritical Systems, 16-th International Conference on Transport Theory, Atlanta (1999)

Rayn84 J.Raynal, Mater. Of Workshop on Nuclear Model Computer Codes. 16 Jan - 3 Feb. 1984. Trieste.

Rayn94 J. Raynal, Notes on ECIS94, *CEA Saclay Report* CEA-N-2772 (1994)

Rimp95 G.Rimpault. "Algorithmic features of the ECCO cell code for treating heterogeneous fast reactor sub assemblies". International conference on mathematics and computation, reactor physics and environmental analysis. Portland Oregon. April 1995.

Ring97 A. Ringbom et al, Nucl. Phys. **A617** (1997) 316.

Road99 "A Roadmapping for Developing Accelerator Transmutation of Waste (ATW) Technology", A Report tp Congress, DOE/RW-0519, October 1999.

Rose90 P.F. Rose, C.L. Dunford, editors,ENDF-102 - Data Formats and Procedures for the evaluated nuclear data file ENDF-6, BNL-NCS-44945,1990.

Rubb95 C. Rubbia, J.A. Rubio, S. Buono, F. Carminati, N. Fietier, J. Galvez, C. Geles, Y.Kadi, R. Klapisch, P. Mandrillon, J.P. Revol and Ch. Roche, Conceptual Design of a Fast Neutron Operated High Power Energy Amplifier, CERN/AT/95-44(ET), 1995.

Rubb96 C. Rubbia and J. A. Rubio, A Tentative Programme Towards a Full Scale Energy Amplifier. CERN report CERN/LHC/96-11 (EET), 1996.

Rubb97 C. Rubbia, S. Buono, Y. Kadi and J.A. Rubio, *Fast Neutron Incineration in the Energy Amplifier as Alternative to Geologic Storage: The Case of Spain*, CERn/LHC/97-01 (EET), February 1997.

Ruds90 G. Rudstam et al., Radiochimica Acta **49** (1990) 155.

Rydi96 R.A. Rydin, M.L. Woosley, Jr., Methods Developed for Dynamic Analysis of an Accelerator-Based Subcritical Radioactive Waste Burning System, International Conference on the Physics of Reactors PHYSOR-96, Mito, Japan (1996).

Salv94 M. Salvatores, A first approach to data needs and target accuracies for hybrid systems, *Proceedings of the NEA Specialist Meeting on Intermediate Energy Nuclear Data: Models and Codes*, May 30-June 1 1994, Issy-les-Moulineaux, France, 313.

Salv96 M. Salvatores et al. MUSE-1 : A first experiment at MASURCA to validate the physics of sub-critical multiplying systems relevant to ADS. Proceedings of the second international conference on Accelerator Driven Transmutation Technologies and Applications. June 3-7, 1996, Kalmar, Sweden.

Salv96a Salvatores, Schapira, Mouney. French programs for advanced waste management options. Physics and modelisation of spallation. Proceedings 2nd Intal Confce on Accelerator Driven Transmutation Technologies and Applications. Kalmar, Sweden. p 60. 1996.Transmutation Technologies and Applications. June 3-7, 1996, Kalmar, Sweden.

Salv97 Salvatores, Ritter, Slessarev, Tchistiakov, Zaetta. "A multipurpose experimental Accelerator Driven Reactor : The Hadron Concept". Proceedings GLOBAL 97 - Yokohama - Japan. p 428.

Salv97a M. Salvatores, I. Slessarev, A. Tchistiakov, G. Ritter. The potential of Accelerator-Driven-Systems for Transmutation or Power Production Using Thorium or Uranium Fuel Cycles. Nuclear Science and Engineering. Vol 126, Number 3, July 1997.

Schr95 U. Schryber, et. al., Proceedings 14th Conference on Cyclotrons and Applications, Cape Town, p.32, 1995.

Schw82 P. Schwandt et al, Phys. Rev. **C26** (1982) 55.

Sege94 M. Segev, PROSDOR – An IBM-3090 Based Semi-Automated Procedure Linking HERMES MCNPand KORIGEN for the Burnup Analysis of Accelerator Driven Cores, KfK-5328, 1994.

Sege99 M. Segev, C. Broeders, I. Broeders, Significance of Spallation Products in a Fast Spectrum ADS, Forschungszentrum Karlsruhe Internal report, January 1999.

Shub95 Yu.N. Shubin, V.P. Lunev, A.Yu. Konobeyev and A.I. Dityuk,Cross-Section Data Library MENDL-2 to Study Activation andTransmutation of Materials Irradiated by Nucleons of Intermediate Energies, IAEA report, INDC(CCP)-385, May 1995.

Sinc95 J.E. Sinclair and P.J. Agg, *MASCOT and MOP Programs for Probabilistic Safety Assessment, Part A: Overview (MASCOT Version 3C and MOP Version 3A)*, Nirex Report NSS/R336, 1995.

SINQ SINQ: Spallation Neutron Source: http://ww1.psi.ch/www_lns_hn/welcome_sinq.html

Sless97 I. Slessarev, A. Tschistiakov, IAEA-ADS BENCHMARK (Stage1), RESULTS and ANALYSIS, TCM-Meeting, Madrid, 17-19 September 1997.

Smit93 P.A. Smith, *Framework of Integrated Performance Assessment in Kristallin-I*, International Workshop on Research and Development of Geological Disposal. Tokai, Ibaraki (Japan), 15-18 Nov 1993, IV/7-IV/18.

Smit95 P.A. Smith, P. Zuidema and I.G. McKinley, *Assessing the Performance of the Nagra HLW Disposal Concept,* Nagra Bulletin English Edition, 1995, 34-46.

Stam94 T. Stammbach, et al. International Conference on Accelerator Driven Transmutation Technology and Applications, Las Vegas, p.229, 1994.

Steh91 B. Stehle, D3D und D3E, Zweige eines FORTRAN-Programms zur Lösung der stationären dreidimensionalen Multigruppen Neutronendiffusions-gleichungen in Rechteck-, Zylinder- und Dreieckgeometrie, KfK-4764,1991.

Stei64 M. Steinberg, G. Watsak, B. Manowitz, Neutron Burning of Long-Lived Fission Products for Waste Disposal, Brookhaven National Laboratory Report BNL-8558 (1964)

Stor88 R. Storck, et al., *PAGIS, Performance Assessment of Geological Isolation Systems for Radioactive Waste, Disposal in Salt Formations*, Commission of the European Communities, EUR 11778 EN, 1988.

Svir83 M.I. Svirin, *Proceedings of the Conference on Neutron Physics*, Kiev, Vol.3, (1984) 294.

Taki92 Takizuka et al. ''Overview on nuclear design problems of accelerator-based transmutation systems with emphasis on the target facilities and their interfaces with accelerator'', Specialists' meeting on accelerator-based transmutation, PSI, Switzerland, 24-26 March 1992.

Taki95 T. Takizuka et al., Accelerator-driven Transmutation, http://inisjp.tokai.jaeri.go.jp/ ACT95E/11/11-3.HTM

Tamu82 T. Tamura, T. Udagawa and H. Lenske, Phys. Rev. **C26** (1982) 379.

Teol92 *Final Disposal of Spent Nuclear Fuel in the Finnish Bedrock*, Technical Plans and Safety Assessment, Teollisuuden Voima Oy, YJT-92-31E, 1992.

Tuce97 K. Tucek, J. Wallenius, W. Gudowski and A. Soltan, IAEA Accelerator Driven System Neutronic Benchmark, IAEA Workshop, Madrid, September 1997.

VanD96 H. Van Dam, Delayed Neutron Effectiveness in a Fluidized Bed Fission Reactor, Ann. Nucl. Energy, 23, 41 (1996)

Vass78 . R.G. Vassylkov, Vi.I. Goldanskii et al., Atomnaya Energiya 48, 329 (1978)

Vaz95 P. Vaz, Review of Existing Planned Proton Accelerators and Neutron Beams in the Intermediate Energy Range, Proc. of Second Specialists' Meeting on 'Shielding Aspects of Accelerators, Targets, and Irradiation Facilities', CERN, Switzerland, 12-13 Oct. 1995, OECD Nuclear Energy Agency.

Venn93 F. Venneri, C.D. Bowman, R. Jameson, Accelerators address Nuclear Waste Problems, Physics World 6,8 p.40, Aug. 1993.

Venn98a F. Venneri, et al., Proceedings 6th International Conference on Nuclear Engineering, 1998.

Venn98b F. Venneri, Presentation for MIT Technical Review, January 1998.

Voig68 J.Voignier, "Study of Interaction of 14 MeV Neutrons with U-238," Report CEA-R-3503 (1968)

Volc98 G. Volckaert, et al., *Long-term Environmental Impact of Underground Disposal of P&T Waste*, paper presented at 5th International Information Exchange Meeting on Actinide and Fission Product Partitioning and Transmutation, OECD/NEA, Mol, November 1998.

Vona94 H.Vonach, A.Pavlik, M.B.Chadwick, R.C. Haight, R.O. Nelson, S.A. Wender, and P.G. Young, "207, 208Pb(n,xn) Reactions for Neutron Energies from 3 to 200 MeV," Phys. Rev. C50, 1952 (1994)

Wahl85. A. Wahl, Phys. Rev. C 32 184 (1985)

Woll75 D. Woll, GRUCAL, Ein Programmsystem zur Berechnung makroskopischer, Gruppenkonstanten, KFK 2108, 1975.

Woos96 M.L. Woosley, Jr., R.A. Rydin, Dynamic Analysis of an Accelerator-Based Subcritical Radioactive Waste Burning System, 2-nd International Conference on Accelerator-Driven Transmutation Technologies and Applications, Kalmar, Sweden (1996)

Wu79 J.R.Wu, C.C.Chang , H.D.Holmgren, "Charged particle spectra: 90 MeV Protons on 27Al, 58Ni, 90Zr, and 209Bi," Phys. Rev. C19, 698 (1979)

Yama98 Yamane Y. and Pázsit I. Heuristic derivation of Rossi-alpha formula with delayed neutrons and correlated source. Ann. Nucl. Energy 25, 1373-1382 (1998)

Yefi99 E. Yefimov, B. Gromov, M. Leonchuk, Yu. Orlov, D. Pankratov, "Problems Of Molten Lead-Bismuth Target Development For Accelerator-Driven Systems", Proceedings of the 3rd International Conference on Accelerator Driven Transmutation Technologies and Aplications – ADTTA99, Praha , 7 - 11 June 1999.

Youi98 Youinou. "Étude conceptuelle de réacteurs nucléaires sous-critiques couplés à un accélérateur de protons". PhD Thesis. Université de Provence. Marseille. France.

Zuid93 P. Zuidema, I.G. McKinley, P.A. Smith, E. Curti, R. Klos, M. Hugi, M. Niemeyer, *Kristallin-I Performance Assessment: First Results*, 1993 International Conference on Nuclear Waste Management and Environmental Remediation, Prague (Czech Republic), 5-11 Sep 1993, 721.